The regulation of myeloid cell survival: Emerging roles for the pro-survival protein HAX1

Pranvera Sadiku

Academic Unit of Respiratory Medicine

Department of Infection and Immunity

University of Sheffield

Thesis submitted for the degree of Doctor of Philosophy

September 2014

Abstract

The regulation of myeloid cell apoptosis is critical in both the control of inflammation and homeostasis. HAX1, a ubiquitously expressed multifunctional protein is thought to play a key role in cell survival. *HAX1* mutations in the human result in premature apoptosis of bone marrow myeloid progenitor cells and a profound PMN (peripheral blood neutrophils) deficiency, suggesting HAX1 plays a critical role in PMN homeostasis. Human PMN are genetically intractable and Hax1 homozygous mice have been shown to die at 14 weeks of age. The molecular pathways in which HAX1 is involved are therefore yet to be elucidated. We hypothesised that HAX1 would play a critical role in constitutive cell death through effects on mitochondrial membrane stability and that *hax1* deficient zebrafish embryos would have defective PMN development and survival.

HAX1 expression was studied in primary PMN (prepared from venous blood of healthy volunteers), myeloid leukaemia cell line PLB-985 and wild type zebrafish embryos by western blotting, RT-PCR and *in situ* hybridisation. *HAX1* was knocked down in the human myeloid leukaemia cell line PLB-985 and *hax1* deficient zebrafish mutants were created in an MPO driven GFP transgenic line using antisense morpholino oligonucleotides (MO) or TALEN technology.

PLB-985 and primary PMN express multiple *HAX1* isoforms at the mRNA level, including the full-length isoform. I present data revealing the modulation of HAX1 in response to inflammatory stimuli in PLB-985 and show that HAX1 expression decreases during constitutive ageing of PMN. Zebrafish express multiple isoforms of *hax1*, providing novel evidence for alternative splicing of the gene in the model organism. *hax1* MO injected embryos exhibit a reduction in PMN numbers, which may be due either to a loss of Hax1 or to the concomitant developmental delay observed. The *hax1* targeting TALEN generated efficiently modified the *hax1* gene and was successfully transmitted through the germline. Preliminary data suggest that the *HAX1* knockdown in PLB-985 cells and the *hax1* homozygous mutation generated in the zebrafish are not important in PMN lifespan.

Acknowledgements

Firstly, I would like to thank my primary supervisor Lynne Prince and co-supervisor Stephen Renshaw for their continued guidance and support throughout the course of my studies. Thanks to Lynne Prince for my training, for the constant motivation in our meetings and through emails and most of all for her patience. Thanks to Steve Renshaw for his input and help. I am really happy and grateful that I have had the chance to be supervised by both of you. I also wish to give special thanks to the Medical Research Council for funding my project.

I would like to thank all of the members of the Infection and Immunity department and of the Centre for Developmental and Biomedical Genetics in Sheffield for making it a pleasant environment to work in. Thank you to Julie Bennett for her help with molecular biology, Kathryn Higgins for help with PMN preps and Vanessa Singleton for always ensuring that reagents arrived on time and the lab ran smoothly. Thank you to the blood donors for making our research possible and everyone who carried out PMN preps and spared cells for my work. I would also like to thank Nikolay Ogryzko, Catherine Mottram, Kate Hammond and Anne Robertson for their help and training in zebrafish work and data analysis using Volocity® software. Thanks to James Robertson for the help with and input into the polymerosome experiments. Very big thanks to Stone Elworthy for his guidance and help with the ZFN and TALEN work.

Thank you to Marzieh Fanaei, Selina Parmar, Jamil Jubrail, Kirsty Wilson for their moral support and Martin Bewley for the funny (mostly science) jokes that always made me laugh. I would also like to thank my family for their unconditional love and support. Thanks to my brothers, sister (Ilirida) and cousins/best friends (Hana, Kreni and Lulja) for listening to me, being interested in what I had to say about my research (even when they didn't quite understand it) and for always putting a smile on my face. A final and very special thanks goes to my parents for their endless encouragement, patience and making me believe that I could get this far.

Table of Contents

List of Figures

List of Abbreviations

AIF- apoptosis inducing factor

ANOVA- analysis of variance

Apaf-1- apoptosis protease activating factor

APS- Ammonium persulfate

ARDS- acute respiratory distress syndrome

ATP-adenosine triphosphate

Bad- Bcl-2 associated agonist of cell death

BAL- bronchoalveolar lavage

Bak- Bcl-2 associated antagonist/killer

Bax- Bcl-2 associated x protein

Bid- BH3 interacting domain death agonist

Bik- Bcl-2-interacting killer

Bim- Bcl-2 like 11

Bcl-2- B cell lymphoma 2

Bcl-x- Bcl-2 associated x protein

BH domain- Bcl-2 homology domain

CHX- cyclohexamide

COPD- chronic obstructive pulmonary disease

CXCR- C-X-C chemokine receptor

DAMP- danger associated molecular pattern

DFP- diisopropyl fluorophosphate

DISC - death-inducing signalling complex

DMF- dimethylformamide

DMSO- dimethyl sulfoxide

DNA- deoxyribonucleic acid

dpf- days post fertilisation

EBNA5- Epstein-Barr virus nuclear antigen 5

EBNA-LP- Epstein-Barr virus nuclear antigen leader protein

EF1-α - elongation factor 1- α

FADD- Fas associated death domain

FCS- foetal calf serum

GAPDH- Glyceraldehyde 3-phosphate dehydrogenase

GCSF- granulocyte colony-stimulating growth factor

GFP- green fluorescent protein

GM-CSF- granulocyte-macrophage colony-stimulating factor

Grb7- growth factor receptor-bound protein 7

HAX1- HCLS-1 associated protein X1

HBSS- Hank's buffered saline solution

HCLS-1- hematopoietic cell-specific Lyn substrate

HCV - Hepatitis C virus

HK- heat killed

hpf- hours post fertilisation

hpi- hours post injury

HRP- horseradish peroxidase

ICAM-1- intracellular adhesion molecule 1

IL- interleukin

IRF-interferon-regulatory factor

LPS- lipopolysaccharide

Mcl-1- myeloid cell leukemia sequence 1

MO- morpholino oligonucleotide

MPO- myeloperoxidase

mRNA- messenger ribonucleic acid

NADPH- nicotinamide adenine dinucleotide phosphate

NETs- neutrophil extracellular traps

NF-κB- nuclear factor kappa-light-chain-enhancer of activated B cells

NLR- nucleotide binding oligomerisation domain receptors

Omi- serine protease HtrA2

PAF- platelet activating factor

PAGE- polyacrylamide gel electrophoresis

PAMPs- pathogen-associated molecular patterns

Parl- presenilin- associated, rhomboid-like protein

PBMC- peripheral blood mononuclear cells

PBS- phosphate buffered saline

PCR- polymerase chain reaction

PECAM-1- Platelet Endothelial Cell Adhesion molecule 1

PI- protease inhibitor

PKD2- polycystic kidney disease protein 2

PMN- polymorphonuclear neutrophil/s

PMSF- phenylmethylsulfonyl fluoride

PPP- platelet poor plasma

PRP- platelet rich plasma

PRRs- pattern recognition receptors

PVDF- Polyvinylidene fluoride

RA- retinoic acid

ROS- reactive oxygen species

RT-room temperature

RT-PCR- reverse transcription PCR

SCN- severe congenital neutropenia

SDS- sodium dodecyl sulphate

siRNA- short interfering RNA

STSP- staurosporine

TALEN- transcription activator-like effector nuclease

TEMED- Tetramethylethylenediamine

TGF-β- transforming growth factor β)

TLR- Toll-like receptor

TNF- tumour necrosis factor

UTR- untranslated region

VDAC- voltage dependent anion channel

XIAP- X-linked inhibitor of apoptosis protein

ZFN- zinc finger nuclease

1 General introduction

1.1 Immunity

The mammalian immune system consists of various cell types and signalling cascades essential in maintaining homeostasis and defence against pathogenic microorganisms. The immune system can be arbitrarily divided into two components, innate and adaptive immunity. The innate immune system is the first line of defence against pathogens. It is primarily mediated by the professional phagocytes polymorphonuclear neutrophils (PMN) and macrophages (Silva 2010). These cells recognise microorganisms through a limited number of pattern recognition receptors (PRRs), which are highly conserved among species from plants to mammals (Takeuchi & Akira 2010). This is in contrast to adaptive immunity, which utilises a large repertoire of specific receptors found on B and T lymphocytes and is capable of generating 'immunological memory' (Zinkernagel et al. 1996). An acquired immunity response is highly specific and is mediated in the later phase of infection. It is characterised by the clonal expansion of lymphocytes bearing antigen-specific receptors.

1.2 Inflammation

1.2.1 Leukocyte recruitment

Inflammation and the clinical symptoms and signs of inflammatory disease were first described by the Roman Cornelius Celsus, in the first century. The four key signs of inflammation were defined as: redness, swelling, heat and pain (Rather 1971). It was later established that an imbalance of these four "cardinal signs" leads to the development of disease. In the second century A.D., impaired function was identified as the fifth "cardinal sign" of inflammation (Rather 1971). Robert Koch and Louis Pasteur later went on to hypothesise that microorganisms are a major cause of an inflammatory

response. It is now accepted that a controlled inflammatory response is initiated as a host defence mechanism against pathogens.

1.2.2 Pattern recognition receptors

Inflammation is characterised by increased blood flow, vascular dilation, capillary permeability and leukocyte recruitment to the site of infection or injury. It is in part initiated by the tissue resident macrophages and mast cells that act as sentinels and recognise highly conserved pathogen-associated molecular patterns (PAMPs). This “pattern recognition” event occurs through PRRs such as Toll-like receptors (TLRs) and nucleotide binding oligomerisation domain receptors (NLRs), expressed by macrophages and mast cells (Takeda et al. 2003; K. S. Kobayashi et al. 2005). TLRs are the most well characterized PRRs and play a major role in the recognition of both endogenous and exogenous stimuli (Takeda et al. 2003). They recognise PAMP signals across Gram positive and negative bacteria and viruses (Takeda et al. 2003).

PRRs can also recognise and bind to danger associated molecular patterns (DAMPs) such as ATP (adenosine triphosphate) and mRNA (messenger ribonucleic acid) released from damaged or stressed cells (Gallucci & Matzinger 2001; Kariko et al. 2004). This enables the immune system to not only distinguish between ‘self’ and ‘non-self’ but also between ‘healthy’ and ‘damaged self’. PRR ligation results in the activation of a signalling cascade, which culminates in the activation of a number of transcription factors including NF-κB (nuclear factor kappa-light-chain-enhancer of activated B cells) and interferon-regulatory factor (IRF) (Baldwin Jr. 1996; Kawai & Akira 2007).

PRR signalling results in the production of numerous inflammatory factors (Medzhitov 2008). These include chemokines, cytokines and pro-inflammatory lipid mediators that can elicit local and systemic inflammatory

responses, which highlights the role of PRRs in leukocyte recruitment. Leukocytes are recruited to sites of infection and inflammation through functional gradients of chemokines, which are cytokines with chemoattractant function and in addition to leukocytes are also produced by endothelial, stromal and epithelial cells (Kumar & Sharma 2010). This process is known as chemotaxis.

Leukocyte recruitment from the circulation into tissues is essential for the development and appropriate maintenance of an inflammatory response. The type and length of the response are governed by the inflammatory trigger (Medzhitov 2010). The fate of inflammation is regulated by neutrophils, macrophages, mast cells and dendritic cells, which sense the pro-inflammatory signals and in turn release inflammatory mediators to regulate the duration and amplitude of the response. Neutrophils are among the first leukocyte type to accumulate at the inflamed tissue (Nathan 2006). During inflammation, these cells combine their anti-infectious role with a pro-inflammatory role (Weiss 1989; Ward & Lentsch 1999).

1.3 PMN

PMN were first discovered by Elie Metchnikoff as migrating and phagocytosing cells in starfish larvae in response to inserted rose thorns (Cavaillon 2011). The cells are on average 10 µm in diameter and have a characteristic lobulated-chromatin dense nucleus (Korchak et al. 1983). They belong to a group of leukocytes known as granulocytes that are characterized by the presence of granules in the cytoplasm. Based on the histological properties of the granules, granulocytes can be divided into PMN, eosinophils and basophils. PMN constitute 60 % of the circulating leukocyte population in the blood (Smith 1994). They are produced in the bone marrow and it is estimated that in the human, between 5×10^{10} and 10×10^{10} are formed each day (Summers et al. 2010).

1.3.1 PMN terminal differentiation

PMN production and differentiation from hematopoietic stem cells in the bone marrow is modulated by two cytokines known as granulocyte colony-stimulating growth factor (GCSF) and granulocyte-macrophage colony-stimulating factor (GM-CSF) (Cannistra & Griffin 1988). The cells first appear in the human marrow cavity at 10-11 weeks post-conception (Slayton et al. 1998) and mature to become terminally differentiated cells within 14 days (Haylock et al. 1992). The majority of a PMN's life is spent in the bone marrow and under physiological conditions only 2 % of the cells are found in the circulation (Semerad et al. 2002).

PMN terminal differentiation, termed granulopoiesis, begins during the myeloblast and promyelocyte stages at which point proliferation is switched to differentiation (Glasser & Fiederlein 1987). During the promyelocytic cell stage, in addition to losing the ability to undergo cell division, the cells form the first granules known as azurophilic granules. These granules are defined by a high content of myeloperoxidase, defensins and proteases such as PMN elastase (Borregaard et al. 1993; Pham 2006). Differentiation of promyelocytic cells progresses into the development of myelocytes and metamyelocytes (Glasser & Fiederlein 1987). During these states, nuclear segmentation is initiated and the cells form secondary granules required for respiratory burst and bactericidal activity (Borregaard & Cowland 1997). Metamyelocytic cells differentiate into band PMN, which in turn go on to become segmented neutrophils (Glasser & Fiederlein 1987). Segmented PMN have segmented nuclei and form secretory and tertiary granules characterised by a high content of enzymes such as gelatinase and lysozyme (Borregaard & Cowland 1997). During stress and infection the rate of PMN differentiation can increase by 10-fold (Cannistra & Griffin 1988).

1.3.2 PMN migration to the site of infection/injury

PMN circulate in the blood in a relatively functionally quiescent state until stimulated by an infection (Southgate et al. 2008). These cells exist in numerous subpopulations in various states of activation ranging from the inactive resting state to the fully activated state (Gallin 1984). Primed PMN acquire a state of pre-activation and this enables them to produce a more powerful response once fully activated.

PAMP binding induces sentinel cells to produce numerous pro-inflammatory cytokines including interleukin-1β (IL-1β), tumour necrosis factor-α (TNF- α), chemokines and other lipid mediators (Zeytun et al. 2010). These act to rapidly recruit PMN to the inflammatory peripheral tissues. PMN extravasation occurs in the postcapillary venules and pulmonary capillaries (Downey et al. 1993). Their recruitment has been shown to involve both selectin and integrin dependent mechanisms (Adams & Shaw 1994; Springer 1994).

A multistep sequential adhesion cascade is initiated on contact of free-flowing PMN to the activated vascular endothelium. It is thought that the vasculature acts as a fast-track system for PMN whereby PMN approach the injured or infected site as closely as possible within the blood vessel (McDonald et al. 2010). During the first step of the PMN adhesion cascade known as tethering, PMN become transiently adherent to the endothelium (Springer 1994). Tethering results in rolling of PMN along the endothelium, which involves PMN L-selectins and E- and P-selectins expressed on the endothelial wall (Lawrence & Springer 1991; Lawrence & Springer 1993; Phillips et al. 1995; Moore et al. 1995; McEver & Cummings 1997). During the rolling step, PMN transmigration into the inflammatory site is promoted through the production of chemoattractants such as platelet-activating factor (PAF) and Interleukin-8 (IL-8) (Walz et al. 1987). These are immobilised on the luminal surface of endothelial cells via glycosaminoglycans (Premack &

Schall 1996; Matsumoto et al. 1997). Chemoattractant production results in the activation of PMN, which in turn leads to firm adhesion to the endothelial cells. This occurs through PMN β_2-integrins (Zimmerman et al. 1992). In order to prevent cytotoxic damage to the host, PMN activation appropriately occurs in regions proximal to the inflammatory site (Swain et al. 2002).

Following PMN activation, β_2-integrins bind to their physiological ligand Intercellular Adhesion Molecule 1 (ICAM-1) with enhanced affinities allowing firm adhesion to occur (Sligh Jr. et al. 1993; Stewart & Hogg 1996). Once PMN have firmly bound to the endothelium, numerous surface molecules including Platelet Endothelial Cell Adhesion molecule 1 (PECAM-1), ICAM-1, CD44 and CD47 facilitate transmigration to the peripheral tissue (Diamond et al. 1990; Muller et al. 1993). PMN movement across the endothelial cell layer and basement membrane is also known as diapedesis and has been shown to almost always occur through the endothelial cell borders (Sumagin & Sarelius 2010; Woodfin et al. 2011).

Once into the interstitial tissue, PMN migrate to the site of injury or infection along a gradient of immobilised chemoattractants and this process is known as haptotaxis (Foxman et al. 1999). PMN sense the gradients through G-protein-coupled-seven-transmembrane glycoprotein receptors and receptors for the chemoattractant, C-X-C chemokines (Premack & Schall 1996; Yokomizo et al. 1997). The ligation of these receptors to the chemoattractants results in the activation of numerous signalling cascades regulating PMN degranulation, reactive oxygen (ROS) production, cytoskeletal organisation, cell adhesion and motility (Cox et al. 1997; Thelen & Didichenko 1997; Nobes & Hall 1999).

1.3.3 The role of PMN in infection

The principal role of PMN is to destroy invading microorganisms at sites of infection through binding and ingestion, a process known as phagocytosis, and degranulation in areas where phagocytosis of pathogens is not possible (Bellocchio et al. 2004; Lotz et al. 2004; Brinkmann et al. 2004). Granule proteins and chromatin are also released by PMN that form extracellular fibres known as neutrophil extracellular traps (NETs) (Brinkmann et al. 2004). NETs bind Gram positive and Gram negative bacteria and prevent their spreading while simultaneously ensuring a high exposure to anti-microbial granule contents for destroying the pathogen. PMN antimicrobial activity is caused primarily by the production of ROS and the antimicrobial and hydrolytic proteins found in their granules (Spitznagel 1990; Quinn & Gauss 2004). Following PMN activation, oxygen consumption of the cell increases dramatically and this process is termed the respiratory burst (Babior 1984). It involves the enzymatic complex, nicotinamide adenine dinucleotide phosphate (NADPH) oxidase (DeLeo & Quinn 1996). This complex generates superoxide anion (O^{2-}), which in turn can react with other molecules to form ROS including hydrogen peroxide, which are critical in the killing of ingested microorganisms (Babior 1984; Nathan 1987)). Proteins such as myeloperoxidase present in PMN granules amplify the toxic effects of the hydrogen peroxide through the generation of hypochlorous acid and chloride anions (Klebanoff 1968).

In addition to their ability to phagocytose, PMN can also resolve infections through the release of ROS and granules containing degradative enzymes (Dransfield & Rossi 2004; El Kebir & Filep 2010). PMN responses to infection can therefore result in considerable damage to host tissues themselves (Melley et al. 2005). This means that PMN apoptosis has to be a finely controlled process by extrinsic and intrinsic factors in order to maintain a balance between PMN defence functions and safe clearance (Savill, Wyllie, et al. 1989; Bianchi et al. 2006; Luo & Loison 2008).

1.3.3.1 PMN granule content and action against pathogens

Human PMN are characterised by the existence of multiple granules varying in morphology and size (Borregaard & Cowland 1997). Whilst some PMN granules such as the azurophilic granule predominantly contain antimicrobial and degradative enzymes that are released into the phagolysosome, others are specifically destined for extracellular release (Cowland et al. 1995; Lollike et al. 1995). Azurophilic granules contain numerous antibiotic proteins including myeloperoxidase and serine proteases (Fouret et al. 1989). These compartments are though to be mobilised upon phagocytosis of pathogens. Furthermore, the contents of these granules result in the activation of numerous cells including epithelial cells, macrophages and lymphocytes (Owen & Campbell 1999).

Other PMN granules are myeloperoxidase negative and can be divided into secondary and tertiary granules (Kjeldsen et al. 1992). These differ in their secretory and content properties. Secondary granules are known as specific granules and contain high levels of potent antimicrobial agents such as the peptidoglycan cleaving protein lysozyme and lactoferrin, which binds to iron and can also cause irreversible damage to bacterial cell membranes resulting in cell lysis (Cramer et al. 1985; Lollike et al. 1995; Chapple et al. 1998). Conversely, tertiary granules are also known as gelatinase granules as a result of comprising the highest content of gelatinase (a metalloprotease) out of all of the different granule types (Kjeldsen et al. 1992). These granules contain numerous metalloproteases, stored in an inactive form and capable of degrading structural and extracellular matrix components upon proteolytic activation (Lazarus et al. 1968; Kjeldsen et al. 1992; Borregaard & Cowland 1997).

1.3.3.2 PMN apoptosis

Circulating PMN have a short life span, estimated to be between 8 and 20 hours (Savill, Henson, et al. 1989; Luo & Loison 2008). The short-half life of

circulating PMN is a result of constitutive apoptosis, which is essential for the resolution of inflammation and maintenance of homeostasis (Luo & Loison 2008). PMN that have been recruited to tissue where they are required to resolve infection, live longer in order to maximise their immunologic potential (1-4 days) (Elbim & Estaquier 2010).

Apoptosis is the major mechanism regulating PMN number, and the mechanisms controlling apoptosis will be discussed in section 1.6 (Shi et al. 2001). PMN undergoing apoptosis are unresponsive to extracellular stimuli and express signals that target the cells for recognition and phagocytosis by scavenger receptors expressed by macrophages (Savill et al. 1990; Haslett et al. 1994; Savill & Haslett 1995). Prolonged PMN lifespan can result in the increased disease severity of numerous non-infectious inflammatory diseases including chronic obstructive pulmonary disease (COPD), chronic lung disease, rheumatoid arthritis and asthma (Kotecha et al. 2003; Pletz et al. 2004; Filep & El Kebir 2009; Wong et al. 2009; Brown et al. 2009; Moriceau et al. 2010; Baines et al. 2010). Concomitant with delayed apoptosis, the prolonged production of pro-inflammatory mediators by tissue neutrophils also contributes to the perpetuation of inflammation. In contrast, accelerated PMN apoptosis can lead to a reduction in PMN number and may prevent efficient responses to invading pathogens (Carlsson et al. 2004; Klein et al. 2007). A precise balance between PMN defence properties and safe clearance is therefore crucial for the maintenance of homeostasis.

The constitutive rates of apoptosis in PMN are tightly regulated compared to other leukocyte types. It has been shown that PMN can undergo apoptosis even in the absence of extracellular signals (Filep & El Kebir 2009). Apoptosis can also however, be accelerated by some cytokines and death receptor ligand binding on the surface of the cells, although this is not thought to be an important mechanism of PMN cell death (van Raam et al. 2006). Although it remains controversial, it is thought that the mitochondria of

PMN play a crucial role in regulating the programmed cell death pathways in these cells (Maianski et al. 2004). PMN survival can be extended by inflammatory cytokines such as TNF-α, GM-CSF and LPS while simultaneously preserving cellular function (Lee et al. 1993).

1.4 Inflammation resolution

The primary goal of an acute inflammatory response is elimination of infectious agents with spontaneous resolution, in turn restoring homeostasis and limiting excessive host tissue damage (Van Dyke & Kornman 2008). Once the pathogen has been cleared, there is a progressive decrease in PMN recruitment due to an increase in the secretion of anti-inflammatory cytokines and a return of endothelial cells to their resting state. There is also a switch in expression from anti-inflammatory to pro-resolution endogenous lipid mediators such as protectins, lipoxins and maresins that act as "stop signals" (Bannenberg & Serhan 2010). These inhibit PMN chemotaxis, adhesion and transmigration (Diamond et al. 1999; Bannenberg & Serhan 2010).

The induction of PMN apoptosis plays a key role in inflammation resolution. It has been shown that following phagocytosis of bacteria, PMN apoptosis is, in some cases, significantly accelerated (Kobayashi et al. 2003). Apoptosis results in impaired PMN functional capacity causing reduced chemotaxis, phagocytosis, degranulation and respiratory burst, therefore limiting further inflammation (Whyte, Meagher, et al. 1993; S. D. Kobayashi et al. 2005). The subsequent ingestion of PMN by macrophages (efferocytosis) is the major mechanism for PMN clearance at the site of inflammation (Savill & Haslett 1995; Savill 1997). Apoptotic PMN express phosphotidylserine on their cell surface, which triggers their recognition and phagocytosis by macrophages (Savill et al. 1993; Homburg et al. 1995). In human and mice, removal of PMN also occurs in the bone marrow, spleen and in the liver, in

Kupffer cells (Savill, Wyllie, et al. 1989; Savill et al. 2002; Furze & Rankin 2008).

Efferocytosis is critical in inflammation resolution not only by removing the source of the inflammation but also by a phenotypic switch to a pro-resolution phenotype consistent with inflammation resolution and tissue repair (Fadok et al. 1998). For example, the production of pro-inflammatory cytokines such as GM-CSF, IL-1β, IL-8 and leukotriene C4 is inhibited in the phagocytosing macrophages and anti-inflammatory genes such as TGF-β (transforming growth factor β) and PAF are expressed (Fadok et al. 1998; Gerber & Mosser 2001). Although it has been shown in mice that Fas ligand (FasL)/Fas death receptor mediated apoptosis is not essential for regulating PMN lifespan during an acute inflammatory response (Fecho & Cohen 1998), macrophages can trigger PMN apoptosis by expressing FasL on their surface and releasing soluble FasL, which binds to the Fas receptor on PMN (Brown & Savill 1999). This however is not thought to be an important mechanism of PMN death but may be considered as an anti-inflammatory response (Renshaw et al. 2000).

Emerging evidence exists for a new route of inflammation resolution. This involves a mechanism known as retrograde chemotaxis or reverse migration. The use of the zebrafish tissue injury model has shown that during this process, PMN migrate away from the wound or infection site and back into the vasculature (Mathias et al. 2006). PMN velocity and directionality were shown to be the same to and from the wound highlighting that the reverse migration is an active process and not due to random mobility. Elks *et al*. were later able to show that a delay in reverse migration contributes to delayed inflammation resolution in response to hypoxia, previously thought to result only from reduced PMN apoptosis (Elks et al. 2011). Evidence for the existence of retrograde chemotaxis in humans has been generated by Buckley *et al*., who have shown that about 0.25 % of PMN from healthy

donors and 1-2 % of PMN in patients with systemic inflammation exhibited a reverse transmigration PMN phenotype as determined by a distinct profile of cell-surface receptors generated from *in vitro* data (Buckley et al. 2006).

1.5 PMN in disease

1.5.1 Inflammatory disease

PMN form part of the first line of defence against invading pathogens and as such do not have the ability to differentiate between 'self' and 'non-self'. Their non-specificity and powerful toxic defences can therefore cause considerable damage to the surrounding normal tissue. Persistence of PMN can result in increased damage to the host tissue and impair the wound healing. Delayed PMN apoptosis has been shown to result in exacerbated and prolonged inflammation (Gilroy et al. 2004). This can have severe pathological consequences.

Delayed PMN apoptosis has been identified as a component of many diseases. The inappropriate suppression of apoptosis has been shown to correlate with the disease severity and outcome. In patients with acute respiratory distress syndrome (ARDS), reduced PMN apoptosis is thought to be mediated by enhanced GM-CSF production (Matute-Bello et al. 1997). This is also the mechanism implicated in supressing PMN apoptosis in sepsis and acute coronary artery disease. Persistent pulmonary neutrophilia, as detected in bronchoalveolar lavage (BAL) fluid from neonates with respiratory distress syndrome, has been shown to be associated with the development of chronic lung disease in adolescence (Kotecha et al. 2003).

COPD is one of the leading causes of death in the world. The main causative factor is cigarette smoke (Franklin et al. 1956). The disease is characterised by persistent local and systemic inflammation, which result in impaired lung function and ultimately lung failure. The PMN is the most

abundant cell type situated in the bronchial wall and lumen of COPD patients (Martin et al. 1985; Pesci et al. 1998). There are also enhanced levels of primed circulating PMN (Koenderman et al. 2000; Oudijk et al. 2006). Although the mechanisms underpinning dysregulated neutrophil function in COPD patients are not fully know, a reported delay in PMN apoptosis in COPD patients may be due to enhanced activation of NF-κB (Brown et al. 2009).

Supressed PMN apoptosis is also known to play a role in the destruction of cartilage and bone in rheumatoid arthritis (Mohr et al. 1981). This occurs in the synovial fluid of rheumatoid arthritis patients where PMN are the most abundant inflammatory cells, along with higher levels of lactoferrin, an iron chelating glycoprotein present in the secondary granules of PMN (Furmanski & Li 1990; Wong et al. 2009). It was later shown that lactoferrin itself acts as a PMN survival factor in rheumatoid arthritis and may be responsible for the extended PMN survival in the rheumatoid joint (Wong et al. 2009).

1.5.2 Accelerated PMN apoptosis

Transient increase in PMN survival during infection is essential for the optimal elimination of pathogens. Accelerated PMN death therefore, can result in impaired anti-microbial function and recurrent infections. Severe congenital neutropenia is a type of immunodeficiency characterised by severe neutropenia with absolute PMN counts below 0.5 x 10^9/l (Haddy et al. 1999). The disease is associated with recurrent systemic bacterial infections due to an insufficient number of circulating PMN. These disorders result mostly from genetic defects in genes such as PMN elastase (ELA2), growth factor independent transcription repressor (GFI1), glucose-6-phosphatase 3 (G6PC3) and HCLS-(hematopoietic cell-specific Lyn substrate 1) associated protein X1 (HAX1) (Klein et al. 2007; Boztug et al. 2009; Boztug & Klein 2011). Some pathogens can also shorten PMN lifespan through their ability to accelerate PMN apoptosis in order to impair PMN-mediated defences

(Colamussi et al. 1999; Allen et al. 2005; Elbim et al. 2009). For example, the cystic fibrosis pathogen *Pseudomonas aeruginosa* produces pyocyanin, which attenuates recruitment into the lung by causing increased PMN apoptosis and resulting in persistent colonisation (Allen et al. 2005).

1.6 Molecular mechanisms of apoptosis

The term 'apoptosis' was first coined by Kerr *et al*. to described active, inherent programmed cell death as an essential mechanism for tissue homeostasis and as a distinct process from necrotic cell death (Kerr et al. 1972). Apoptosis occurs in two distinct stages. In the first stage the nucleus and the cytoplasm condense leading to cell fragmentation, but with plasma membranes still preserved. During this phase chromatin condensation and nuclear fragmentation occur. These morphological changes define apoptosis (Kroemer et al. 2005). In the second stage, the apoptotic bodies formed are rapidly engulfed by resident phagocytic cells preventing the release of cellular contents into the surrounding area and without affecting the tissue function and architecture. The activation of precursor caspases is required for the manifestation of apoptotic features in both the intrinsic and extrinsic pathways (Fuentes-Prior & Salvesen 2004). Caspases are cysteine proteases that cleave after an aspartate residue (Yuan et al. 1993).

1.6.1 The extrinsic Apoptotic pathway

The extrinsic cell death pathway is initiated by extracellular signals and involves death receptor-mediated interactions (Locksley et al. 2001). Members of the tumour necrosis factor (TNF) cytokine family such as TNF-α and FasL can bind to their receptors on the PMN and induce apoptosis (Liles et al. 1996). Trimeric ligand binding to the transmembrane death receptors recruits adaptor proteins and engages signal transduction via cytoplasmic 'death domains' (Ashkenazi & Dixit 1998; Lavrik et al. 2003). For example, FasL and TNF- α binding to their corresponding receptors results in the

recruitment of adaptor proteins including Fas associated death domain (FADD) adaptor protein, which in turn associates with procaspase-8 (Kischkel et al. 1995). The protein complex formed is known as the death-inducing signalling complex (DISC). It results in the activation of caspase-8, which in turn cleaves caspase-3 which then go on to cleave hundreds of substrates in the cell including a DNAse, which degrades chromatin (Scaffidi et al. 1998)

1.6.2 Intrinsic (mitochondrial) apoptotic pathway

In most vertebrate cells, programmed cell death occurs through the intrinsic, or mitochondrial, pathway of apoptosis (Green & Kroemer 2004). During various forms of intracellular stress such as DNA damage, cytokine deprivation and viral infection the outer mitochondrial membrane becomes permeabilised (Hakem et al. 1998; Adams 2003). This results in the release of the mobile electron transporter cytochrome c (cyt c) into the cytoplasm and recruitment of the initiator caspase-9 via Apaf-1 (apoptosis protease activating factor) (Liu et al. 1996; Susin et al. 1996; Zou et al. 1997). This in turn leads to the formation of the apoptosome, a macromolecular complex in which precursor caspase-9 is activated due to allosteric change and dimerization. Once caspase-9 is activated, it cleaves executioner caspase-3 and -7 and in turn triggers the execution phase of apoptosis (Adams 2003).

Whether PMN contain fully functioning mitochondria is subject to controversy (Borregaard & Herlin 1982; Fossati et al. 2003). However, studies have shown that tubular networks, which form mitochondria, although limited in number, can be visualized in PMN (Bainton et al. 1971; Maianski et al. 2002; Fossati et al. 2003). Mitochondria of human PMN are unique in that they are thought to mainly play a role in apoptosis and are not involved in generating energy for the cell in the form of ATP (Maianski et al. 2004). Mitochondria also control apoptosis by acting as sensors of endogenous factors such as intracellular ions Ca^{2+} and K^{+} (van Raam et al. 2006; Giacomello et al. 2007).

Loss of mitochondrial membrane potential has been identified as an early marker of apoptosis (Fossati et al. 2003) and indeed maintenance of the mitochondrial membrane potential is essential in delaying apoptosis during infection (Taneja et al. 2004).

1.6.3 The regulation of the mitochondrial apoptotic pathway by the Bcl-2 protein family

Apoptosis of PMN and other cell types is controlled by a balance between pro- and anti-apoptotic members of the Bcl-2 (B cell lymphoma 2) family. These proteins regulate the integrity of the mitochondrial membrane (Adams & Cory 1998). By definition, each member of the Bcl-2 family contains at least one BH domain (Bcl-2 homology) out of four (BH1-4) (Zha et al. 1996). The formation of homo- and hetero-dimers between Bcl-2 family members is crucial for the fine control of the programmed cell death pathway (Zha et al. 1996; Adams & Cory 1998). The regulation of apoptosis by these proteins is complex and not well understood. There are two main subfamilies of Bcl-2 proteins: pro-apoptotic and anti-apoptotic proteins which although share BH domain sequences, are structurally and functionally distinct (Adams & Cory 1998).

1.6.3.1 Pro-apoptotic proteins

These Bcl-2 proteins promote apoptosis by using their BH3 domain to bind to anti-apoptotic proteins and inhibit their effects (Zha et al. 1996; Adams & Cory 1998). The first pro-apoptotic Bcl-2 protein member to be identified was alternatively spliced Bax (Bcl-2 associated x protein), which exists in a single membrane and two cytosolic forms (Oltvai et al. 1993). Bax was shown to bind to Bcl-2 and act as an antagonist of the protein. In an IL-3 (Interleukin 3) cytokine dependent cell line, overexpression of Bax was shown to result in accelerated apoptosis (Oltvai et al. 1993). Conversely, mice deficient in pro-apoptotic Bax and Bak (Bcl-2 associated antagonist/killer) were shown to be

unable to induce apoptosis when exposed to cell death stimuli and therefore are essential for this process to occur (Wei et al. 2001). These findings highlighted the requirement for the balance between pro- and anti- apoptotic Bcl-2 protein members in the control of cell fate.

Pro-apoptotic proteins act by utilising their BH3 α-helical region in order to bind into a cleft formed by the BH1, BH2 and BH3 domains of anti-apoptotic proteins (Zha et al. 1996; Adams & Cory 1998). The BH3 domain is essential for the pro-apoptotic function of the Bcl-2 family (Zha et al. 1996; Adams & Cory 1998). The proteins have been shown to function by causing the release of pro-death factors such as cyt c and Apaf-1 into the cytoplasm (Shimizu et al. 1999; Wei et al. 2000).

The BH3 only protein Bad (Bcl-2 associated agonist of cell death) is the dominant transcript in PMN but other pro-apoptotic proteins Bax, Bak and Bik (Bcl-2-interacting killer) have also been shown to be expressed (Moulding et al. 2001). A study on mice deficient in Bim (Bcl-2 like 11) demonstrated that granulocyte numbers were increased several fold as a result of extended cell survival in comparison to control mice (Bouillet et al. 1999). The pro-apoptotic Bcl-2 family members in PMN have been shown to be extremely stable with long half-lives emphasising the ability of PMN to rapidly undergo apoptosis (Moulding et al. 2001).

1.6.3.2 Anti-apoptotic proteins

The Bcl-2 anti-apoptotic proteins are essential for cell survival and bind to pro-apoptotic Bcl-2 members to inhibit their function (Adams & Cory 1998). These pro-survival proteins inhibit the release of pro-apoptotic factors such as cyt c and Apaf-1 from the mitochondria into the cytosol in order to prevent programmed cell death (Susin et al. 1996; Yang et al. 1997; Kluck et al. 1997). Although they have been shown to be functionally redundant as the overexpression of any of the members protects cells from apoptosis, genetic

studies have revealed the differential expression of the proteins in different cell types (Susin et al. 1996; Adams 2003).

The pro-survival Bcl-2 proteins utilise the BH1 and BH2 domains to bind pro-apoptotic Bcl-2 members (Yin et al. 1994). These domains are essential for their function and are also used in homodimerisation with a BH4 domain on the second molecule (Zha et al. 1996). It has been proposed that anti-apoptotic proteins also regulate the voltage dependent anion channel (VDAC) that in turn modulates mitochondrial membrane potential and the release of cyt c from the mitochondria (Shimizu et al. 1999).

The Bcl-2 protein was the first member to be identified in a t(14:18) chromosomal translocation where its overexpression in humans causes follicular lymphomas (Tsujimoto & Croce 1986). The protein is essential for the survival of mature lymphocytes (Veis et al. 1993; Hamasaki et al. 1998). The pro-survival proteins Bcl-x (Bcl-2 associated x protein) and Mcl-1 are both indispensable in embryonic development since mice deficient in Mcl-1 fail to implant whereas Bcl-x deficiency in mice results in an embryonic lethal phenotype (Motoyama et al. 1995; Rinkenberger et al. 2000). Conversely, the A1 protein is required for PMN survival (Veis et al. 1993; Hamasaki et al. 1998).

PMN express three anti-apoptotic proteins Mcl-1, A1 and Bcl-x but unlike other cell types they do not express Bcl-2 (Rinkenberger et al. 2000; Moulding et al. 2001). Mcl-1 and A1 are thought to be regulated at the protein stability level and have been shown to undergo rapid turnover in PMN (Moulding et al. 2001). Mcl-1 is the key anti-apoptotic protein in PMN with high levels of expression shown in freshly isolated PMN (Derouet et al. 2004). Its levels inversely correlate with the number of apoptotic PMN (Moulding et al. 1998). The more recently identified pro-survival protein, HAX1, has been shown to have weak homology to the anti-apoptotic Bcl-2

proteins (Suzuki et al. 1997). Its structure and function will be discussed in the following paragraphs.

1.7 HCLS-1 associated protein X1 (HAX1)

HAX1 was first identified as a novel 35 kDa protein interacting with HS1 (hematopoietic cell-specific Lyn substrate) in B lymphocytes (Suzuki et al. 1997). HS1 is a substrate of Src tyrosine kinases and is specifically expressed in cells of hematopoietic lineage. HAX1 binding to the amino terminal of the HS1 protein was thought to implicate HAX1 in B lymphoma cell signal transduction. Since its identification, it has been established that the HAX1 gene is ubiquitously expressed in human and murine tissues and the protein is primarily localized in the mitochondria and to a lesser extent in the endoplasmic reticulum and nuclear envelope (Suzuki et al. 1997; Hippe et al. 2006).

Importantly, autosomal recessive mutations of the HAX1 gene resulting in HAX1 deficiency cause Kostmann disease (severe congenital neutropenia), a condition characterized by impairment of myeloid differentiation and a lack of circulating PMN in the blood (Klein et al. 2007). This finding provides strong evidence for the function of HAX1 as a key modulator of myeloid cell survival and homeostasis. Therefore, further study into the role of HAX1 protein could enhance our understanding of this field.

1.7.1 *HAX1* genetic organization, transcription and conservation

The human genome contains two *HAX1* genes (Lees et al. 2008). The first is located on chromosome 1 (1q21.3) within the epidermal differentiation complex and the second is a processed pseudogene found on chromosome X (Xq28). The *HAX1* gene on chromosome 1 contains seven exons in total and has been shown to give rise to eight studied transcript variants through alternative splicing and intron retention (Lees et al. 2008). Most of the

alternative splicing in humans results from an internal splice site in exon 2, which generates transcripts without various regions of the exon. Lees *et al*. show that the mRNA sequence for *HAX1 006* contradicts a previously published sequence for the same isoform (Lees et al. 2008). This does not necessarily mean that one of the sequences is incorrect. It is likely that there are other *HAX1* isoforms, which are yet to be identified. Lees et al. who identified additional PCR products resulting from the retention of the introns also support this notion.

At least six of the isoforms out of the eight are transcribed in any one particular tissue with no significant differences in the patterns of expression between different cell types. Transcripts of *HAX1 001*, *HAX1 003, HAX1 005, HAX1 006* and *HAX1 008* were shown to be expressed in all cell types whereas the rest of the isoforms *HAX1 002, HAX1 004 and HAX1 007* are only expressed in certain cell types. The existence of these isoforms adds a level of regulation to HAX1 expression and also may account for the many different roles of HAX1, which is to be expected for a protein with numerous cellular functions.

The *HAX1* gene is highly conserved between human, mouse, rat, chimpanzee and macaque highlighting its essential function in the cells of these organisms (Jeyaraju et al. 2009). Similar sequences have also been found in the zebrafish, *Danio* rerio. The mouse *Hax1* cDNA shares 86 % identity with the human *HAX1* cDNA (Hippe et al. 2006). However, there are two *Hax1* genes in the mouse genome and they encode only three distinct variants of *Hax1*. Seven alternatively spliced *Hax1* variants have been identified in the rat up to date with similar splicing to that of the human gene (Grzybowska et al. 2006). Elevated levels of *Hax1* mRNA are seen in the liver, kidney and testis of mice and in the testis of rat (Grzybowska et al. 2006; Hippe et al. 2006). However in the human, mRNA levels are the highest in skeletal muscle (Lees et al. 2008).

HAX1 Isoform	Predicted protein size	Expression and roles
001	31.6 kDa	>Ubiquitously expressed >Mutations in the 5' region of exon 2 result in neutropenia only
002	28.6 kDa	Expressed in PBMCs, oral keratinocytes and some fibroblasts
003	14.2 kDa	Ubiquitously expressed
004	26.1 kDa	>Expressed in fibroblasts, oral keratinocytes and some PBMCs >Mutations in the 3' region of exon 2 result in neutropenia and neurological and neuropsychological abnormalities
005	32.4 kDa	Ubiquitously expressed
006	21.8 kDa	>Expressed in fibroblasts, PBMCs and some oral keratinocytes >Expressed in cell lines: breast carcinoma, colon adenocarcinoma and melanoma cell lines
007	10 kDa	Expressed in PBMCs, oral keratinocytes and some fibroblasts
008	7.5 kDa	Ubiquitously expressed

Table 1.1 Difference in the expression and mutation of HAX1 isoforms in human (Information extracted from Lees et al. 2008).

1.7.2 Molecular and physiological roles of HAX1 protein

1.7.2.1 Domain structure, function and cellular localisation

The human *HAX1* gene was first isolated from a B lymphoma cDNA library and cloned into yeast cells for use in a yeast two-hybrid system identifying the binding partners of hematopoietic lineage cell-specific protein 1 (HS1) (Suzuki et al. 1997). Suzuki *et al* described HAX1 as a hydrophilic protein with no significant homology to any other proteins. Fig. 1.1 shows the HAX1 putative domain organisation and some of its binding partners.

Some similarity was shown to Nip3, a protein, which interacts with adenovirus EIB 19-kDa protein and Bcl-2(Suzuki et al. 1997). A putative PEST sequence (aa 104-117) was also identified, which indicates that the protein can be rapidly degraded in a regulated manner. It was proposed that HAX1 contains two BH domains, BH1 (aa 37-56) and BH2 (aa 74-89) and a putative hydrophobic transmembrane domain (aa 261-271) at the C-terminus (Suzuki et al. 1997). Another feature of HAX1 is an acid box (amino acids 30-41) with unknown function, identified by analogy with the fibroblast growth factor receptor (Lees et al. 2008).

Although the existence of the BH domains is supported by some recent studies, contradictory reports have demonstrated that the proposed BH domains are not recognised even when using relaxed thresholds in conserved protein domain searches (Chao et al. 2008; Jeyaraju et al. 2009; Fadeel & Grzybowska 2009). In addition to this, the predicted secondary structures for these regions are highly disordered in HAX1 whereas the *bona fide* BH domains are well structured with hairpin motifs formed by hydrophobic α-helices (Jeyaraju et al. 2009). Furthermore, the putative BH domains of the HAX1 sequence are poorly conserved in mammals and no conservation of the sequence is found in distantly related species (Jeyaraju et al. 2009).

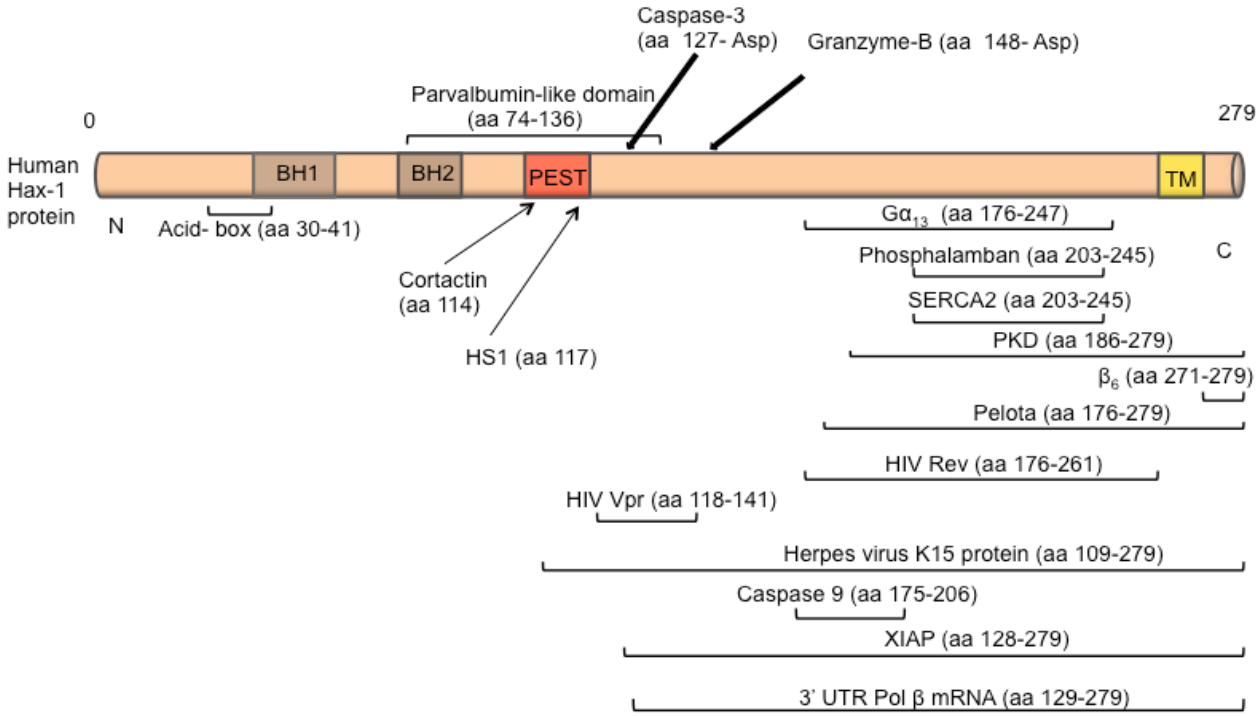

Figure 1.1 Domain structure organization of human HAX1 and sites of interaction with other proteins

The dominant human HAX1 isoform is composed of 297 amino acids (Suzuki et al. 1997). The locations of the two putative BH domains (BH1 and BH2), PEST sequence, putative transmembrane domain (TM) and acid-box are shown. Sites of interactions between HAX1 and other proteins identified to date are indicated. Caspase-3 and Granzyme-B cleavage sites on HAX1 are also indicated by the thick black arrows. Most of the interactions of HAX1 with other proteins occur at the C-terminus of the protein. The schematic figure draws information from numerous studies on the interactions and cleavage of HAX1 referenced throughout the text.

There is also some controversy as to whether HAX1 is an integral mitochondrial membrane protein or a peripherally associated one. Chao *et al* reported that HAX1 is localised on the inner and outer mitochondrial membrane with the protein exposed to the intermembrane space (Chao et al. 2008). However, other researchers disagree and have emphasised that the putative transmembrane domain does not contain enough hydrophobic amino acids in order to span the lipid bilayers (Jeyaraju et al. 2009; Fadeel & Grzybowska 2009). A long stretch of a minimum of 20 mostly hydrophobic residues is required to form an α-helix which is capable of spanning the lipid bilayers and no such region is found anywhere in the HAX1 sequence. Although HAX1 is selectively concentrated at the mitochondria, it has been shown that some HAX1 has also been detected in the nuclear envelope, sarcoplasmic and endoplasmic reticulum in different cell types of human and mouse models (Suzuki et al. 1997; Gallagher et al. 2000; Hippe et al. 2006; Zhao et al. 2009). This differential localisation is likely to reflect the different roles and binding partners of HAX1 in different cell types.

1.7.2.2 HAX1 putative binding sites for RNA

Regulated RNA metabolism is maintained through multiple specific and non-specific protein-RNA interactions. *In vitro* as well as *in vivo* studies in yeast, rat and HeLa cells have revealed that HAX1 binds to mRNA (Al-Maghrebi et al. 2002; Sarnowska et al. 2007). So far only two HAX1 binding targets have been identified. The first is a stem loop structure in the highly conserved 3' untranslated region (UTR) of the cytoskeletal protein vimentin involved in cell migration (Al-Maghrebi et al. 2002). The second HAX1 target was shown to be an evolutionary conserved hairpin motif at the UTR region of the mRNA encoding for DNA polymerase β (Sarnowska et al. 2007). HAX1 binding regions on DNA polymerase β and vimentin mRNA are not evolutionarily conserved and the protein products of their mRNAs are functionally and structurally distinct (Al-Maghrebi et al. 2002; Fadeel & Grzybowska 2009). It can therefore be speculated that HAX1 binding and regulation is different for each mRNA and that there may be many other HAX1 mRNA binding targets in the cell.

1.7.2.3 Regulation of cell migration by HAX1

Over the past few years, a number of studies have generated evidence linking HAX1 function to cell motility. Gallagher *et* al reported that HAX1 interacts with polycystic kidney disease protein 2 (PKD2) and showed that HAX1 co-localizes with this protein in the cell body as well as cellular processes and lamellipodia (Gallagher et al. 2000). In the same study, a link between PKD2 and the cytoskeleton was established by the finding that HAX1 interacts with cortactin, an HS1 protein family member and an F-actin associated protein expressed in most tissues except for lymphoid cells (Suzuki et al. 1997; Gallagher et al. 2000). In a second study, it was shown that HAX1 interacts with $G\alpha_{13}$, the α-subunit of the heterotrimeric G protein 13 involved in stimulating cell migration (Radhika et al. 2004). HAX1 forms a quaternary complex with $G\alpha_{13}$, Rac and cortactin where HAX1 is predicted to sequester $G\alpha_{13}$ from cell adhesion signalling pathways and tethering it to the cytoskeleton (Radhika et al. 2004). A

third study investigating the HAX1 involvement in cell migration reported HAX1 binding to the β_6 cytoplasmic tail of the integrin $\alpha_v\beta_6$, which regulates clathrin-mediated endocytosis of this integrin (Ramsay et al. 2007). Silencing of HAX1 with short interfering RNAs led to reduced $G\alpha_{13}$- and $\alpha_v\beta_6$- mediated cell migration in Gα13 expressing NIH3T3 cells and in oral squamous cell carcinoma cell lines, respectively (Radhika et al. 2004; Ramsay et al. 2007).

Phosphorylated growth factor receptor-bound protein 7 (Grb7), a cell migration protein has also been reported to interact with HAX1 in mammalian cells (Siamakpour-Reihani et al. 2010). Grb7 is an adaptor protein involved in cell migration and although it is known that it mediates signal transduction through a focal adhesion kinase pathway, its specific downstream binding partners are unknown. Overexpression of Grb7 has been shown to result in increased cell migration and the development of metastases (Tanaka et al. 1998). HAX1 also binds to the cytoskeletal protein Pelota (PELO), which is involved in cytoskeleton organization, cell growth and spreading (Burnicka-Turek et al. 2010). Cell migration is important in both the movement of PMN during inflammation and in metastatic cancers. HAX1 has been shown to be upregulated in a number of cancers (Ramsay et al. 2007). The above-mentioned studies in addition to the evidence for the HAX1/vimentin mRNA interaction provide a connection between HAX1 protein and signalling pathways of cell migration, however these studies do not present any mechanisms of specific HAX1 action and no such interactions have been described for PMN. Further study in this area may shed new light into how these mechanisms work.

1.7.2.4 Interactions with viral proteins

Viral protein function and their use to hijack and manipulate host cell proteins are slowly being revealed. Viruses utilise any means possible to manipulate host cell regulatory pathways in their favour. Studies into HAX1 interactions with virus-encoded proteins provide data on binding of

proteins from four different viruses. The first two viral proteins to be identified as HAX1 binding partners were EBNA-LP (Epstein-Barr virus nuclear antigen leader protein) and EBNA5 (Epstein-Barr virus nuclear antigen 5) (Kawaguchi et al. 2000; Dufva et al. 2001). Both of these proteins had previously been thought of as nuclear proteins involved in B-cell immortalization but the interaction with HAX1 suggested a function for these proteins in the cytoplasm. K15 protein of Kaposi's sarcoma-associated herpes virus or herpes virus 8 is another protein shown to bind to HAX1 (Sharp et al. 2002). Infection of HeLa cells with K15 did not have any effects on the HAX1 blocking of Bax-induced apoptosis indicating that HAX1 may act in a Bax-independent fashion. Human immunodeficiency virus (HIV) type 1 viral protein R (Vpr) has also been reported to bind to HAX1 and dislocate it from the mitochondrial membrane, resulting in membrane permeability and apoptosis. HAX1 also binds to a second HIV protein, Rev, delocalising the viral protein from the nucleus into the cytoplasm (Modem & Reddy 2008). HAX1 overexpression was shown to unexpectedly inhibit Rev function by preventing RNA binding.

The last protein identified so far to bind to HAX1 is the Hepatitis C virus (HCV) core protein (Banerjee et al. 2009). In the same study, HAX1 presence was shown to increase tumour suppressor gene p53 expression upon anticancer drug treatment of HepG2 cells. It is unknown why or how this occurs but it suggests a further link for HAX1 to cell cycle check points.

Many pathogens hijack and modulate host cell apoptosis pathways to their own benefit. The virus-encoded proteins known to bind to HAX1 *in vitro* as well as *in vivo* are mostly involved in suppressing apoptosis in order for efficient viral replication to occur. It may therefore be reasonable to assume that these proteins utilize HAX1 as a strategy of ambushing the apoptotic machinery. However, a direct biological significance of HAX1 interactions with the virus-encoded proteins is yet to be revealed.

1.7.2.5 HAX1 involvement in cell fate

The weak homology and similar cellular distribution of HAX1 to Bcl-2 proteins led Suzuki *et al* to hypothesize that HAX1 plays a role in promoting cell survival by interacting with proteins distributed in the mitochondria region (Suzuki et al. 1997). Their preliminary data showed that overexpressed HAX1 protected the T-lymphoma cell line, Jurkat from apoptosis in response to apoptosis inducing stimuli. Subsequent studies have supported this hypothesis (Sharp et al. 2002; Li et al. 2009; Jitkaew et al. 2009). Consistent with these findings, HAX1 silencing by siRNA caused human melanoma A375 cells to undergo apoptosis (Li et al. 2009). HAX1 knockout mutations in mice are lethal, with failure of mice to survive longer than 14 post-natal weeks (Chao et al. 2008). This is because of a failure to eat or drink due to loss of motor coordination and activity. In addition, extensive apoptosis of neurons and lymphocytes occurs.

HAX1 downregulation occurs in response to apoptosis signals and it is thought to trigger the induction of caspase-dependent apoptosis in immortalised human B cell lines (Jitkaew et al. 2009). HAX1 overexpression was also shown to reduce Bax-mediated apoptosis to background levels in HeLa cells (Sharp et al. 2002). HAX1 overexpression has been reported in several tumours including in breast cancer, lung cancer and melanoma (Trebinska et al. 2010). These findings support a role for HAX1 in the inhibition of apoptosis and the involvement of this protein in carcinogenesis.

1.7.2.6 Interactions with factors involved in the apoptotic pathway

As described earlier in the text, loss of mitochondrial membrane potential leads to the release of protein factors such as cyt c and the serine protease HtrA2 (Omi) from the intermembrane space into the cytosol. This results in the activation of caspase-9, which in turn activates caspase-3. HAX1 has been shown to interact with Omi, a mitochondrial serine protease that translocates to the cytosol and cleaves inhibitor of

apoptosis proteins (Verhagen et al. 2002), caspase-9 and caspase-3 (Cilenti et al. 2004; Han et al. 2006; Chao et al. 2008). *In vitro* and in vivo studies have shown that HAX1 is also a target of Omi (Cilenti et al. 2004). The degradation of HAX1 occurs early in the apoptotic process, while Omi is still localized to the mitochondria (Cilenti et al. 2004). However, detailed information on the HAX1 cleavage products is not provided.

In a subsequent study, inhibition of apoptosis in lymphocytes was shown to require interactions of HAX1 with the mitochondrial proteases Parl (presenilin- associated, rhomboid-like) and Omi (Chao et al. 2008). The authors of this study proposed a model in which HAX1 binding to Parl led to the presentation and cleavage of Omi by Parl. Mature Omi prevents the accumulation of pro-apoptotic Bax. It was suggested that reduced levels of processed Omi in HAX1 knockout mice and the similarity of the phenotypes of HAX1 and Omi deficient mice provide some proof for this mechanism (Jones et al. 2003). However, an article by Jeyaraju *et al* claims that the interaction of HAX1 to Parl is an *in vitro* artefact (Jeyaraju et al. 2009). The authors also argue that the two proteins are confined to distinct cellular compartments and that Parl does not require presentation of proteins by HAX1. In support of this, HAX1 deficiency does not completely abolish the expression of mature Omi (Chao et al. 2008). The proposed actions of HAX1 implicated in the regulation of programmed cell death are illustrated in Fig. 1.2.

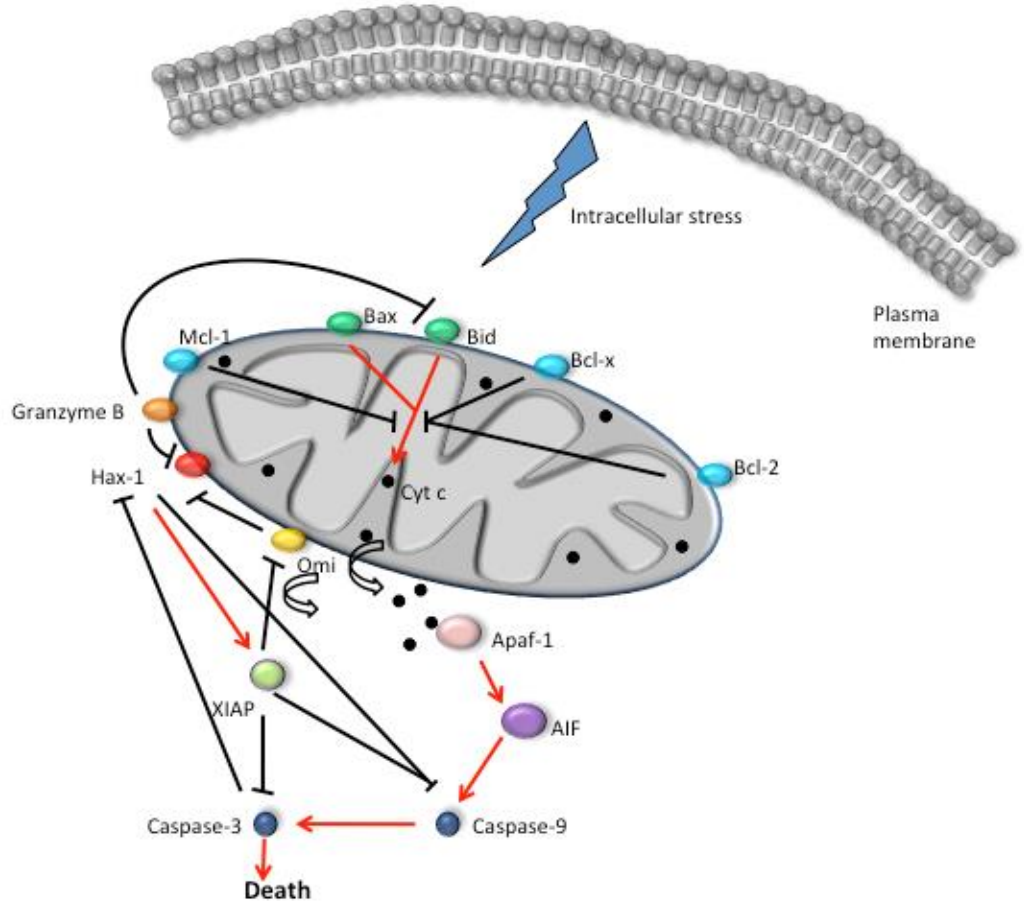

Figure 1.2 HAX1 involvement in the apoptotic pathway

A simplified diagram of the mitochondrial apoptotic pathway and the role of HAX1 in this process. HAX1 binds to and is cleaved by factors involved in apoptotic signalling. It binds to pro-survival proteins enhancing their activity and preventing the activation of the caspases. Intracellular stress leads to the inhibition of anti-apoptotic proteins such as Bcl-2 and Bcl-x by the pro-apoptotic Bcl-2 proteins (Adams 2003). This causes the release of several apoptotic factors into the cytoplasm including cyt c, AIF (apoptosis inducing factor) and Omi (Liu et al. 1996; Kluck et al. 1997; Yamaguchi et al. 2003) and this results in the activation of Apaf-1 (apoptosis protease activating factor) (Zou et al. 1997). In turn, Apaf-1 activates the caspase cascade, which ultimately leads to cell death (Zou et al. 1997). Omi and caspase 3 cleave HAX1 abolishing its pro-survival effects (Cilenti et al. 2004; Lee et al. 2008). Information from different studies has been drawn for this figure and is referenced in the text.

HAX1 has been identified as a binding target of caspase-9 in cardiac myocytes (Han et al. 2006). Overexpression of HAX1 inhibited caspase-9 activation while silencing of the *HAX1* gene using siRNA resulted in significant apoptosis of adult cardiac myocytes. In a separate study, suppression of *HAX1* by siRNA in HepG2 cells did not have any effect on caspase-9 processing upon induction of apoptosis, suggesting cell-specific roles of *HAX1*. A study by Lee *et al* identified the association of HAX1 with caspase-3 (Lee et al. 2008). Caspase-3 cleaves HAX1 *in vitro* at Asp 127, which is found in the N-terminal region of the protein. As both caspase-9 and -3 are cytoplasmic proteins it becomes difficult to understand how these interactions occur when the interacting proteins are confined to different cellular compartments. Han *et al* suggested that the HAX1/caspase-9 interaction in cardiac myocytes occurs at the mitochondrial membrane as a result of some translocation of caspase-9 to the mitochondria (Han et al. 2006).

Two recent studies have reported HAX1 binding to XIAP (X-linked inhibitor of apoptosis protein) and granzyme B (Han et al. 2010; Kang et al. 2010). XIAP inhibits apoptosis by preventing the activation of caspases (Srinivasula & Ashwell 2008). The interaction of HAX1 with this protein is believed to inhibit apoptosis by suppressing the polyubiquitinylation of XIAP therefore enhancing the stability of the protein and preventing it from proteosomal degradation. XIAP deficient mice fail to produce a distinct phenotype indicating that the HAX1 interaction may not be essential for inhibition of apoptosis by HAX1. This could also be explained by the possible existence of a compensatory mechanism from other IAPs in the cell suggesting that other IAPs may also be acting by interacting with HAX1 (Harlin et al. 2001). Granzyme B is the second serine protease to cleave HAX1. The protein also cleaves Bid (BH3 interacting domain death agonist) into tBid therefore directly activating downstream apoptotic proteins resulting in the loss of the mitochondrial membrane potential.

1.7.3 Roles of HAX1 in PMN

1.7.3.1 Involvement of HAX1 in Ca2+ signalling

Changes in calcium concentration in the cell are an important determinant of apoptosis (Giacomello et al. 2007). HAX1 has been reported to interact with key regulators of Ca^{2+} homeostasis (Vafiadaki et al. 2007; Vafiadaki * et al. 2009; Vafiadaki et al. 2009). Phosphalamban (PLN) and the sarco(endo)plasmic reticulum (SR) Ca^{2+} transport ATPase (SERCA2) are such proteins which bind HAX1 (Vafiadaki et al. 2007; Vafiadaki * et al. 2009). The protective effects of HAX1 increased in the presence of PLN whereas overexpression of SERCA2 abolished these effects in response to hypoxia-induced cell death. HAX1 overexpression has been shown to reduce SERCA2 pump activity in cardiomyocytes and led to reduced calcium cycling and contractility (Zhao et al. 2009). In a recent study, iterative similarity searches identified novel insect HAX1 homologs which are parvalbumin-like Ca^{2+} binding proteins (Kokoszynska et al. 2010). The findings suggest that there is a putative single EF-hand calcium binding protein in HAX1. These data further support a role for HAX1 in Ca^{2+} homeostasis and cell survival. This is particularly interesting because calcium homeostasis is an important factor in PMN apoptosis (Whyte, Hardwick, et al. 1993).

1.7.3.2 The importance of HAX1 in PMN apoptosis

As previously mentioned, HAX1 deficiency in humans has been shown to cause severe congenital neutropenia (SCN) (Klein et al. 2007). Further studies have shown that HAX1 isoform-dependent phenotypes may exist. Lees *et al* identified isoforms 001, 002 and 005 as the isoforms likely to be responsible for myeloid survival (Lees et al. 2008). Another study associated isoform 001 with severe congenital neutropenia whereas mutations in isoform 002 were linked to neurologic symptoms including neurodevelopmental delay and epilepsy (Germeshausen et al. 2008).

Hax1 SCN results from reduced levels of anti-apoptotic Bcl-2 proteins and extensive cyt-c release into the cytoplasm in bone marrow myeloid progenitor cells leading to premature apoptosis (Carlsson et al. 2004). Klein *et* al. isolated $CD34^+$ cells from patients with SCN, transduced them with vectors encoding *HAX1* and differentiated the cells *in vitro* to become myeloid precursor cells (Klein et al. 2007). These cells displayed significantly delayed loss of mitochondrial membrane potential in response to valinomycin when compared with cells transduced with a control marker gene and those from healthy individuals. Peripheral blood PMN from patients with SCN were also shown to undergo accelerated apoptosis compared to PMN from healthy donors. Consistent with these findings, PMN from SCN patients were shown to be associated with constitutive release of cyt c from mitochondria as well as defective Bcl-2 protein expression (Carlsson et al. 2004). The Klein *et al* study provides strong support for a unique role of HAX1 in PMN since although it is a ubiquitously expressed gene, it does not have the same effects leading to extensive apoptotic death in any other cell type.

There are a number of mechanisms by which HAX1 could regulate PMN numbers. As discussed earlier, the protein could be directly involved in modulating apoptosis through the maintenance of the mitochondrial membrane stability. Conversely, the protein may be involved in the GM-CSF signalling pathway, which is vital in the regulation of PMN production and differentiation. One could also speculate that HAX1 plays a role in the migration of the PMN out of the bone marrow and therefore, mutations of the gene result in persistence of the cells in the bone marrow leading to increased apoptosis.

1.8 Zebrafish as a model of PMN inflammation

Zebrafish (*Danio rerio*) have emerged as a good model organism due to their high fecundity, high stocking densities and optical clarity of the embryos and larvae (Lieschke & Currie 2007). Zebrafish embryo development is rapid with a functional heart and circulating blood cells developing within the first 30 hours post fertilisation (hpf) (Stainier et al. 1993). The transparent zebrafish larvae allow excellent visualization of fluorescent proteins in cellular processes (Renshaw et al. 2006). The generation of the *Tg(mpx::GFP)i114* (myeloperoxidase::green fluorescent protein) transgenic line has allowed visualisation of PMN through GFP expression under the PMN-specific myeloperoxidase promoter (Renshaw et al. 2006). This has meant that zebrafish can be used as an *in vivo* model for the genetic analyses of inflammatory responses.

Zebrafish PMN (sometimes called heterophils) are visible in the circulation 48 hours post fertilisation (hpf) (Lieschke et al. 2001). The cells are functionally orthologous to their human counterpart, in that they contain granules, are the first cell type to migrate towards the wound/infection site and phagocytose bacteria (Lieschke 2001; Colucci-Guyon et al. 2011). The zebrafish innate immune system exists in isolation from the adaptive immune system until approximately 4 weeks post fertilisation when the latter is established allowing segregation of pathways and molecular mechanisms involved in the two immune systems (Trede et al. 2004).

Using time-lapse imaging, zebrafish PMN have been shown to migrate to the wound site (sterile inflammation) (Mathias et al. 2006). During the resolution of the local inflammatory response the cells migrate back into the vasculature (Mathias et al. 2006; Colucci-Guyon et al. 2011). Direct in vivo quantitation of the tissue neutrophil lifespan has demonstrated that the resting PMN cell has a half-life of approximately 5 days (Dixon et al. 2012).

Many different tools and genomic resources have been established for use in the zebrafish in order to genetically manipulate the organism (Trede et al. 2004; Martin & Renshaw 2009). The genetic tractability of the organism has enabled the use of both forward-, through random ENU mutagenesis, and reverse-genetic approaches. Microinjection of morpholinos or mRNA (messenger ribonucleic acid) into the transparent larvae in the early stages of development can result in transient downregulation or overexpression, respectively (Hammerschmidt et al. 1999; Nasevicius & Ekker 2000). Alternatively, stable overexpression and knockdown can also be achieved through the use of cell-specific promoters and tol2 transposon system. Conversely, the recently established knockout technology using zinc finger (ZF) and transcription activator-like effector (TALE) nucleases can be utilised for selective gene knockout.

A further advantage of using zebrafish as model organisms is the high molecular and genetic similarity to humans (Eimon et al. 2006; Lieschke & Currie 2007). The zebrafish genome sequencing project has led to the annotation of most of the genome (http://www.sanger.ac.uk/resources/zebrafish/genomeproject.html). It has been shown that the zebrafish genome contains structural and functional homologs of most of the Bcl-2 protein family and caspases, which control the mitochondrial apoptotic pathway (Kratz et al. 2006). Morpholino oligonucleotides have been used to show that like the human, zebrafish innate immunity also involves the cytosolic adaptor protein MyD88 (myeloid differentiation factor 88), which has a central role in innate and adaptive immunity (Van Der Sar et al. 2006).

Progress has also been made in the study of monogenic disease affecting the PMN. For example, Deng *et al* developed models of Rac2 disease (Ras-related C3 botulinum toxin substrate 2) demonstrating defects in PMN migration and proliferation (Deng et al. 2011). In a second study using a WHIM (Warts, Hypogammaglobulinemia, Infections, and Myelokathexis) syndrome model where the G-protein-coupled chemokine

receptor CXCR4 was mutated, it was shown that zebrafish PMN are trapped in the bone marrow (Walters et al. 2010). These findings establish that zebrafish are a relevant model for studying programmed cell death and inflammation. In addition, further support comes from protein sequence analysis of human and zebrafish Hax-1, which shows that the two orthologues have evolved from a common ancestor (Fig. 1.3).

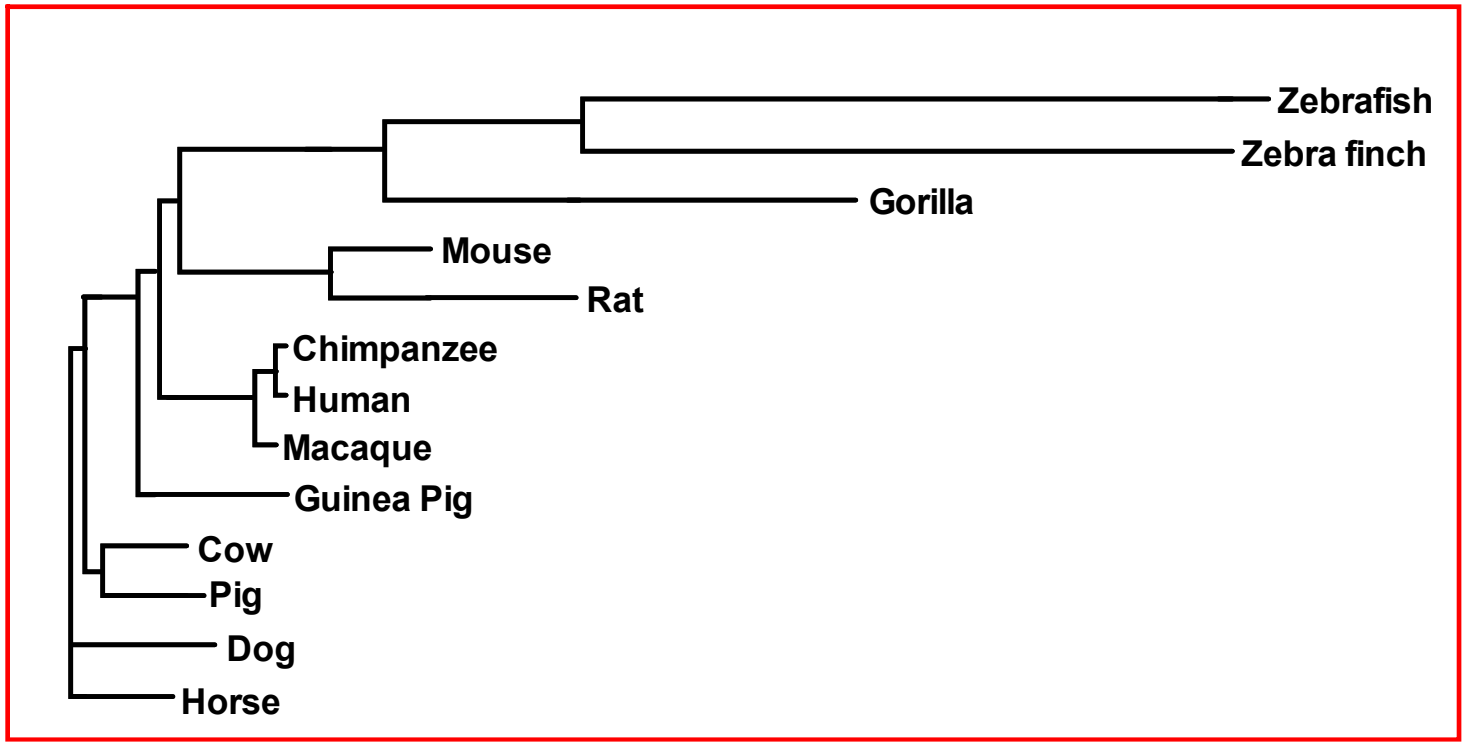

Figure 1.3 Evolution of the Hax-1 protein. ClustalW 2.1 Protein sequence alignment of Hax-1 from a number of different species in the form of a phylogenetic tree.

Zebrafish (Danio Rerio), Chimpanzee (Pan troglodytes), Cow (Bos taurus), Dog (Canis familiaris) Chromosome 7, Gorilla (Gorilla gorilla), Guinea Pig (Cavia porcellus), Horse(Equus caballus), Human (Homo sapiens), Macaque(Macaca mulatta), Mouse (Mus musculus), Pig(Sus scrofa), Rat(Rattus norvegicus), Zebra Finch(Taeniopygia guttata). The protein sequences were deduced from ENSEMBL.

1.9 Hypothesis, aims and Objectives:

The regulation of myeloid cell apoptosis is vital in both the control of inflammation and homeostasis. Persistence of PMN has been shown to be involved in the pathogenesis of numerous pulmonary diseases including COPD and acute respiratory distress syndrome. PMN have an exquisitely short half-life in the circulation due to constitutive apoptosis however, PMN longevity can increase several fold following migration into the tissue in response to injury or infection. PMN survival is dysregulated in inflammatory diseases, where PMN persist in the tissue and cause significant tissue damage. Currently, there are no effective therapeutic regimes that can effectively reduce PMN numbers in the tissue in order to resolve inflammatory disease. Further investigation into the mechanisms which regulate PMN apoptosis will lead to a better understanding of the molecular pathology of inflammatory diseases and may aid identification of new therapeutic targets.

HAX1 is a ubiquitously expressed gene with predominant localisation in the mitochondrial membrane. In a study by Klein et al it was shown that homozygous recessive mutations of the *HAX1* gene in the human result in Severe Congenital Neutropenia, a disease associated with premature apoptosis of bone marrow myeloid progenitor cells and a profound PMN deficiency. This suggests that HAX1 plays a pivotal role in PMN homeostasis and survival. The evidence generated thus far from other studies on HAX1 function infers that HAX1 is a very complex protein with a multitude of roles in multiple important cellular processes. These multiple roles of HAX1 in cellular processes make it an important target for further research. Although it is not clear how HAX1 functions in apoptosis and survival of cells, there is strong evidence emphasizing its importance in PMN and pathology. Therefore, our aim is to increase our understanding of the roles of HAX1 in myeloid cells, specifically PMN, in order to gain a better understanding of how PMN survival is controlled, with an overall aim of improving therapeutic strategies for PMN

inflammatory diseases. I hypothesise that HAX1 plays a critical role in PMN survival and homeostasis. More specifically I hypothesise that:

a.) HAX1 expression is modulated during induced and constitutive cell death

b.) HAX1 deficient zebrafish will have defective PMN development and survival

The main objectives of this thesis are:

a.) To determine the expression and regulation of HAX1 in primary neutrophils and PMN-like cell line PLB-985

b.) To define the effects of HAX1 knockdown on the mitochondrial stability of myeloid cells using flow cytometry

c.) To establish *in vivo* models of zebrafish Hax1 deficiency using morpholino, ZFN and TALEN technology and investigate the effects on PMN development and survival.

A range of techniques will be utilised in order to establish the role of HAX1 in myeloid cells using *in vitro* and *in vivo* models. My aim is to modify the techniques already in use in order to create a working model for studying HAX1 function in the zebrafish. Western blotting and RT-PCR will be used in order to identify HAX1 expression patterns during resting and stimulation of cells. HAX1 function will also be investigated in PLB-985 cells (myeloid leukaemia cell line) through knockdown studies using HAX1 siRNA technology. In order to study the effects of loss of Hax1 in zebrafish embryos, a *hax1* splice morpholino will be used to knockdown *hax1* mRNA expression. *hax1* knockout will be attempted using both CoDa (context-dependent assembly) zinc finger nuclease and TALEN (transcription activator like effector nuclease) mutagenesis approaches in order to study the effects of *hax1* gene mutation and loss of Hax1 function in the zebrafish.

2 Materials and Methods

2.1 In-vitro techniques

2.1.1 Reagents

Reagents used were purchased from Sigma-Aldrich, Poole, UK unless otherwise stated. qVD-OPh was purchased from R&D Systems, Abingdon, UK. GM-CSF was purchased from PeproTech, London, UK. Pyocyanin was prepared by Dr Lynne Prince (Usher et al. 2002), heat killed *E. coli* and heat killed *S. aureus* (SH1000, obtained from Professor Simon Foster (Dept. of Molecular Biology and Biotechnology, University of Sheffield, Sheffield, UK) were prepared from overnight cultures which were heat-treated for 10 min at 100 °C. All restriction enzymes and buffers were from NEB, (Biolabs, Hertfordshire, England) unless otherwise stated. The ON-TARGETplus Cyclophilin B (Cyc B) control siRNA (D-001820-01, human NM_000942) and the *HAX-1* ON-TARGETplus SMARTpool siRNA (L-012168-01-0005, human *HAX1*, NM_001018837) were from Thermo Fisher Scientific, Lafayette. CO, USA.

2.1.2 Mammalian cell culture

Adult PMN (polymorphonuclear neutrophils) were harvested from peripheral venous blood of healthy volunteers (under the approval of South Sheffield Regional Ethics Committee) using either an Optiprep™ (Axis-Shield, Upton, Huntingdon, UK) or Percoll® (Sigma-Aldrich, Poole, UK) gradient.

2.1.3 Leukocyte isolation and purification

4.4 ml of the anti-coagulant, trisodium citrate (3.8 %) from single use sterile ampulets (Martindale Pharmaceuticals, Essex, UK) were added per 35.6 ml of blood. In order to separate the blood cells from the blood plasma and platelets, the lid was covered in parafilm and the tube spun at 350 g for 20 min at room temperature (RT). Once spun, the upper platelet-rich plasma layer (PRP- upper phase) was harvested gently,

taking care not to disturb the interface. The upper platelet-rich plasma was then spun for 20 min at 800g to pellet the platelets leaving the platelet-poor plasma (PPP) supernatant. The PPP was then transferred to a fresh tube.

2.1.3.1 Dextran sedimentation

6 ml of 6 % dextran T-500 (3g dextran powder in 50ml 0.9% saline, Sigma-Aldrich, Poole, UK) was added to the erythroid/cell-rich layer (lower interphase) and the volume was made up to 50 ml with sterile 0.9% saline and the tube was inverted to mix, avoiding formation of air bubbles. The lid was loosened and the cells were undisturbed for 20-30 min at RT to allow the sedimentation of the red blood cells to occur. Following dextran sedimentation the upper white cell layer was harvested carefully and spun at 320 g for 6 min. The supernatant was discarded and the leukocyte pellet was then subjected to either an Optiprep™ (Axis-Shield, Huntingdon, UK) or a Percoll ® gradient (Sigma-Aldrich, Poole, UK).

During the centrifugation of the leukocyte pellet, 1X Hanks Buffered Saline Solution (HBSS) was made fresh each time from 10X stock. For one tube of blood a total volume of 50 ml of 1X HBSS was made; 45 ml of Baxter Sterile Irrigation water (Baxter Healthcare Corp., Deerfield, Illinois, USA) were added to 5 ml of 10X HBSS. Three drops of Sodium Bicarbonate were added to adjust the pH to ~7.

2.1.3.2 Construction of the Optiprep™ gradient

The white cell soft pellet generated in section 2.1.3.1 was gently resuspended in 2 ml of 20% PPP in HBSS without Ca^{2+} and Mg^{2+} (GIBCO HBSS- from Life Technologies) and topped up to 6 ml. Optiprep™ (4 ml) was added to the cells to make the volume 10 ml. After gently inverting to mix, 10 ml of the 1.095 Optiprep™ layer (3 ml Optiprep™ + 8.036 ml of 20 % PPP in HBSS) was carefully overlaid over the 10 ml of the white cell layer followed by a further 10 ml of the 1.080

Optiprep™ (3 ml Optiprep + 10.435 ml of 20 % PPP in HBSS). The final layer was formed by the addition of 10 ml 20% PPP in HBSS. The gradient was centrifuged at 1978 g for 30 min at 20 °C without the brake. A single gradient was used to isolate PMN from up to 80 ml of blood.

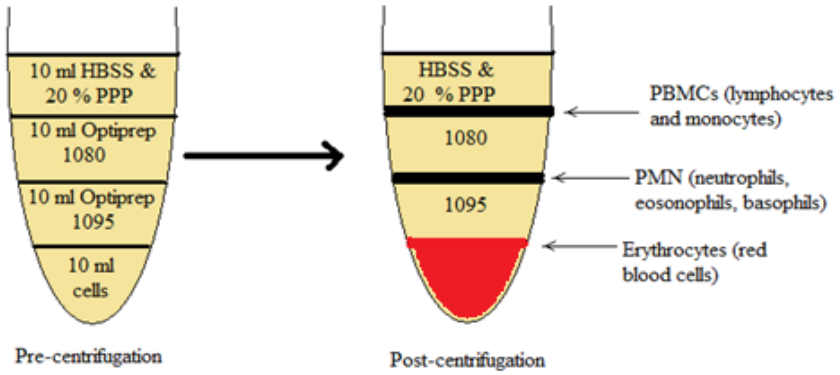

This yielded three populations of cells: the erythrocyte layer at the bottom of the tube, the PMN layer in the middle phase and PBMCs (peripheral blood mononuclear cells) in the upper phase.

2.1.3.3 Construction of the plasma-Percoll® gradient

The pelleted leukocytes from section 2.1.3.1 were resuspended in 1.5 ml of PPP. The Percoll® gradient solutions were prepared. The lower phase (51 %) was made up by adding 1.02 ml of 90 % Percoll® (1ml of 100 % Percoll was added to 9ml 0.9 % saline) and 0.98 ml PPP. The upper phase (42 % Percoll®) was made up by adding 0.84 ml of 90 % Percoll® to 1.116 ml of PPP. The lower phase (2ml total volume) was placed in the bottom of a 15 ml polystyrene centrifuge tube. A fresh sterile Pasteur pipette was then used to carefully overlay the upper phase on top, tilting the tube slightly whilst doing so. The white cell soft pellet generated in section 2.1.3.2 and resuspended in 1.5 ml PPP was then overlaid onto the upper phase. The gradient was subsequently spun at 320 g for 11 min without a brake at RT. A single gradient was used for isolation of PMN from up to 80 ml of blood. The centrifugation of the plasma-Percoll® gradient also yields three layers of cells with the erythrocytes residing at

the bottom of the tube, the PMN at the interphase between the 51% and 42% Percoll® layers and the PBMCs at the top of the 42% layer.

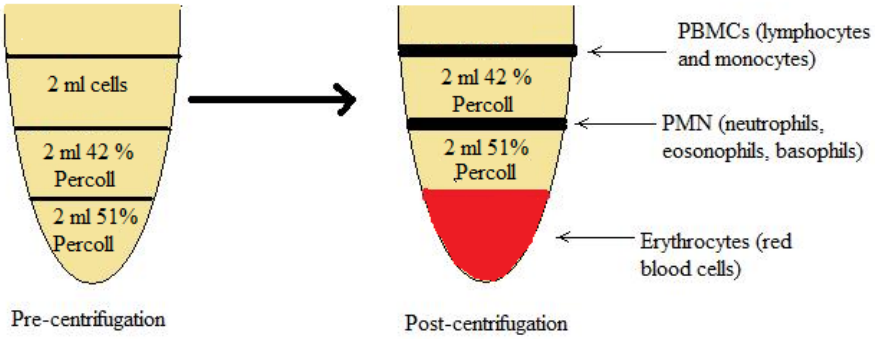

2.1.3.4 Harvesting the gradient

A Pasteur pipette was used to collect the cells from just above the interface avoiding any extra liquid from the gradient layers. The cell layers were transferred to fresh 50 ml falcon tubes and washed in HBSS (without Ca2+ and Mg2+) to remove any contaminating gradient material as follows. Each tube was made up to 40 ml with 20 % PPP in HBSS. A cell count was then carried out using a haemocytometer. The cells were then pelleted at 320 g for 6 min and either further purified as described in section 2.1.3.5 or resuspended in pre-warmed supplemented RPMI 1640 media.

2.1.3.5 Ultrapurification of PMN using a negative magnetic selection

In order to further purify the PMN and remove residual contaminating cells, the PMN layer from either purification method in sections 2.1.3.2 and 2.1.3.3 was subjected to a negative magnetic selection column using a custom antibody cocktail (Stem Cell Technologies, Meylan, France). Column buffer was prepared by adding 1 ml of FCS to 49 ml HBSS (without Ca^{2+} and Mg^{2+}). The cells were resuspended in column buffer at $1x10^8$ cells per ml of buffer. 65 µl of antibody cocktail (Sabroe et al. 2002) were added and the cells were incubated at RT for 15 min with occasional gentle swirling followed by a further 15 min incubation with

magnetic colloid beads added at 50 µl/1x10^8 cells (Stem Cell Technologies, Meylan, France). During this incubation a magnetic MACS® Separation (Miltenyi Biotec, Surrey, UK) column was pre-equilibrated with 10 ml column buffer. The cells were subsequently run through the column, which bound to the colloid beads attached to antibody with contaminating cells. Any remaining PMN in the column were washed off with an extra 10 ml column buffer. The ultrapure PMN were then counted using a haemocytometer, spun and resuspended in RPMI 1640 media.

2.1.4 Cytospin analysis of PMN purity and death

To determine the purity and assess PLB-985 and PMN apoptosis morphologically, 50-100 µl of cells at 5x10^6/ml were cytocentrifuged onto microscope slides and visualised by light microscopy. Duplicate cytospins slides were prepared for each treatment. Cells were added to chambers and spun at 300g for 3 min (Shandon Cytspin 3, Thermo Scientific, Hemel Hempstead, UK). Cytospins slides were fixed with 100 % methanol and stained with Quick- Diff stains (Gentaur, London, UK). The slides were mounted with DPX (Fisher Scientific, Loughborough, UK) and covered with cover slips. The slides were observed under a Zeiss Axioplan microscope using the 100x oil immersion lens. PMN, PBMC and eosonophils were distinguished on the basis of their morphology and PMN apoptosis was assessed on the basis of characteristic morphological changes. Healthy PMN have multi-lobed nuclei and are round whereas apoptosing cells loose their nuclear morphology and shrink. A total count of 300 PMN or 100 of PLB-985 cells was recorded for each slide unless otherwise stated. A purity count was carried out on the untreated control at 0 h where a total of 600 cells were scored on the basis of cell type from the two slides.

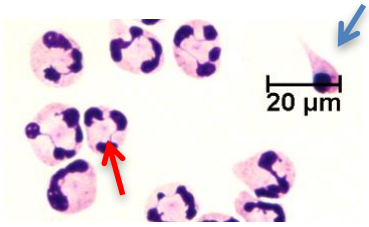

Figure 2.1 PMN Apoptosis

A micrograph of PMN cells from cytocentrifuge preparations. During apoptosis PMN shrink and undergo chromatin condensation. PMN were scored as healthy (red arrow) and apoptotic (blue arrow) based on morphological changes.

2.1.5 PLB-985 cell maintenance

PLB-985 cells - human acute myeloid leukaemia cell line (from the German Collection of Microorganisms and Cell Cultures – DMSZ) were grown in 1640 RPMI medium containing 10% FBS (Autogen Bioclear, Wiltshire, UK) and 100 U/ml Penicillin and 100 U/ml Streptomycin (Pen/Strep) at 37℃ in a humidified atmosphere of 5 % CO_2 in tissue culture incubator (Sanyo, Loughborough, UK). PLB-985 cells were maintained between $2x10^5$ cells/ml to $2x10^6$ cells /ml of media. Cells were grown in 75 cm^2 culture flasks until they reached 80% confluence and then passaged. To induce differentiation to a PMN-like morphology, cells were cultured in medium supplemented with various reagents at 3 x 10^5 cells per ml for a number of days.

2.1.6 Mycoplasma testing of PLB-985

Mycoplasma tests were carried out by the department lead technician on the cell culture medium on a monthly basis using EZ-PCR mycoplasma test kit, which uses mycoplasma specific primers to detect DNA by PCR (Geneflow, Staffordshire, UK). Tests were carried out according to manufacturer's instructions.

2.1.7 PLB-985 differentiation into PMN-like cells

PLB-985 cells were seeded at 0.5 x 10^6 cells/ml one day prior to transfer into differentiation media. The next day the cells were pelleted at 200 g for 2 min and re-suspended in differentiation media at 0.3 x 10^6. The cells were in the log phase of growth at this stage. The differentiation stimuli tested were: 0.5 µM Retinoic Acid (RA), 0.75 µM RA, 1 µM RA, 1 µM RA and DMF (dimethylformamide), 1 µM RA and 1.25 % (v/v) DMSO (dimethyl sulfoxide) and 1.25 % DMSO. The cells were incubated in 24 well plates in a total of 1 ml volume per well for 5 days at 37℃ in a humidified atmosphere of 5 % CO_2 in tissue culture incubator (Sanyo, Loughborough, UK). Two cytocentrifuge slides were prepared on each day. A cell count was carried out using a haemocytometer and 1x10^6 cells were lysed for protein on day1 -5 of the differentiation process as described in section 2.1.10.1.

2.1.8 Transfection of PLB-985 cells

PLB-985 cells were seeded at 4 x 10^5 cells/ml one day prior to the transfection to ensure cells were equilibrated. The cells were transfected using the Nucleofector V system from Amaxa Biosystems according to manufacturer's manual. Briefly, after centrifugation at 300 g for 3 min, 4 x 10^6 cells were gently resuspended in 100 µl of nucleofection solution containing 3 µg of siRNA and transfections were performed with the program C-023. The siRNA target sites are shown in Fig. 2.2. Immediately following transfection, the PLB-985 cells were transferred to RPMI 1640 media at a final concentration of 3 x 10^5. The cells were incubated at 37℃ with 5 % CO_2 for 10 or 24 h. At 10 h or 24 h after transfection, the cells were harvested and either lysed for RNA (described in section 2.1.15), protein extraction (section 2.1.10.1) or processed for flow cytometry (section 2.1.9). Cytospins of the cells were prepared at each time-point in order to assess cell death.

Figure 2.2 Identification of human *HAX1* siRNA target sites

The *HAX1* ON-TARGETplus SMARTpool siRNA (L-012168-01-0005, human *HAX1*, NM_001018837) used for the gene knockdown in the PLB-985 cell line targets four different sites of the mRNA. *HAX1 001* sequence is shown with alternating exons displayed in upper- and lowercase. The siRNA target sites found on exon 2 (red, pink) exon 3 (blue) and exon 7 (yellow) are highlighted.

2.1.9 Detection of changes in mitochondrial inner transmembrane potential (Δψm) in PLB-985 cells

A distinctive feature of early-programmed cell death is mitochondrial membrane instability resulting in commitment of cells to undergoing apoptosis. Changes in mitochondrial membrane potential were detected using a 5,5′, 6,6′-tetrachloro-1, 1′, 3,3′ tetraethylbenzimidazolo-carbocyanine iodide (JC-1; Sigma-Aldrich). Two x 10^6 PLB-985 cells from each control, mock (nucleofection solution only) or *HAX1* siRNA transfected conditions were pelleted and resuspended in complete RPMI media at 1 x 10^6/ ml. The cells were transferred to a 24 well plate at 1 x 10^6 cells per well. Cells were treated with valinomycin [3 or 5 µM] for 3 h in order to induce the collapse of mitochondrial membrane potential of these cells. Cells were then pelleted and resuspended in 300 µl of RPMI 1640 media without serum and antibiotics containing 10 µM JC-1 dye. An unstained untreated PLB-985 cell control was also prepared by resuspension in just the serum- and antibiotic-free media. The samples were left to stain for 15 min at 37 °C. This was followed by washing in 1ml PBS and resuspension in 300 µl of PBS. The samples were kept on ice until analysed by flow cytometry. Loss of Δψm was demonstrated by a gain of fluorescence on the FL-1 channel of a FACS Calibur flow cytometer (BD Biosciences - Pharmingen). At least 10000 cells were analysed for each experimental condition. Analyses of data was carried out by the flow cytometry analysis software FloJo (software version 9.3.2 (Tree Star, Inc.).

2.1.10 Protein extraction

2.1.10.1 Preparation of whole cell lysates

PLB-985 and PMN cells from section 2.1.3 were washed with ice-cold Dulbecco A PBS (Oxoid, Hampshire, England). The cells were then lysed in 10 µl of PI cocktail (protease inhibitor), PMSF (phenylmethylsulfonyl fluoride) and DFP (Diisopropyl fluorophosphate) containing water (see below) per 10^6 cells. The sample was vortexed vigorously and an

equivalent volume of hot SDS-PAGE loading buffer (Appendix 7.1.1) was added. The sample was boiled for ~5 min and stored at -80°C until required.

PI, PMSF and DFP containing water (500 µl)	Volume (*µl*)
PMSF (100mM)	5
DFP (100mM)	5
PI (Roche Complete protease inhibitor cocktail (Roche Applied Science, Lewes, UK) dissolved in 1.5 dH_2O)	20
dH_2O	470

2.1.11 Western Blotting

Protein extracts from Section 2.1.10.1 were analysed by western blotting. The samples were first subjected to SDS-PAGE gel electrophoresis using either a 12 or 15 % SDS-PAGE resolving gel. The proteins were then wet transferred to Immobilon-P 0.45 µM PVDF (Polyvinylidene fluoride) transfer membrane (Merck Millipore, Billerica, MA). The membrane was then immunostained with a primary antibody against the preferred protein. This was followed with immunostaining with a secondary antibody conjugated to horseradish peroxidase (HRP). The proteins were visualised using the EZ-ECL enhanced chemiluminescence detection kit for HRP (Geneflow, UK).

2.1.11.1 SDS-PAGE Electrophoresis

The gel running apparatus (Protean 2 gel assembly, Bio-Rad, Berkeley, CA) was wiped clean and assembled. Acrylamide gels were made by mixing the reagents listed in Appendix 7.1.2. APS (Ammonium persulfate) and TEMED (Tetramethylethylenediamine) were added just before the gel was ready to be poured. The gel was overlaid with 100 % isopropanol in order to remove any air bubbles. Once the gel had set, the isopropanol was washed off with distilled water. Stacking gels were made by adding together the reagents listed in Appendix 7.1.3. Combs were inserted to form wells and the gels were left to set for ~15 min. Once the gels had set, the gel apparatus was dismantled and the gels were transferred to

gel tanks. The gels were immersed in running buffer (Appendix 7.1.4) and the combs were carefully removed. Whole cell lysates were loaded into individual lanes alongside 15 µl of ColorPlus Prestained Protein Ladder, Broad Range (10-230 kDa) (New England Biolabs, UK) to allow sizing of the proteins. The gels were run at 120-180 volts using a PowerPac 300 from BioRad until the blue dye reached the gel front. The gel was removed from the gel apparatus carefully using flat- end tweezers and immersed in 1X transfer buffer (Table 5) for ~ 5 min.

2.1.11.2 Wet protein transfer

Proteins were transferred using the Geneflow wet transfer Kit. PVDF membrane was immersed in 100 % methanol for ~ 5 min in order to activate the membrane. It was then transferred to transfer buffer (1X) (Appendix 7.1.5). In a plastic tray containing 1X transfer buffer, two transfer buffer soaked fibre pads were placed on the black side of the gel holder cassette. One piece of filter card was then placed on top of this followed by the gel and the PVDF membrane on top. Any bubbles were removed using tweezers and gloved hands. The second piece of filter card was then placed on top of the PVDF membrane followed by another two transfer buffer soaked fibre pads. Lastly, the cassette was closed using the red side of the cassette. The gel holder cassette was then placed in the buffer tank and the transfer was run at 100 V for 70 min. Ponceau S (0.1 % w/v in 5 % acetic acid) staining was used to assess the protein transfer and the protein loading. 1X TBS (Tris Buffered Saline) buffer (Appendix 7.1.6) was used to wash off the stain. The membrane was then blocked with blocking buffer for 1 ½ – 3 h (depending on antibody used) at RT.

Blocking Buffer (5% Marvel non-fat milk powder in TBS Tween (Appendix 7.1.7):

1 g Marvel milk powder + 20 ml 1X TBS Tween (0.1% Tween-20)

2.1.11.3 Immunostaining of PVDF membrane

Blocked membranes were then transferred to a 50 ml Falcon tube containing diluted primary antibody in 4 ml of blocking buffer and incubated overnight at 4℃ on a rolling platform. Concentrations and dilutions of primary antibodies are listed in Appendix 7.2.1. After incubation with primary antibody, the membrane was washed with 1X TBS-Tween three times for 10 min each time on a shaker at RT. The membrane was then incubated with secondary antibody (Appendix 7.2.2) conjugated to HRP in 5 ml of blocking buffer on an orbital rotator for 1 h at RT. After incubation with secondary antibody, the membrane was washed again three times with 1X TBS-Tween for 10 min each time with shaking.

2.1.11.4 Chemiluminescent detection of immobilized proteins (Western blotting)

Detection of specific proteins on the immunoblot was carried out using the EZ-ECL Chemiluminescence Detection Kit according to the manufacturer's specifications. The membranes were exposed to a Hyperfilm™ chemiluminescence film (GE Healthcare Life Sciences, Uppsala, Sweden) in a Hypercassette™ (GE Healthcare Life Sciences, Uppsala, Sweden) The membranes were sealed in plastic film and stored at 4℃.

2.1.12 Stripping and re-immunostaining of western blot membranes

Stored membranes were blotted in water for 2 min. The membranes were then stripped in 0.2 M sodium hydroxide for 15 min on a shaker. This was followed by two 5 min washes with water and two 5 min washes with 1X TBS-Tween on a shaker. The membrane was blocked for 1 ½ - 3 h in blocking buffer. Immunostaining was carried out as described on section 2.1.11.3.

2.1.13 Western Blot Densitometry Analysis

Western blots were scanned and images saved in TIFF format. Bands were analysed using Image J (free software, Rasband, 1997) following online instructions (http://www.navbo.info/DensitometricAnalysysNIH image.pdf) and have been labeled as relative fold change from the untreated control. In occasions where relative band density was calculated, the band density is displayed as a percentage of the actin control band.

2.1.14 Total RNA (ribonucleic acid) extraction and assessment of RNA quality

Total RNA was extracted from ultrapure PMN (5-10 x 10^6 cells), PLB-985 (0.5-1 x10^6cells) cells and 10-100 zebrafish embryos using TRI reagent (Sigma-Aldrich, Gillingham, Dorset, United Kingdom) according to the protocol supplied by the manufacturer. 200 µl of TRI-reagent were used for 20 or less embryos and 1ml for more than 50 embryos and the embryos were forced through a needle to ensure full lysis. Total RNA was resuspended in 30 µl of sterile H_2O for injections. The RNA was quantified using a Nanodrop™ 1000 spectrophotometer (Thermo Scientific). The 260/280 and 260/230 ratios were also noted down to evaluate the purity and quality of the RNA. The RNA was then immediately either converted to cDNA (Section 2.1.16) or stored at -80℃. For some experiments the quality of the RNA was also assessed by RNA agarose gel electrophoresis. Agarose gel (50 ml) was prepared by adding 0.5 g of RNA agarose to 38.5 ml of dH_2O and boiling in the microwave. 5 ml of 10X MOPS (3-(N-morpholino) propanesulfonic acid) and 8.5 ml of formaldehyde were then added to the agarose in a fume hood and the gel was poured and left to set. The gel was immersed in 1X MOPS running buffer and the comb was removed. RNA (2 µl) loading buffer was added to 1 µl of RNA and the total 3 µl were loaded into each lane. The gel was run at 70 V for 10-20 min.

2.1.15 RT-PCR (Reverse-transcription polymerase chain reaction)

All RT-PCR reagents, buffers and enzyme used were from Promega, Biotec (Madison, WI) unless otherwise stated. Unless otherwise stated PCR was carried out using Taq polymerase.

2.1.15.1 Reverse Transcription of mRNA into cDNA (Deoxy-ribonucleic acid)

RNA (29 µl, containing between 1-3 µg of RNA) was added to 1 µl of oligo dT_{15} (deoxythymidine) primer and heated to 70℃ for 5 min in a PCR machine. Control tubes containing only water were also prepared. While primer annealing was occurring, RT master mix was made for the number of samples plus two extra, as some master mix is lost during pipetting.

Master Mix (per tube):

● 5 X MMLV RT Reaction Buffer	10 µl
● RNAsin	1.25 µl
● 100 mM dNTPs (deoxynucleotide thriphosphates)	1.25 µl
● MMLV Reverse Transcriptase	2 µl
● Nuclease- free H_2O	5.5 µl
Total volume:	20 µl

20 µl of RT master mix were then added to the 30 µl of the sample and the samples were gently mixed by pipetting and placed in the PCR machine. Negative RT control tubes containing no MMLV RT were also set up in order to assess whether there is any contaminating genomic DNA in the sample. The tubes were incubated at 40℃ for 1 h and the reaction was inactivated by heating for 2 min at 94℃. The cDNA was then used as a template for amplification by PCR or stored at -20℃ until required.

2.1.15.2 Amplification of human and zebrafish cDNA by PCR using Taq polymerase

Two microlitres of cDNA generated as described in section 2.1.11.3 were subsequently used in the PCR amplification unless otherwise stated. The following were combined in a PCR:

Master Mix (made for number of samples + 2 extra tubes)

- 10 X PCR Reaction Buffer (without $MgCl_2$) 5 µl
- 25 mM $MgCl_2$ 1.5 µl
- 10 mM dNTPs 1 µl
- 10 mM Forward Primer 0.7 µl
- 10 mM Reverse Primer 0.7 µl
- Taq (DNA Polymerase- 5u/ µl) 0.25 µl
- Nuclease- Free H_2O 13.85 µl

Total volume: 23 µl

The master mix (23 µl) was added to 2 µl of cDNA from the RT reaction (Section 2.1.11.3) and the sample was mixed gently. Negative PCR control tubes were also prepared containing H_2O instead of cDNA. Elongation factor 1- α (EF1-α) (zebrafish samples) and Glyceraldehyde 3-phosphate dehydrogenase (GAPDH) (human samples) primers were used as positive control PCR primers. Zebrafish and human primer sequence and optimal annealing temperatures are shown in 7.3. EF1-α and GAPDH are ubiquitously expressed genes and can be used as standards in zebrafish and humans respectively for normalizing samples. In order to identify the optimal primer annealing temperature, temperature gradients of the human *HAX1* primers (50-68℃) were carried out with both PMN and PLB-985 cDNA. The tubes were placed in a PCR block and the following thermal cycling was carried out:

- 1. 94℃- 2 min (1 cycle)
- 2. 94℃- 30 sec
- 3. *Optimal primer annealing temperature- 1 min*
- 4. 72℃- 30 sec
- 5.Go to step 2 (29/34 X)
- 6. 72℃- 2 min
- 7. Hold step- 4℃.

PCR products were stored at -20℃.

2.1.16 *hax1* transcript - specific primer design for Zebrafish mRNA

Primers were designed using the NCBI Primer design tool to test whether chosen sequences were suitable primer sequences. It was assumed that the zebrafish gene would be spliced in the same way as the human gene and the primers were modelled using the splicing pattern described by Lees *et al* (which uses the VEGA annotation of alternatively spliced HAX1 isoforms) and the zebrafish *hax1* gene sequence (Lees et al. 2008). Annealing temperature gradients were carried out in order to identify the optimal primer annealing temperatures. The primer sequences and their optimal annealing temperatures are shown in Appendix 7.3.1. The genomic sequence of zebrafish *hax1* with highlighted primer annealing regions is shown in Appendix 7.4.

2.1.17 Amplification of zebrafish cDNA and gDNA by PCR using Phusion® High-Fidelity DNA Polymerase

Unless otherwise stated, 0.5 µl of zebrafish cDNA were used in the PCR amplification. The following were combined in a PCR reaction, on ice:

gDNA/cDNA	0.5 µl
water	make up to 20 µl
10 µM forward primer	0.5 µl
10 µM reverse primer	0.5 µl
10 mM each dNTPs (Promega)	0.4 µl
Phusion 5 X HF Buffer (NEB)	4 µl
Phusion® DNA Polymerase	0.2 µl

The samples were mixed gently and added to a preheated thermocycler and cycled as follows:

- 1. 98℃- 30 sec (1 cycle)
- *2. 98℃- 10*
- *3. Optimal primer annealing temperature - 15 sec*
- *4. 72℃- 5 sec*
- 5. Go to step 2 (34 X)

- 6. 72℃- 5 min
- 7. Hold step- 4℃.

PCR products were stored at -20℃.

2.1.18 PCR gel electrophoresis

PCR products were examined on agarose (Melford Labs) gels. The desired % gel was made by adding a specific amount of agarose (w/v) to 1X TAE (Tris-acetate) buffer and the melting in a microwave. 3 µl of ethidium bromide (BDH Electran) were added once the agarose had cooled and the gel was poured. After the gel had set, the comb was removed and the gel placed in a tank immersed in 1X TAE buffer (Appendix 7.5). Samples were loaded in each lane alongside the DNA ladder, Hyperladder I (Bioline, London, United Kingdom) to allow sizing of the PCR products.

2.1.19 QIAquick PCR Clean-up and gel extraction

PCR products were extracted and purified using the QIAquick gel extraction kit protocol (QIAGEN, Valencia, CA) according to manufacturer's instructions. The DNA was eluted in in 50 µl of sterile H_2O for injections (Braun) and samples were stored at -20℃ until sequencing. PCR clean up (with the Guanidine HCl step) was carried out according to the QIAquick PCR Purification Kit (QIAGEN, Valencia, CA) manual. Remaining PCR product was eluted into 30 µl of sterile H_2O. PCR products were sent for sequencing to the Core Genomics Facility (University of Sheffield, Medical School).

2.1.20 Colony PCR

Well-separated transformant colonies were PCR amplified in order to screen for inserts. The following were added to a PCR tube per colony and mixed gently:

9 µl water

10 µl PCR Reddymix (Thermoscientific)

1 µl 10 µM each left and right primer

A small amount of each colony was added to the PCR mix using a p200 pipette tip. The tubes were then added to a preheated thermocycler and cycled as follows:

- 1: 94 °C 2min
- 2: 94 °C 20sec
- 3: initially 60 °C (then a 0.2 °C reduction per cycle) 20 sec 4:72 °C 45sec
- 5: go to step 2) 29 X
- 6: 72 °C 3min
- 7: 10 °C hold

Each p200 pipette tip containing a colony was also used to streak out to give single colonies on selective plates. In order to verify the sequence, colonies with the correct sized PCR product were Sanger sequenced following ExoI-SAP treatment. On ice, 3.2 µl of ExoI-SAP mix were added to each PCR tube containing the PCR reactions. ExoI-SAP mix for 10 reactions was produced by adding 1.7 µl of NEB exonuclease I and 32 µl of shrimp alkaline phosphatase (USB, Cleveland, OH, USA). Following the addition of ExoI-SAP to each PCR reaction, tubes were incubated on a preheated thermocycler at 37°C for 45 min and then 80 °C for 15 min.

2.1.21 Whole mount *in situ* Hybridization (WISH) probe synthesis

The full-length *hax1* coding sequence was cloned in a pCR-BLUNT II-TOPO plasmid vector (Appendix 7.6) according to the manufacturer's instructions (Invitrogen, Carlsbad, CA). The plasmid DNA was purified by a high speed MIDIprep of a colony containing the vector with the gene according to manufacturer's protocol (QIAGEN, Valencia, CA). The plasmid DNA was then eluted into 1 ml of water. In order to generate the anti-sense probe the plasmid was linearized with an XhoI restriction digest. A SpeI digest was carried out to generate the sense probe. 100 µl

of plasmid DNA were mixed with 11 µl of NEB Buffer 4,1.2 µl of BSA and 3 µl of the relevant restriction enzyme. A vector containing the coding sequence for the positive control L-Plastin (anti-sense) was also linearized using 20 µg of plasmid DNA, 31 µl of water, 10 µl of NEB Buffer 3, 1 µl of BSA and 5 µl of NotI restriction enzyme.

The digests were incubated at 37 °C for 2 h. Following the incubation the whole mixtures were loaded into 3 wells each an 0.8 % agarose gel (section 2.1.18) and the plasmids resolved by electrophoresis at 100 Volts for 1 h and 20 min. The plasmid DNA was quantified on a Nanodrop™ 1000 spectrophotometer (Thermo Scientific). The purified linear DNA probes were *in vitro* transcribed using a T7 and Sp6 RNA digoxygenin (DIG) labelling kit (Roche) for the *hax1* sense and anti-sense probes respectively. A T7 RNA digoxygenin (DIG) labelling kit was used to transcribe the L-Plastin probe. 1 µg of linear plasmid DNA was added to 2 µl of transcription buffer, 1 µl of RNAse inhibitor, 1 µl T7/SP6 RNA polymerase, 2 µl NTP-DIG-RNA and 5.6 µl of sterile water then incubated for 2 h at 37 °C. The plasmid DNA template was removed by digestion with an additional 2 µl of TURBO DNAse in a further 30 min incubation at 37 °C. The RNA was precipitated by the addition of 4 µl of Lithium chloride, 1 µl EDTA (pH8), 75 µl and ethanol (100 %) at -80 °C overnight. The next morning, the RNA was pelleted by centrifugation at 14000 rpm for 30 min at 4 °C. The RNA pellet was then gently washed in 1 ml of 70 % ethanol followed by a further 10 min centrifugation for 10 min at 4 °C, 14000 rpm. The supernatant was removed and the pellet was air-dried and resuspended in 20 µl of sterile water. Presence of RNA was confirmed by agarose gel electrophoresis of 0.5 µl of RNA on a 0.8 % agarose gel. 80 µl of formamide (Sigma-Aldrich) were added to the resuspension and the RNA was stored at -80 °C.

2.1.22 Synthesis of capped zebrafish *hax1 001* mRNA for microinjection

The pCR-BLUNT II-TOPO *hax1 001* plasmid generated in section 2.1.21 was subjected to an EcoRI restriction digest to allow excision of the *hax1 001* insert. The restriction digest was carried out by adding 11.8 µl of water, 0.2 µl of 100X BSA (NEB), 2 µl of RE 10X buffer H and 1 µl of EcoRI (Promega, Biotec, Madison, WI) to 5 µl of the Zero Blunt TOPO vector containing the *hax1 001* insert. The digest was incubated at 37 °C for 3 h. The EcoRI restriction digest products were analysed by agarose gel electrophoresis. The excised *hax1 001* insert was gel purified as described in section 2.1.19. The purified insert was quantified using a Nanodrop™ 1000 spectrophotometer (Thermo Scientific). The insert was ligated O/N to EcoRI linearized pCS2+ plasmid vector by adding 50 ng of linearized pCS2+ to 33 ng of *hax1* insert, 1 µl of 10X T4 ligase buffer and 1 µl of T4 DNA ligase (Promega, Biotec, Madison, WI) in a final volume of 10 µl. The ligation product was transformed into One Shot TOP10 *E. coli* competent cells (Invitrogen Life Technologies, Carlsbad, CA) according to manufacturer's protocol. Transformed cells were streaked onto carbenicillin selective plates and grown O/N at 37 °C. Carbenicillin plates were made by adding carbenicillin antibiotic at 50 µg/ml to autoclaved LB agar.

The next morning, 12 well-separated colonies were used to inoculate 5 ml of carbenicillin selective cultures and the cultures grown O/N at 37 °C. The plasmid DNA was purified using a QIAgen plasmid MINIprep kit according to manufacturer's instructions (Valencia, CA). The plasmid DNA was screened for insertion of the *hax1 001* segment by agarose gel electrophoresis using 1 µl of plasmid DNA loaded onto a 1 % agarose gel. The plasmid DNA from colonies with a shift in size from ~4000 bp to ~5000 bp was then subjected to PCR with *hax1 001* primers (Appendix 7.3) using Reddymix (ThermoScientific) according to the manufacturer's instructions. The PCR products were ExoI-SAP treated as described in section 2.1.20 followed by Sanger sequencing in order to determine the orientation of the *hax1* insert in the pCS2+ plasmid vector. A clone with

the correct orientation was used to inoculate a 50 ml selective culture and the culture grown O/N at 37 °C. The following morning, the *hax1 001* containing pCS2+ plasmid was purified from the O/N culture using a QIAgen plasmid MIDIprep kit (Valencia, CA) according to the manufacturer's protocol. The plasmid DNA was linearized using NotI. 20 µg of plasmid DNA were mixed with 20 µl of buffer 3 (NEB), 2 µl of 100X BSA, 4 µl of NotI in a total volume of 200 µl. The digest was incubated at 37 °C for 2 h. The linearized plasmid DNA was then purified using a QIAgen PCR clean-up kit as described in the manufacturer's manual. Purified linear plasmid DNA was transcribed into mRNA from the SP6 promoter using an Ambion Sp6 mMessageMachine transcription kit (Austin, TX). The following were assembled into a PCR tube:

5 µl linear pCS2+ *hax1 001* (10 µg)
10 µl NTP/CAP
2 µl buffer
1 µl RNAse free water
2 µl Sp6 polymerase

The contents of the tube were mixed gently and incubated at 37 °C for 2 h. The plasmid DNA template was degraded by adding 1 µl of DNAse and incubating at 37 °C for 30 min.

In order to purify the mRNA, synthesized mRNA was mixed 400 µl of Phenol Chloroform and 480 µl of RNAse free water. The mixture was vortexed and spun at 13000 rpm at 4 °C for 15 min. To further purify and concentrate the plasmid DNA, 400 µl of the upper layer were transferred into an Amicon ultra 0.5 ml centrifugal filter device (Millipore, Billerico, MA, USA) and the column inserted into a tube according to the manufacturer's instructions. The tube was then centrifuged at 14000 at RT for 10 min. Following centrifugation, the column was transferred to a fresh tube and spun at 1000g at RT for 2 min. In order to quantify the RNA, the purified capped mRNA was then subjected to agarose gel electrophoresis. 1 µl of mRNA was loaded alongside Hyperladder I

(Bioline, London, United Kingdom) on a 1% agarose gel. The purified capped mRNA was diluted with RNAse free water and 50 pg (1 nl) were injected into each embryo as described in section 2.2.3.

2.1.23 Isolation of genomic DNA from single zebrafish embryos

Dechorionated embryos were lysed in 50 µl of embryo digestion buffer (10 mM Tris Hcl pH8, 1 mM EDTA, 0.3 % Tween-20, 0.3 % NP-40). Following a 10 min incubation at 98 °C, the embryos were transferred to ice and 4 µl of Proteinase K (25 mg/ml) were added. The embryos were then incubated for a further 3 h at 55 °C followed by a 10 min incubation at 98 °C. 650 µl of ammonium acetate solution were added to the lysate and mixed. Ammonium acetate solution for 10 samples was made up by adding 2.63 ml of 7.5 M ammonium acetate to 4.2 ml of water. The gDNA was extracted using 700 µl of chloroform and spinning at 14000 g for 1 min at RT. The top aqueous layer (~650 µl) was then transferred to a new tube and 1 µl of GlycoBlue (Ambion, Austin, TX) was added to the sample for visualisation of pelleted nucleic acid. The gDNA was precipitated using 650 µl of propan-2-ol at RT and centrifugation at 14000g for 30 min at 4 °C. The pelleted gDNA was washed with 1 ml 70 % ethanol. Following centrifugation at 14000 g at 4 °C for 1 min, the supernatant was discarded and the sample pulse spun to bring down residual supernatant, which was then removed. The gDNA pellet was then air dried at RT for 1 min only followed by resuspension in 50 µl of water. The gDNA was stored at -20 °C.

2.1.24 Isolation of genomic DNA from a pool of zebrafish embryos

Genomic DNA (gDNA) was extracted from a pool of 10-50 embryos. Dechorionated embryos were lysed in 700 µl of embryo digestion buffer (10 mM Tris Hcl pH8, 1 mM EDTA, 0.3 % Tween-20, 0.3 % NP-40). Following a 10 min incubation at 98 °C, the embryos were transferred to ice and 30 µl of Proteinase K (25 mg/ml) were added. The embryos were then incubated for a further 3 h at 55 °C followed by a 10 min incubation at 98 °C. 700 µl of 1:1 phenol/chloroform solution were added to the

lysate and mixed by inversion. The tube was spun at 14000 g for 1 min at RT. The top aqueous layer (~450 µl) was then transferred to a new tube and 700 µl of chloroform were added to the solution. This was mixed by inversion and spun at 14000g for 1 min at RT. The gDNA was precipitated by transferring the aqueous layer (~450 µl) to a new tube containing 250 µl of 7.5 M ammonium acetate and 700 µl of propan-2-ol. The sample was centrifuged at 14000 g for 30 min at 4 °C. The pelleted gDNA was then washed in 1 ml of 70 % ethanol followed by a spin again at 14000 g at 4 °C for 1 min. Following the centrifugation, the supernatant was discarded and the sample pulse spun to bring down residual supernatant, which was then removed. The gDNA pellet was then air dried at RT for 1 min only followed by resuspension in 100 µl of water. The gDNA was stored at -20 °C.

2.2 In-vivo techniques

2.2.1 Whole mount *in situ* Hybridization (WISH)

All WISH buffer formulas are shown in Appendix 7.7. Uninjected and *hax1 001* mRNA injected *nacre* embryos at 24 hours post fertilization (hpf) were fixed overnight in 4 % para-formaldehyde (PFA made in phosphate buffered saline; PBS) at 4 °C. The embryos were then transferred into 100 % methanol and stored at -20 °C. Up to 20 embryos per eppendorf were fixed in this way. The embryos were rehydrated by 5 min washes in 1 ml of a methanol series of 75 %, 50 % and 25 % made up in PBS and 100 % PBT (PBS with 0.1 % Tween-20). This was followed by a 15 min 1:1000 treatment in 10 µg/ml Proteinase K (Sigma-Aldrich) in PBT then fixing for a second time in 4 % PFA for 20 min. This was followed by five 5 min washes in PBT and incubation in a pre-hybridization buffer for 5 h at 70 °C. The embryos were incubated in probe-hybridization buffer (1:200 dilution of RNA in formamide from section 2.1.21 in pre-hybridization buffer) for 15 h at 70 °C. Excess RNA probe was removed by successive washes with 100 % brief HybWash and 15 min washes in 75 %, 50%, 25 % HybWash with 2X SSC at 70 °C. A 2X Saline-sodium citrate (SSC) wash followed by two 30 min washes

with 0.2X SSC at 70 °C followed. The embryos were then washed for 10 min in a series of 0.2X SSC of 75%, 50 %, 25 % and 0% made up in PBT at RT. The embryos were incubated at RT in blocking solution (PBT, 2 % sheep serum; v/v, 2 mg/ml BSA) for several hours. This was followed by incubation in Blocking solution containing 1:5000 anti-DIG-AP antibody (Roche) overnight at 4 °C with gentle shaking. Excess primary antibody solution was washed of with six 15 min washes in PBT. During the last wash, the embryos were transferred to a 24 well plate. The embryos were then washed with staining wash solution three times, 5 min each time. This was followed by incubation in staining solution containing NBT (Roche) and BCIP (Roche) and the embryos were monitored with a dissecting microscope. Once the desired staining was achieved, the staining solution was removed and the reaction was stopped by adding 1 ml of 1 mM EDTA in PBS (pH 5.5) for 5 min. The embryos were fixed in 4 % PFA for 30 min and stored at -20 °C in methanol. Before imaging, the embryos were rehydrated with brief washes in 75 %, 50 % and 25 % methanol made up in PBS. Whole fish embryos were mounted in 80 % glycerol and imaged using a Nikon SMZ1500 stereomicroscope with a DS-Fi1 camera. Images were taken at multiple Z-planes. NIS elements software was used to generate the focused images.

2.2.2 Morpholino phosphorodiamidate antisense oligonucleotides (MO) design

Hax-1 splice blocking and translation start site blocking MOs were designed to target the splice acceptor of exon 3 and translation start site according to instructions on the http://www.gene-tools.com/Oligo_Design website. The MO oligonucleotides were obtained from Gene Tools, LLC (Corvalis, OR, USA). The sequence of the Hax-1 splice site MO was: 5’ AAACCTGATGGGAAGAAGCAGAACA 3’ and that of the translation start site MO 5’ GCTCATTTATGGACAGAATCCTGAG 3’. A p53 translational blocking MO was also used (5’ GCGCCATTGCTTTGCAAGAATTG 3’). Before injection the MOs were diluted with sterile H_2O and phenol red (for visualization).

2.2.3 Zebrafish maintenance and microinjection

Adult zebrafish were maintained at 28 °C in a 14 h light/dark cycle in approved Home Office facilities in the Centre for Developmental and Biomedical Genetics aquaria at the University of Sheffield. All zebrafish experiments were performed under the UK Home Office Project License 40/3325 in accordance with Home Office legislation. Wild-type zebrafish (AB and EKK strains) and transgenic *Tg(mpx::GFP)i114* fish (Renshaw et al. 2006) were set up for spawning late in the afternoon. Embryos were collected the next morning and grown at low density (~50 embryos per petri dish) in E3 media (Appendix 7.8). If embryos were required for RNA extraction they were then anesthetised with Tricaine methanesulfonate (MS222) before dechorionation and processing for genomic DNA (gDNA) or RNA extraction.

2.2.4 Microinjection of embryos with MO and capped mRNA

Transgenic zebrafish Tg(mpx:GFP)i114 were marbled overnight. The embryos were collected the following morning and ~50 embryos were aligned on a microinjection petri dish. The embryos were injected at the 1-4 cell stage using 1-2 nl of diluted MO or RNA using a pulled Kwik-Fil^{tm} borosilicate glass capillary (World Precision Instruments) and a pneumatic picopump (PV830) and air compressor micromanipulator (World PrecisionInstruments), and a Leica S6D 100 dissecting microscope with a Leica L2 light source. The end of the needle was broken off using very fine forceps and the volume to be injected was quantified using a graticule. Phenol red was added to the diluted MO or RNA (1 µl in 10 µl final volume) for visualization of injecting under the microscope. After injection, embryos were placed in E3 media and incubated at 28.5℃. Dead and unviable embryos were removed after 1 hpf (hour post fertilization). Dead embryos were also removed after 6 and 24 h. Embryos required for total RNA extraction were dechorionated and lysed in TRI reagent (Section 2.1.15).

2.2.5 Analysis of total zebrafish PMN counts

Embryos were mounted in 1 % low melting point agarose containing MS222 in a 40 mm dish with a section of the base replaced by a microscopy glass coverslip. Images of embryos were captured using Volocity® software (Perkin Elmer, Cambridge, UK) through a Nikon Eclipse TE2000U inverted microscope 2x objective with 20 z planes. Merged z-stacks were generated using Volocity®. PMNs were counted at 35, 48 and 72 hpf by eye from taking images of embryos on and counting the green fluorescent protein (GFP) labeled PMN by eye.

2.2.6 Tail-fin transection of *Tg(mpx:GFP)i114* embryos and analysis of PMN recruitment and resolution from the site of injury

Dechorionated embryos were anesthetized by addition of MS222 to the E3 media at a density of 10 embryos per petri dish. In order to trigger an inflammatory response complete transection of the tail was performed midway between the terminal point of the aortic venous loop and the distal most part of the tail on 2-3 dpf embryos using a microsurgical knife (World Precision Instruments, Hertfordshire, UK) as previously described by Loynes *et al.* (Renshaw, Loynes et al. 2006). Post transection, the embryos were transferred to fresh E3 media and incubated at 28 °C for either 6 h (for analysis of recruitment of PMN to the site of injury) or 24 h (for analysis of PMN resolution from the site of injury) post injury (hpi). At the appropriate time point images of whole fish embryos were taken using a 2x objective on a Nikon Eclipse TE2000U inverted microscope and PMN at the site of injury were counted by eye.

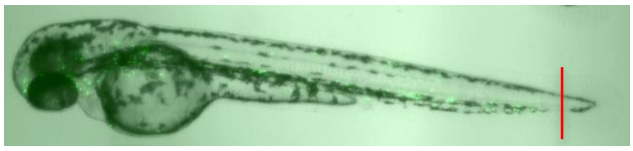

Figure 2.3 Site of tail-fin transection

An image of a 2 dpf embryo generated on a Nikon Eclipse TE2000U inverted microscope using a 2x objective. The red line indicates the site of transection.

2.2.7 Generation of a zebrafish *hax1* targeting CoDA ZFN

2.2.7.1 Adding zinc fingers to the generic backbones

In order to insert the F1, F2 and F3 zinc fingers (Appendix 7.13.1) into the generic backbones, the following were assembled in a tube on ice:

PCR reaction Components	
1ul	generic backbone amplicon
14ul	water
4ul	5 X Phusion HF buffer
0.5ul	10mM each dNTPs
0.5ul	10uM each F1+F2F3 primers
0.4ul	Phusion HF

PCR cycling parameters
1:95 °C 2min
2:95 °C 20sec
3:50 °C 20sec
4:72 °C 5min
5:go to step 2) 19x
6:72 °C 3min
7:10 °C hold

The contents of the tube were mixed gently, added to a preheated thermocycler and cycled as shown above. Primers for the left ZFN were added to the pCS2-Flag-ZFP-FokI-DD generic backbone and the right ZFN zinc finger primers to the pCS2-HA-ZFP-FokI-RR generic backbone.

2.2.7.2 Generation of plasmid sticky ends

The remainders of the left and right ZFN PCR products were then purified using a QIAquick PCR clean-up kit (with the guanidine HCl step), according to manufacturer's protocol. In order to create plasmid DNA sticky ends and allow self-ligation of the plasmids into circular form, the resulting plasmid constructs (ZFN plasmids) were digested with restriction enzyme AgeI by adding the following components to a PCR tube, on ice:

Reaction components
• 44 µl of the eluted PCR product
• 34 µl of water
• 5 µl of NEB buffer I
• 1 µl of AgeI

The AgeI digested left and right ZFN expression vectors containing the F1, F2 and F3 zinc fingers were then purified using a QIAquick PCR clean-up kit (with the guanidine HCl step) according to manufacturer's instructions and eluted in 50 µl of water.

2.2.7.3 Circularisation of the ZFN backbone plasmids

To generate a circular construct the left and right ZFN encoding plasmids were self-ligated by assembling the following components into a PCR tube:

Reaction components
• **2 µl of the eluted AgeI digested PCR product** • **2.5 µl of 2X NEB quick ligase buffer** • **0.5 µl of NEB quick ligase**

This was mixed gently and incubated at room temperature (RT) for 5 min prior to transferring to ice. The entire reactions were then each used to transform 25 µl of NEB 10-beta competent *E. coli* (New England Biolabs, Ipswich MA) according to the manufacture's instructions. Transformed cells (150 µl) were streaked on Ampicillin (50 µg/ml) selective LB agar plates and grown overnight (O/N) at 37 °C.

2.2.7.4 Preparation of ZFN capped RNA for microinjection

The two purified plasmids from section 5.1.1.3 encoding the left and right ZFN plasmids were linearised using NotI restriction enzyme. The following components were assembled in a tube, on ice:

ZFN linearization components Reaction components
• **6 µg of each the left and right ZFN plasmids** • **247 µl of water** • **30 µl of NEB buffer 3** • **3 µl of 10 mg/ml BSA (NEB)** • **20 µl NotI**

The digest was incubated at 37 °C for 1 h. The linearised plasmid DNA was then purified using a QIAquick PCR clean-up commercial kit as described in (section 2.1.19) and eluted into 30 µl of water. The plasmids were then used to *in vitro* synthesise capped RNA via Ambion's Sp6 mMessageMachine transcription kit (Austin, TX). The following were assembled into a PCR tube at RT:

***In vitro* transcription components**
• **3 µl 400 ng/µl Left and Right ZFN plasmid DNA** • **5 µl NTP CAP mix** • **1 µl 10X buffer** • **1 µl enzyme mix**

The contents of the tube were gently mixed and incubated at 37 °C for 2 h. Following the *in vitro* RNA synthesis, the plasmid DNA template was degraded by adding 1 µl of DNAse turbo (Ambion, Austin, TX) to the sample and incubating at 37 °C for a further 20 min. The *in vitro* synthesised capped RNA was then purified using a QIAGEN RNeasy Minelute kit according to manufacturer's protocol. The capped RNA was eluted with 18 µl of RNAse free water.

2.2.7.5 Preparation of zebrafish *hax1* ZFN target sequence for Roche Titanium 454 sequencing

In order to allow Roche Titanium 454 sequencing of the ZFN target site, the *hax1* target site was first amplified using LHax1ZF454 and RHax1ZF454 primers (Appendix 7.13.2). The following components were assembled into a PCR tube on ice and PCR carried out using the following conditions:

PCR reaction Components	
1 µl	20 X diluted genomic DNA
14 µl	water
4 µl	5X Phusion HF buffer
0.4 µl	10 mM each dNTPs
1 µl	10 uM each primer
0.2 µl	Phsion HF

PCR cycling parameters
1:95 °C 30 sec
2:95 °C 10sec
3:50 °C 15sec
4:72 °C 5 sec
5:go to step 2) 34 X
6:72 °C 5min
7:10 °C hold

2.2.8 Generation of a zebrafish *hax1* targeting TALEN

2.2.8.1 TALEN assembly stage I

Following identification of a suitable *hax1* TALEN targeting site (described in Chapter 5), the first stage assembly reactions were set up on ice as follows:

Left TALEN Part A components
1 µl pNI1 (150 ng/µl)
1 µl pHD2 (150 ng/µl)
1 µl pNI3 (150 ng/µl)
1 µl pNN4 (150 ng/µl)
1 µl pNN5 (150 ng/µl)
1 µl pNN6 (150 ng/µl)
1 µl pNI7 (150 ng/µl)
1 µl pHD8 (150 ng/µl)
1 µl pHD9 (150 ng/µl)
1 µl pHD10 (150 ng/µl)
1 µl pFUS_A (100 ng/µl)
4 µl water
2 µl T4 ligase buffer (NEB)
2 µl T4 ligase (NEB)
1 µl BsaI (NEB)
Total volume: 20 µl

Left TALEN Part B components
1 µl pHD1 (150 ng/µl)
1 µl pNG2 (150 ng/µl)
1 µl pNG3 (150 ng/µl)
1 µl pHD4 (150 ng/µl)
1 µl pFUS_B
10 µl water
2 µl T4 ligase buffer (NEB)
2 µl T4 ligase (NEB)
1 µl BsaI (NEB)
Total volume: 20 µl

Right TALEN Part A components
1 µl pHD1 (150 ng/µl)
1 µl pNG2 (150 ng/µl)
1 µl pNG3 (150 ng/µl)
1 µl pHD4 (150 ng/µl)
1 µl pNI5 (150 ng/µl)
1 µl NG6 (150 ng/µl)
1 µl pHD7 (150 ng/µl)
1 µl pNI8 (150 ng/µl)
1 µl pNG9 (150 ng/µl)
1 µl pHD10 (150 ng/µl)
1 µl pFUS_A (100 ng/µl)
4 µl water
2 µl T4 ligase buffer (NEB)
2 µl T4 ligase (NEB)
1 µl BsaI (NEB)
Total volume: 20 µl

Right TALEN Part B components
1 µl pNI1 (150 ng/µl)
1 µl pNG2 (150 ng/µl)
1 µl pHD3 (150 ng/µl)
1 µl pNI4 (150 ng/µl)
1 µl pNG5 (150 ng/µl)
1 µl HD6 (150 ng/µl)
1 µl pFUS_B
8 µl water
2 µl T4 ligase buffer (NEB)
2 µl T4 ligase (NEB)
1 µl BsaI (NEB)
Total volume: 20 µl

A list of the plasmids required for Golden Gate TALEN construction is shown in Appendix 7.17. For part A assembly, the first ten RVD modules were excised from the plasmids in which they were stored and ligated to array plasmid pFUS_A. For part B assembly the rest of the RVD modules were ligated to array plasmid pFUS_B. The plasmids were thawed and mixed. Each reaction was mixed by gentle pipetting and cycled following the parameters shown on the right.

Temperature cycling parameters
1: 37 °C 5 min
2:16 °C 10 min
3: go to step 1 9 X
4:50 °C 5 min
5:80 °C 5min
7:10 °C hold

2.2.8.2 TALEN assembly stage I plasmid purification

In order to remove the non-ligated linear DNA fragments, 1 µl each of 10 mM rATP and plasmid safe nuclease (Epicentre Biotechnologies) was added to each of the four cloning reactions. The samples were mixed gently by pipetting and incubated at 37 °C for 1 h. Three µl of each reaction were used to transform 12.5 µl of NEB 10-beta competent E. coli (New England Biolabs, Ipswich MA) according to the manufacture's instructions. Spectinomycin selective X-gal LB agar plates were used for streaking of 50 µl of transformed cells and overnight incubation at 37 °C followed. Three medium sized well-separated white colonies were picked for each transformation reaction and used to inoculate 6 ml cultures of Spectinomycin selective LB. The cultures were incubated O/N at 37 °C with shaking. Plasmid DNA was purified from overnight cultures using a QIAGEN MINI prep kit (with the PB buffer wash) as described in the manufacturer's protocol. The purified DNA was eluted into 50 µl of water.
In order to asses whether the RVD modules of the Part A and B of the left and right *hax1* specific TALEN were correctly aligned, each array plasmid containing the RVD modules was subjected to a diagnostic digest with NheI and XbaI restriction enzyme (NEB). Four µl of each plasmid eluate were transferred to a tube containing 6 µl of restriction enzyme master mix of the following components:

Assembly stage I: Diagnostic digest master mix	
• **22 µl**	**water**
• **5 µl**	**10 X NEB2 buffer**
• **0.5 µl**	**10 mg/ml BSA**
• **1 µl**	**NheI**
• **1 µl**	**XbaI**

The digests were incubated at 37 °C for 1 h.

2.2.8.3 TALEN assembly stage II

Part A and B of each subunit were combined with the following components in the reaction:

Assembly stage II components	
5 µl	water
4 µl	eluted Part A plasmid
4 µl	eluted Part B plasmid
1 µl	pLRNG (150 ng/ µl)
1 µl	pCAG-T7-TALEN 75 ng/ µl)
2 µl	10 X T4 DNA ligase buffer (NEB)
2 µl	T4 DNA ligase (NEB)
1 µl	Esp3I

Temperature cycling parameters
1: 37 °C 5 min
2:16 °C 10 min
3: go to step 1 9 X
4:50 °C 5 min
5:80 °C 5min
7:10 °C hold

The components of the left and right subunits were mixed by gentle pipetting and cycled as shown above.

The resulting left and right *hax1* specific pCAGT7-TALEN plasmids were then transformed into 25 µl of NEB 10-beta competent *E. coli* (New England Biolabs, Ipswich MA) using 2 µl of the Golden Gate reaction according to manufacturer's protocol. Following streaking of 50 µl of the transformed cells onto carbenicillin Xgal LB agar plates and growth O/N at 37 °C, a well separated white colony was picked for each subunit and used to inoculate a 125 ml carbenicillin selective LB culture. This was followed by O/N incubation at 37 °C. The plasmid DNA was purified from each of the two O/N cultures using a Nucleobond Midi Kit (Macherey-Nagel, Düren, Germany) according to manufacturer's manual. During the second wash, the plasmid DNA was split into six 1.5 ml eppendorf tubes and precipitated using isopropanol. The supernatant was completely removed and the plasmid DNA pellet washed in 1 ml of 70 % ethanol. Following centrifugation, the supernatant was completely removed once again and the DNA pellet left to dry for 1 min. The plasmid DNA pellets in each of the six tubes were resuspended in 20 µl of water and pooled into

a single tube. In order to quantify the plasmid DNA, 1 µl of each the left and right subunit was diluted with 99 µl of water and absorbance at 260 nm was measured using a spectrophotometer.

2.2.8.4 TALEN assembly stage II: Diagnostic digest

In order to assess the TALEN stage II assembly, the left and right TALEN subunit plasmids were subjected to a BamHI and XbaI restriction digest. The digestion components of each reaction are shown below:

Assembly stage II: Diagnostic digest components
• **7 µl water** • **1.5 µl Nucleobond purified pCAGT7-TALEN construct 100ng/µl** • **0.1 µl 100 X BSA** • **0.5 µl BamHI** • **0.5 µl Xbal**

The contents of the digestion reaction were mixed by pipetting and incubated at 37 °C for 1 h.

2.2.8.5 TALEN assembly stage II: Diagnostic digest

The left and right *hax1* specific TALEN encoding constructs were also linearised with NotI restriction enzyme to enable *in vitro* transcription of the TALEN subunit:

Construct Linearization Components
• **6 µg Left TALEN construct** • **6 µg Right TALEN construct** • **3 µl 10 mg/ml BSA** • **30 µl 10 X NEB buffer 3** • **30 µl NotI (NEB)**

The digestion reaction was mixed by gentle pipetting and incubated at 37 °C for 1 h. Following linearization, the plasmid DNA was purified using a QIAquick PCR clean-up kit. The plasmid was run through two purification columns

and eluted with 30 µl of water.

2.2.8.6 Preparation of *hax1* exon 2 targeting TALEN RNA for microinjection

In order to synthesize *hax1* specific TALEN capped RNA, an Epicenter T7 Message Max ARCA kit was used to *in vitro* transcribe the NotI linearised TALEN encoding plasmids. The following components were assembled in a tube at RT:

TALEN *In vitro* transcription components
• **5.5 µl 400 ng/µl linear plasmid DNA**
• **2 µl 10 X buffer**
• **8 µl NTP CAP mix**
• **2 µl 100 mM DTT**
• **0.5 µl Scriptguard**
• **2 µl enzyme mix**

The contents of the tube were mixed gently and incubated at RT for 30 min. In order to eliminate the template plasmid DNA, 1 µl of DNAse was added o the sample and incubated at 37 °C for 15 min. The RNA was then purified using an RNeasy MinElute clean-up kit (QIAGEN, Valencia, CA) according to manufacturer's protocol. The purified RNA was eluted with 14 µl of water.

2.2.9 *In vivo* PMN tracking during recruitment to the site of injury

Embryos were anesthetized with MS222 and tail fin transections were performed 30 min prior to commencement of tracking. Embryos were mounted immediately after injury using 1 % low melting point agarose and the tail fins were imaged using Volocity® build 5.3.2 on a Nikon Eclipse TE2000U inverted microscope with the 10 X NA 0.3 PlanFluor objective and an Orca-AG camera (Hammatsu). 5 z stacks were taken through the tail fin at every 2 minute intervals over a focal depth of 100 µM over a period of 3 h. Volocity® was used to generate measurements such track length, average velocity (µm/sec) for the duration of the track, bearing (degree) and the meandering index (a ratio of displacement from

the origin to track length). In order to generate the final images, a calculated point spread function was generated followed by deconvolution for 30 iterations using Volocity®.

2.3 Statistical Analysis

Statistical analysis was performed using Version 5.0 GraphPad Prism (San Diego, CA). Data sets were analysed using either a One-Way ANOVA with a Bonferroni's post test (all pairs of columns compared) or unpaired student's t-tests. Significance is represented by *p≤ 0.05, **p≤ 0.01, ***p≤ 0.001 and ****p≤ 0.0001.

2.4 Bioinformatics

Nucleotide and protein sequence searches were carried out using NCBI (National Centre for Biotechnology Information) Basic Local Alignment Search Tool (BLAST) (http://blast.ncbi.nlm.nih.gov/Blast.cgi). Gene sequence were searched and extracted from the Ensembl genome browser (http://www.ensembl.org/index.html). Sequencing traces were viewed using FinchTV (Finch TV 1.4.0, Geospiza, (http://www.geospiza.com/finchTV). Nucleotide and protein alignments were carried out using Clustal Omega (EMBL-EBI; http://www.ebi.ac.uk/Tools/msa/clustalo/). The plasmid editor ApE (http://biologylabs.utah.edu/jorgensen/wayned/ape/) and SeqBuilder software (DNAstar; Lasergene, Madison, WI, USA) were used to generate vector constructs and restriction maps for the ZFN and TALEN assembly.

3 Results- The expression, regulation and role of HAX1 in human myeloid cells

3.1 Introduction

The human *HAX1* gene is found on chromosome 1 and contains seven exons in total (Lees et al. 2008). It has been shown to give rise to eight transcript variants through alternative splicing and intron retention (Lees et al. 2008). The gene is highly conserved across many species including rat and mice highlighting its essential function (Mirmohammadsadegh et al. 2003; Grzybowska et al. 2006; Hippe et al. 2006; Lees et al. 2008). The HAX1 protein is known to function to maintain mitochondrial stability thereby promoting cell survival (Suzuki et al. 1997; Sharp et al. 2002; Klein et al. 2007). A role for HAX1 in cell survival is also supported by reports on HAX1 overexpression in several tumours including breast cancer, lung cancer and melanoma (Trebinska et al. 2010).

Human *HAX1* deficiency leads to Kostmann disease, a severe congenital neutropenia (SCN) characterized by low numbers of circulating PMN and increased apoptosis of PMN progenitor cells in the bone marrow (Klein et al. 2007). It has been suggested that HAX1 plays a key role in PMN survival pathways but the possible mechanism is unknown (Klein et al. 2007).

To date, the expression, regulation and function of HAX1 in primary human PMN has not been described. The aims of this chapter were to study the expression of HAX1 at the mRNA and protein level in PMN and the myeloid cell line, PLB-985 and create *HAX1* deficient cells by siRNA transfection of PLB-985 cells. The role of *HAX1* knockdown in key survival assays was explored. Knockdown of *HAX1* in primary human PMN was also attempted.

3.2 Results

3.2.1 Expression of *HAX1* in tissue cell lines and PMN

In order to investigate the expression of *HAX1* in a panel of human cell types, *HAX1* isoform expression was examined using RT-PCR in three cell lines (Beas2B, HeLa and PLB-985), primary peripheral blood mononuclear cells (PBMC) and ultrapurified PMN (>97 % pure) (Fig. 3.1). Published *HAX1* isoform primer pairs were first optimised for their annealing temperature in both PLB-985 and PBMC cDNA (results not shown) (Lees et al. 2008). cDNA for the PBMC and PMN PCRs was pooled from three individual donors in order to reduce donor variability. Primers for transcripts *004* and *007* yielded multiple bands at all of the annealing temperatures tested (50 - 65 °C) and therefore were omitted from the panel.

Amplification of *GAPDH* was used as a loading control. Two negative controls consisting of PCR reactions without template at both the RT and PCR step were also included and no DNA was amplified for any primer pair. Fig. 3.1 shows that the full-length isoform *HAX1 001* (151 bp) along with isoforms *002* (1009 bp), *003* (316 bp), *005* (165 bp) and *008* (297 bp) are expressed in ultrapure PMN and all the other cell types tested. Expression of *HAX1 006* is inconclusive following 35 cycles of PCR due to the lack of a band at the predicted size (548 bp) in the PBMC positive control (Lees et al. 2008). A number of additional bands were present in the PCRs designed to specifically amplify isoform *HAX1 002* and *HAX1 008* and are detected in all cell types, labeled with an asterisk. These additional isoforms were also noted in the previous study by Lees *et al* (Lees et al. 2008).

a.)

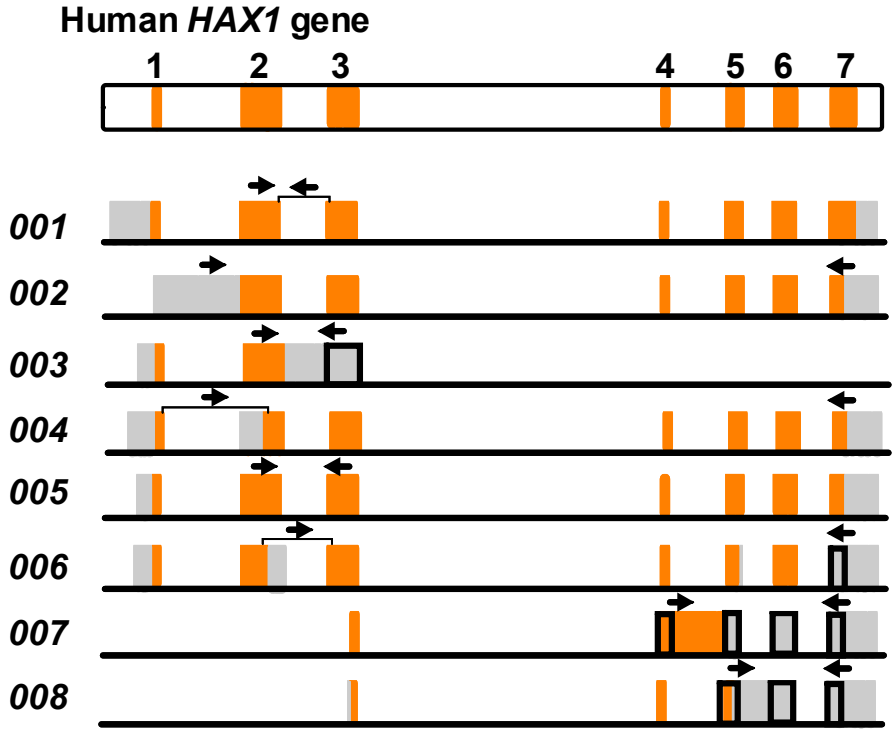

Figure 3.1 Multiple *HAX1* transcripts are expressed in human cell lines and myeloid cells

a.) Image adapted from Lees *et al*. indicating the human *HAX1* primer binding sites (black arrows) used to amplify the different predicted transcript variants (*001-008*) in human cells (Lees et al. 2008). The exons (orange) numbered 1-7 and non-protein coding regions (grey) are also shown.

b.)

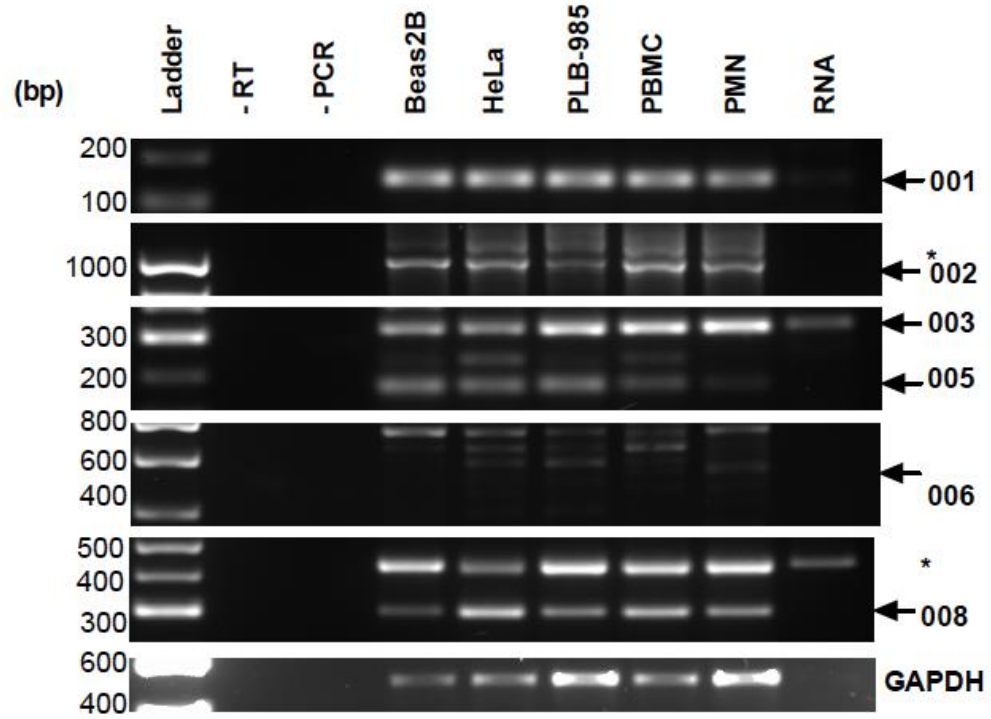

Figure 3.1 Multiple *HAX1* transcripts are expressed in human cell lines and myeloid cells

b.) Total RNA was extracted from Beas2B, HeLa, PLB-985, PBMC and PMN followed by reverse transcription of 2 µg of total mRNA. PBMC and PMN RNA was extracted from three independent donors, reverse transcribed and the cDNA was pooled. The cDNA (4 µl) was amplified using each of the primer pairs, Hax-1 001-008 designed by Lees *et al.* (Lees, Hart et al. 2008). A primer pair specific for GAPDH was used as a loading control. 35 PCR cycles were carried out for all primer pairs shown and bands were separated by agarose gel electrophoresis and visualised using a UV transilluminator. A no template control was included in both the Reverse transcriptase (-RT) and PCR (-PCR) step. Also shown are the results obtained from total RNA extracted without the reverse transcription (RNA). Other putative isoforms are labeled with an asterisk.

HAX1 expression at the protein level was assessed using two commercially available antibodies (obtained from GeneTex and BD Biosciences) raised to two different epitopes of the HAX1 protein. Fig. 3.2 indicates the regions of the protein that each of the antibodies recognize. The overall domain structure of the eight putative isoforms is also presented in Fig. 3.2 indicating the putative isoforms that are likely to be detected by the two different HAX1 antibodies. Whole cell lysates derived from a number of different tissue cell types were subjected to SDS-PAGE and identical membranes were probed with each antibody. Both antibodies detected a band just above the 30 kDa marker that corresponds to full-length HAX1 (32 kDa) (Fig. 3.3). HAX1 is highly expressed in tissue cell lines including PLB-985, which was used as a positive control for HAX1 expression from this point onwards (Tucker et al. 1987).

HAX1 bands were clearly visible in PMN whole cell lysates derived from three independent donors. The existence of bands between the 20 and 25 kDa and at 15 kDa markers should also be noted and may be of interest. Higher molecular weight bands (>35 kDa) were visible with both the GeneTex and BD Biosciences antibody however; this was less evident in the immunoblot incubated with the HAX1 antibody obtained from BD Biosciences. For bands of 30 kDa and below, some similarity of the pattern and intensity of banding between the PMN whole cell lysates and the PMN-like cell line PLB-985 is apparent in both western blots.

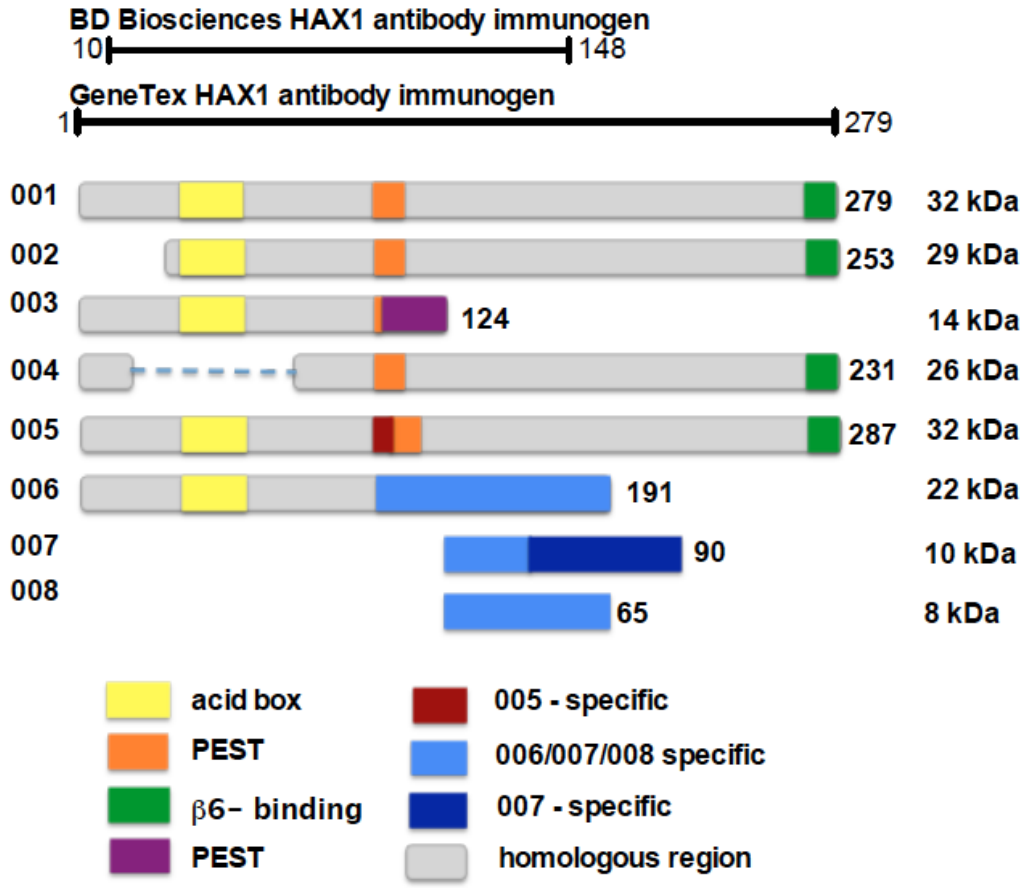

Figure 3.2 HAX1 antibody binding sites

Image adapted from Lees *et al*. showing putative HAX1 isoform domain structure and immunogenic regions for the BD Biosciences and GeneTex antibodies. Each of the eight putative human HAX1 protein isoforms are shown and known domain structures are indicated. Amino acid length and weight of proteins is shown on the right. The monoclonal BD Biosciences Hax-1 antibody was raised against the human HAX1 amino acids 10-148, whereas the polyclonal GeneTex antibody was raised against a recombinant fragment corresponding to the region within amino acids 1 and 279 of full-length isoform 001.

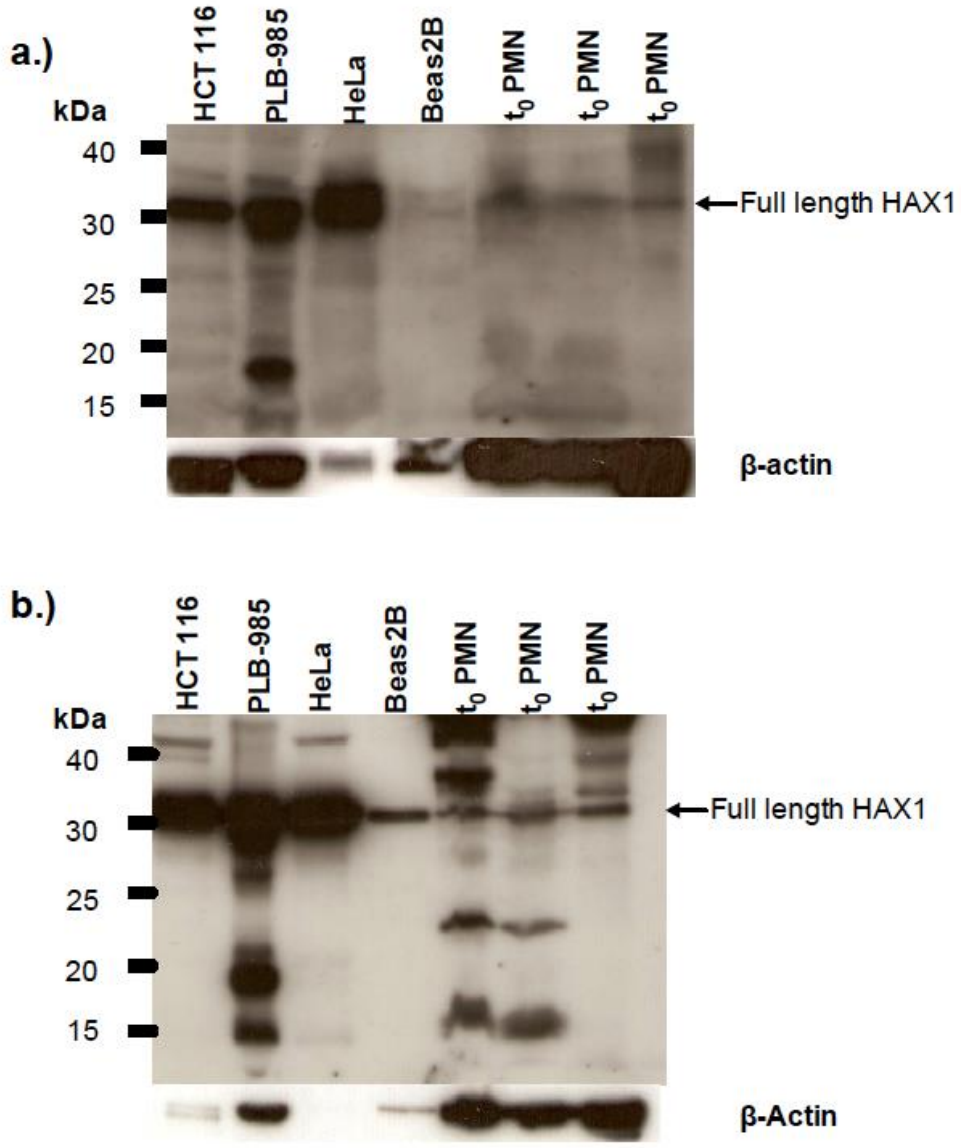

Figure 3.3 Detecting HAX1 at the protein level

Western blots of whole cell lysates from PMN and a number of different human cell lines. Lysates from the same sample were loaded in each SDS-PAGE gel. Immunoblots were stained with the BD Biosciences antibody (1:400) **a.)** and the GeneTex antibody (1:1000) **b.)**. The cell lines from left to right and number of cells loaded per lane are: HCT116 - Human colon carcinoma ($1.5x10^6$ cells), PLB-985- a myeloid leukemia cells ($1x10^6$ cells), HeLa- cervical cancer cells ($5x10^5$ cells), B2B-bronchial epithelial cell line ($2x10^5$ cells). Protein extracted from $2x10^6$ PMN cells was loaded in each lane. Position of protein markers is shown on the left. The membranes were stripped and reprobed with β-actin antibody to assess the loading.

3.2.2 Modulation of HAX1 expression during PMN lifespan

To test whether HAX1 protein levels are regulated during PMN cell ageing, lysates were prepared from PMN incubated at 37˚C (5 % CO_2) for 0, 6 and 18 h. Since PMN contain significant amounts of proteases, which may cleave proteins during the lysis process and therefore affect detection of HAX1, lysates were prepared in the presence or absence of the protease inhibitor, Diisopropylfluoro-phosphate (DFP) in addition to the standard protease inhibitor cocktail. PMN morphological changes and apoptosis rates during constitutive cell death are shown in Fig. 3.4. PMN are seen to shrink and lose their nuclear morphology during apoptosis (Fig. 3.4 a.).

After 18 h in culture more than two thirds of the PMN were apoptotic (66.67% ±11.01) (Fig. 3.4. b.). PMN whole cell lysates at 0, 6 and 18 h in the presence or absence of the protease inhibitor (DFP) were prepared and identical samples were loaded in each of the two western blots shown in Fig. 3.5. Membranes were immunostained with anti-HAX1 antibodies obtained from BD Biosciences (Fig. 3.5 a.) and GeneTex (Fig. 3.5 b.). HAX1 protein levels decreased with aging of PMN, which was observed with both antibodies (Fig. 3.5). While both antibodies give rise to higher molecular weight bands (>35 kDa), Fig. 3.5 (b.) shows that the GeneTex HAX1 antibody produces a number of additional bands of high intensity corresponding to 15 kDa, 22 kDa and 27 kDa protein sizes which do not appear to be regulated during PMN cell death.

The addition of DFP appeared to have no effect on full-length HAX1 during cell lysis but it was clearly seen to have an effect on β-actin where a stronger β-actin signal was detected in the presence of DFP and also the lower molecular weight HAX1 bands (Fig. 3.5). Since the immunoreactivity of HAX1 was reliable for both antibodies, the BD Biosciences HAX1 antibody was used in all western blots shown from hereon.

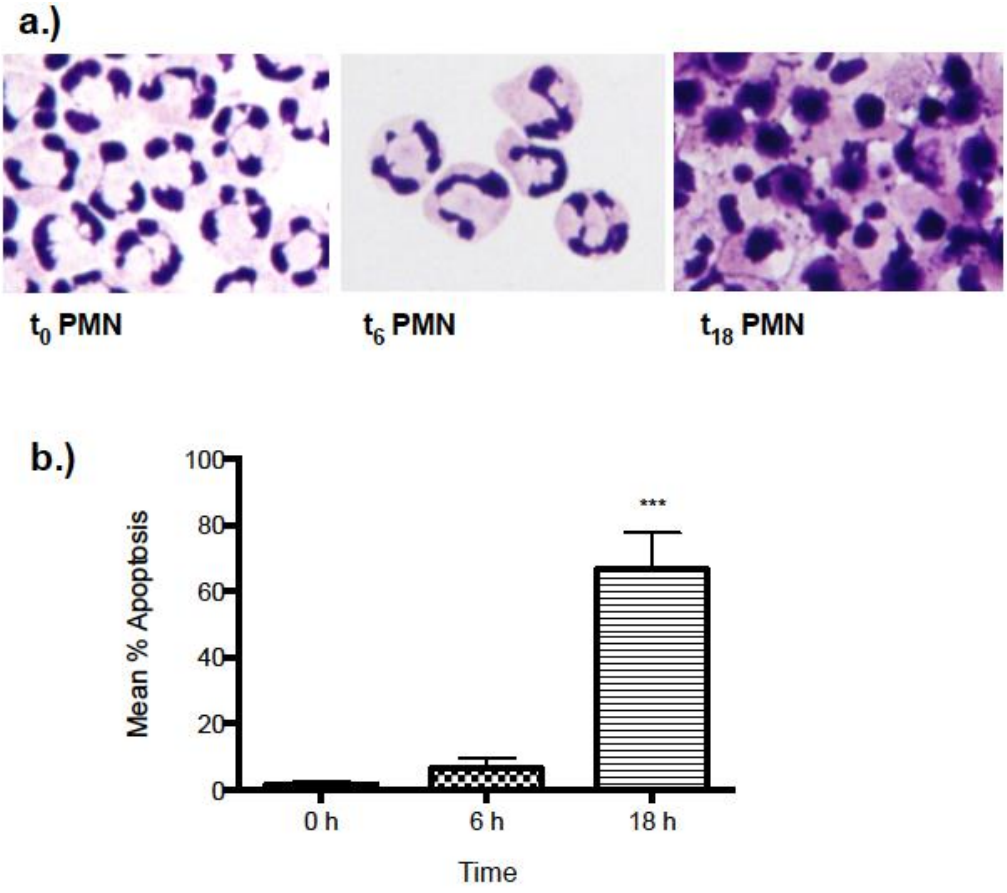

Figure 3.4 Constitutive PMN apoptosis

a.) Morphological assessment of constitutive PMN death**.** PMN were either cytospun immediately (t_0) or cultured in media for 6 (t_6) and 18 h (t_{18}). Cytocentrifuge slide preparations were fixed and stained with Diff-quick solutions 1 and 2 and visualised using a light microscope with X400 magnification. Representative micrographs of cells at different time-points are shown in **a.).** PMN underwent constitutive death displaying morphological changes consistent with apoptosis. Fig**. b.)** shows mean ± SEM percent apoptosis from four independent experiments (n=4), three of which were used to generate samples for the western blots probed with HAX1 antibody shown in Fig. 3.5. Healthy and apoptotic cells were counted from duplicate cytospins. Data were analysed using a one-way ANOVA with Bonferroni's post-test:; ***p≤ 0.0001 test vs untreated; n=4.

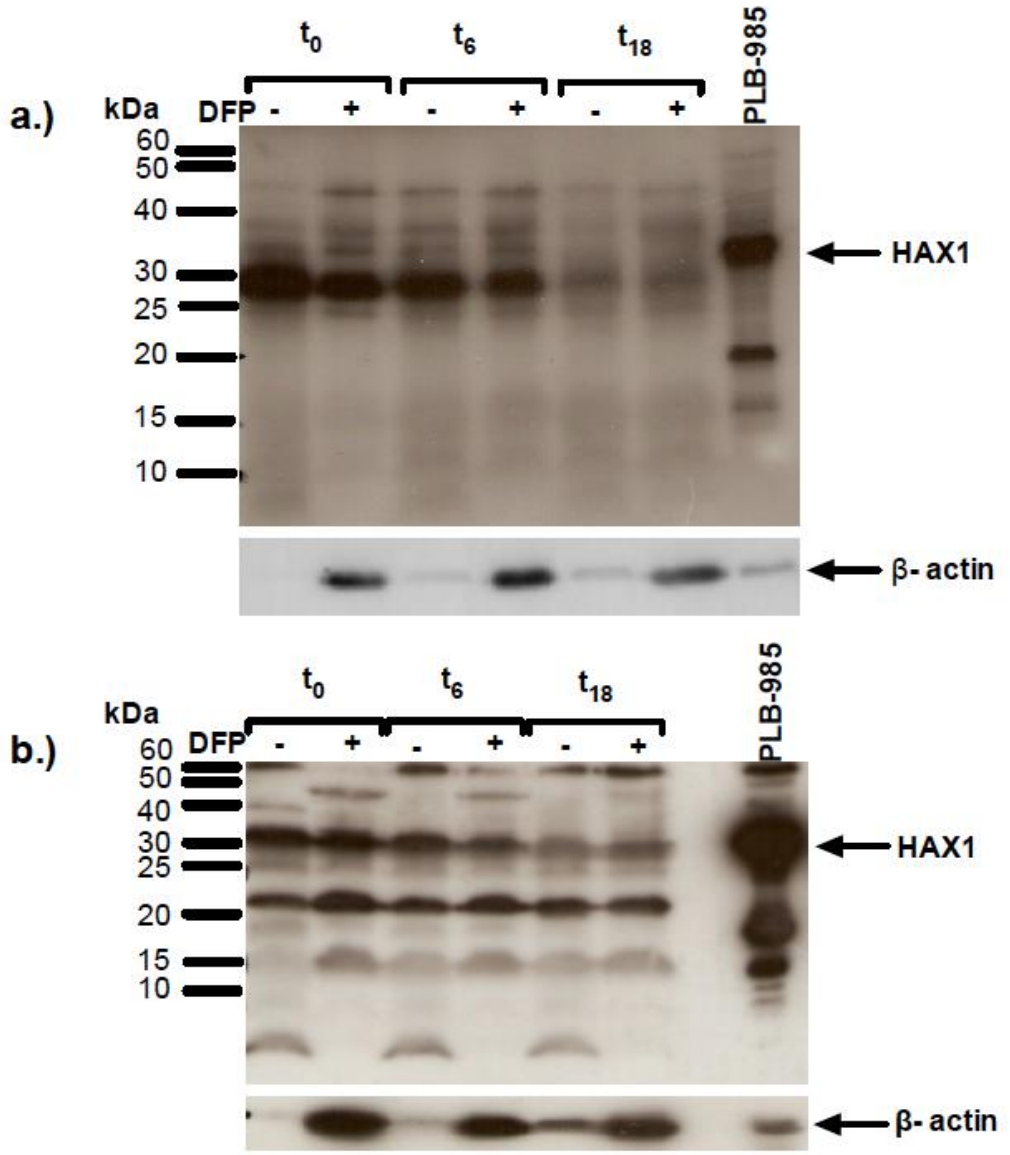

Figure 3.5 HAX1 protein levels decrease during PMN constitutive death

Ultrapure PMN cultured for 0, 6 or 18 h were lysed in the presence or absence of the protease inhibitor DFP. Identical samples were subjected to two western blots. Protein from $2x10^6$ cells was loaded in each lane. **a.)** The membrane was immunostained with Hax-1 antibody from BD biosciences. Blot is representative of three independent experiments (n=3). **b.)** The membrane was immunostained with Hax-1 antibody from GeneTex. Blot is representative of a single experiment. Both blots were stripped and reprobed with antibody to β- actin in order to assess the loading.

The HAX1 expression levels during PMN ageing were analysed by densitometry. The fold changes in HAX1 levels relative to the β-actin loading control significantly reduced at 6 and 18 h time-points compared to 0 h (Fig. 3.6). The reduction in HAX1 levels with time was accompanied by increased apoptosis as shown in Fig. 3.6 (a.). A rapid fall in HAX1 levels in the first 6 h was followed by a gradual decrease from 6-18 h. Fig. 3.6 (b.) shows that the rapid fall in the protein level occurs in the first 6 h of culture and only a small number of cells are apoptotic at this time-point.

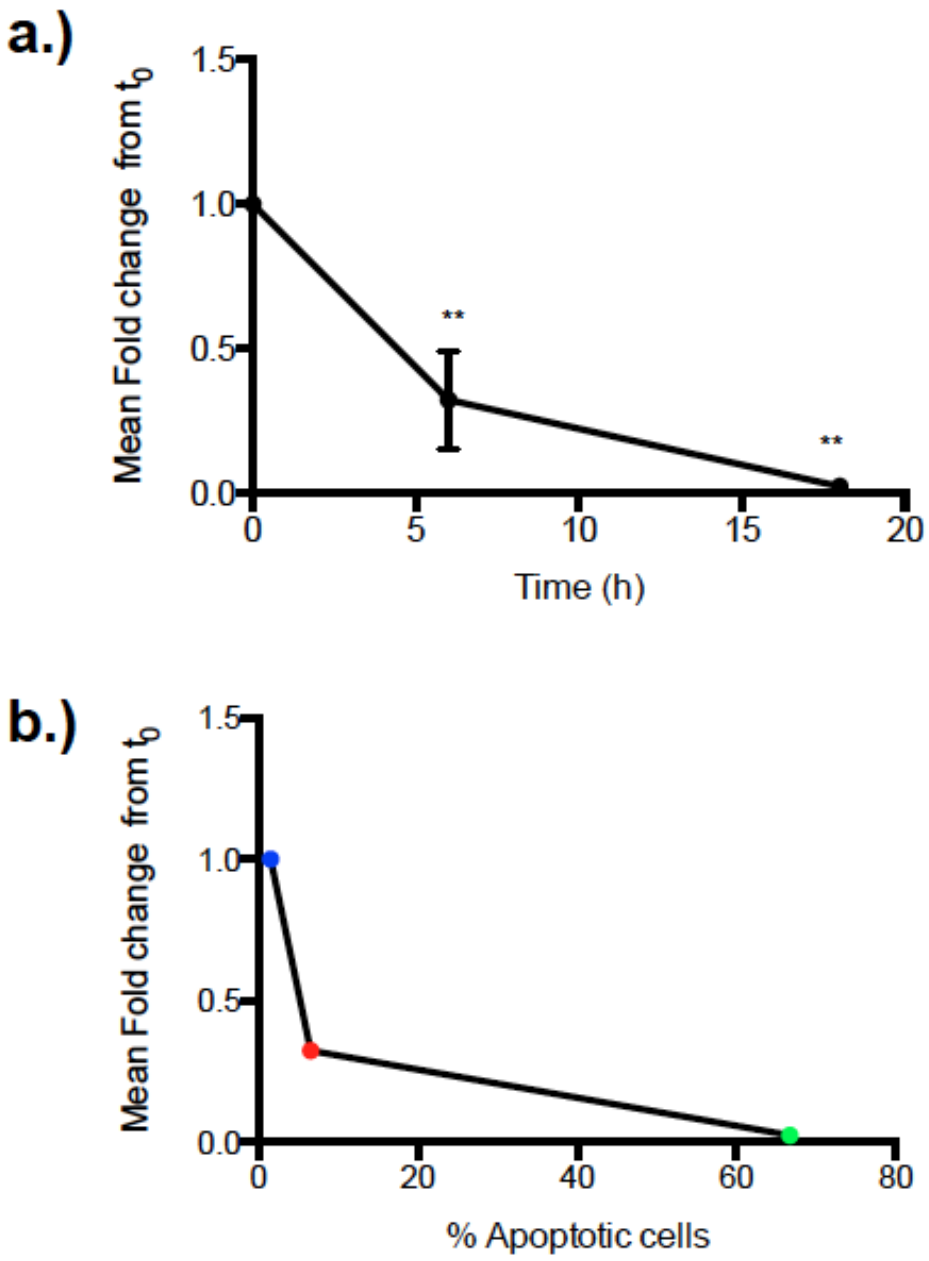

Figure 3.6 Densitometry analysis of HAX1 expression during constitutive cell death

Full-length HAX1 immunoreactive band intensity from 3 independent experiments was quantitated by densitometry and relative expression compared to β-actin control was calculated. Fold change from t_0 (expressed as 1) is shown on the y-axis and time (h) on the x-axis (**a**.). Data from three different time-points (t_0, t_6, and t_{18}) were analysed. (One-way ANOVA with Bonferroni's post-test:; **p≤ 0.001, test vs untreated; n=3). (**b**.) The mean fold change (n=3) was plotted against % apoptosis (n=4) at 0 h (blue point), 6 h (red point) and 18 h (green point).

3.2.3 Regulation of HAX1 in response to inflammatory and death-inducing stimuli

HAX1 mRNA expression was previously shown to be upregulated in response to GM-CSF and LPS in a microfluidics study using human PMN (Kotz et al. 2010). GM-CSF is known to enhance Mcl-1 stability in PMNs (Klein et al. 2000; Derouet et al. 2004). GM-CSF, the potent pan-caspase inhibitor qVD-OPh and heat killed bacteria are known to prolong PMN survival (Brach et al. 1992; Caserta et al. 2003; Baran et al. 1996). Conversely, the bacterial endotoxin pyocyanin and the protein biosynthesis inhibitor cyclohexamide (CHX) have been shown to induce PMN apoptosis (Usher et al. 2002; Gong et al. 1993). To investigate whether HAX1 is regulated at the protein level by these factors that modulate apoptosis, PMN were incubated with inflammatory and death-inducing stimuli and HAX1 expression was explored by western blotting (Fig. 3.7). Ultrapure PMN were cultured in the absence and presence of GM-CSF, pyocyanin, heat killed (HK) *E. coli*, HK *S. aureus*, qVD-OPh and CHX for 6 and 18 h. Cytocentrifuge slides and protein lysates were prepared at the appropriate time-point. HAX1 expression increased relative to the untreated PMN control in response to all of the inflammatory stimuli (GM-CSF, qVD-OPh, HK *E. coli* and HK *S. aureus*). It remained unchanged in response to pyocyanin and CHX. The combined CHX and qVD-OPh treatment of PMN also resulted in increased HAX1 levels.

Densitometric analysis from three independent experiments did not reveal statistically significant changes. This is shown in Fig. 3.8 (a.) and (b.) after 6 h and Fig. 3.8 (c.) and (d.) after 18 h time-points. Changes in HAX1 expression were accompanied by changes in PMN apoptosis rates as assessed by counts on cytocentrifuge slide preparation (Fig. 3.9). The inflammatory stimuli, GM-CSF, qVD-OPh, HK *E. coli* and *S. aureus*, resulted in decreased apoptosis of PMN. On the other hand, CHX lead to significantly increased apoptosis at both 6 and 18 h. Interestingly, cells

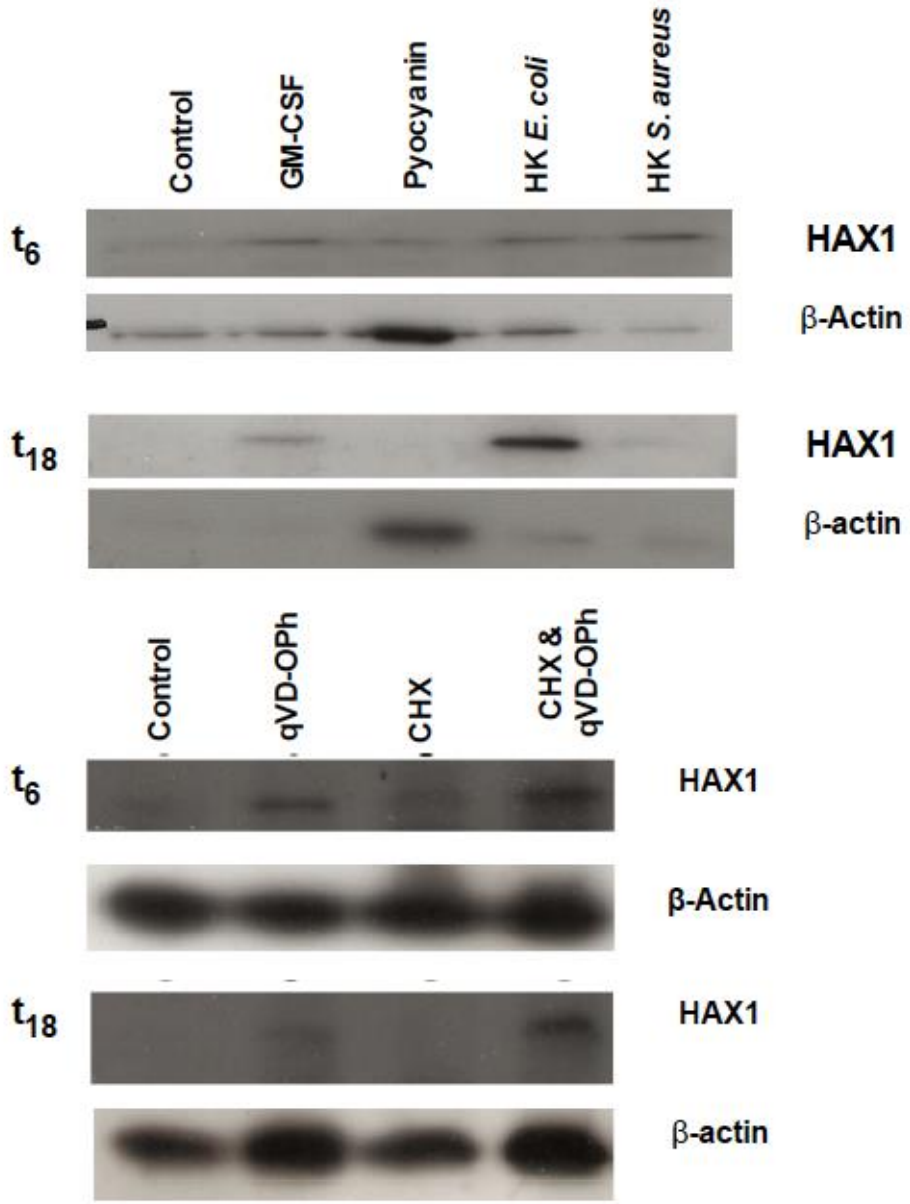

Figure 3.7 Full length HAX1 expression in PMN after treatment with inflammatory stimuli and death inducing agents

Cells were cultured with GM-CSF 50 units / ml, Q-VD.OPh (1 μM), CHX (100 μM), pyocyanin (50 μM), heat killed *E. coli* (MOI = 10) or heat killed *S. aureus* (MOI = 10) for 6 and 18 h. At the relevant time-point, cells were lysed and lysates were subsequently subjected to western blotting. 2 x 10^6 lysed cells were loaded per lane. The western blots were immunostained with HAX1 antibody and stripped and re-immunostained with β-actin antibody to assess the loading. Immunoblots are representative of 3 independent experiments.

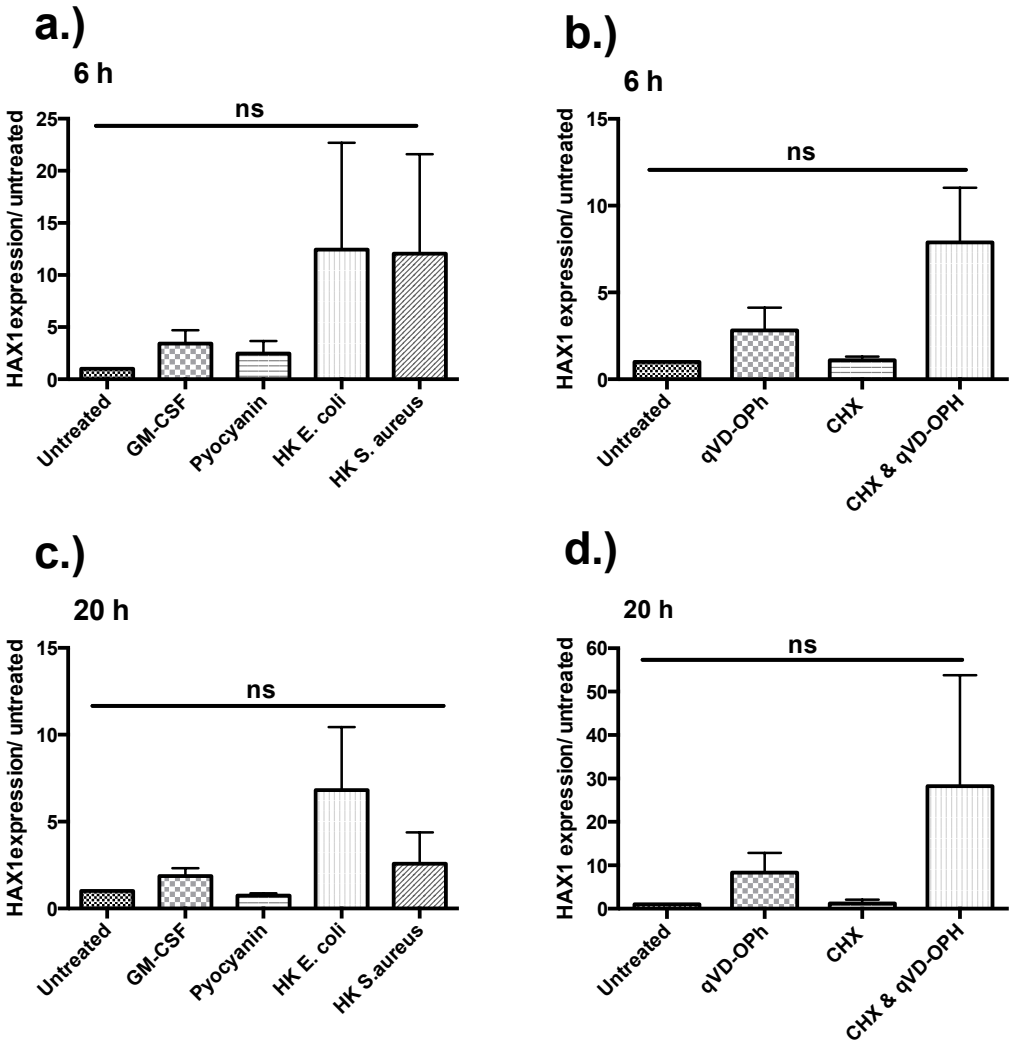

Figure 3.8 Mean fold change in HAX1 expression from untreated control in response to inflammatory and death inducing stimuli

PMN were treated as indicated for 6 h (**a.** & **b.**) or 18 h (**c.** & **d.**) and whole cell lysates prepared as described in section 2.1.10. Samples from three independent experiments were subjected to western blotting for the detection of HAX1 and β-actin loading control. Full-length HAX1 immunoreactive band intensity from 3 independent experiments was quantitated by densitometry and relative expression normalized to the untreated control sample was calculated and is shown on the y- axis in response to each stimulus as well as in the untreated control PMN. Relative densitometry data were analysed using a one-way ANOVA with Bonferroni's post-test, n=3 (ns indicates not significant).

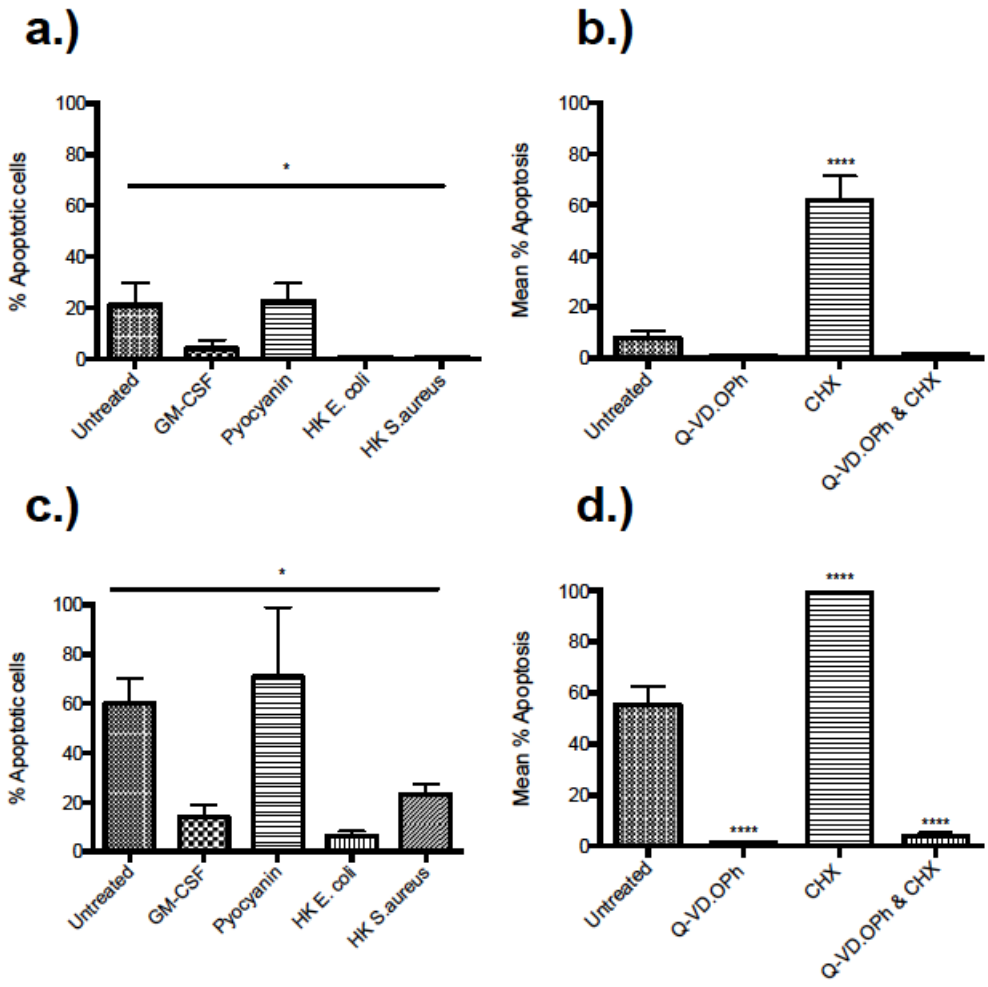

Figure 3.9 Regulation of Apoptosis in response to inflammatory and death inducing stimuli

PMN were treated as indicated for 6 (**a.** & **b.**) or 18 h (**c.** & **d.**) and cytocentrifuge slides were prepared. Slides were fixed and stained with Diff-quick solutions 1 and 2 and visualized using a light microscope with X1000 magnification. Apoptosis rates were scored from duplicate slides and % apoptotic cells are shown for each condition. (One-way ANOVA with Bonferroni's post-test; overall ANOVA for **a.** and **c.** * p≤ 0.05, Bonferroni's post-test ns, **a.** n=4, **c.** n=3; **b.** and **d.**) One-way ANOVA with Bonferroni's post-test; ****p≤ 0.0001, test vs untreated, n=4).

with the combined treatment of CHX and qVD-OPh were significantly less apoptotic at 18 h with qVD-OPh preventing the CHX induced death.

3.2.4 Regulation of HAX1 expression in PLB-985 cells by death inducing agents

In order to establish whether PLB-985 cells have a similar HAX1 expression and regulation profile to PMN, PLB-985 cells were incubated with the death inducing agents CHX and staurosporine (STSP, a protein kinase inhibitor) for 3 h in the presence and absence of qVD-OPh. Cytocentrifuge slides and whole cell lysates were prepared as described in sections 2.1.4 and 2.1.10 respectively. Changes in HAX1 expression were explored by western blotting. In contrast to the media control, incubation with 100 µM CHX and STSP resulted in the appearance of additional HAX1 specific bands indicated by the red arrows in Fig. 3.10 (a.). When cells were co-incubated with the pan-caspase inhibitor qVD-OPh these bands disappeared. Percent apoptosis of control and treated cells from 3 independent experiments is shown in Fig. 3.10 (b.). Interestingly, the loss of the HAX1 specific lower molecular weight bands in cells with the combined CXH or STSP and qVD-OPh treatment was accompanied by abrogation of the CHX-induced apoptosis. PLB-985 cells treated with STSP were significantly more apoptotic than the control. The accelerated apoptosis was inhibited by qVD-OPh. The morphology of these cells is shown in Fig. 3.10 (c.).

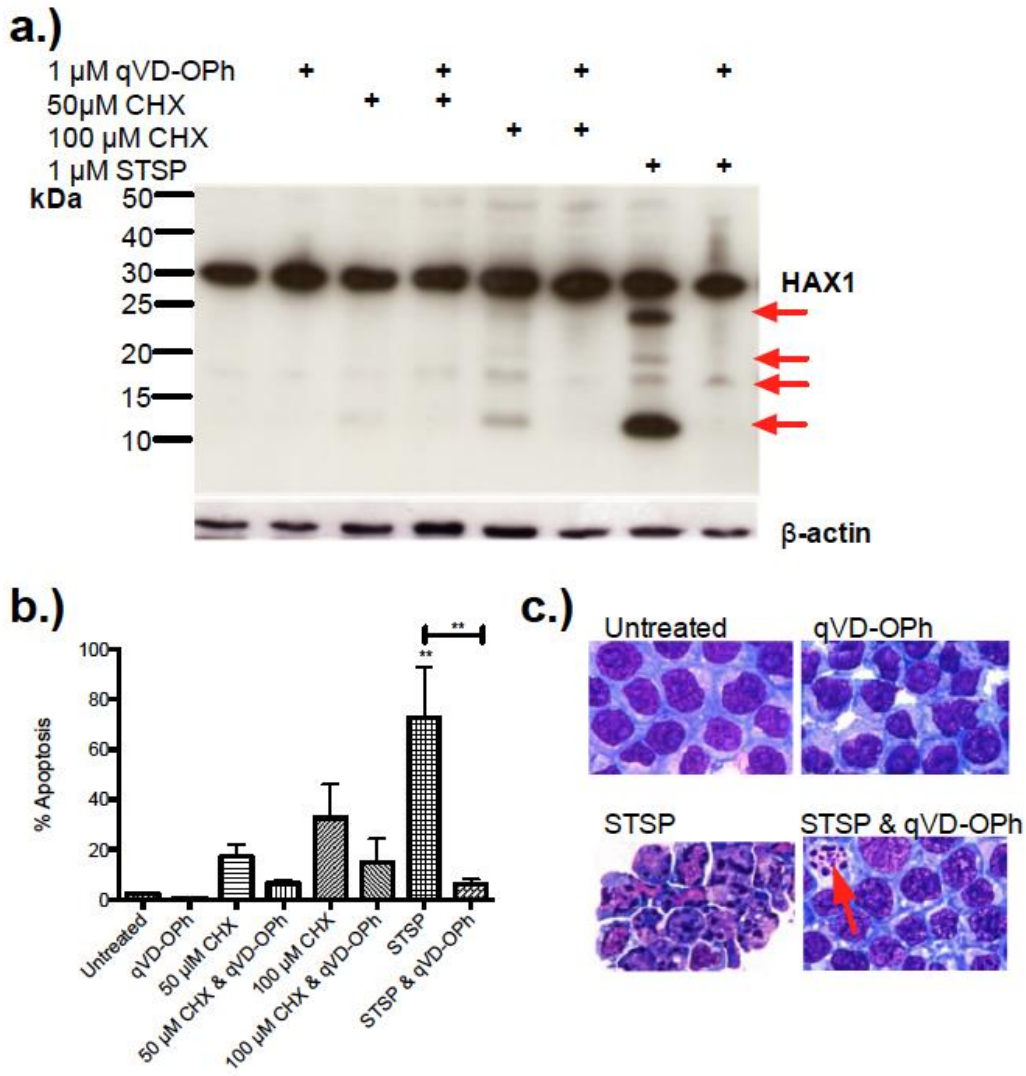

Figure 3.10 HAX-1 is regulated in response to CHX and STSP in PLB-985 cells

PLB-985 cells were incubated with CHX and STSP for three hours with or without a 30 min pre-incubation with qVD-OPh. Protein from $1x10^6$ cells was loaded in each lane and subjected to western blotting (**a.**). The blot was immunostained with HAX1 antibody followed by stripping and re-immunostaining with β-actin in order to assess protein loading. Percentage apoptosis scored from cytocentrifuge slide preparations from the same experiments is shown (bars represent mean ± SEM) in Fig. **b.** (bars represent mean ± SEM). Data were analysed using a one way ANOVA with Bonferroni's post-test:; **p≤ 0.0012 test vs untreated and STSP vs STSP & qVD-OPh; n=3 with qVD-OPh and n=4 without qVD-OPh). **c.** Light micrographs of control, STSP, and combined STSP & qVD-OPh treated PLB-985 cells. An apoptotic PLB-985 cell is indicated by the red arrow.

3.2.5 HAX1 protein levels decrease during PLB-985 differentiation

Healthy cells were treated with various differentiation stimuli over five days; a cell count was carried out on each day followed by preparation of duplicate cytocentrifuge slides. The effectiveness of the differentiation media was assessed by analysis of morphological changes and was compared to primary human PMN. Fig. 3.11 shows images of PLB-985 cells taken on day 4. The arrows indicate the appearance of promyelocytes, metamyelocytes and band cells at different stages of differentiation.

The various stimuli had similar effects on the PLB-985 differentiation state. All stimuli yielded band cells and cells with nuclear indentations in comparison to the round nucleated undifferentiated promyelocytes. Differentiation by combined RA and DMSO treatment of cells generated most PMN-like cells on day 5 (data not shown) however, the combination was toxic to the cells and would not yield high enough numbers of cells to lyse for protein. PLB-985 differentiation was achieved using 1 µM RA in the following experiments.

PLB-985 cells differentiated for 5 days were lysed to generate whole cell protein lysates as described in section 2.1.10. Two cytocentrifuge slides were also prepared to assess the morphological changes. The lysates were subjected to western blotting for the detection of HAX1 protein. Full-length HAX1 levels were downregulated with increased differentiation (Fig. 3.12 a.). Densitometry data analyses of two independent PLB-985 differentiation experiments up to day 3 is shown in Fig. 3.12 (b.) and demonstrates the same trend. Interestingly, as the level of full-length HAX1 protein (~30 kDa) decreased, a second lower molecular weight band (~ 28 kDa) was observed.

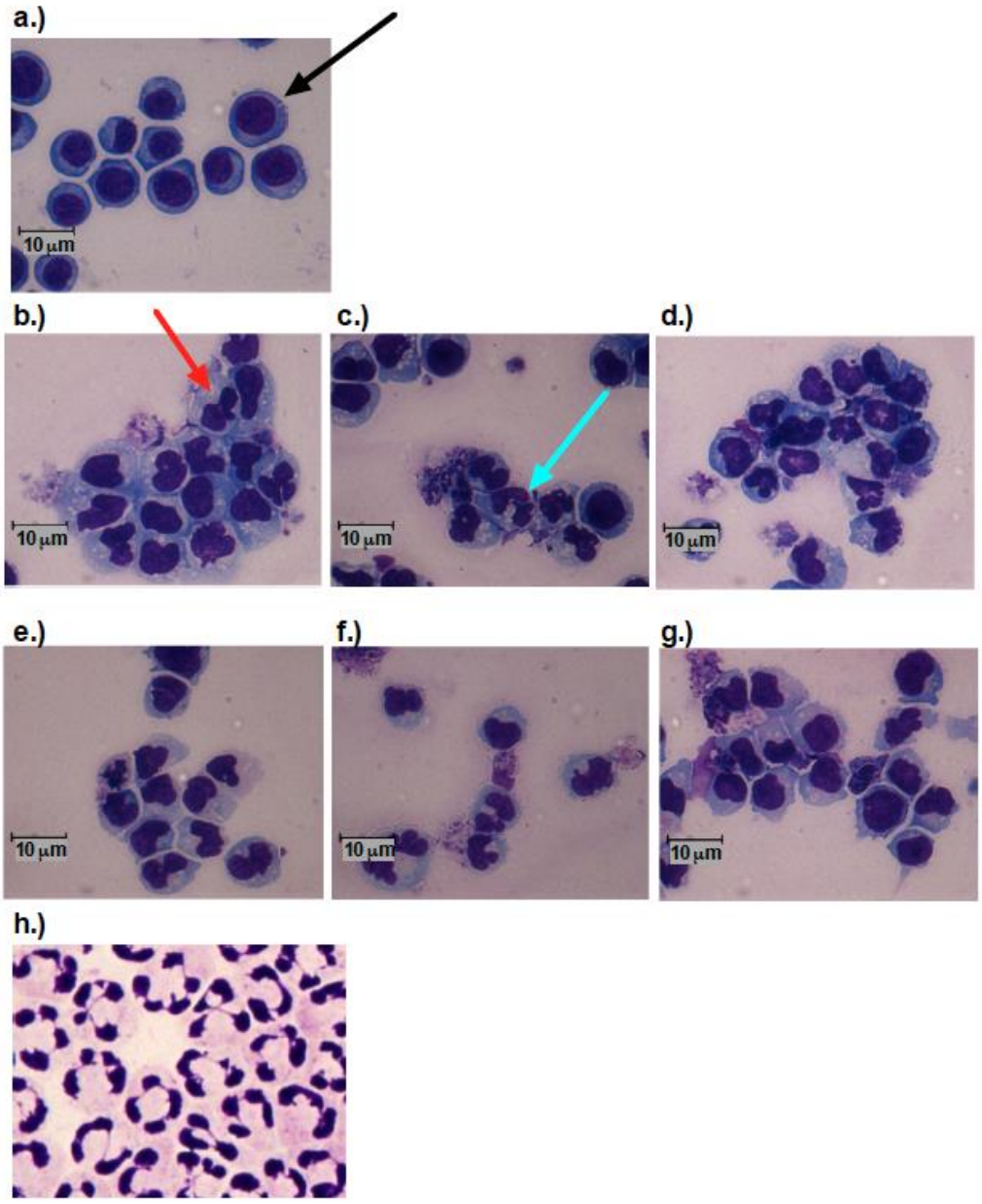

Figure 3.11 Induction of morphological changes during PLB-985 differentiation into PMN-like cells by different stimuli

Undifferentiated PLB-985 cells were cultured in media (**a.**), 0.5 µM RA (**b.**), 0.75 µM (**c.**), 1 µM RA (**d.**), 1 µM RA & 0.5 % DMF (**e.**), 1 µM RA & 1.25 % DMSO (**f.**) or 1.25 % DMSO (**g.**) for four days. A primary PMN image is also shown for comparison. Duplicate cytocentrifuge slides were prepared for each of the conditions and cell morphology assessed by light microscopy. Images were taken at X400 magnification, (black arrow- promyelocyte, cyan arrow- band cell, red arrow- metamyelocyte). Images shown are representative of n=3.

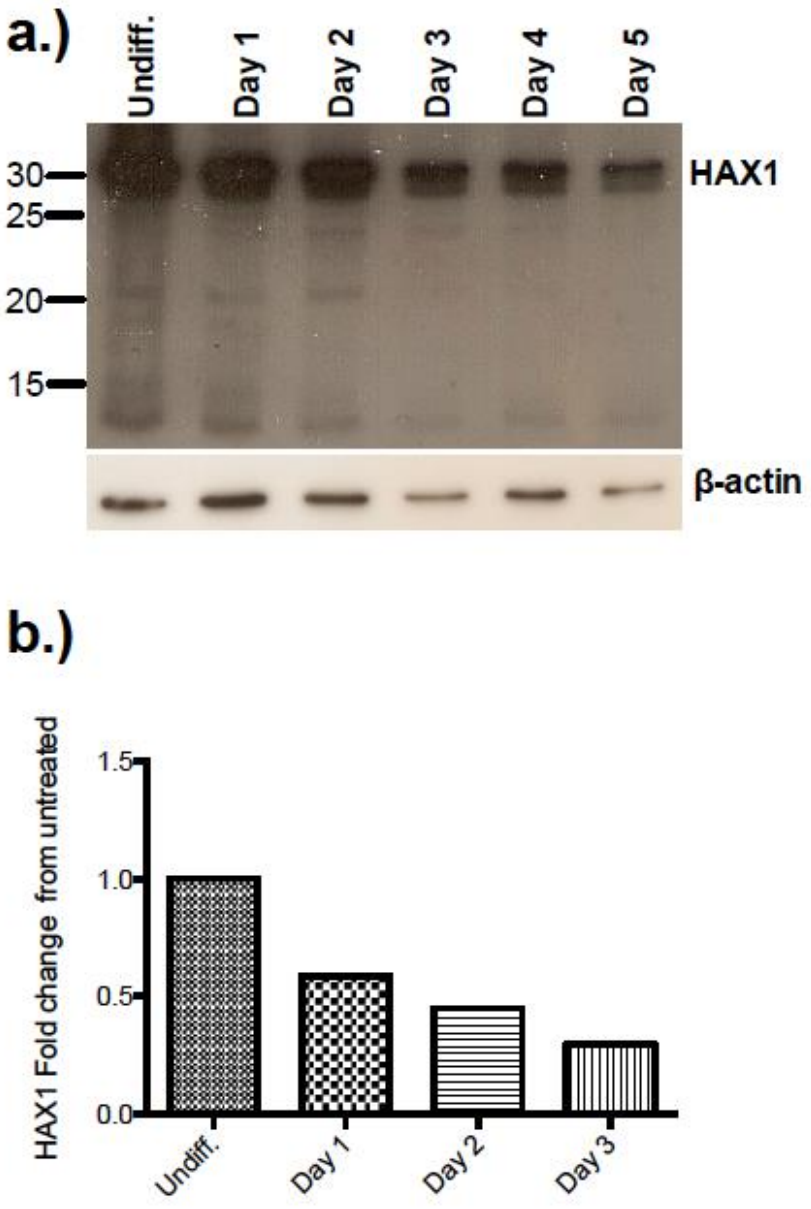

Figure 3.12 HAX1 protein levels are downregulated during PLB-985 differentiation

PLB-985 cells were differentiated over 5 days using 1 μM RA. At the appropriate time-point two cytocentrifuge slides were prepared in order to assess the differentiation and the rest of the cells were lysed for protein. The lysates were subjected to western blotting and blots immunostained with HAX1 antibody **(a.)**. Protein levels were quantitated using Image J as fold change from t_0 (undiff., expressed as 1) relative to the β-actin control and densitometric data showing HAX1 degradation with over 3 days is shown in (**b.**).

3.2.6 Transient knock-down of gene expression in PLB985 cells

In order to test the hypothesis that HAX1 is important in myeloid cell survival and homeostasis, HAX1 specific siRNA (short interfering RNA) strategies to knockdown *HAX1* in PLB-985 cells were followed. siRNAs work by targeting the specific mRNA for degradation via the RNAi (RNA interference) pathway thus preventing gene expression (Martinez et al. 2002). Dharmacon ON – TARGETplus SMART pool siRNA was used which comprised 4 different siRNAs targeting six of the published isoforms, isoforms 001 – 006 (Lees et al. 2008). PLB-985 cells were transfected using the Amaxa nucleofection system™.

3.2.7 Transient Cyclophilin B knock-down in PLB-985 cells

The Amaxa nucleofection system™ had previously been used in PLB-985 cells by others but only for the purpose of delivering plasmid DNA into the cells (Chen et al. 2007). To test the ability of the Amaxa nucleofection system™ to knockdown genes in PLB-985, Amaxa mediated siRNA gene knockdown of the housekeeping gene Cyclophilin B (Cyc B) was optimised. Fig. 3.13 shows successful Cyc B knockdown in PLB-985 cells. Cyc B siRNA transfected cells showed a reduction in Cyc B expression when compared with untransfected and mock-transfected cells (cells that underwent electroporation in the presence of nucleofection solution V without any siRNA) relative to GAPDH levels.

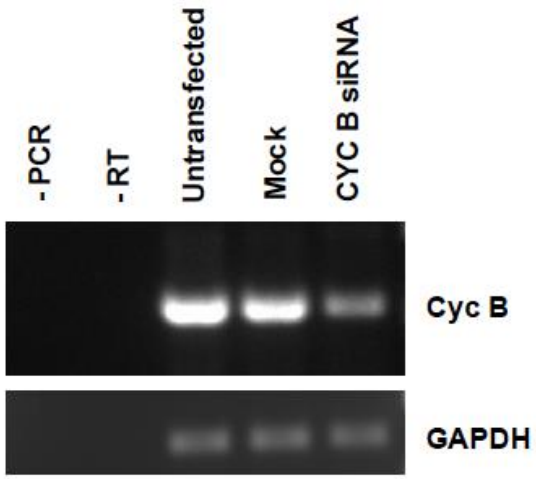

Figure 3.13 Cyclophilin B knockdown in PLB-985 cells

PLB-985 cells (3 x 10^6) were transfected with Cyc B siRNA or nucleofection solution V only (Mock control) and cultured for 24 h following transfection. Total RNA was then extracted from control untrasfected, mock transfected and CYCB siRNA transfected cells. Following reverse transcription the cDNA was amplified using primers specific for either Cyc B or GAPDH loading control and samples were subjected to agarose gel electrophoresis. A no template control was included in both the reverse transcription (-RT) and PCR (-PCR) step.

3.2.8 Transient *HAX1* knock-down in PLB-985 cells and its effect on apoptosis and mitochondrial membrane stability (Δψm)

Since we determined that Cyc B gene expression could be disrupted using siRNA transfected via the Amaxa nucleofection system™, we went on to investigate the effects of *HAX1* knockdown in PLB-985 cells. *HAX1* ON–TARGETplus SMART pool siRNA was transfected into PLB-985 cells and knockdown was analysed at the mRNA level by RT-PCR and protein level by western blotting. The siRNA was designed to target four different regions of the mRNA spanning all of the isoforms published by Lees *et al.* (Lees et al. 2008). HAX1 levels were visibly reduced at 10 h and 24 h following transfection in response to HAX1 siRNA when compared to the untransfected and scrambled siRNA controls (Fig. 3.14 a.). *HAX1* knockdown had no effect on apoptosis rates at 24 h post transfection (n=6) (Fig. 3.14 b.). In addition, the knockdown was without effect on mitochondrial membrane permeability (Δψm), an early marker for commitment of PMN to apoptosis, when compared to the untransfected and mock-transfected controls assessed by JC-1 staining (Fig. 3.15). The potassium ionophore valinomycin (Val) is known for its role in inducing apoptosis through its actions on decreasing Δψm (Janeway Jr. & Medzhitov 2002). Val treated cells underwent a large dissipation of Δψm as shown by the profound increase in FL-1 signal in all conditions. The *HAX1* siRNA transfection did not enhance the loss of Δψm in these experiments.

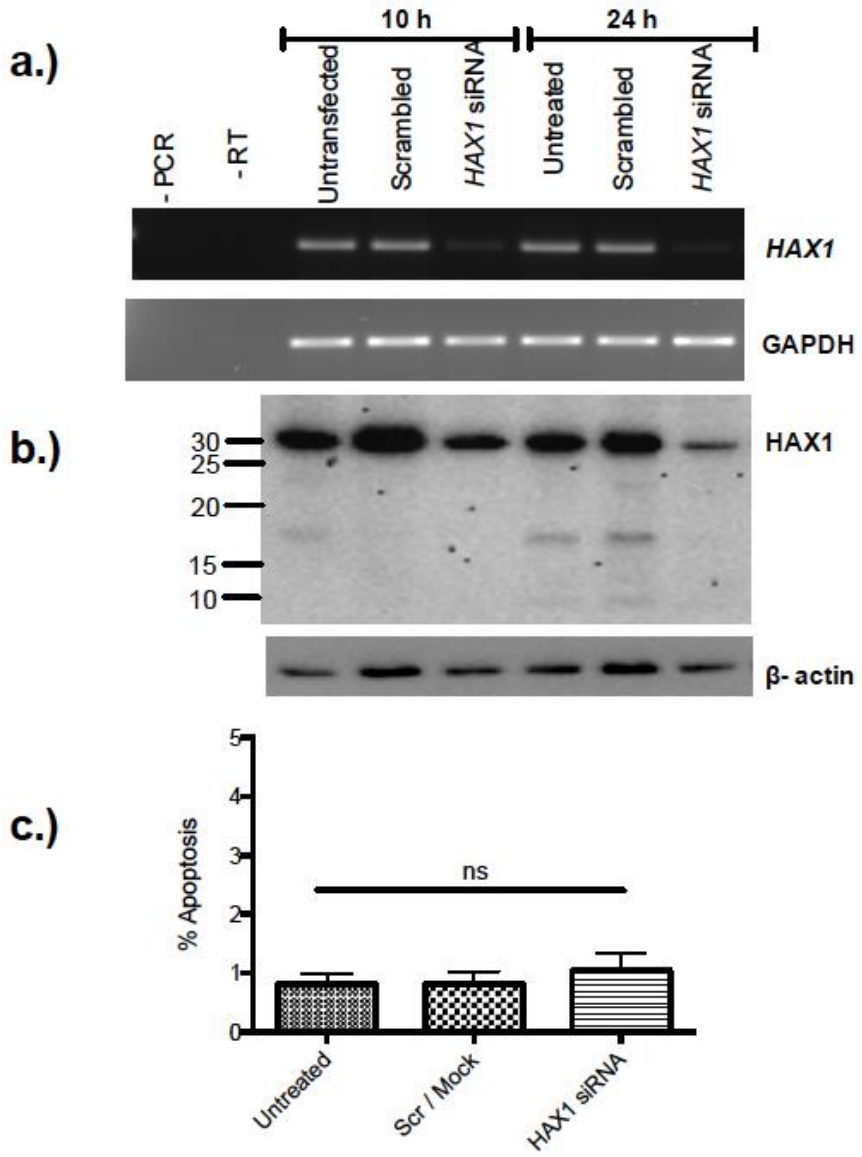

Figure 3.14 Transient *HAX1* knockdown in PLB-985 cells does not induce apoptosis

PLB-985 cells (3 x 10^6) were transfected with scrambled, *HAX1* siRNA or nucleofector solution V only (mock) using Amaxa. RNA and protein were extracted at 10 and 24 h (n=6) and knockdown was assessed by RT-PCR (**a.**) and western blotting (n=2) (**b.**). Percent apoptosis was quantified by light microscopy at 24 h post-transfection (**c.**). Apoptosis counts from six independent experiments are shown and were analysed using a one way ANOVA with Bonferroni's post test; n=6). ns indicates not significant.

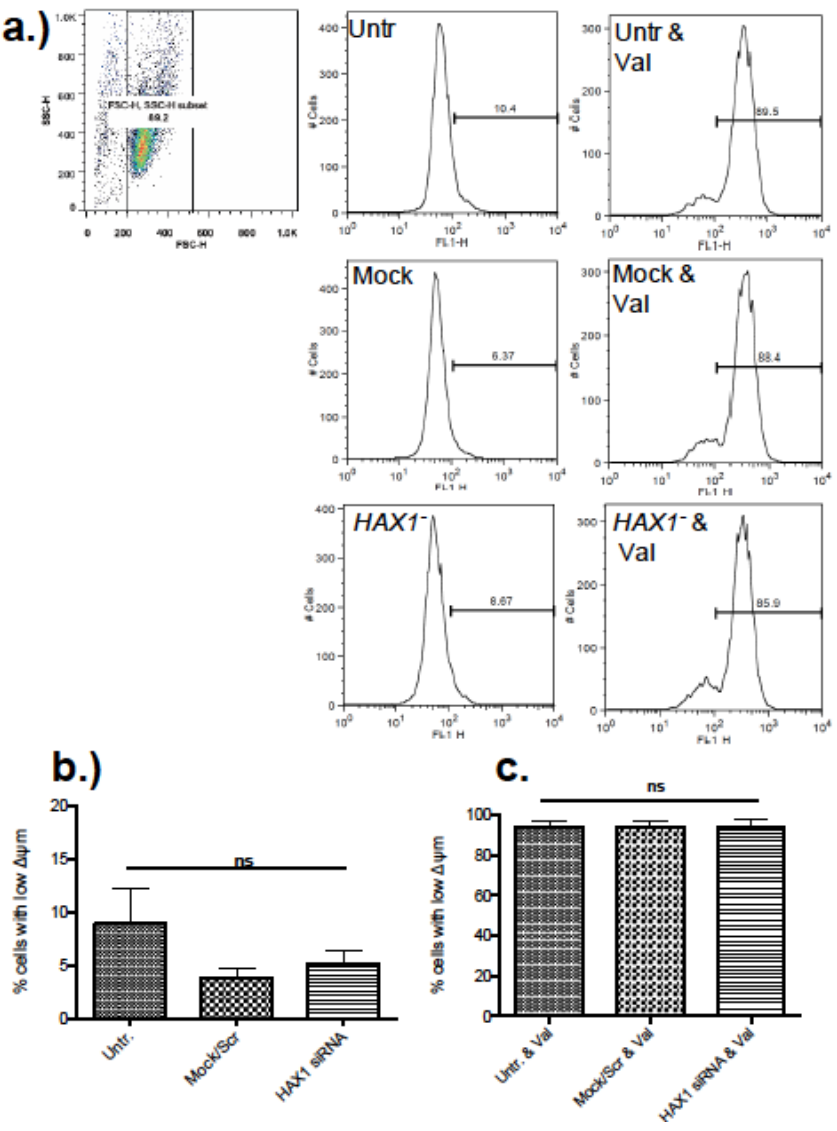

Figure 3.15 The effect of *HAX1* knockdown in PLB-985 cells on mitochondrial transmembrane potential (Δψm)

PLB-985 cells were transfected with scrambled control siRNA, *HAX1* siRNA or nucleofector solution V only (mock). Loss of Δψm was detected using the cationic dye JC-1 in control and knockdown cells at 24 h post-transfection in cells with and without a 3 h treatment with 5 µM valinomycin (Val). Gain of green fluorescence (FL-1) indicative of loss of Δψm was measured in intact cells identified by forward (FSC) and side scatter (SSC) characteristics using flow cytometry. Representative histograms are shown in Fig. **a.**. Basal changes in control and *HAX1* knockdown cells are shown in Fig. **b.** and changes induced by Val are shown in Fig. **c.**; bars represent mean % ±SEM, (one way ANOVA with Bonferroni's post-test, p≤ 0.05, n=3).

3.2.9 The effect of *HAX1* siRNA encapsulated polymerosomes on *HAX1* levels in human PMN

A recent study has shown that polymerosomes (nanometre-sized vesicles) can be utilised as nanovectors for the delivery of active proteins into cells and targeting of intracellular mechanisms (Canton et al. 2013). Polymerosomes are non-cytotoxic and have also been used for rapid and efficient intracellular delivery of nucleic acids (Lomas et al. 2008). During my studies, a member of Dr Steve Renshaw's lab (James Robertson) has generated unpublished evidence that knockdown of Mcl-1 accelerates PMN apoptosis *in* vitro using polymerosome encapsulated siRNA. PLB-985 cells are undifferentiated myeloid progenitors and therefore differ from PMN in many ways and therefore in order to investigate whether HAX1 knockdown has an effect on PMN apoptosis, we attempted to knockdown the gene in primary human PMN using polymerosome encapsulated *HAX1* siRNA. These experiments were carried out in collaboration with James Robertson, who had previously optimized the technique. Cells were treated with GM-CSF in order to prolong survival, allowing enough time for efficient delivery of the siRNA and gene knockdown. Untreated and PBS treated controls were included. Cells were incubated with polymerosomes containing 20 μM *HAX1* siRNA (prepared in PBS). Following 30 h of culture, the cells were harvested for protein and mRNA. Since Mcl-1 is known to play a role in PMN apoptosis, encapsulated Mcl-1 siRNA was also used as a positive control. Samples were subjected to RT-PCR and western blotting. Fig. 3.16 shows that the *HAX1* and Mcl-1 siRNA encapsulated polymerosomes were unsuccessful in knocking down the respective genes in PMN tested at the transcript and protein level for HAX1 and only protein level for Mcl-1.

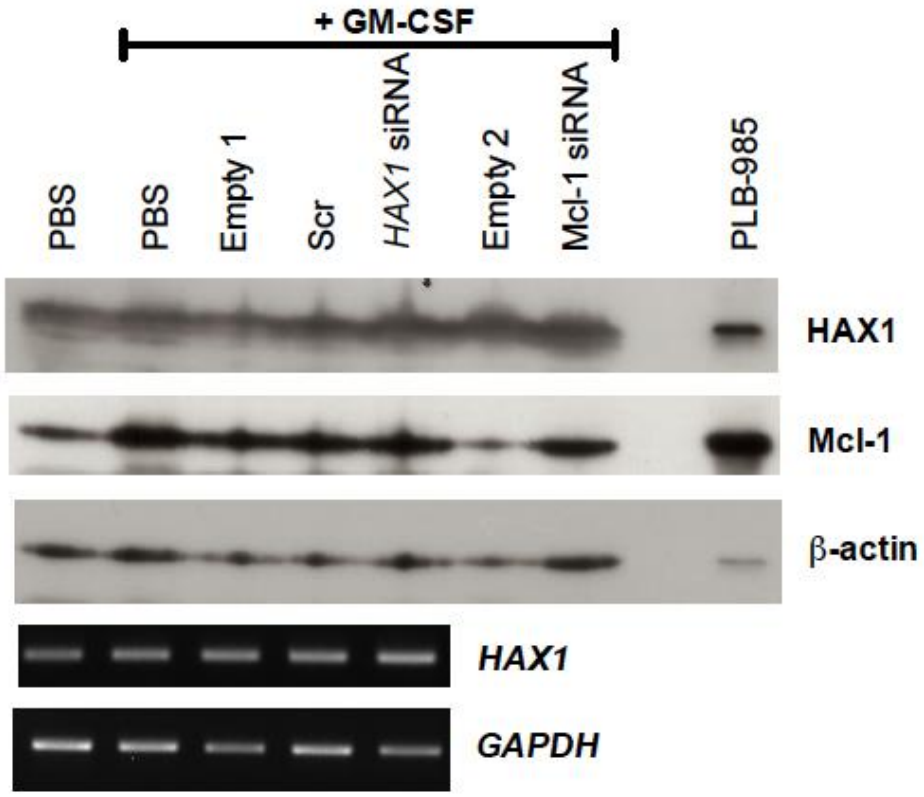

Figure 3.16 Effects of polymerosome encapsulated *HAX1* siRNA on PMN HAX1 protein levels

Ultrapurified cells were cultured with 20 μM polymerosome encapsulated siRNA and 50 u of GM-CSF for 30 h. Since the encapsulation efficiencies were different for the *HAX1* and Mcl-1 siRNAs, two different doses of empty polymerosome were applied to control for the number of polymerosomes added to the cells (Empty 1 and Empty 2). A PBS control in the presence and absence of GM-CSF was also included. At the appropriate time point the cells were lysed for RNA (0.5 x 10^6) and protein (2 x 10^6) and analysed by RT-PCR and western blotting. Once probed with HAX1 the western blot was then stripped and re-immunostained with MCL1 antibody. This was followed by a second stripping and reprobing with β-actin to assess the loading. Images are representative of 3 independent experiments (n=3).

3.3 Summary

The aim of this chapter was to investigate the expression, regulation and function of HAX1 in PMN and PLB-985 cells. Expression was analysed at both the transcript and protein level. siRNA technology was applied in order to test the effects of *HAX1* knockdown on cell survival and mitochondrial membrane potential.

I found that human PMN and PLB-985 cells express multiple *HAX1* isoforms at the mRNA level including the full-length isoform 001. HAX1 expression in human PMN and PLB-985 cells at the protein level was also confirmed. Although HAX1 protein levels were shown to increase in response to anti-apoptotic factors, GM-CSF and qVD-OPH as well as heat killed bacteria, the increase in HAX1 expression is likely to reflect the apoptosis rates. In PLB-985 cells, incubation with death inducing stimuli generated lower molecular weight HAX1 specific bands. Interestingly, HAX1 levels decreased as PLB-985 cells gained a more PMN-like morphology during differentiation. Furthermore, I found that transient knockdown of *HAX1* in PLB-985 did not affect basal apoptosis rates or mitochondrial membrane stability.

3.4 Discussion

3.4.1 HAX1 expression in human myeloid cells

3.4.1.1 HAX1 isoforms

Lees *et al*. first reported the existence of multiple HAX1 isoforms in a panel of different cell types (Lees et al. 2008). This study found that at least six isoforms are transcribed in any one particular tissue. There was no specific expression pattern associated with the cell types. In the same study, it was demonstrated that at least two out of three PBMC samples expressed all of the isoforms. Therefore, the PBMC sample used for this thesis functioned as a positive control for the expression of the different HAX1 transcript variants. In agreement with Lees *et al.* findings, the

transcript expression in this chapter shows numerous isoforms exist in PMN and PLB-985 cells.

I have shown that PMN express the full-length HAX1 (001 - 31.6 kDa) variant at both the transcriptional and protein level. This is the most abundant isoform in many different cell types (Lees et al. 2008). Isoforms *002*, *003*, *005* and *008* were also detected in PMN, PLB-985, HeLa and Beas2B cells at the mRNA level. The lack of *006* expression demonstrated in this chapter is in agreement with Lees *et al*. who revealed a restricted distribution of this isoform in their panel of 19 human cell lines (Lees et al. 2008). Isoform 006 detection was limited to cell lines VB6 (squamous cell carcinoma,), BT20, T47D, ZR75 (all of which are breast carcinomas), SW620 (colon adenocarcinoma) and A375M (melanoma) (Lees et al. 2008).

Isoform 005 (32.4 KDa) is also a common isoform with a very similar protein size to 001 (31.6 KDa). Therefore, if this isoform were also to be expressed in PMN we would be unable to distinguish between the two isoforms on a conventional western blot and it is possible to mistake one isoform for the other. Our transcript expression data demonstrate that *HAX1 005* is not very highly expressed in PMN and that the HAX1 immunoreactive band present at 30 kDa is most likely to represent isoform 001. Further experiments such as antigen competition or protein sequencing of the immunoreactive product would be required to be certain of the exact protein species. Bands <30 kDa in size are also visualised in the panel of cells by western blotting. We can speculate as to the potential isoform identity of the remaining bands based on previous work by Lees *et al*. (Lees et al. 2008).

Although our transcript data does not identify any myeloid cell lineage specific isoforms, HAX1 specific bands are visible in PMN as well as PLB-985 cells in the western blots (Fig. 3.3). Both HAX1 antibodies bound to bands lower than 30 kDa in size. On analysis of the sizes of the putative HAX1 protein variants generated by Lees *et al*. through *in silico*

translation, it becomes apparent that the 15 kDa band seen in both PLB-985 and PMN cells may correspond to isoform 003 while the 23 kDa band only visible in the PMN samples could correspond to isoform 006. All three isoforms (001, 003 and 006) contain exon 2, which is mutated in Kostmann syndrome patients (Klein et al. 2007; Lees et al. 2008), suggesting that exon 2 is critical for PMN function. These three bands appear to be specific to the PLB-985 and PMN cells at the protein level and could play myeloid specific roles.

Using the BD Biosciences HAX1 antibody, Germeshausen *et al* showed that in HL-60 cells HAX1 runs as a doublet at ~35 kDa with the upper band being described as isoform 001 and the lower band described as isoform 004 (Germeshausen et al. 2008). Although bands are detected around the 30-35 kDa size in our western blots the high expression of full-length HAX1 in the PLB-985 cells combined with the low resolution of the western blots does not allow us to verify the expression of isoform 004. However, this is visible in Fig. 3.12 (a.) showing the expression of HAX1 during PLB-985 differentiation where lower numbers of lysed cells were used. The possibility that these bands are phosphorylated forms of the same isoform was ruled out in a study carried out by Lees *et al.* who saw no modulation of the bands after treatment with serine, threonine and tyrosine phosphatase inhibitors prior to lysing cells for western blot analysis (Lees et al. 2008).

Higher molecular weight >50 kDa HAX1 forms have also been implicated in the regulation of apoptosis (Yap et al. 2011). Bands larger than 50 kDa in size are visible in our western blots when immunostaining with BD and GeneTex HAX1 antibodies. Yap *et al* found that ~65 kDa, ~50 kDa and 25 ~ kDa protein bands showed restricted expression to normal breast epithelium and were absent from tumorigenic breast epithelium (Yap et al. 2011). This led them to propose that these forms may promote cell death. Control of apoptosis in this fashion is seen with Mcl-1 (Bae et al. 2000). Although Mcl-1 is a pro-survival protein, a truncated transcript variant of Mcl-1 known as Mcl-1s possesses only the pro-apoptotic BH3

domain and its expression results in apoptosis. If this were the case with HAX1 then levels of these HAX1 isoforms would be expected to increase during apoptotic cell death. Our results indicate that the additional HAX1 bands described by Yap *et* al. do not appear to be upregulated during PMN cell death (Fig. 3.5).

3.4.2 Mechanisms of HAX1 regulation in myeloid cells

3.4.2.1 Regulation of PMN apoptosis

Our data generated by western blotting suggest that HAX1 protein levels decrease with the increasing age and apoptosis of PMN (Fig. 3.6). Since the HAX1 reduction occurs in conjunction with increased apoptosis rates, it raises the question whether HAX1 protein is simply being degraded by caspase activity during the late stages of apoptotic cell death or whether the reduction in HAX1 levels is upstream of the caspase activation and would therefore play a causative role in mediating cell death. HAX1 protein has previously been identified as a substrate of caspase 3 and is cleaved at Asp127 during apoptosis (Lee et al. 2008). This study suggests that a loss of hax1 may reflect an event that occurs once the apoptotic process has been engaged rather than being upstream of apoptosis.

The decrease in HAX1 protein level in Fig. 3.6 (b.) is time dependent and appears to precede apoptosis in the sense that the percentage of apoptotic cells at the 6 h time-point is very low, however HAX1 levels are reduced by more than half. This may suggest that HAX1 plays a role in PMN survival and that HAX1 protein degradation may occur upstream of the activation of the apoptotic pathway. Since morphological changes only appear after the onset of apoptosis further work would be required to investigate this.

3.4.2.2 HAX1 expression during PLB-985 differentiation

In agreement with previous transcript data, HAX1 protein levels decreased as PLB-985 differentiated from less prolific to more terminally differentiated and PMN-like cells (Theilgaard-Mönch et al. 2005). In support of this, a paper published during this PhD also reported the decrease in HAX1 protein expression as PLB-985 cells differentiated (Cavnar et al. 2011). This suggests that HAX1 may play more important roles in undifferentiated myeloid cells. The high expression in the myeloid progenitors may protect the cells from apoptosis and loss of HAX1 with time as cells become terminally differentiated could allow PMN to rapidly undergo apoptosis. A recent study showed myeloid cells derived from congenital neutropenia patients with *HAX1* deficiency were arrested at the myeloid progenitor cell stage with increased predisposition to apoptosis, supporting a role for HAX1 in the differentiation pathway of myeloid cells (Morishima et al. 2013).

3.4.2.3 Effects of HAX1 knockdown on PLB-985 Apoptosis and Mitochondrial stability

If HAX1 is functionally more important in progenitor myeloid cells then HAX1 knockdown in PLB-985 cells would provide a good system for investigating HAX1 function. However, PLB-985 cells are a cell line and caution should be taken when interpreting data obtained from cell lines, particularly in models of cell death.

The function of HAX1 in myeloid cells was investigated by transiently knocking down *HAX1* in PLB-985 cells using siRNA. Percentage apoptotic death of the PLB-985 cells that had been transfected with *HAX1* siRNA was compared to that of cells transfected with non-specific scrambled siRNA or mock-transfected controls. Interestingly, these studies showed that HAX1 had no effect on PLB-985 and mitochondrial membrane stability (a common component of cell death) or apoptosis assessed by morphological analysis of cytospin preparations. Due to the lack of expression of phosphotidyl-serine in undifferentiated PLB-985

cells we were unable to confirm this finding by Annexin V binding by flow cytometry (Huynh et al. 2002). It is important to note that Fig. 3.14 shows that although most of HAX1 is knocked down at both the transcript and protein level, a very small amount of protein remains and may be sufficient to inhibit any phenotype.

Published studies on HAX1 knockdown in cell lines provide contradictory data. Contrary to our findings, *HAX1* targeting by siRNA in a study carried out by Li *et al.* resulted in increased apoptosis of melanoma cells (Li et al. 2009). Further support for a role of HAX1 in apoptosis is provided by Sun *et al.* demonstrating that HAX1 knockdown inhibited the malignant phenotypes of EC9706 cells while overexpression of the gene promoted cell proliferation against cisplatin in the same cell line (Sun et al. 2012). During the course of my studies, a study was published containing work carried out on PLB-985 cells. In agreement with our knockdown data, it was found that *HAX1* knockdown by lentiviral shRNA technology in PLB-985 cells showed no decrease in the basal level of apoptosis and only a mild increase in apoptosis in response to H_2O_2 (Cavnar et al. 2011). HAX1 was shown to instead be involved in regulating PMN adhesion and chemotaxis through GTP-ase RhoA (Cavnar et al. 2011).

Analysis of cell death in the *Hax1* $^{-/-}$ mouse however, suggests that HAX1 does have a role in PMN apoptosis since the lack of HAX1 was reported to have an effect on PMN apoptosis (Chao et al. 2008). Although the authors of the study focused on the effect of the *Hax1* knockout in lymphocytes and studies in granulocytes were limited, they presented a single piece of evidence where they demonstrated that G-CSF deprived PMN from the *Hax1* null mice were more apoptotic than PMN from wild type mice.

Controversial data suggests that the mitochondrion plays a central role in PMN apoptosis (Maianski et al. 2004). Klein *et* al. have previously generated strong support for an essential role of HAX1 in maintaining mitochondrial membrane stability (Klein et al. 2007). They showed that

circulating $CD34^+$ cells isolated from SCN patients underwent accelerated apoptosis due to loss of Δψm, which was prevented by transduction with a HAX1 encoding retrovirus. Further support for an anti-apoptotic function of HAX1 comes from mammalian studies investigating HAX1 protein-protein interactions in the mitochondria. It has been proposed that in human cardiac myocytes HAX1 directly interacts with caspase 9 in the mitochondria and inhibits its activation (Han et al. 2006). The protein has also been shown to present Omi (high-temperature regulate A2) to mitochondrial PARL (pre-senilin associated, rhomboid-like) and facilitate its processing into an active protease which in turn prevents the accumulation of the pro-apoptotic protein Bax (Chao et al. 2008).

It has previously been shown that *HAX1* deficiency is associated with defective expression of the mitochondrial protein Bcl-2 and constitutive release of cytochrome c from the mitochondria (Carlsson et al. 2004). In viral models, the HIV Vpr protein was shown to interact with HAX1 and cause it to dislocate from its normal residence in the mitochondrial membrane to the cytosol (Yedavalli et al. 2005). This would imply that perhaps a global decrease in HAX1 levels and therefore its dislocation from the mitochondria causes mitochondrial instability in myeloid cells and results in the onset of apoptosis. This does not appear to be the case in PLB-985 cells in our studies as transient *HAX1* knockdown did not affect basal changes in the mitochondrial membrane potential when analysed by JC-1 staining in *HAX1* knockdown and control transfected cells.

3.5 Conclusion

I have provided evidence for HAX1 expression at both the transcript variant and protein level in primary human PMN and a number of cell lines including the myeloid leukaemia cell line, PLB-985. I have shown that HAX1 protein levels decrease as PMN undergo constitutive apoptosis. Using the caspase inhibitor qVD-OPh and a number of inflammatory stimuli, I have demonstrated that HAX1 protein levels are

higher in response to these stimuli when compared to control untreated cells and that this is accompanied by reduced apoptosis rates. This suggests that the increased HAX1 levels in response to the PMN survival stimuli are likely to reflect the apoptosis rates and result directly from caspase inhibition by qVD-OPh. Furthermore, I have determined that HAX1 protein levels are regulated during PLB-985 differentiation and apoptosis. Finally, I have provided evidence that HAX1 knockdown in PLB-985 cells does not affect basal PMN apoptosis and mitochondrial membrane stability. The high complexity generated by the appearance of a multiple HAX1 banding pattern in western blotting and PCR techniques, in addition to the lack of tools for the genetic manipulation of human primary PMN and the limitations of using the cell line PLB-985 highlight a need for a new model for the study of HAX1 function in PMN survival.

4 Results- *hax1* expression and transient knockdown in *Danio rerio*

In the previous chapter, I discussed the limitations of the studies of *HAX1* function in the human and the lack of evidence for HAX1 function from patient data. In the model organism, the mouse, a *Hax1*$^{-/-}$ null mutation resulted in postnatal lethality (Chao et al. 2008). Therefore, the *in* vivo role of HAX1 in PMN remains unknown and there is need for new tools to discover its immediate molecular, cellular, and developmental functions.

The zebrafish have emerged as a powerful research model for the study of vertebrate development and haematopoiesis. Following fertilisation, zebrafish embryos survive with only the innate immune system for 4-6 weeks (Lam et al. 2004). This temporal separation provides an excellent opportunity for the study of innate immunity in isolation *in vivo*. Many of the components of zebrafish innate immunity have remarkable similarities to their mammalian counterparts (Lieschke 2001). The transparent larval model also allows visualisation of the PMN through the use of the *Tg(mpx:GFP)i114* transgenic line (Renshaw et al. 2006). These properties together with the availability of a large range of tools for the study of genetic factors drove us to utilise the zebrafish for the *in vivo* study of *hax1* gene function.

To date there have been no studies examining zebrafish *hax1* variant expression or function. The exon/intron organization of the zebrafish *hax1* gene is the same as that of the human, comprising 7 exons. Based on this, I hypothesized that the splicing of the zebrafish *hax1* gene is similar to that reported for the human *HAX1* gene with multiple variants arising from alternative splicing and intron inclusion. The aim of this chapter was to investigate the expression of *hax1* mRNA in the zebrafish embryos and to validate the use of morpholinos as a suitable tool for studying *hax1* function in vertebrate embryos.

4.1 RNA extraction from zebrafish embryos

To assess whether total RNA extracted from zebrafish embryos using the TRI reagent protocol (Section 2.1.15) is of good quality and therefore can subsequently be used for RT-PCR, RNA was extracted from EKK and AB embryos at 1-4 days post fertilization (d.p.f). Total RNA was then resolved on a 1% denaturing agarose gel. Fig. 4.1 shows that all of the RNA samples have two sharp bands which correspond to 28S and 18S rRNA (ribosomal RNA). In most lanes the 28S rRNA band is more intense than the 18S rRNA with no visible smearing under the 18 S rRNA band indicating that the RNA is intact and of good quality. This showed that RNA extraction from zebrafish embryos using TRI reagent yields good quality RNA that can be used in downstream processing reactions such as RT-PCR.

4.2 Multiple *hax1* transcript variants are expressed in the zebrafish

In order to study Hax1 function in the zebrafish it was first necessary to explore the *hax1* transcript expression. Due to the same exon-intron structure (Figure 4.2 a.), I hypothesized that the splicing of the zebrafish *hax1* gene is similar to that seen in the human and designed isoform specific primers based on this hypothesis. *hax1* primers were designed to selectively amplify the following transcript variants: *001* (964 bp), *002* (1150 bp), *003* (1625 bp), *005* (130 bp), *007* (907 bp) and *008* (592 bp). Two extra sets of primers were also designed. The first pair was intended to amplify additional variants that may have arisen from splicing occurring between exon 1 and 7 of the gene (variant *x*- 818 bp). The second primer pair was designed to amplify multiple transcript variants; this set of primers is denoted simply as *hax1* (984 bp) and is likely to amplify variants *001, 002* and *003*. The primer annealing temperatures for each primer pair were optimised on a gradient of 55- 65 °C using cDNA from embryos at 1 and 2 dpf. Primer sequences and binding sites are shown in Appendix 7.3.

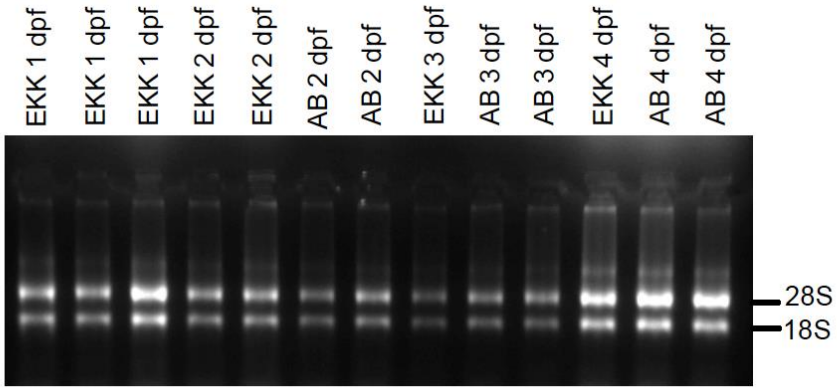

Figure 4.1 Assessment of RNA qualities extracted from zebrafish embryos at various stages of development

Total RNA was extracted from embryos of EKK and AB strains at 1-4 dpf using TRI reagent. The quality of the RNA was assessed by denaturing agarose gel electrophoresis. RNA bands were visualised using a UV transilluminator. The 18S and 28S rRNA bands are shown.

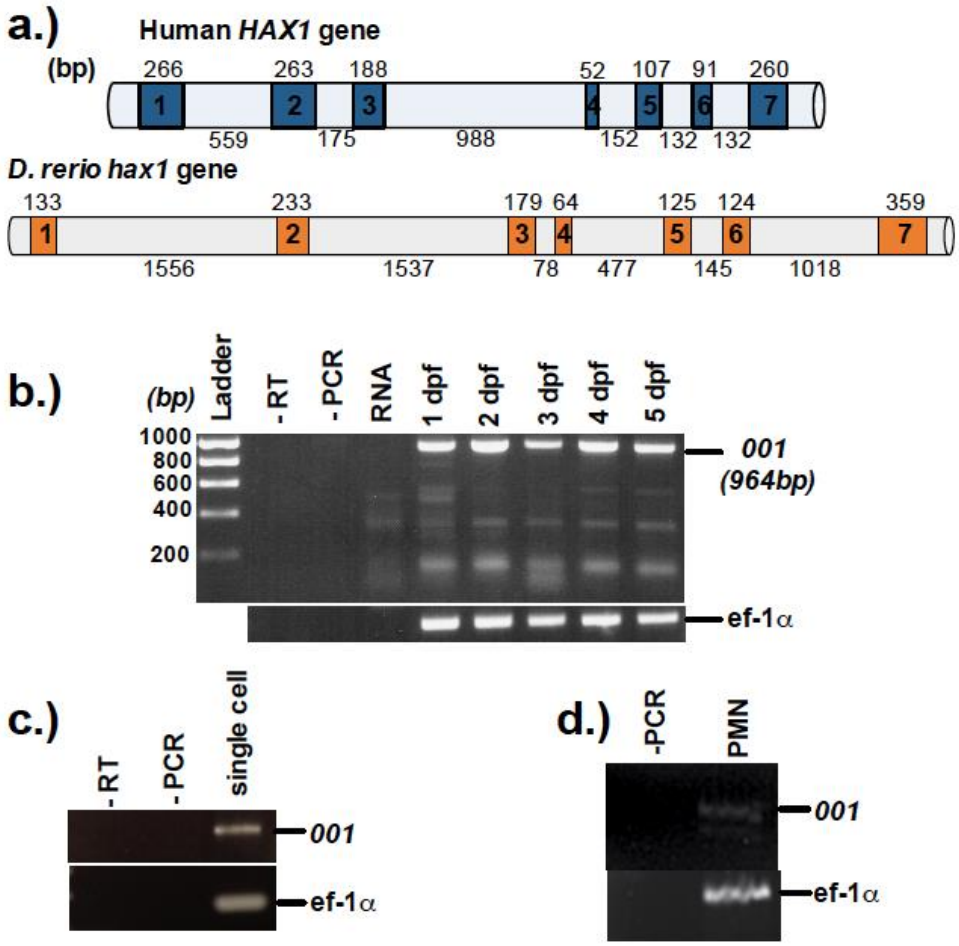

Figure 4.2 Zebrafish express the putative *hax1* full length transcript at different stages of development

a.) Exon-intron structure of the human and zebrafish *hax1* genes. Exons are shown in blue (human) and orange (zebrafish). **b.)** RNA was extracted from *Tg(mpx:GFP)i114* embryos at different stages of development (1-5 dpf) using TRI reagent. This was followed by RT-PCR using primers for amplification of *hax1 001* (full length) with Phusion High-Fidelity DNA Polymerase. The results obtained from total RNA extracted from 2 dpf embryos without the reverse transcription (RNA) and a no template control for the RT (-RT) and PCR (-PCR) steps are also included. **c.)** RNA was extracted from zebrafish embryos at the single cell stage (single cell) and RT-PCR was carried out using *hax1 001* and ef-1 α loading control primers. **d.)** cDNA from adult *Tg(mpx:GFP)i114* zebrafish FACS sorted GFP +ve (PMN) cells was amplified by PCR using *hax1* specific primers (isoform x primers). Also shown is a negative PCR control lacking the template cDNA (-PCR) and the results from PCR with the ef-1 α loading control. PCR bands were resolved by agarose gel electrophoresis and visualised using a UV transilluminator.

To examine the expression of *hax1* full-length transcript *001* in zebrafish embryos at different stages of development. RNA extracted from embryos at 1-5 dpf was subjected to RT-PCR. The PCR products were resolved by agarose gel electrophoresis. Fig. 4.2 (b.) shows that a band corresponding to *hax1 001* was visible in embryos at all of the developmental stages tested, 1-5 dpf. Lower molecular weight bands are also visible but at a much lower intensity. Amplification of *ef-1α* was used as a loading control and also produced an amplicon at the expected size in all of the samples tested. The two additional negative controls consisting of reactions without template at the RT and PCR step were clear for both the *hax1 001* and *ef-1α* primer pairs.

It has previously been shown that some mRNAs are maternally transferred to fertilised zebrafish eggs playing essential roles in the early stages of embryonic development (Dosch et al. 2004). The onset of gene activation in the zebrafish is delayed until the midblastula transition at which stage the embryo consists of around 1000 cells (Kane & Kimmel 1993). To investigate whether *hax1 001* mRNA is maternally transferred, RNA was extracted from embryos at the single cell stage. This was followed by RT-PCR for the detection of *hax1 001*. PCR analysis shows that *hax1 001* is present in the single cell embryo mRNA (Fig. 4.2 c.). A band of the expected size was also visible in the RT-PCR reaction carried out using the *ef-1α* loading control primers while the negative RT-PCR controls remained clear.

In order to determine the presence of the *hax1 001* transcript in the adult zebrafish PMN, the cDNA of PMN was subjected to 35 cycles of PCR with *hax1* 001 and *ef-1α* primers. To visualise the bands PCR products were separated by agarose gel electrophoresis and imaged using a UV transilluminator. Emily Hogget, a former BMedSci student in Dr Renshaw's lab, prepared the cDNA. Briefly, RNA was extracted from PMN of *Tg(mpx:GFP)i114* zebrafish adult tissue sorted by FACS (fluorescence activated cell sorting), gated on the green fluorescence-positive events. It was then reverse transcribed to generate cDNA. Due to

limited sample availability I was only able to carry out the PCR on the PMN sample once. PCR analysis shows that a band of the expected size for the transcript was detected in the PMN sample (Fig. 4.2. d.). Variant *001* from zebrafish embryos was cloned into a TOPO blunt vector and sequenced to confirm expected splicing pattern. As in the human, zebrafish *hax1 001* is comprised of all seven exons of the gene. Blast analysis of the sequencing output is shown in Fig. 4.3.

Having established that the full-length *hax1 001* transcript is expressed in zebrafish embryos, I next investigated whether other putative transcript variants resulting from alternative splicing and/or intron inclusion are also expressed. The same RNA extracted from embryos at 2 dpf and used in the RT-PCR analysis of variant *001* (Fig. 4.2) was subjected to RT-PCR using primers specific for the different *hax1* isoforms. PCR products of the expected sizes were detected for putative transcript variants *002*, *007* and *008* (Fig. 4.4). I was unable to reliably detect variants *003 and* 005 in zebrafish embryos. Multiple PCR bands were visible in the reactions with primers specific for isoform *003 & 005* and *007*. Some of these bands were also detected in the sample not subjected to reverse transcription (-RNA) confirming that these were generated from the amplification of contaminating genomic DNA and not cDNA. Primers for isoform *007* did not always produce the same pattern of banding as highlighted by Fig. 4.4 (b.). Primers amplifying isoform *x* (labelled as *x*) also produced a strong band at ~ 800 bp. Fig. 4.4 also shows the PCR products for the positive PCR primers, *ef-1α* with relatively high levels found in the samples indicating that the samples were likely to have good quality cDNA for amplification with *hax1* primers. The existence of additional species visible with all of the primer pairs except that amplifying *hax1* variant *008* should be noted.

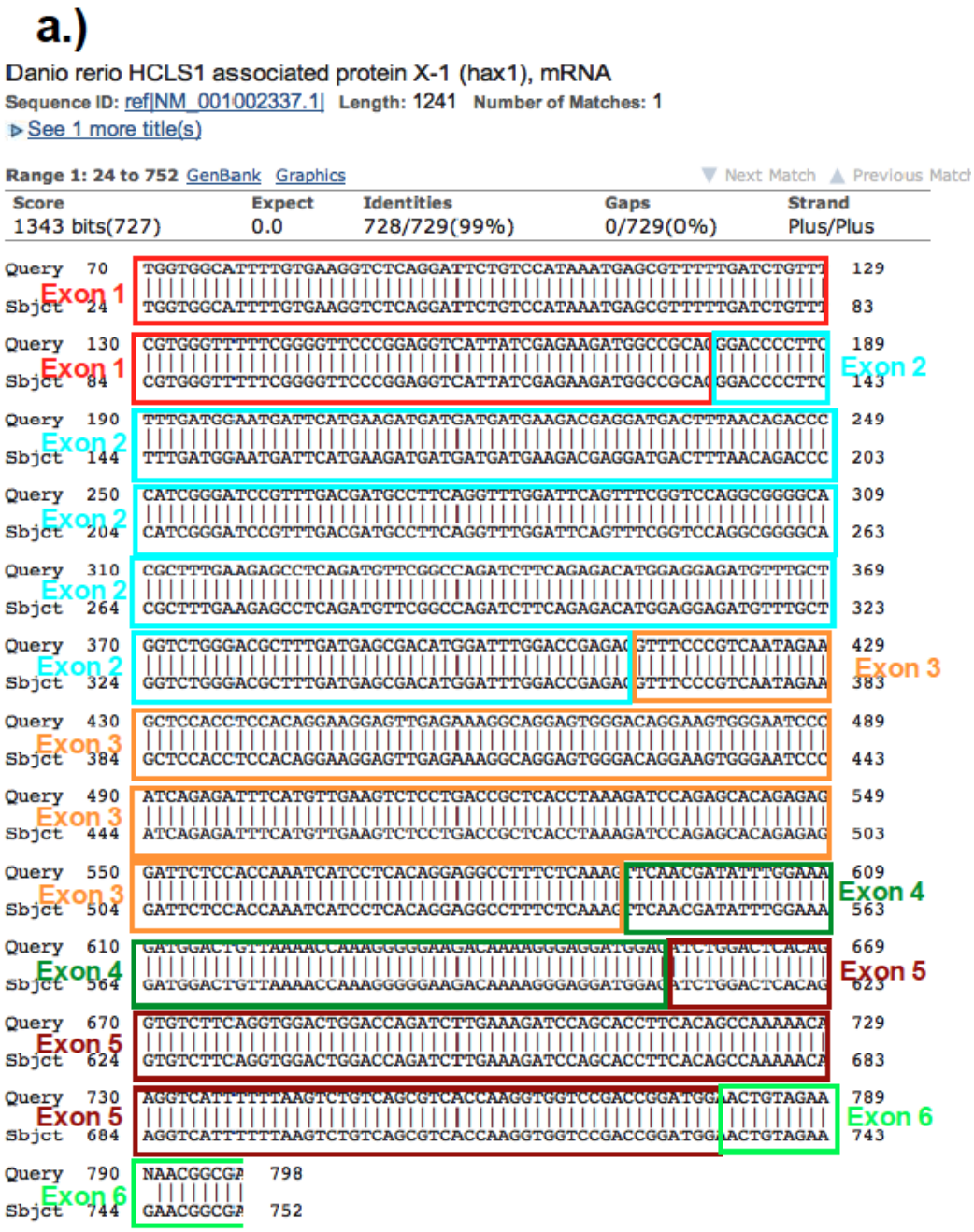
a.)
Danio rerio HCLS1 associated protein X-1 (hax1), mRNA
Sequence ID: ref|NM_001002337.1| Length: 1241 Number of Matches: 1
See 1 more title(s)
Range 1: 24 to 752 GenBank Graphics
Next Match Previous Match
Score 1343 bits(727)
Expect 0.0
Identities 728/729(99%)
Gaps 0/729(0%)
Strand Plus/Plus
Query 70 TGGTGGCATTTTGTGAAGGTCTCAGGATTCTGTCCATAAATGAGCGTTTTTGATCTGTTT 129
Sbjct 24 TGGTGGCATTTTGTGAAGGTCTCAGGATTCTGTCCATAAATGAGCGTTTTTGATCTGTTT 83
Exon 1
Query 130 CGTGGGTTTTTCGGGGTTCCCGGAGGTCATTATCGAGAAGATGGCCGCAGGACCCCTTC 189
Sbjct 84 CGTGGGTTTTTCGGGGTTCCCGGAGGTCATTATCGAGAAGATGGCCGCAGGACCCCTTC 143
Exon 1
Exon 2
Query 190 TTTGATGGAATGATTCATGAAGATGATGATGATGAAGACGAGGATGACTTTAACAGACCC 249
Sbjct 144 TTTGATGGAATGATTCATGAAGATGATGATGATGAAGACGAGGATGACTTTAACAGACCC 203
Exon 2
Query 250 CATCGGGATCCGTTTGACGATGCCTTCAGGTTTGGATTCAGTTTCGGTCCAGGCGGGGCA 309
Sbjct 204 CATCGGGATCCGTTTGACGATGCCTTCAGGTTTGGATTCAGTTTCGGTCCAGGCGGGGCA 263
Exon 2
Query 310 CGCTTTGAAGAGCCTCAGATGTTCGGCCAGATCTTCAGAGACATGGAGGAGATGTTTGCT 369
Sbjct 264 CGCTTTGAAGAGCCTCAGATGTTCGGCCAGATCTTCAGAGACATGGAGGAGATGTTTGCT 323
Exon 2
Query 370 GGTCTGGGACGCTTTGATGAGCGACATGGATTTGGACCGAGACGTTTCCCGTCAATAGAA 429
Sbjct 324 GGTCTGGGACGCTTTGATGAGCGACATGGATTTGGACCGAGACGTTTCCCGTCAATAGAA 383
Exon 3
Query 430 GCTCCACCTCCACAGGAAGGAGTTGAGAAAGGCAGGAGTGGGACAGGAAGTGGGAATCCC 489
Sbjct 384 GCTCCACCTCCACAGGAAGGAGTTGAGAAAGGCAGGAGTGGGACAGGAAGTGGGAATCCC 443
Exon 3
Query 490 ATCAGAGATTTCATGTTGAAGTCTCCTGACCGCTCACCTAAAGATCCAGAGCACAGAGAG 549
Sbjct 444 ATCAGAGATTTCATGTTGAAGTCTCCTGACCGCTCACCTAAAGATCCAGAGCACAGAGAG 503
Exon 3
Query 550 GATTCTCCACCAAATCATCCTCACAGGAGGCCTTTCTCAAACTTCAACGATATTTGGAAA 609
Sbjct 504 GATTCTCCACCAAATCATCCTCACAGGAGGCCTTTCTCAAACTTCAACGATATTTGGAAA 563
Exon 3
Exon 4
Query 610 GATGGACTGTTAAAACCAAAGGGGGAAGACAAAAGGGAGGATGGACATCTGGACTCACAG 669
Sbjct 564 GATGGACTGTTAAAACCAAAGGGGGAAGACAAAAGGGAGGATGGACATCTGGACTCACAG 623
Exon 4
Exon 5
Query 670 GTGTCTTCAGGTGGACTGGACCAGATCTTGAAAGATCCAGCACCTTCACAGCCAAAAACA 729
Sbjct 624 GTGTCTTCAGGTGGACTGGACCAGATCTTGAAAGATCCAGCACCTTCACAGCCAAAAACA 683
Exon 5
Query 730 AGGTCATTTTTTAAGTCTGTCAGCGTCACCAAGGTGGTCCGACCGGATGGAACTGTAGAA 789
Sbjct 684 AGGTCATTTTTTAAGTCTGTCAGCGTCACCAAGGTGGTCCGACCGGATGGAACTGTAGAA 743
Exon 5
Exon 6
Query 790 NAACGGCGA 798
Sbjct 744 GAACGGCGA 752
Exon 6

Figure 4.3

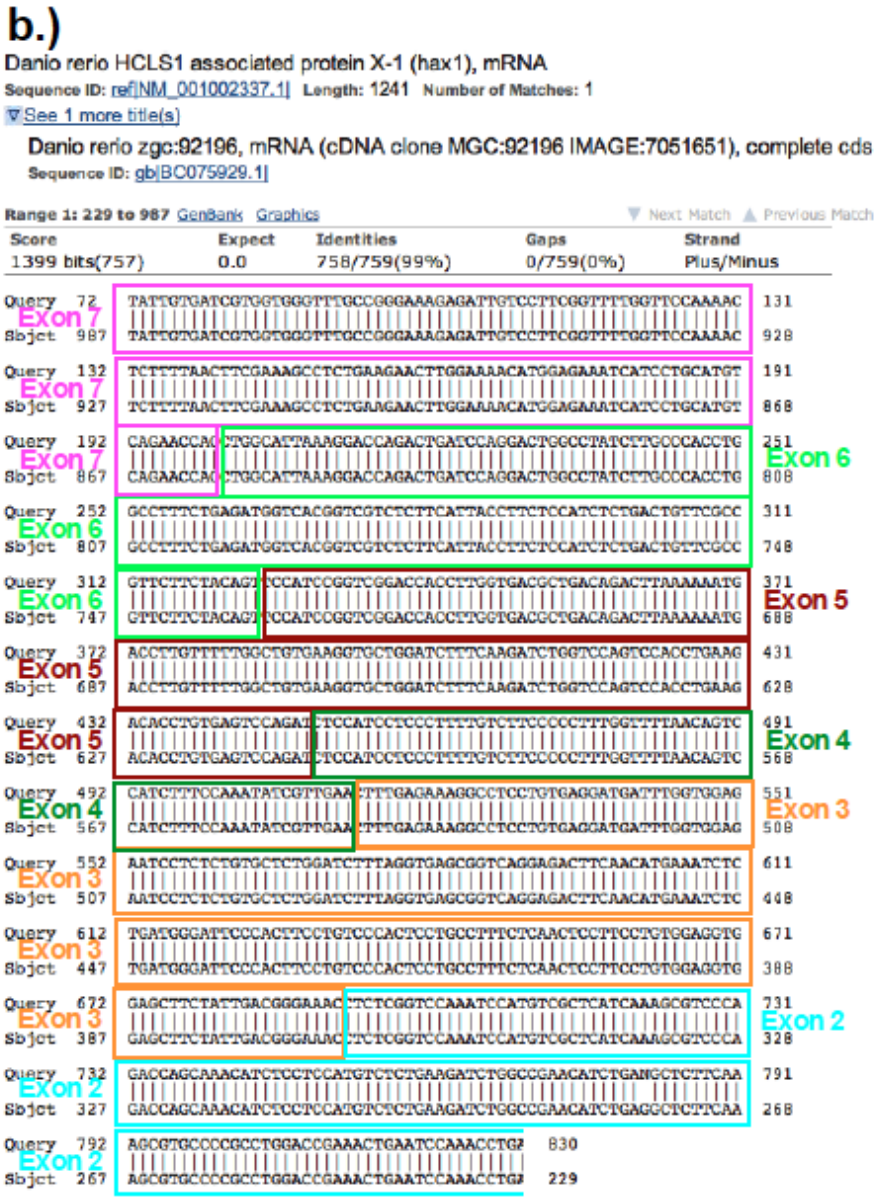

Figure 4.3 *hax1 001* expression in zebrafish embryos

The DNA fragment amplified using primers for *hax1 001* was TOPO cloned into a Zero BLUNT® TOPO® plasmid vector and Sanger sequenced using M13 forward and reverse primers. The output sequences from the M13F (**a.**) and M13R (**b.**) were then subjected to a nucleotide Blast search. The *hax1* specific fragment contained only *hax1* exonic regions. The *hax1* exon structure was deduced from the Ensembl sequencing data.

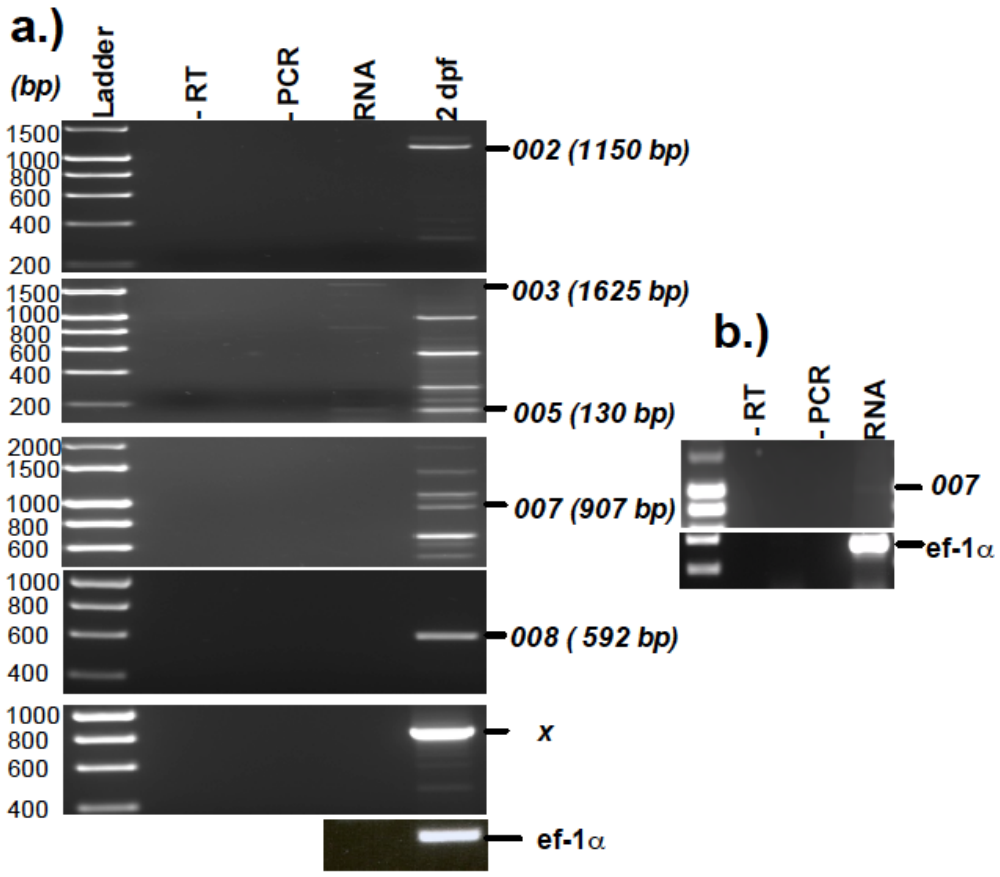

Figure 4.4 Zebrafish embryos express multiple putative *hax1* transcript variants

a. Detection of *hax1* isoforms using RT-PCR (35 cycles) with Phusion High-Fidelity DNA Polymerase in RNA extracted from *Tg(mpx:GFP)i114* embryos at 2 dpf. 2□ µl of template cDNA were used for each PCR reaction. 2 PCR products were analysed by agarose gel electrophoresis. A no template control was included in both the Reverse transcriptase (-RT) and PCR (-PCR) step. Also shown are the results obtained from total RNA extracted from 2 dpf embryos without the reverse transcription (RNA) and the ef-1 α loading control. **b.** Detection of *hax1 007* in a second sample of cDNA from day 2 embryos.

Fig. 4.5 is a schematic illustrating the human and zebrafish *hax1* genetic organisation and the putative *hax1* isoforms detected in embryos at 2 dpf (Figures 4.3 and 4.4). The green coloured arrows indicate primer-binding sites of the putative variants expressed in embryos at 2 dpf (Fig. 4.5). Transcript variants *008* and *x* were gel extracted, purified and sequenced. Sequencing confirmed expected splicing pattern at the 3' end of variant *008* with intron 5-6 being retained at the mRNA level. Blast analysis of the sequence extracted from the strong band produced by *hax1* isoform *x* primers revealed that variant *x* is full-length *hax1* variant *001* since the primers anneal to the first and last exon of the transcript and the Sanger sequence shows that the transcript contains exons 2-6. Blast analyses output data for transcript variant x (*001*) sequence with the isoform *x* primers and variant *008* is shown in Appendices 7.9 and 7.10 respectively.

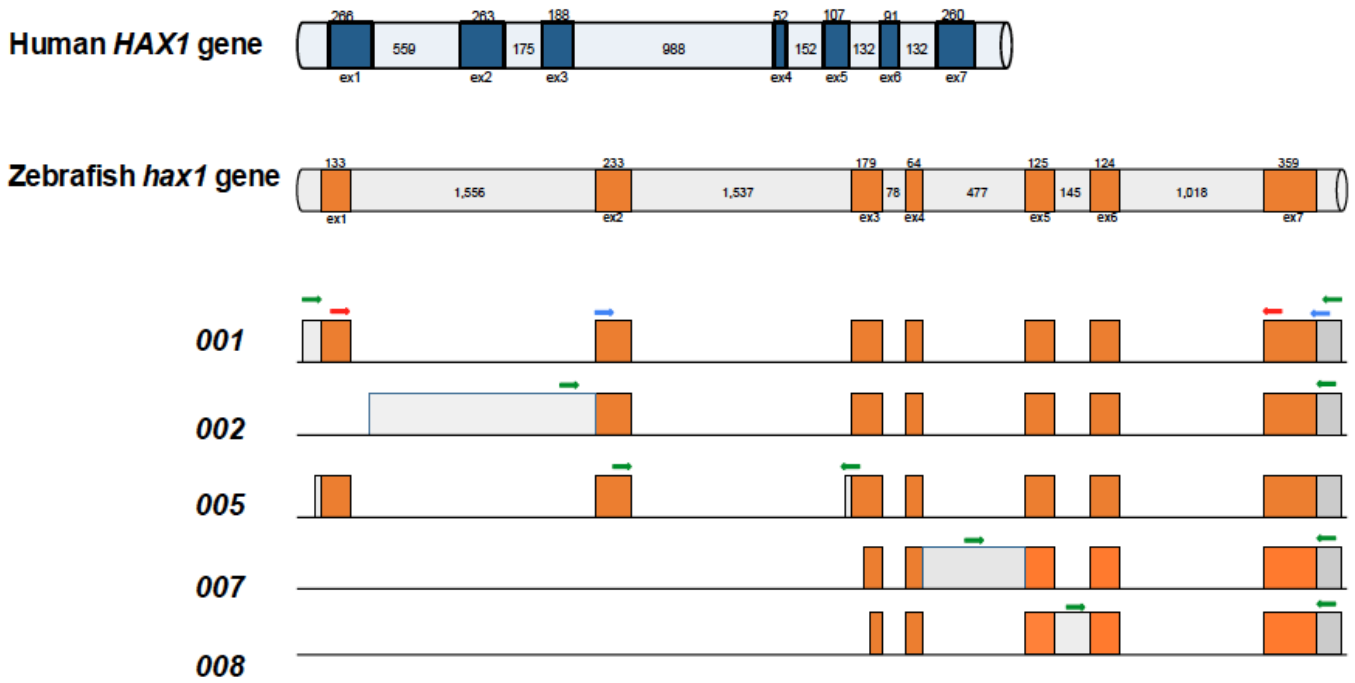

Figure 4.5 The structure of the *Danio rerio hax1* gene and putative mRNA variants

hax1 gene structure showing exonic (orange/blue, ex 1-7) and intronic (grey) regions. The human and zebrafish genes are shown. Putative zebrafish *hax1* transcript variants detected by RT-PCR are listed with primer binding sites indicated by the arrows (green). Numbers above the exons and in the intronic regions denote size in basepairs (bp). Red arrows indicate binding of *hax1* specific primers to identify additional isoforms arising from alternative splicing and intron inclusion between exons 1 and 7 (*isoform x*). Blue arrows indicate binding sites for primers used to amplify multiple isoforms of *hax1*. PCR products obtained from these primers will be labelled simply as *hax1*. Please note diagram is not to scale.

4.3 HAX1 putative protein sequence analysis

4.3.1 HAX1 protein sequences are conserved across many different species

In order to investigate the sequence similarities between human (*Homo sapiens*), zebrafish (*Danio rerio*), macaque (*Macaca mulatta*), rat (*Rattus norvegicus*) and mouse (*Mus musculus*) Hax1 protein, sequences were extracted from the Ensembl Genome browser and aligned using ClustalW2 (Fig. 4.6). Previously identified regulatory regions are highlighted (Han et al. 2006; Fadeel & Grzybowska 2009; Li et al. 2012). Although the zebrafish Hax1 sequence is the most divergent, a single alignment of zebrafish Hax1 001 protein and human full length HAX1 (data not shown) shows that there is still 40 % identity and 70% similarity. Fig. 4.6 shows that an acid box, a region consisting mainly of acidic residues has been conserved through evolution in all of the species included in the alignment. The zebrafish sequence also differs to the rest in that it shown reduced similarity at the putative PEST sequence and transmembrane domain regions in comparison to the other species. A search for PEST signals using ePESTfind (http://emboss.bioinformatics.nl/cgi-bin/emboss/epestfind) in the zebrafish Hax1 protein could only generate weak PEST sites.

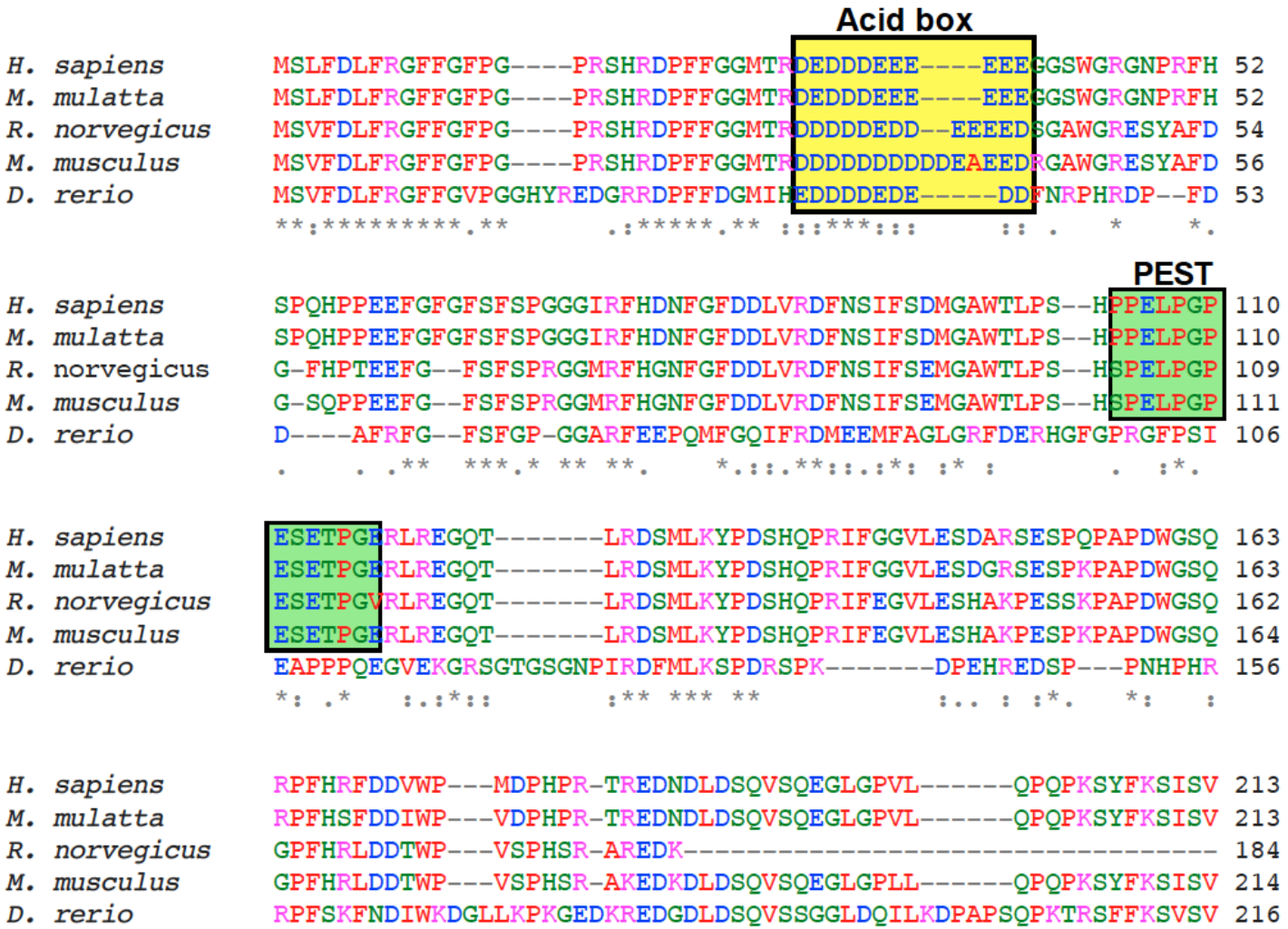

Figure 4.6 Bioinformatic analysis of HAX1 protein sequences from different species

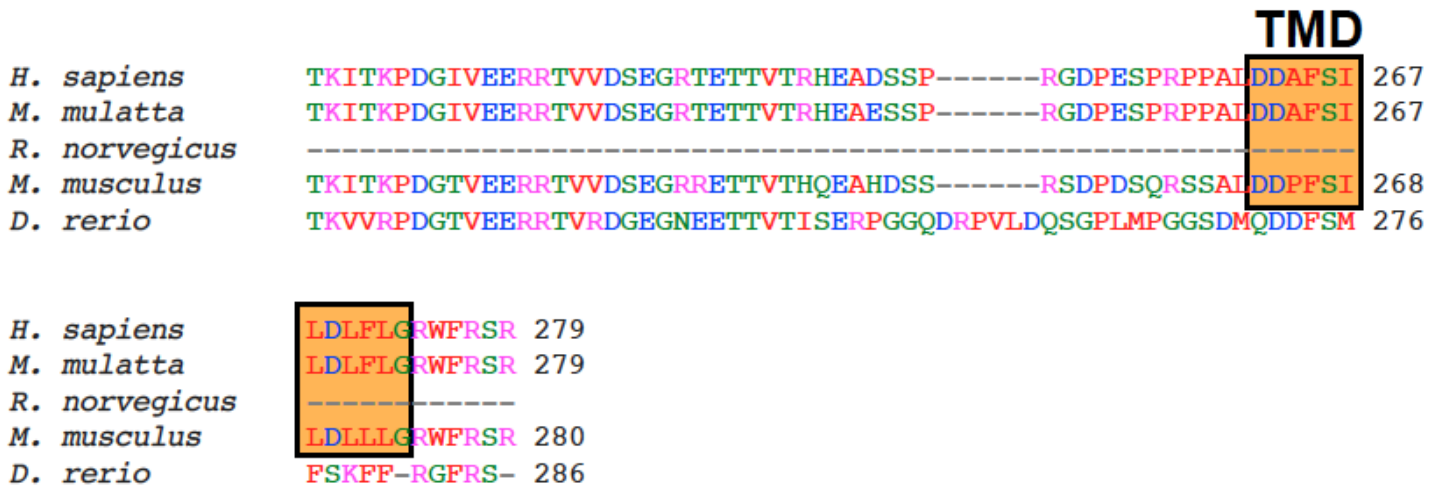

Figure 4.6 Bioinformatic analysis of HAX1 protein sequences from different species

A comparison of HAX1 protein sequences from five different species (*Homo sapiens*- human: ENSP00000329002, *Macaca mulatta*- macaque: ENSMMUP00000014178, *Rattus norvegicus*- rat: ENSRNOP00000064877, *Mus musculus*- mouse: ENSMUSP00000078661, and *Danio rerio*- zebrafish:ENSDARP00000053379) using a CLUSTALW2 multiple sequence alignment (http://www.ebi.ac.uk/Tools/msa/clustalw2/). The protein sequences were taken from the Ensembl Genome Browser website (http://www.ensembl.org/index.html). Putative regulatory regions were identified through literature searches and are highlighted (Fadeel and Grzybowska 2009; Li, Hu *et al*. 2012).

4.3.2 Sequence analysis of zebrafish putative Hax1 protein isoforms

Cloning and sequencing of variant *001*, RT-PCR of bands at the expected sizes for isoforms *002*, *005*, *007* and 008 and sequencing of the *008* PCR band allowed me to predict the splicing pattern of each variant and perform *in silico* translation. The intron exon boundaries for isoforms 001, 002, 007 and 008 were identified using Ensembl Genome Browser. A splice site predictor was used to identify a splice site with the highest score in the 3' region of intron 2-3 of transcript *005* which would result in the inclusion of 452 bases of this intron. Open reading frames were found for all of the isoforms. The open reading frames of isoforms 005 and 008 were quite short and may represent incomplete coding sequences. An alignment of the isoform sequences is presented in Fig. 4.7. All three isoforms 001, 002 and 003 contained the acid box. Variations from the Hax1 001 are described in the following paragraph.

The putative Hax1 002 isoform lacks a short region of the N-terminal as a result of the absence of exon 1 and uses an alternative splice site found in exon 2 in frame with the Hax1 001 stop codon. Inclusion of exon 1 in the 002 mRNA sequence did not make a difference in the protein sequence generated. Putative isoform 005 is likely to be a truncated version of Hax1 001. It contains an identical N-terminal sequence to isoform 001 with the exception of the last six amino acids at the 3' end of the protein. Both potential isoforms 007 and 008, however, lack the N-terminal of isoform 001. These isoforms are almost identical to the C-terminus of Hax1 001.These two isoforms use a splice site in exon 3. Inclusion of intron 4-5 in isoform 007 generates an isoform specific region comprising 26 amino acids, which is in frame with the Hax1 001 stop codon and reverts back to the Hax1 001 reading frame. In the putative isoform 008 inclusion of intron 5-6 would also results in a 008 specific 3'

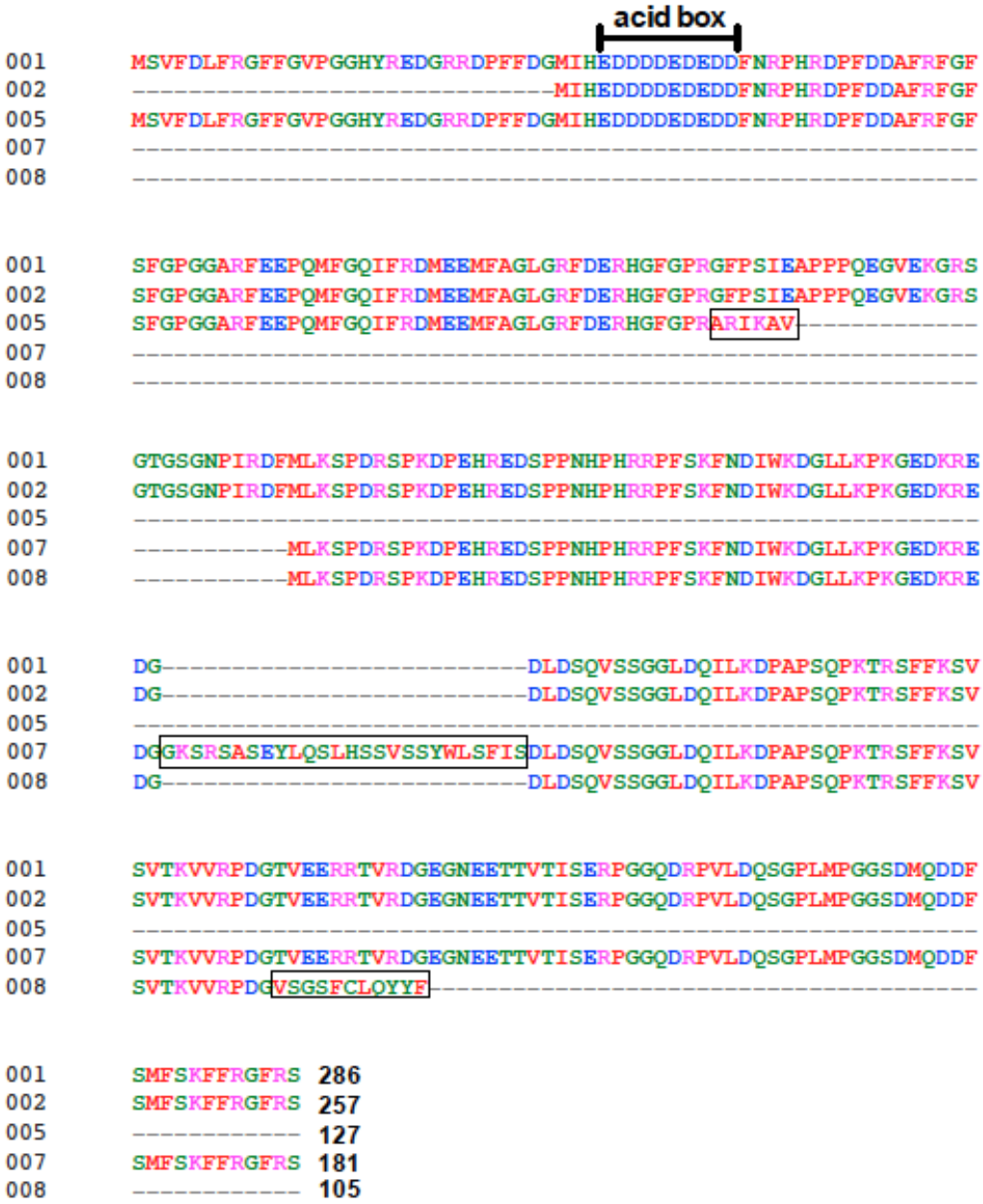

Figure 4.7 Sequence alignment of the zebrafish Hax1 001 isoform and predicted isoforms 002, 005, 007 and 008

Using the predicted mRNA variant data from Fig. 4.5, the transcript sequences were *in silico* translated using the Expasy translate tool (http://web.expasy.org/translate/). The longest open reading frames were then aligned using Clustal Ω. The exon intron boundaries used were those found on the Ensembl Genome Browser (http://www.ensembl.org/index .html). A *hax1 005* internal splice site at the 3' of intron 2-3 was identified using a splice site predictor (Reese, Eeckman et al. 1997). Black boxes indicate isoform specific sequence. Numbers at the end of each sequence represent length of the protein sequence.

end and early termination of the protein sequence. It should be noted that transcript variants *005*, *007* and *008* are only hypothetical. Cloning and sequencing would be required to confirm the complete splicing pattern.

4.4 Microinjection of high *hax1* splice site morpholino oligonucleotide (MO) doses results in the death of *Tg(mpx:GFP)i114* embryos

Many studies investigating the role of HAX1 have shown that it is a multifunctional protein and so the disruption of its expression in the zebrafish was likely to affect many different pathways. To investigate the role of Hax1 in the zebrafish *in vivo* model, *hax1* knockdown by morpholino (MO) was carried out in one cell stage embryos. An exon 3 splice acceptor targeting MO was designed to prevent correct splicing of the gene. At least three *hax1* transcript variants express exon 3 (variants *001*, *002* and *005*) and therefore this MO is likely to affect multiple *hax1* variants. The dose of MO for injecting was optimized on the basis of using a dose which would lead to </= 40 % death after injection. Embryos were injected with varying doses of *hax1* MO as indicated in Fig. 4.8. High doses, 2nl of 2mM - 1 nl of 0.5 mM, resulted in highly dysmorphic embryos (data not shown) and reduced viability of embryos (>79 % death) at 24 hours post fertilization (hpf). After numerous injections with different doses of the *hax1* splice MO, the optimized dose chosen was 1 nl of 0.25 mM MO which generated a death rate of ~33% at 24 hpf. Most of the embryos injected with this dose showed varying degrees of dysmorphology.

4.4.1 RT-PCR analysis of *hax1* MO injected zebrafish embryos at 12 hpf

In order to establish whether the *hax1* MO targeting exon 3 splicing has any effect on *hax1* mRNA levels, one cell stage *Tg(mpx:GFP)i114* embryos were injected with 1 nl of 0.25 mM MO. *hax1 splice* MO injected embryos were grouped based on their morphology: healthy-looking

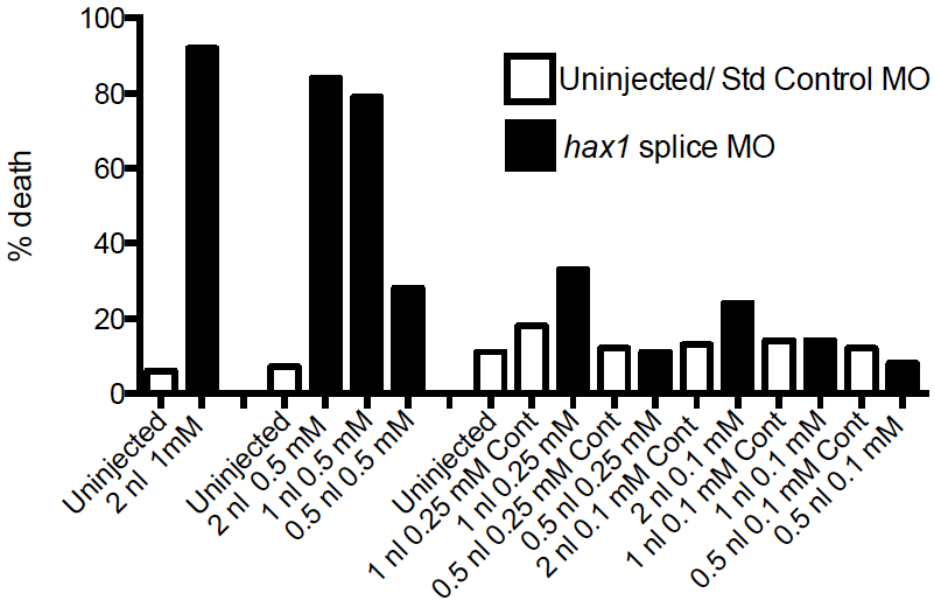

Figure 4.8 Optimisation of *hax1* splice MO concentration

Tg(mpx::gfp)i114 embryos at the 1-4 cell stage were injected with varying amounts of *hax1* MO on three different occasions. Embryos were then incubated at 28 °C for 24 h. Non-viable embryos were removed 1 h after injection and remaining healthy embryos were counted. At 24 hpf, the number of healthy embryos was counted once again and % number of dead embryos (% death) was calculated (excluding non-viable embryo counts 1 h following injection).

(normal), mildly dysmorphic (mild) and severely dysmorphic (severe) in order to investigate whether this would be linked to the extent of knockdown in the *hax1* mRNA level (Fig. 4.9). When compared to uninjected and standard control MO injected embryos, *hax1* splice MO injected embryos did not appear to have the expected reduced levels of isoform *001* mRNA tested by the two different sets of primers. However, the *hax1* splice MO injection appears to induce the expression of a very high molecular weight species (>2500 bp) indicated by the red arrows in Fig. 4.9. Lowering the PCR cycle number from 30 to 25 cycles showed that *hax1* mRNA levels were reduced but not abolished in severely dysmorphic embryos when compared to the uninjected control (Fig. 4.9 b.). The 2500 bp band was still visible and is indicated by the red arrow. It was thought that splicing into an alternative cryptic splice site found only a few bases into the 5' end of exon 3 may have been used instead of the targeted splice site, which would yield an amplicon of a similar size to the full-length *hax1* transcript and therefore undistinguishable by standard RT-PCR. As a result, the PCR product was sequenced and blast analysis of the data carried out. Comparison to the normally splice full-length *hax1* sequence showed no evidence of alternative splicing into the cryptic splice site.

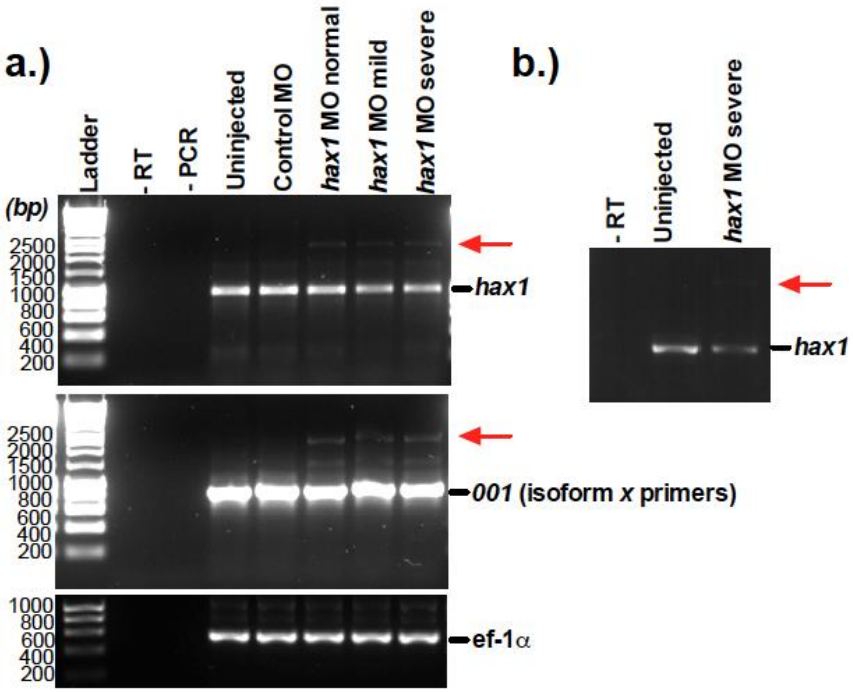

Figure 4.9 Analysis of *hax1* splice MO injected zebrafish embryos at 12 hpf

a.) *Tg(mpx:GFP)i114* embryos at the 1-4 cell stage were injected with 1 nl of 0.25 mM standard control (Control MO) and *hax1 splice* MO and grouped into 3 categories: embryos with a normal morphological phenotype (*hax1* MO normal), embryos that were mildly dysmorphic (*hax1* MO mild) and embryos that were severely dysmorphic (*hax1* MO severe). Total RNA was extracted from embryos at 12 hpf. 2 µg of RNA were used for each RT reaction. Negative RT (- RT) and PCR (- PCR) controls containing water instead of RNA and cDNA respectively are also shown. *hax1* was amplified using two sets of primers. PCR products after 30 cycles were analysed by agarose gel electrophoresis. Red arrows indicate the appearance of an additional band in the *hax1* MO injected embryos. Note not all Hyperladder marker sizes are shown. **b.)** Repetition of PCR using uninjected and *hax1* splice MO injected embryo cDNA with a reduced number of PCR cycles (25) and *hax1* primers.

4.4.2 Disruption of *hax1* gene expression results in abnormal development and lower total PMN counts

To test whether a longer time-point after MO microinjection results in a further decrease in *hax1* mRNA levels, embryos were injected with either standard control or *hax1* splice MO and incubated for 24 h. RNA extracted from the embryos using TRI reagent was subjected to RT-PCR with hax1 primers. Microinjection of hax1 splice MO resulted in either a decrease in *hax1* mRNA level (Fig. 4.10 a.) or the appearance of a high molecular weight band ~2500 bp (Fig. 4.10 b.). This band was not seen in the standard control MO injected sample and was also used as an indicator of disruption of *hax1* transcription. After each experiment, embryos were collected at 24 hpf, RNA extracted and knockdown (decrease in hax1 mRNA level, appearance of ~2500 bp band or combination of both) was determined by RT-PCR analysis; any experiments not showing knockdown were discarded. RT-PCR analysis results representative of 6 independent experiments are shown in Fig. 4.10 a. and b.. The mRNA was also amplified with positive control *ef-1α* primers that show constant levels of the transcript in all samples.

The effect of *hax1* knockdown on whole embryo PMN numbers of zebrafish was assessed using Volocity® software. Uninjected, standard control MO and *hax1* splice MO injected *Tg(mpx:GFP)i114* embryos (morphants) were incubated at 28 °C for 35 and 48 h. At the relevant time point, embryos were mounted in 1% low melting point agarose and imaged under a 2x objective on a Nikon Eclipse TE2000U inverted microscope. GFP labelled PMN were counted from at least six embryos in each experiment. At 35 hpf, *hax1* MO knockdown significantly reduced total PMN number compared to uninjected and standard control morpholino injected embryos (Fig. 4.10 c.). There was no significant difference between uninjected and standard control injected embryos (Fig. 4.10 c.). In half of the experiments (3 out of six), *hax1* MO injected embryos failed to survive to 48 h. Total PMN counts were carried out in the three experiments where injected embryos did survive past 48 hpf

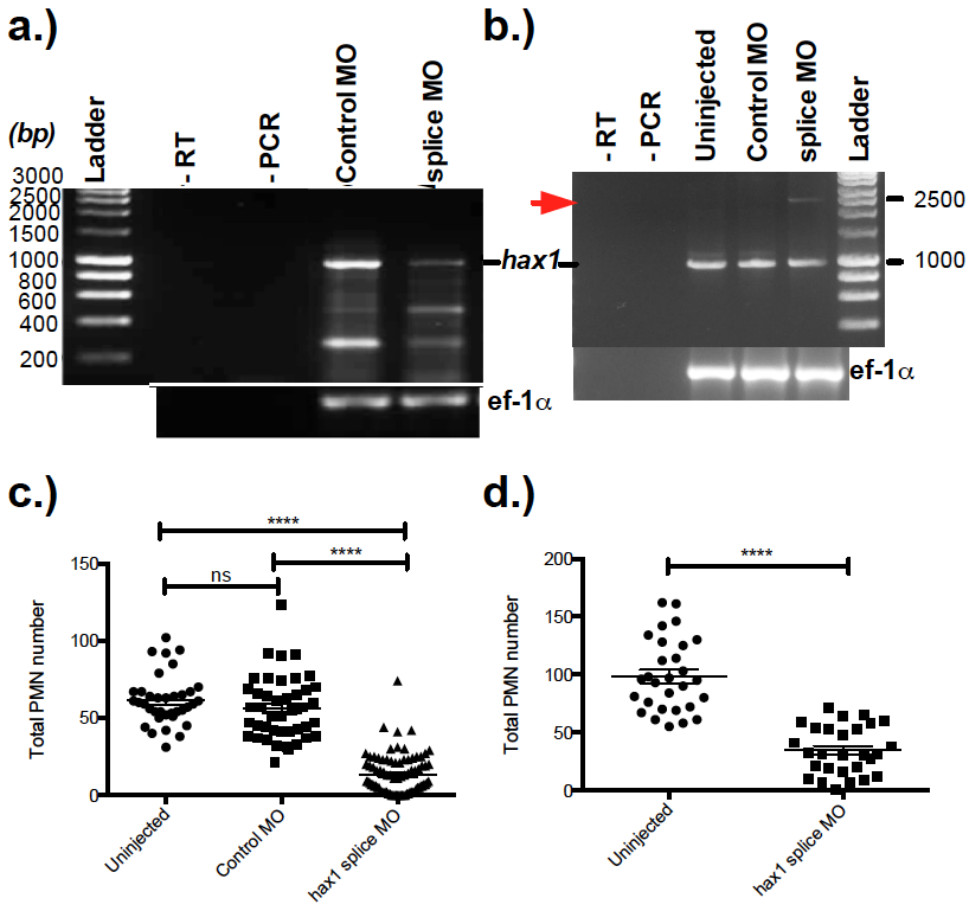

Figure 4.10 *hax1* RT-PCR analysis and PMN whole embryo counts of *Tg(mpx:GFP)i114* embryos following injection with *hax1* splice MO

RT-PCR analysis of total RNA from uninjected, standard control and *hax1* morpholino injected (1 nl of 0.25 mM- splice MO) *Tg(mpx:GFP)i114* zebrafish embryos at 24 h post injection. cDNA was amplified using *hax1* and positive control ef-1 α primers. DNA bands after 30 cycles of PCR were separated by agarose gel electrophoresis and visualised using a UV transilluminator. A no template control was included in both the Reverse transcriptase (-RT) and PCR (-PCR) step. PCR results shown in **a.** and **b.** are representative of 6 independent experiments. Red arrow indicates presence of additional band in *hax1*MO injected cDNA. Whole embryo PMN counts were carried out at 40 hpf (**c.**) (uninjected n=3, control and *hax1* MO n=4) and 48 hpf (**d.**) (n=3**)** from at least 6 embryos per condition on each independent experiment. Total PMN numbers at 40 hpf from three independent experiments were analysed using a one way ANOVA with Bonferroni's post test; ****p≤ 0.0001. Total PMN counts at 48 hpf were analysed using an unpaired t-test, ****p≤ 0.0001.

(Fig. 4.10 d). PMN counts in *hax1* morphants remained low (mean±SEM: 34.54 ± 3.939) compared to the uninjected control (mean±SEM: 98.62 ± 5.826) (Fig. 4.10 d.).

On morphological analysis, most of the *hax1* splice MO embryos were developmentally delayed compared to the healthy control uninjected (Fig. 4.11 a.) and standard control MO injected embryos (Fig. 4.11 b.).The *hax1* MO injected embryos at 48 hpf were classified into four groups based on gross morphology and developmental delay. Micrographs taken using the brightfield and GFP channels are shown in Fig. 4.11 a-e. The groups were: healthy embryos which resembled the morphology of the uninjected and control MO injected embryos, curly tailed embryos (curly, Fig. 4.11 c.), embryos with a curly tail and brain swelling (brain swelling, Fig. 4.11 d.) and severely dysmorphic embryos (severe, Fig. 4.11 e.). The reduced number of PMN in the *hax1* morphants is also apparent from the micrographs taken using the GFP channel. Embryos were sorted into the four different morphological groups and RNA extracted. RT-PCR analysis revealed that although there was no difference in the *hax1* mRNA levels between the controls (uninjected, standard control MO) and the hax1 splice MO injected morphants (curly, brain swelling, severe) (Fig. 4.11 f.); the ~2500 bp band (red arrow) was still visible at a very low intensity in the *hax1* PCRs of the curly, brain swelling and severely dysmorphic groups.

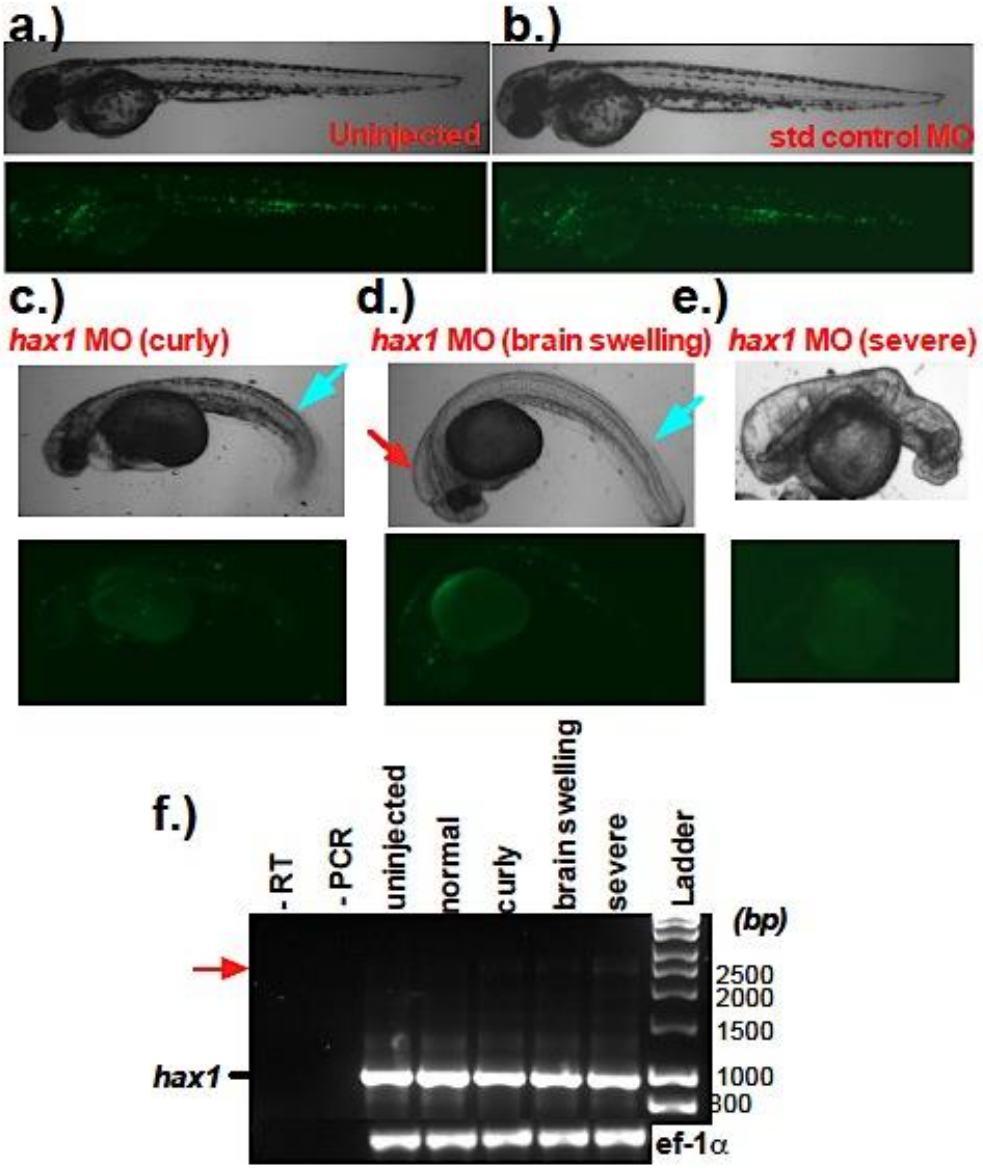

Figure 4.11 RT-PCR and morphological analysis 48 hpf following injection with *hax1* splice site MO

a-e.) Representative micrographs showing uninjected, standard control MO injected and *hax1* MO injected embryos with brain swelling (red arrow) and curly tail (cyan arrow) at 48 hpf. **f.)** RT-PCR analysis of total RNA from standard control and *hax1* morpholino injected *Tg(mpx:GFP)i114* zebrafish embryos 48 h following injection. RT-PCR was carried out using *hax1* and positive control ef-1α primers. PCR bands were separated by agarose gel electrophoresis. A no template control was included in both the Reverse transcriptase (-RT) and PCR (-PCR) step. *hax1* MO injected embryos fell into four categories: normal morphology, curly tail (curly), brain swelling & curly tail (brain swelling), and severely dysmorphic (severe) embryos. Red arrow indicates additional 2500 bp *hax1* specific band. Note not all Hyperladder marker sizes are shown.

4.4.3 RT-PCR and morphological analysis of embryos co-injected with *hax1* and p53 MO

A study evaluating the off-target effects of sequence-specific gene knockdowns demonstrated that p53 activation is a side effect of morpholino injection and siRNA silencing (Robu et al. 2007). In order to assess whether the developmental delay in *hax1* morphants was mediated by p53 activation, a p53 MO (0.4mM) was co-injected with the *hax1* splice MO. Amplification of mRNA with *hax1* primers shows the appearance of the ~2500 bp band in the *hax1* and combined *hax1 p53* morphants (Fig. 4.12 a.). Negative reverse transcription controls were carried out for each sample of RNA and were all clear. RT-PCR analyses using the ef-1α loading control primers shows ef-1α levels were uniform in all PCR samples.

While the *hax1* morphants failed to survive to 48 hpf, the co-injection with *p53* MO prevented the death of the embryos. However, most of the co-injected embryos remained highly dysmorphic even with the *p53* co-injection. The morphologies of uninjected, standard control MO and *hax1 p53* MO co-injected embryos at 48 hpf are displayed in Fig. 4.12 b. Total numbers of PMN from embryos of the same experiment were counted at 40 hpf (Fig. 4.12 c.). Total PMN numbers were considerably lower in *hax1* and co-injected morphants when compared to sibling controls (uninjected and control MO injected). The difference appeared to persist at 48 hpf (Fig. 4.12 d.).

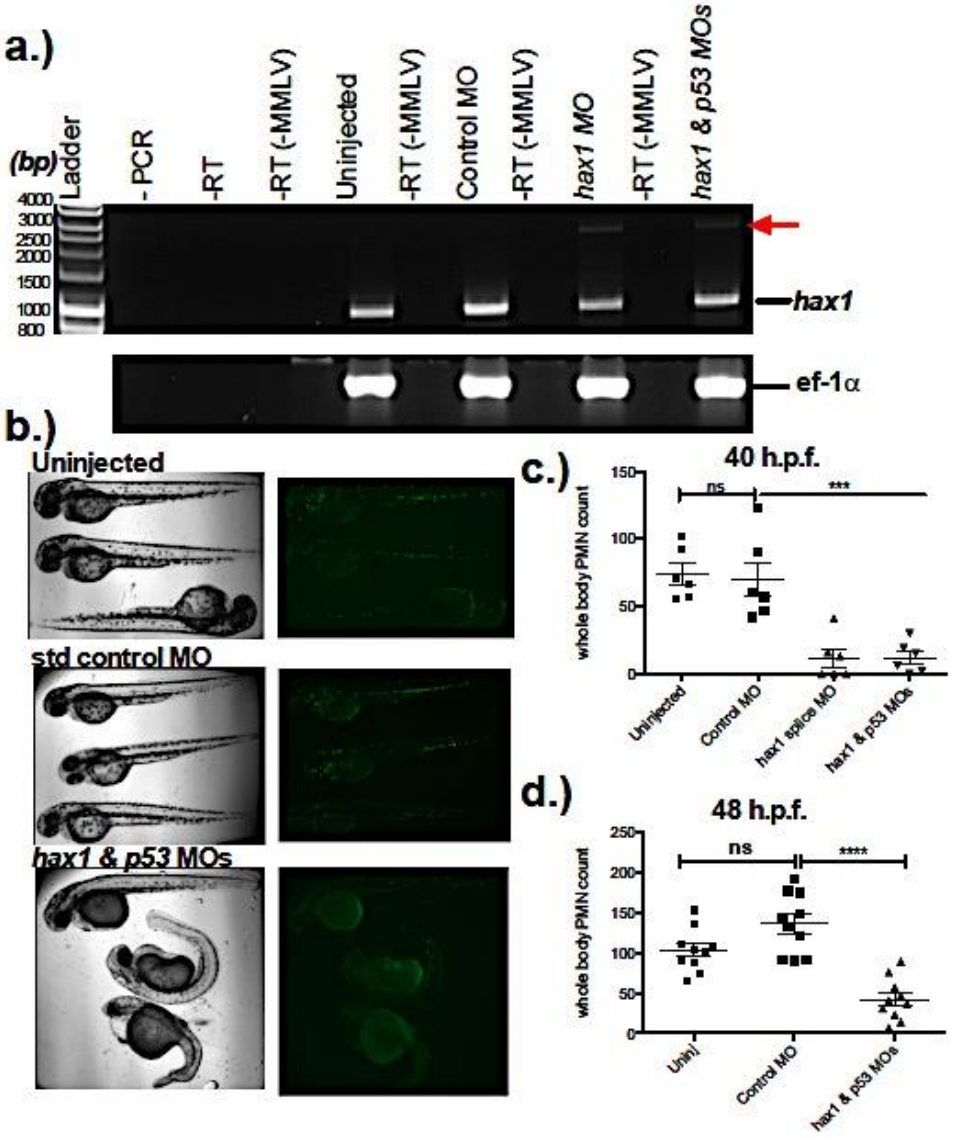

Figure 4.12 Analysis of i114 embryos co-injected with *hax1* and *p53* MO

a.) *Tg(mpx:GFP)i114* embryos at the 1-4 cell stage were injected with standard control MO, *hax1* MO or co-injected with 1nl *hax1* and p53 MOs (n=1). Total RNA was extracted 24 h following injection and RT-PCR was carried out using *hax1* and loading control primers ef-1α. The PCR products were separated by agarose gel electrophoresis and bands were detected using a UV transilluminator. **b.)** Micrographs of uninjected and injected embryos at 48 h post injection. Total PMN counts were carried out on images taken using the GFP channel from 6 embryos at 40 h (n=6 performed as a single experiment) (**c.**) and 10 embryos at 48 h (n=10 performed as a single experiment) (**d.**) following injection. Total PMN counts were analysed using a one way ANOVA with Bonferroni's post test;$p<0.0001$. Bars represent mean values ±SEM.

4.5 *hax1* splice site MO induces aberrant splicing of the gene in zebrafish embryos

To explore whether the *hax1* specific ~2500 bp visible only in the RT-PCRs using *hax1* morphant mRNA is a result of altered pre-mRNA splicing of the gene, the band was cloned into a pCR-BLUNT II-TOPO vector and sequenced using M13 primers. PCR bands were excised from the gel and purified from pooling lanes 1-4 (Fig. 4.13 a.). The purification was assessed by agarose gel electrophoresis. Fig. 4.13 b. shows that a sufficient amount of the large DNA band was purified from the gel extract to allow subsequent cloning. Once the ~2500 bp PCR product was inserted into pCR-BLUNT II-TOPO and transformed into Amp resistant TOP10 comptetent *E.* coli, colony PCR was carried out with M13 primers to confirm insertion of the ~2500 fragment into the pCR-BLUNT II-TOPO. PCR analysis of colony 1 containing the ~2500 bp insert is shown in Fig. 4.13 c**.** Sequencing of the plasmid vector from a mini-preparation from colony 1 revealed that the ~2500 band seen in the *hax1* morphants is due to aberrant splicing of the *hax1* gene (Fig. 4.13 d.). Blast analysis of the sequencing output showed that the band amplified using the *hax1* primers generated a 2599 bp product consisting of exon 2, intron 2-3, exon 3, intron 3-4, exon 4, exon 5, exon 6 and exon 7. The exon/intron organization of the zebrafish gene, the normal splicing of variant *001* and *002* in the region amplified by *hax1* primers (green arrows) and the abnormal splicing as a result of the *hax1* MO injection are shown in Fig. 4.13 d. *In silico* translation of the mRNA species generated as a result of the MO injection reveals premature truncation of the protein sequence due to intron 2-3 being maintained in the transcript (Fig. 4.14).

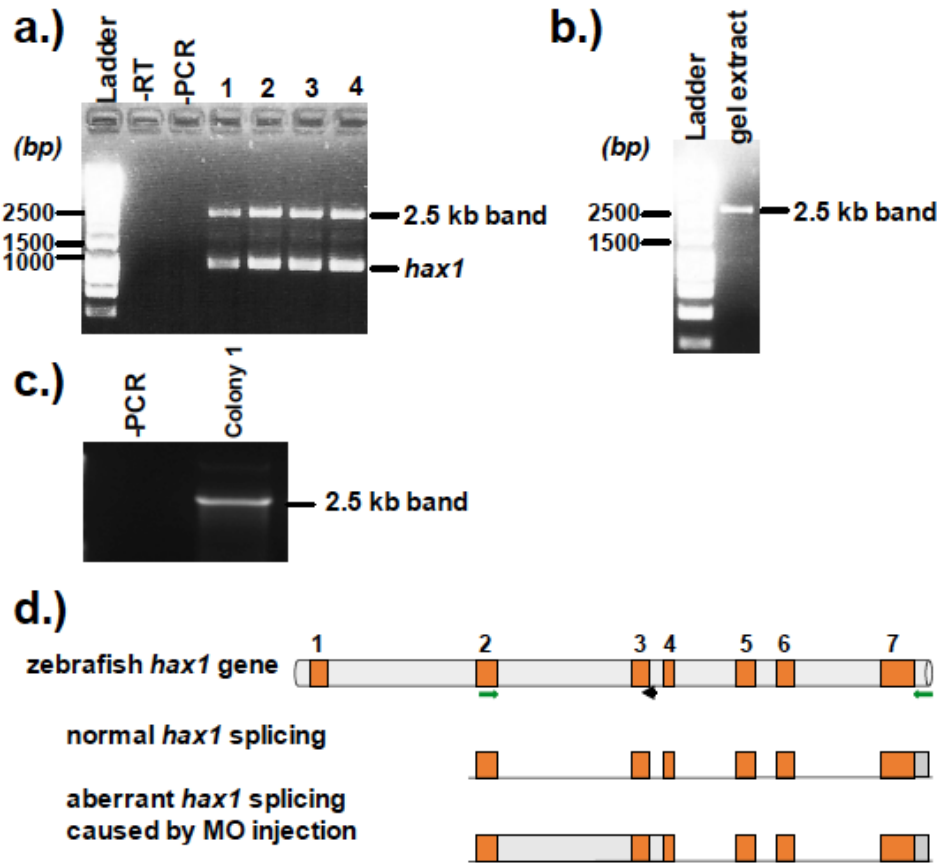

Figure 4.13 Cloning of alternatively spliced 2500 bp band observed in response to *hax1* splice MO injection

a.) cDNA from *hax1* morphants at 24 hpf was amplified using *hax1 001* primers with a 2 min PCR cycle extension step. Following 35 cycles of PCR, the DNA bands (lanes 1-4) were resolved on an agarose gel and visualised using a UV transilluminator. A no template control at the RT and PCR step is included. Note not all ladder sizes are shown. The 2.5 kb band was gel extracted and PCR purified. Purification of the band was confirmed by agarose gel electrophoresis (**b.**). The 2.5 kb band was inserted into a pCR-BLUNT II-TOPO vector. The TOPO cloning reaction was transformed into competent TOP 10 *E. coli* that were streaked on Amp selective media. **c.)** Colony PCR using M13 primers was carried out to confirm cloning of 2.5 kb *hax1* specific insert into the plasmid. Colony 1 was used to inoculate a 5 ml culture and incubated O/N at 37 °C. **d.)** Plasmid DNA was purified and sequenced. Normal and aberrant splicing induced by the MO injection is shown alongside the gene containing the numbered exons. Green arrows indicate site of *hax1 001* primer binding and the black arrow indicates binding of the *hax1* MO intron 3-4 primer binding site.

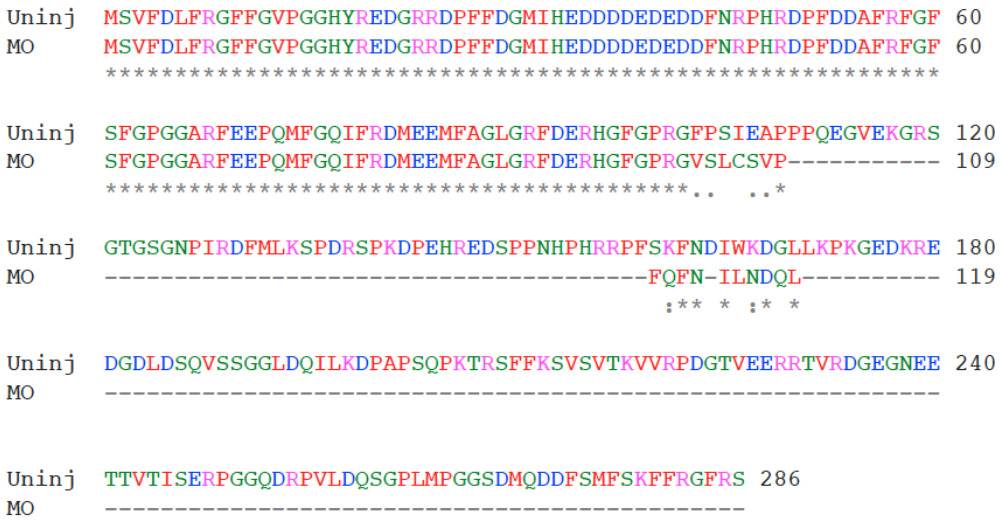

Figure 4.14 The *hax1* splice MO introduces a premature STOP codon

The *hax1 001* mRNA sequence was obtained from cloning and sequencing of *hax1* transcript variant *001* (Uninjected) whereas the sequence of the ~2500 bp band from the *hax1* MO injected embryos (MO) was determined by cloning and sequencing of the band. *In silico* translation of the mRNA sequences was carried out using the Expasy translate tool (http://web.expasy.org/translate/). A CLUSTALW2 alignment (http://www.ebi.ac.uk/Tools/msa/clustalw2/) reveals premature truncation of the *hax1 001* mRNA in the *hax1* splice MO injected embryos.

4.6 Transient knockdown of *hax1* using a translation start site targeting MO and co-injection with the *hax1* splice MO

In order to investigate whether a *hax1* translation start site targeting MO (ATG MO) would replicate the phenotypic changes and reduction in total PMN number seen with the *hax1* splice MO (section 4.5), a *hax1* ATG MO was designed and three different concentrations of the MO were injected into *Tg(mpx:GFP)i114* one cell stage embryos. ATG MOs work by inducing post-transcriptional interference of gene expression. Since the ATG MO does not affect mRNA levels the MO efficiency is not quantifiable by RT-PCR and to date, there are no commercially available zebrafish *hax1* antibodies to allow validation of the knockdown at the protein level. Uninjected, control MO and *hax1* ATG injected embryos were cultured for 48 h after which they were visualized under a Leica MZ10F fluorescent microscope with the GFP+ filter. Total PMN number from 12 embryos per condition was counted by eye. The number of PMN decreased slightly as the concentration of the ATG MO was increased when compared to the uninjected and standard control MO injected groups (Fig. 4.15). The *hax1* ATG MO resulted in very few or no no-viable embryos at 24 hpf and only a slight delay in development even with the highest dose tested (1nl 0.5 mM).

In a second experiment, the dose of the *hax1* ATG MO was increased to 1 mM to test the tolerance of this concentration with respect to embryonic development. The ATG MO was co-injected with 0.2 mM *hax1* splice MO. Note the concentration of the *hax1* splice MO is not the same as the previously optimized dose (section 4.4). The dose of the *hax1* splice MO was lowered in the co-injection with the ATG MO in order to try and reduce off-target effects that may result from p53 activation. In addition, since the *hax1* splice MO alone caused severe embryonic development it was anticipated that any additional *hax1* knockdown by the ATG MO could result in death therefore lowering the splice MO dose could prevent this.

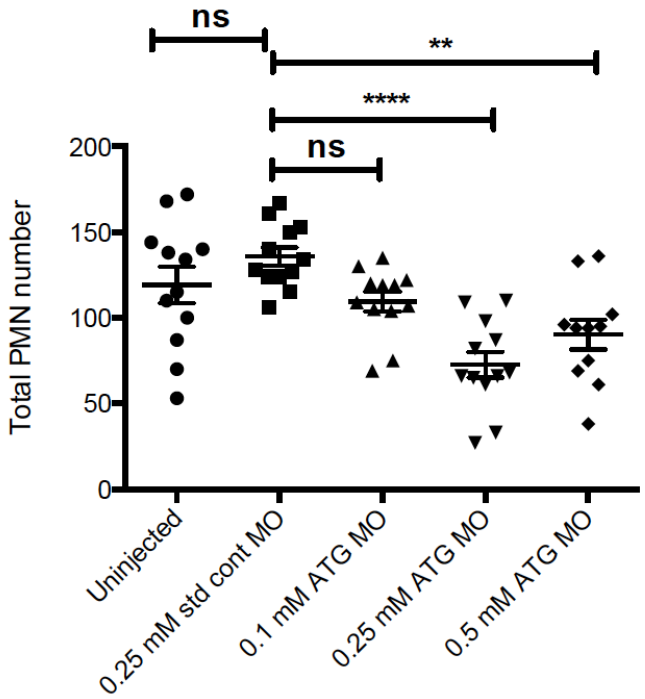

Figure 4.15 Optimisation of *hax1* ATG MO

Tg(mpx:GFP)i114 embryos at the one cell stage were injected with 1nl of standard control MO and varying doses of *hax1* ATG MO as indicated. Micrographs were taken using the GFP channel at 48 hpf. Whole embryo PMN numbers, n=12 performed as a single experiment were analysed using a one way ANOVA with Bonferroni's post test;****p≤ 0.0001. Bars represent mean ±SEM.

Morphological analysis of the embryos shows that in comparison to the healthy uninjected and standard control injected embryos, the *hax1* ATG MO injected alone had a slight delay in development indicated by the curling of the tail in Fig. 4.16. The severity of the tail curling increased in the co-injected morphants particularly with the higher dose of the MOs (1 mM ATG and 0.2 mM splice) however, this delay in development was not as marked as that seen with the 1 nl 0.25 mM *hax1* splice MO injection alone. Analyses of PMN counts at 48 hpf show that total PMN levels were lower in the *hax1* ATG MO injected and *hax1* splice MO & ATG MO co-injected embryos (both doses) when compared to the uninjected and standard control MO injected embryos (Fig. 4.17 a.). This is clearly visible from the micrographs taken using the GFP channel (Fig. 4.16). The ATG injected and MO co-injected embryos survived past 54 hpf and so PMN numbers were also counted at this time point (Fig. 4.17 b.). The PMN numbers in the 1 mM *hax1* ATG MO injected and *hax1* splice MO ATG MO co-injected embryos remained low at 54 hpf .The 1 nl 1 mM ATG and 0.2 mM splice *hax1* MOs co-injection dose generated embryos with the lowest PMN numbers.

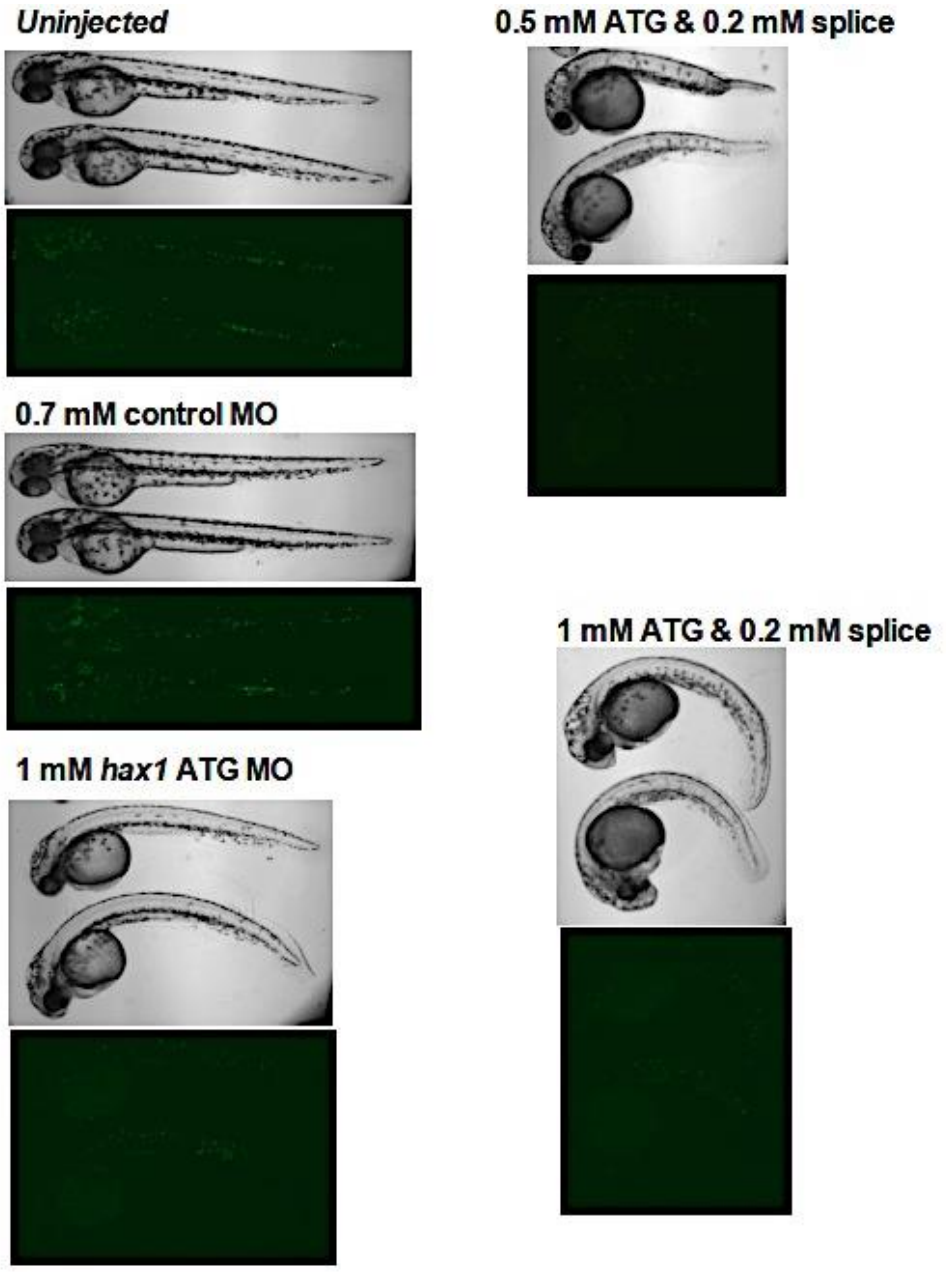

Figure 4.16 Morphological analysis of zebrafish embryos co-injected with *hax1* splice and ATG MO

Tg(mpx:GFP)i114 embryos were injected at the 1- 4 cell stage with standard control MO, *hax1* ATG MO or co-injected with *hax1* ATG and splice MO as indicated. Micrographs using the brightfield and GFP channel were taken at 48 hpf using a 2x objective on a Nikon Eclipse TE2000U inverted microscope. Images are representative of 12 embryos from a single experiment.

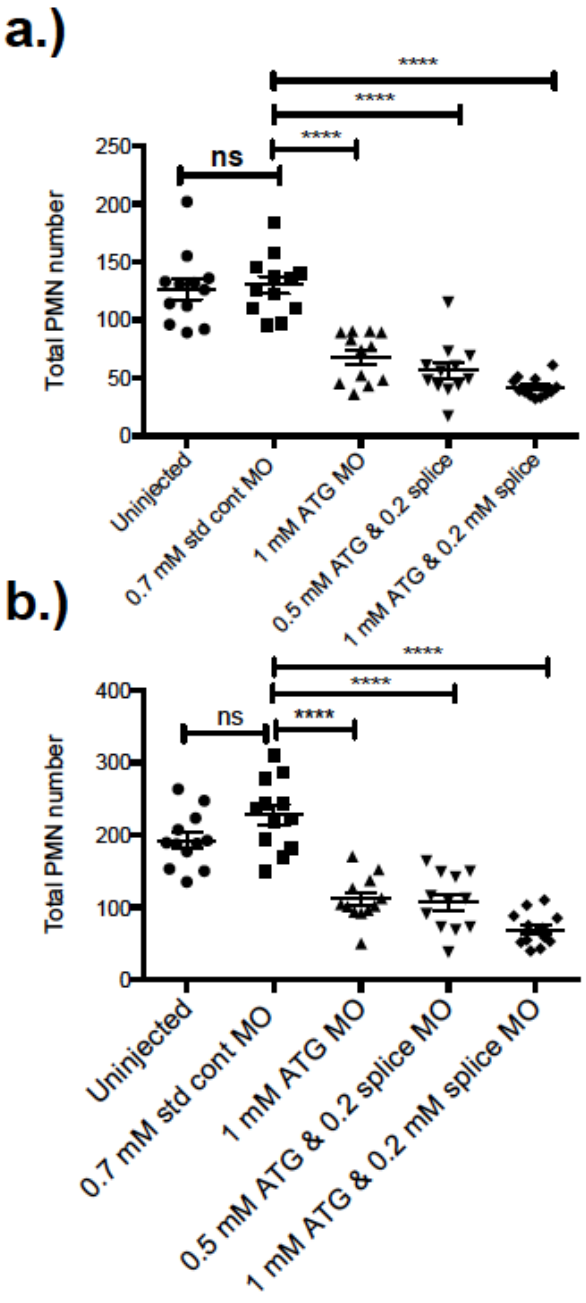

Figure 4.17 The effects of co-injection of *hax1* start MO and *hax1* splice MO on whole body PMN counts

Tg(mpx:GFP)i114 embryos at the one cell stage were injected with 1nl of 1 mM *hax1* ATG MO and co-injected with varying doses of *hax1* splice and ATG MOs as indicated. Micrographs of uninjected and injected embryos were taken at 48 h (**a.**) and 54 h (**b.**) following injection. Total PMN numbers were counted by eye from 12 embryos per condition. Total PMN counts (n=12 performed as single experiments) were analysed using a one way ANOVA with Bonferroni's post test;$p<0.0001$. Bars represent mean ±SEM.

4.7 Generation of *hax1* RNA probes for use in whole-mount *in situ* hybridization (WISH) in zebrafish embryos

WISH is an efficient method used to allow the detection of spatial gene expression patterns in zebrafish embryos. To detect the sites of *hax1* expression in the zebrafish embryo, a full-length *hax 1* antisense and a sense control RNA probe were generated. The region consisting of the full coding sequence of *hax1* (001) was PCR amplified and used as a template for the synthesis of an antisense and sense (negative control) probe (Fig. 4.18). The *hax1 001* coding sequence containing vector was transformed into TOP10 competent *E. coli* as described in section 2.1.21. This was followed by purification from a midi scale DNA preparation. Purified plasmid vector was subjected to PCR with *hax1 001* primers in order to confirm insertion of the template into the plasmid. Agarose gel electrophoresis of the PCR band and visualization using a UV transilluminator confirmed the successful insertion of the *hax1 001* template into the plasmid vector (Fig. 4.18 c.). The plasmid DNA was also sequenced to ensure the sequence of the template was intact and to determine the orientation of the insert. Blast analysis of the sequencing output is shown in Appendix 7.12. SpeI and XhoI restriction digests were then used to linearize the circular plasmid DNA (Fig. 4.18 d.).

Linear DNA was subjected to agarose gel electrophoresis (Fig. 4.18 e.) to allow quantification of each of the plasmids containing the *hax1 001* antisense, *hax1 001* sense negative control and the positive *L-plastin* control (a kind gift from Catherine Loynes, University of Sheffield) probes. Each linearized plasmid was used for the synthesis of the RNA probes labeled with digoxigenin-linked nucleotides. The quality of the RNA probe was assessed by agarose gel electrophoresis and is shown in Fig. 4.18 e**.** A single RNA band was visible for the L-plastin and the *hax1 001* sense probes. The *hax1 001* antisense probe consisted of two bands likely to result from differing secondary structures of the RNA species.

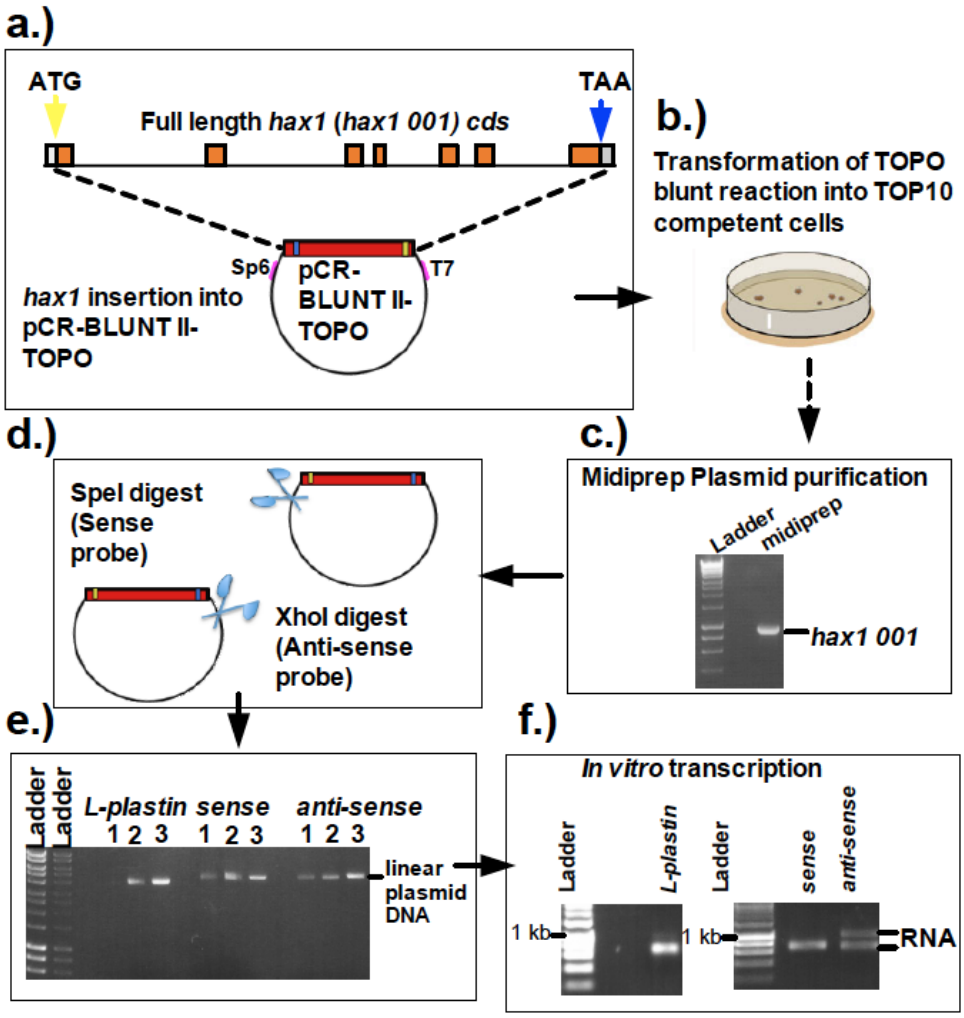

Figure 4.18 Generation of whole mount *in situ* hybridisation *hax1* sense and anti-sense probes

a.) The full length *hax1* cds was cloned into a pCR-BLUNT II-TOPO plasmid vector. **b.)** The TOPO cloning reaction was transformed into competent cells. A single colony was used to inoculate a 50 ml culture and incubated at 37 □C for 12 h. **c.)** The plasmid DNA was then purified and the insert amplified by PCR with *hax1 001* primers. **d.)** Plasmid DNA containing the insert was linearised using SpeI (*hax1* sense probe) and XhoI (*hax1* anti-sense probe) for generation of mRNA using the Sp6 and T7 promoter, respectively. **e.)** 0.1 (lane 1), 0.5 (lane 2) and 1 (lane 3) µl of linearised L-plastin, *hax1* sense and anti-sense plasmid DNA were resolved on an agarose gel to allow quantification using the Hyperladder I band DNA quantities. **f.)** Linearised DNA was *in vitro* transcribed using DIG-labelled NTPs. RNA clean-up was carried out and the RNA was resolved on an agarose gel alongside Hyperladder I and visualised by a UV transilluminator.

4.8 Overexpression of *hax1 001* in zebrafish embryos

4.8.1 Cloning of *hax1 001* into the multifunctional expression vector pCS2+

The pCS2^{+} vector has been shown to permit very effective in vitro expression fusing an artificial 3' UTR with a polyadenylation (poly A) signal to the gene of interest (Turner & Weintraub 1994). This provides increased stability of the mRNA. Since the *hax1 001* full cds containing pCR-BLUNT II-TOPO plasmid vector did not contain a polyadenylation signal, the *hax1 001* insert was excised from the pCR-BLUNT II-TOPO plasmid using EcoRI digestion and cloned into the multifunctional expression vector pCS2^{+} (Fig. 4.19). A colony containing the *hax1* insert (colony 2- Fig. 4.19 b.) was used for the preparation of the plasmid. Sequencing of the plasmid DNA with the M13 reverse primer revealed that the insert was in the correct orientation with the 3' region of the gene adjacent to the SV40 poly (A) signal. Linearization of the plasmid with the NotI restriction enzyme resulted in migration of the plasmid according to its true size (Fig. 4.19 c. and d.). In vitro mRNA synthesis using an SP6 transcription kit (Roche Applied Science) generated capped mRNA for injection into single cell embryos (Fig. 4.19 e.).

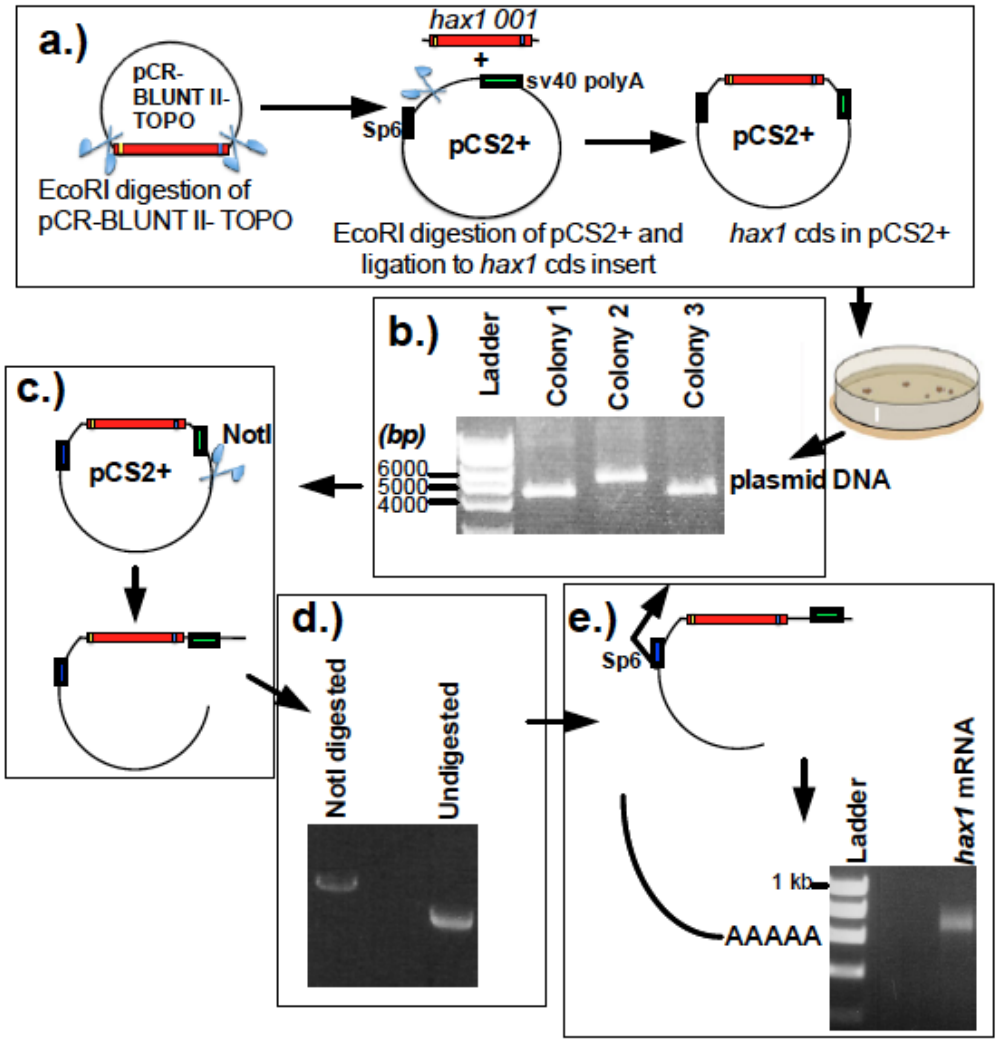

Figure 4.19 Cloning and *in vitro* transcription of zebrafish full length *hax1* into pCS2+

a.) The full length *hax1* cds was excised from pCR-BLUNT II-TOPO by EcoRI digestion and ligated to EcoRI linearised pCS2+ plasmid vector containing SV40 polyA tail. The ligation reaction was transformed into competent *E. coli, which* were subsequently plated on Amp selective media. Single colonies were used to inoculate a 50 ml culture which was incubated O/N at 37 °C. **b.)** The plasmid DNA was then purified and resolved on an agarose gel. Colony 2 contained the *hax1* insert. Plasmid DNA from colony 2 was linearised by digestion with the restriction enzyme NotI. **d.)** Undigested and NotI digested plasmid DNA was resolved on an agarose gel. The linearised plasmid DNA was then *in vitro* transcribed using an SP6 RNA polymerase. *hax1* mRNA was loaded onto an agarose gel and resolved by electrophoresis (**e.**). The mRNA band was visualised using a UV transilluminator.

4.8.2 Whole-mount *in situ* hybridization analysis of uninjected and *hax1 001* mRNA injected embryos

In situ hybridization using the *hax1 001* antisense RNA probe (section 4.8.1) shows that *hax1 001* mRNA is ubiquitously distributed in zebrafish embryos at 24 hpf (Fig. 4.20 a.) with high expression around the brain region. Some non-specific staining is visible in the WISH with the negative control *hax1 001* sense probe. WISH with the L-plastin antisense probe produced the expected staining pattern with staining in the anterior yolk region and posterior intermediate cell mass (ICM). The overexpression of *hax1 001* was also verified by the *in-situ* hybridization. Injection of *hax1 001* mRNA resulted in increased staining with the *hax1* antisense probe (Fig. 4.20 b.) when compared to the uninjected control embryos. As expected, there was no such increase in staining with the sense probe.

4.8.3 RT-PCR analysis of *hax1 001* mRNA injected and *hax1 001 mRNA* splice MO co-injected embryos

In order to assess whether *hax1 001* overexpression could prevent the *hax1* splice MO induced phenotypic changes of the embryos and concomitant decrease in the PMN number, embryos were injected with *hax1* 001 mRNA, *hax1* splice MO or co-injected with *hax1 001* mRNA and *hax1* splice MO. Following a 24 h incubation period, the embryos were anaesthetized and RNA extracted using TRI reagent. RT-PCR with *hax1* primers was used to confirm the overexpression. RT-PCR analysis showed that *hax1* splice MO injection resulted in decreased *hax1* levels, whereas the *hax1 001* mRNA and *hax1 001* and splice MO co-injection led to elevated *hax1* levels (Fig. 4.21).

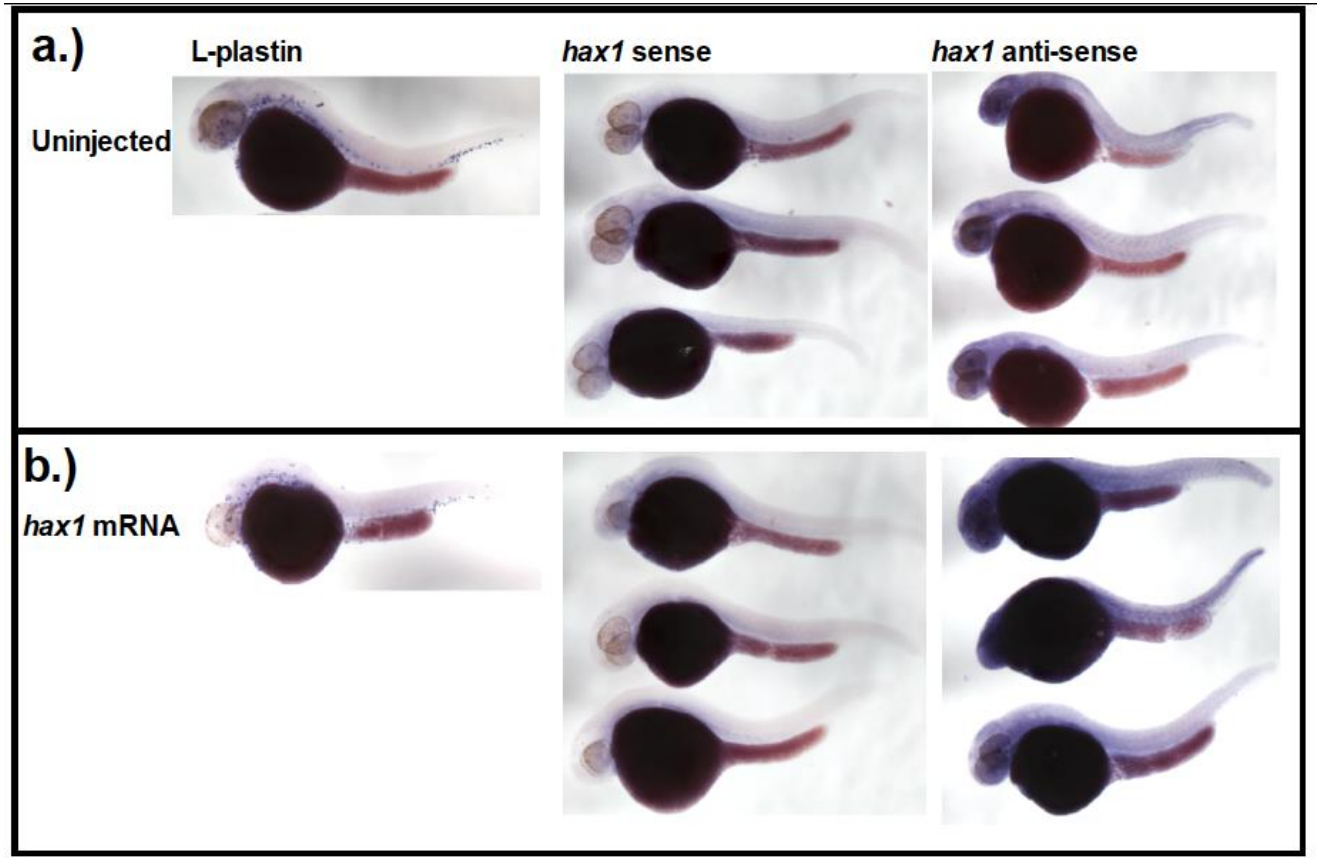

Figure 4.20 *hax1* is ubiquitously expressed in zebrafish embryos

NACRE embryos at the 1 cell stage were injected with 1 nl of *hax1* mRNA at 50 ng/ µl. Uninjected (**a.**) and *hax1* mRNA injected embryos (**b.**) were then subjected to WISH at 24 hpf. An L-plastin anti-sense probe was used as a positive control. A *hax1* sense probe was also included for detection of non-specific binding. Images are representative of at least 15 embryos per condition from a single experiment.

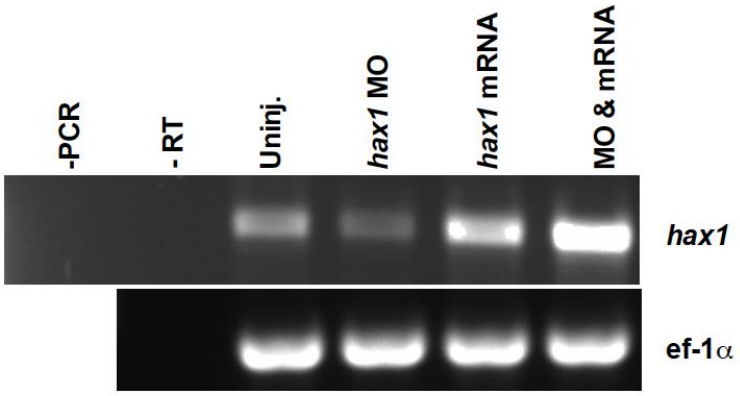

Figure 4.21 RT-PCR analysis of *hax1 001* overexpression in zebrafish embryos at 24 hpf

Tg(mpx:GFP)i114 embryos were injected at the one cell stage with control *mCherry* mRNA (1 nl of 50 ng/µl), *hax1* mRNA (1 nl of 50 ng/µl), *hax1* splice MO and combined *hax1 mRNA* and splice MO. Following injection (24 hpf), total RNA was extracted from the embryos and RT-PCR using *hax1 001* primers carried out. Results for PCR carried out using ef-1α loading control primers are also shown. Negative RT (- RT) and PCR (- PCR) controls containing water instead of RNA and cDNA respectively are also shown.

4.8.4 Effects of *hax1 001* overexpression on embryonic morphology and total PMN number

Having demonstrated both by *in* situ hybridization and RT-PCR that *hax1 001* mRNA injection into single cell embryos results in increased embryonic mRNA levels at 24 hpf, I next examined the effects of *hax1 001* overexpression on embryo morphology and total PMN number. It has previously been shown that injection of *mCherry* mRNA into embryos results in red fluorescing embryos. In experiments where the *mCherry* mRNA was used as a control, embryos were visualized under a Leica MZ10F fluorescent microscope using the red filter at 24 hpf in order to validate the overexpression. In each case, all of the embryos expressed the fluorescent protein indicating efficient injection and translation (data not shown). Control *mCherry* mRNA, *hax1 001* mRNA, *hax1* splice MO injected and *hax1 001* mRNA *hax1* MO co-injected embryos were cultured for 48 h and imaged using a Nikon Eclipse TE2000U inverted microscope with the 2x objective. Representative images are shown in Fig. 4.22 a. The *hax1 001* overexpression did not affect the overall appearance of the embryos. Both the *mCherry* and *hax1 001* mRNA injected embryos remained healthy throughout the course of the experiment. The *hax1* splice MO however, resulted in the characteristic delayed development and dysmorphic phenotype. Co-injection of the *hax1* mRNA with the *hax1* splice MO had no effect on the morphology of the embryos. The co-injected morphants remained developmentally delayed and dysmorphic with similar morphology to the hax1 splice MO only injected group (Fig. 4.22 a).

Total PMN counts of uninjected, mCherry control, *hax1* mRNA, *hax1* splice MO injected and *hax1* mRNA MO co-injected embryos were carried out at 48 hpf (Fig. 4.22 b.). PMN were counted from at least six embryos per condition. The *hax1 001* overexpression had no effect on total PMN numbers when compared to the uninjected and *m*Cherry control groups. As shown earlier in the chapter, the *hax1* splice MO resulted in reduced total PMN number. Co-injection with *hax1 001* mRNA

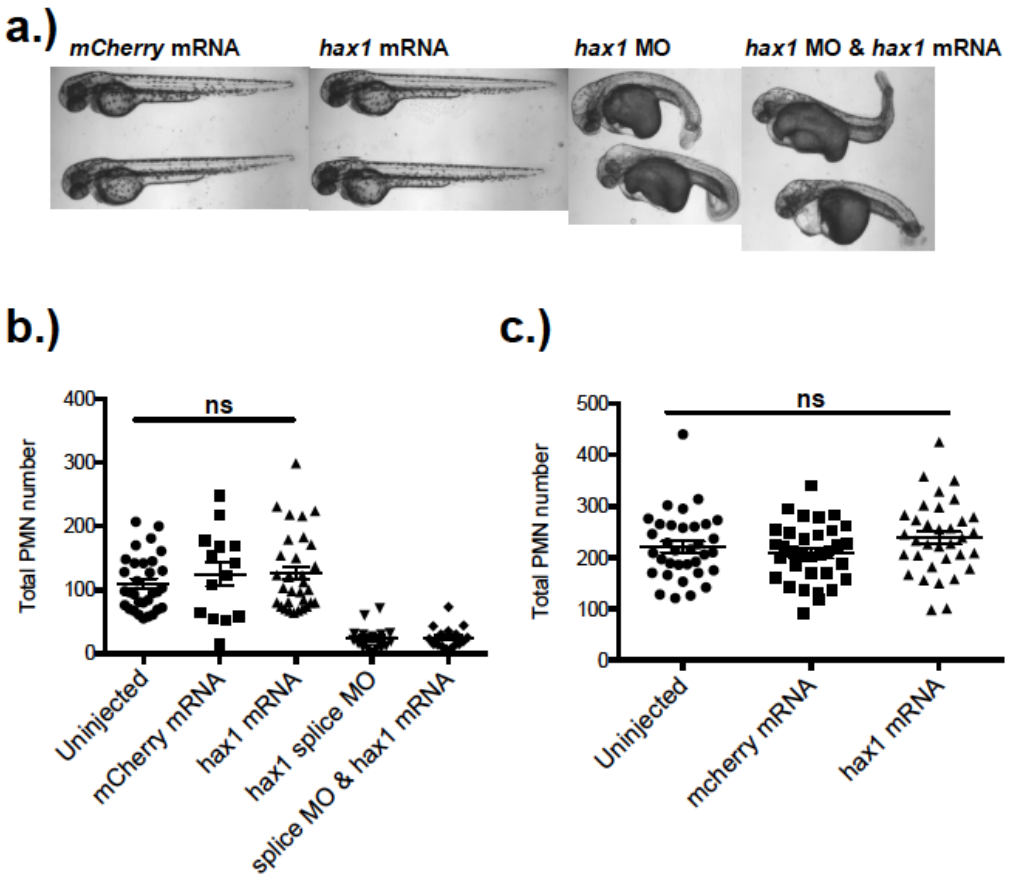

Figure 4.22 Effects of *hax1 001* overexpression in zebrafish embryos

Tg(mpx:GFP)i114 embryos were injected at the one cell stage with control *mCherry* mRNA (1 nl of 50 ng/ µl, *hax1* mRNA (1 nl of 50 ng/ µl), *hax1* splice MO and combined *hax1 mRNA* and splice MO. Following injection (24 hpf), total RNA was extracted from the embryos and RT-PCR using *hax1 001* primers carried out. **a.)** Bright field micrograph of embryos were taken 48 following fertilization**.** Total PMN numbers were counted from at least 6 embryos from each independent experiment at 48 hpf (uninjected and *hax1* mRNA*,* n=3; *mCherry*, *hax1* splice MO, combined *hax1* MO and mRNA, n=2) (**b.**) and 54 hpf. (n=3). Uninjected and *hax1* mRNA injected total PMN counts at 48 hpf were analysed using an unpaired student's t-test, $p<0.05$. Total PMN counts at 54 hpf were analysed using a one way ANOVA with Bonferroni's post test.

did not affect this reduction. Interestingly, MO injected and the *hax1 001* mRNA *hax1* splice MO co-injected embryos failed to survive to 48 hpf in the third experiment. Very few or none survived to 54 hpf in any of the three independent experiments carried out.

In order to test whether the *hax1* 001 overexpression affected PMN number at 3dpf, total PMN counts of uninjected, *mCherry* mRNA and *hax1 001* mRNA injected embryos were also counted at 54 hpf. Statistical analysis shows that there was no difference in the total PMN number between the control (uninjected, *mCherry* mRNA) and *hax1 001* mRNA injected embryos from three independent experiments.

4.9 Summary

The aims of this chapter were to assess *hax1* mRNA expression in zebrafish embryos and study the effects of *hax1* knockdown on total PMN number in zebrafish. Novel evidence for the multiple *hax1* transcript variant expression in the zebrafish embryo is presented through the use of *hax1* isoform specific primers. The full-length *hax1* transcript is expressed throughout embryonic development and in the adult PMN. Via cloning of the (full-length) *hax1 001* cds, the ubiquitous expression of *hax1 001* was determined using *in situ* hybridization of zebrafish embryo at 24 hpf. This observation shows that as in humans, *hax1 001* expression is not restricted to any cell type. Attempts to knockdown *hax1* by injection of a splice MOs were unsuccessful since it is demonstrated that it resulted in developmental delay, which did not correlate with the degree of knockdown. I have shown that these morphants also exhibit a reduction in total PMN numbers and this is likely to be due to the concomitant developmental delay observed. Furthermore, I found that *hax1 001* overexpression did not prevent the splice MO induced developmental delay and reduction in PMN number.

4.10 Discussion

4.10.1 *hax1* transcript expression in *D. rerio*

In this chapter, for the first time I have shown that zebrafish express at least five different *hax1* mRNA variants. This is in accordance with a study carried out by Lees *et al* (Lees et al. 2008), which describes the existence of eight *HAX1* alternative splice variants in human cell types. Transcript variants *001*, *002*, *005*, *007* and *008* were all expressed in embryos at 2 dpf. The RT-PCR data indicate that the *hax1 001* transcript is the most abundantly expressed. The *hax1 001* mRNA was detected in embryos at different stages of development (single cell embryo, 1-5 d.p.f) and in adult zebrafish PMN. These findings support a possible role for *hax1* in the zebrafish embryo development and PMN. The ubiquitous expression of the full-length *hax1* mRNA suggest that *hax1* plays an

important global role in the cells of the zebrafish embryo. The RT-PCR evidence in this thesis for *hax1* maternal mRNA transfer to the fertilized zebrafish egg further supports this notion. Maternal factors have been shown to regulate development prior to the activation of the embryonic genome and our data suggest that *hax1* may be involved in this process (Kane & Kimmel 1993).

To date, *HAX1* alternative splicing has been analysed in the genomes of three different species: the rat, mouse and human. Despite the high sequence similarity between the mouse and human *HAX1* cDNAs, the mouse variants identified so far appear to be distinct (Hippe et al. 2006; Lees et al. 2008). The rat and human variants are similar and are generated mainly from intron retention and the use of internal splice sites in exon 2 (Grzybowska et al. 2006; Lees et al. 2008). Human and zebrafish Hax1 protein share 60 % sequence similarity and 60 % identity at the cDNA level suggesting a similar functional importance. The data generated in this chapter suggests that the splicing pattern of zebrafish *hax1* is also in part analogous to that of the human *HAX1* gene (Lees et al. 2008). PCR bands of the expected sizes were generated for primers specific for transcript variants *001*, *002*, *005*, *007* and *008* indicating that these variants are likely to be spliced in the same manner as the human variants. Cloning and sequencing of the full-length transcript (*001*) confirmed the expected splicing pattern for this variant. Sequencing of the PCR band generated for transcript *008* also verified the expected splicing pattern at the 3' end of the transcript. Additional bands were visible in PCRs with most of the primers indicating that other *hax1* zebrafish isoforms are likely to exist. These data provide further support for a regulatory role of the alternative splicing in assigning variability in Hax1 function.

It is worth noting that in order to fully verify the splicing patterns in isoforms *002*, *005*, *007* and *008*, each transcript should be cloned from the start to stop codon and correct splicing pattern determined by sequencing analysis. A detected PCR band that has the expected size

might not necessarily have the expected splicing pattern. The protein sequences for each isoform discussed below are generated from the predicted splicing pattern of variants *002*, *005*, *007* and *008*. The putative open reading frames of the zebrafish Hax1 isoforms 005 and 008 are quite short and may represent incomplete coding sequences.

The predicted proteins encoded by the zebrafish *hax1* variants show variability at the C- and N-termini. Alternative splicing at the 5' region of the *hax1* mRNA generates three different protein start sites. Hax1 isoforms 001 and 002 appear to have an identical splicing pattern to that described in the human gene with isoform 002 missing a short protein region of the N- terminus of 001 (Lees et al. 2008). *In silico* translation analysis shows that even if exon 1 inclusion occurred in the zebrafish isoform 002, it is still likely to generate the same protein open reading frame.

Whereas the putative human isoform 005 is almost identical to isoform 001 and differs only by 8 amino acids, the zebrafish isoform 005 is a truncated version of the full-length isoform 001 and differs only by 6 amino acids at its C-terminus. The zebrafish isoforms 007 and 008 are also truncated version of isoform 001 and unlike their human counterparts, which show no resemblance to human isoform 001, these two isoforms are almost identical to the C-terminus of zebrafish Hax1 001.

Suzuki *et al* revealed some sequence similarity of the human HAX1 N-terminus to the Bcl-2 family homology (BH) domain regions of the Bcl-2 family (Suzuki et al. 1997). In the rat, the N-terminal region of the protein is thought to contain a localization sequence in two rat-specific transcripts (Grzybowska et al. 2006). Many other groups have reported the C-terminus of the protein to be responsible for protein-protein interactions. For example, interactions with caspase 9 (Han et al. 2006), Omi (Chao et al. 2008), and viral proteins Vpr (Yedavalli et al. 2005), human herpesvirus 8 K15 and HIV-1 REV (Modem & Reddy 2008) are all

reported to occur at the C-terminus of the protein. The alternative splicing at the N-terminus of zebrafish *hax1* may result in changes in the localization, stability or function of the protein. On the other hand, isoform specific regions found in the C-termini of the isoforms could determine the protein-binding partners thus enhancing the control of *hax1* expression in different cell types. The regulation of Hax1 isoform expression and or tissue specific isoform expression may in turn modulate the role of Hax1 in apoptosis signalling.

4.10.2 Zebrafish as a model for studying *hax1* function

In the last twenty years, the zebrafish has become a widely used model for the study of gene function and disease pathogenesis during embryonic development (Lieschke & Currie 2007). One of the many advantages of using the vertebrate model is the unique opportunity for the *in vivo* analysis of genes required for a normally functioning innate immune system. The optical transparency of the embryos allows excellent visualisation of fluorescent proteins in many different cellular processes (Renshaw et al. 2006; Ellett et al. 2011). This property has permitted the identification of numerous blood cell lineages through the generation of many transgenic lines in which GFP expression is driven by cell specific promoters. Embryonic zebrafish myelopoiesis has been shown to generate several cell types including the zebrafish PMN (sometimes termed heterophil), which closely resembles the human PMN. Embryonic PMN are fully functional by 48 hpf further facilitating the study of myelopoiesis in this model (Lieschke et al. 2001).

Though the components interacting with pathogens are more divergent, many of the factors acting downstream of the receptors in zebrafish innate immunity have remarkable similarities to the mammalian counterparts (Lieschke 2001; Stein et al. 2007). Caspases and many of the mammalian Bcl-2 protein family members involved in the control of the intrinsic apoptotic pathway have structural and functional counterparts in the zebrafish (Kratz et al. 2006). This is important because HAX1 has

been shown to bind to numerous factors involved in the intrinsic apoptotic pathway and disruption of the gene in the zebrafish is more likely to reproduce the human phenotype if these factors are conserved through evolution in the zebrafish.

Previous studies have highlighted that there is a striking similarity between zebrafish mutant phenotypes and human disease emphasizing its efficacy as a model system for elucidating pathophysiological mechanisms (Lieschke & Currie 2007). The utility of the zebrafish model therefore becomes particularly valuable in instances where mouse models fail to accurately recapitulate the human disease phenotype. Several studies have shown that mouse models for sever congenital neutropenia (SCN) are not necessarily neutropenic (Belaaouaj et al. 1998; Grenda et al. 2002). Although a single experiment carried out on the *Hax1* knockout mouse indicated a role for Hax1 in suppressing granulocyte apoptosis, the mouse phenotype did not accurately model the phenotype of HAX1 deficient patients, since the mouse phenotype is not limited to neutropenia.

The relevance of the zebrafish as a model for the study of *hax1* function is further emphasized by the high similarity of the zebrafish Hax1 to the human HAX1 protein sequence. Interestingly, both the extreme N-terminal region and that containing the acid box identified by Lees *et al* have been maintained through evolution across species and may underline key roles for these protein regions (Lees et al. 2008). Grzybowska *et al* utilised PSORT prediction software to suggest that the rat Hax1 amino acid residues 1-26 may function in mitochondrial localization (Grzybowska et al. 2006). This particular region corresponds to the N-terminal region with a very high sequence identity found in human, rat, mouse, macaque and zebrafish species.

The function of the N-terminus in mitochondrial localization has been verified by Yap *et al*. who demonstrated that deletion of 59 amino acid residues within the N-terminus of human HAX1 results in the abolishment of its mitochondrial targeting and reduced anti-apoptotic capacity (Yap et al.

2010). Interestingly, mutations in the human in this region of the gene are implicated in the neutropenic phenotype associated with these mutations. Germeshausen *et al* have shown that mutations affecting isoform 001 exclusively result in congenital neutropenia without the neurological phenotype (Germeshausen et al. 2008). This implies that it is this region, which has a functional importance in the PMN. Perhaps mutations in this region prevent the localization of HAX1 to the mitochondria and this in turn is detrimental to its normal function. The high similarity in this region of the zebrafish full-length Hax1 protein to human HAX1 suggests that this region is likely to have a similar function in the zebrafish and we have used this logic to design knockdown tools targeted to this region in order to recapitulate the SCN phenotype in the zebrafish.

4.10.3 The use of MOs to inhibit *hax1* expression in the zebrafish

MOs are a powerful approach to loss of function analysis in the zebrafish (Nasevicius & Ekker 2000). A splice site MO and an ATG MO targeting *hax1* splicing and translation respectively were used in this chapter in order to knockdown *hax1* mRNA levels and study the effects on PMN number. In humans *HAX1* mutations result in SCN as well as severe neurodevelopmental delay (Matsubara et al. 2007; Germeshausen et al. 2008). I have shown that disruption of *hax1* expression in the zebrafish embryo through MOs leads to a reduced PMN number and delay of generalised development. Although it is tempting to speculate that this phenotype is *hax1* specific, due to insufficient knockdown and factors discussed below, it is likely that the developmental delay and reduced PMN number are MO off-target effects.

Detection of *hax1* by RT-PCR analysis of RNA extracted from *hax1* splice site MO injected embryos yielded variable results. In some experiments gene knockdown was visible however, on others knockdown was poor and instead an additional ~2500 bp band was visible. Cloning and sequencing of the additional high molecular weight band identified a *hax1* specific amplicon resulting from a splicing abnormality (Fig. 4.13 d.).

The RT-PCR detection of the maternal *hax1 001* mRNA may explain the variable and poor gene knockdown in these studies. There is evidence for maternal pre-mRNA in eggs demonstrating that they cannot be blocked by splice MOs (Bennett et al. 2007). Some maternal mRNAs can persist in the embryo for up to three days (Alexa et al. 2009). Since the highly abundant *hax1 001* transcript expresses exon 3 and it has been shown in this chapter to be maternally transferred, this demonstrates that the splice-blocking MO cannot fully inhibit the *hax1 001* expression. Yet, the partial disruption of the *hax1* mRNA transcript expression leads to multiple defects in embryonic development indicating an essential embryonic role for the gene. In addition, it also caused a reduction in total PMN number. This raised the question as to whether this phenotype is *hax1* MO specific or a result of off-target effects?

4.10.4 Limitations of using MOs

Despite the large success rate, there are known limitations of utilising MO based gene targeting. One of the main problems with using MOs is that they may have off-target effects. This can occur by MO binding and disruption of a non-related gene. Although this is not likely, a published example of such effects in the zebrafish does exist (Ekker & Larson 2001). A second source of off-target effects is p53 activation (Robu et al. 2007). The induction of the p53-dependent cell death pathway leads to widespread apoptosis (Robu et al. 2007), neural degeneration (Nasevicius & Ekker 2000) and defects in epiboly (Imai & Talbot 2001). Some of these effects were visible with the *hax1* splice MO. Co-injection of MOs with a p53 ATG MO has been shown to rescue the p53-dependent apoptosis phenotype revealing the true effects of MOs (Robu et al. 2007). However, though the co-injection of a p53 ATG MO extended the survival of the embryos it did not appear to alleviate the severe developmental delay. It also did not have an effect on the reduced total PMN number. Although the data are representative of a single experiment and so it is not possible to draw any conclusion from the results, this may suggest that the *hax1* splice MO phenotype specifically

inhibits *hax1* pre-mRNA splicing and that the neurodevelopmental delay and PMN phenotype is specific to *hax1* knockdown. In support of this, MO targeted to cytochrome c oxidase led to neuronal cell death, which was not inhibited by co-injection with a p53 MO (Baden et al. 2007).

The recapitulation of the *hax1* phenotype although less marked using the ATG MO provides further support for the specificity of the *hax1* MO. The *hax1* ATG MO is likely to inhibit the translation of any maternal mRNA as well as zygotic *hax1* transcripts. However, the transcript variant expression data presented earlier in this chapter shows that alternative splicing generates *hax1* transcripts with at least three different ATG start sites hence only transcripts with the same start site as the full-length *hax1* are likely to be affected by the *hax1* ATG MO. This could justify the milder effects of the *hax1* ATG MO on the developmental delay and reduction in PMN number compared to the *hax1* splice MO. The lack of a zebrafish Hax1 antibody means that it is not possible to assess whether the ATG MO has successfully targeted *hax1* however, even if it was available it would not address whether the noted effects are caused solely by the *hax1* knockdown.

The most reliable control for a MO is rescue of the phenotype by co-injection of *in vitro* transcribed mRNA of the targeted gene (Eisen & Smith 2008). Contrary to the above findings, attempts to rescue the *hax1* splice MO induced phenotype by co-injection with *hax1 001* mRNA were unsuccessful. Co-injection did not prevent the characteristic developmental delay or the reduction in the total PMN number. This raises a concern about the specificity of the MO. however, due to the complex organization of the zebrafish *hax1* gene it cannot be ruled out that the phenotypic changes in response to the *hax1* splice MO injection are mediated by the inhibition of transcript variants other than *hax1 001.* On the other hand, this could suggest that full-length zebrafish *hax1* isoform may not play a role in embryonic development or PMN survival and homeostasis. A third explanation may be that the capped *hax1 001* mRNA was not functionally active in the injected embryos. In order to test

whether *hax1 001* mRNA overexpression had an effect in PMN apoptosis and in turn demonstrate that the mRNA was functional, uninjected and *hax1 001* injected *Tg(mpx:GFP)i114* embryos at 30 h were treated with 50 μM pyocyanin in the media for 6 h. Dual staining for the PMN specific Mpx (tyramide signal amplification-TSA) and an apoptotic marker (terminal deoxynucleotidyl transferase dUTP nick end labelling-TUNEL) revealed that the pyocyanin did not have an effect on PMN apoptosis in the embryos (data not shown) and therefore it was not possible to determine whether the *hax1 001* mRNA injection was in fact functional.

Further extensive analysis and characterization of the *hax1* mRNA variants is required in order to establish the exact isoform specificity of the MOs to determine the functional redundancy of the different isoforms. Future work could involve further characterization of the hax1 transcript expression profile using qPCR. The expression of each isoform could also then be tested for maternal transfer. Following this, isoform specific MOs could be designed and injected to test their effects on total PMN number and embryonic morphology. Attempts to rescue the phenotype with mRNA from each isoform could be carried out to test for redundancy and isoform specific functions.

4.11 Conclusion

This work provides novel evidence for the expression of multiple *hax1* transcript variants in the zebrafish embryo with a similar splicing pattern to that found in the human. I have shown that full-length *hax1* isoform *001* is ubiquitously expressed supporting a multifunctional role for the gene in the zebrafish. Furthermore, I have explored the effects of inhibition of the *hax1* gene *in vivo* and shown that this results in decreased total PMN number with concomitant developmental delay. I have shown that overexpression of *hax1 001* did not rescue any of the MO induced effects. In conclusion, due to the insufficient hax1 knockdown using the splice MO and lack of phenotypic rescue by co-injection with *001* mRNA, the reduced total PMN number is likely to be a secondary effect of the

delayed development and not a direct effect of the MO. Further work utilizing stable knockout zebrafish lines was required to validate these findings. The generation of stable *hax1* knockout lines and effect on total PMN number is described in Chapter 5.

5 Results- Creation of *hax1* mutant zebrafish lines

The aim of this chapter was to generate zebrafish *hax1* knockout lines in order to analyse the effect on total PMN number and function and to validate the morpholino data presented in Chapter 4. Zinc finger nucleases (ZFNs) and transcription activator-like effector nucleases (TALENs) are genetically engineered chimeric nucleases designed to specifically bind to DNA sequences (Cathomen & Joung 2008; Sander et al. 2011; Cermak et al. 2011). These proteins comprise a powerful class of tools enabling targeted genetic modification across many different species by induction of double stranded DNA breaks, which are repaired by the error-prone non-homologous end joining (NHEJ) mechanism (Bibikova et al. 2002) (Fig. 5.1). NHEJ generates many different indel mutations including frame-shift mutations resulting in inactivation of the target gene (Muhlrad & Parker 1994).

ZFNs and TALENs are hybrids of a non-specific DNA cleavage domain and a targeting DNA binding domain (Fig. 5.1 b and c.). This chapter describes the detailed protocols for generating a *hax1* targeting nuclease construct, initially by ZFN and subsequently by the newer TALEN approach. In both the ZFN and TALEN approach, the *hax1* binding domains were engineered into generic backbones encoding the FokI nuclease domains.

5.1 *hax1* targeted mutagenesis using the ZFN context dependent assembly (CoDA) approach

The ZFN CoDA approach was first described by Sander et al. (Sander et al. 2011) and is a publicly available platform of reagents and software for creating ZFNs. ZFNs function as dimers with each monomer composed of an engineered zinc finger (ZF) array (ZF domain) fused to a non-specific FokI nuclease domain (Kim et al. 1996). ZFN CoDa

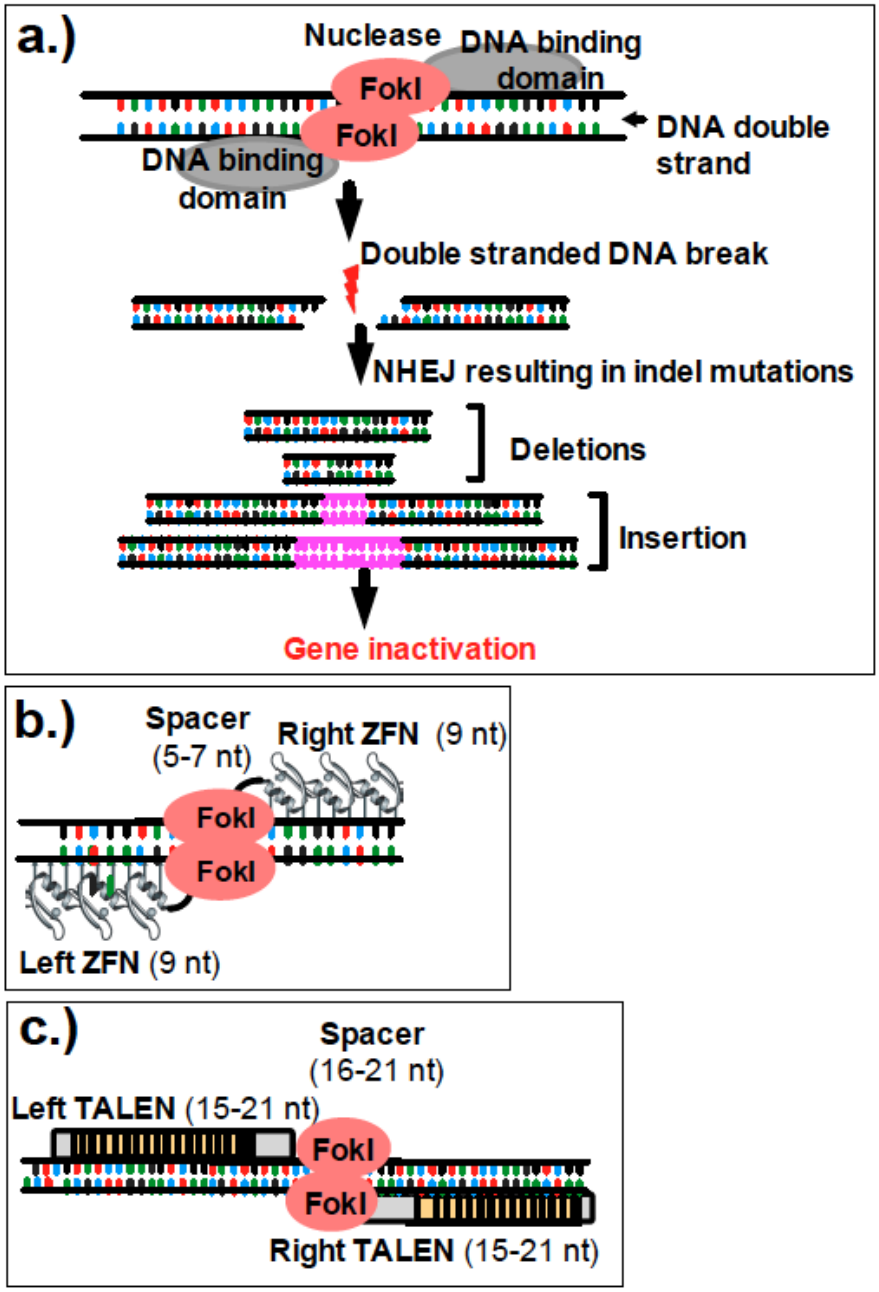

Figure 5.1 Schematic overview of genomic editing using ZFN and TALEN mutagenesis

a.) Outcome of gene targeting using engineered nucleases (ZFN and TALEN). Binding to the target site induces a double stranded mutation. A non-homologous error-prone joining mechanism then repairs the DNA break introducing indel mutations resulting in gene inactivation (Bibikova et al. 2002). The structure of a ZFN nuclease (**b.**) and TALEN (**c.**). Two monomeric molecules are required to bind the target DNA to enable Fok I to dimerise and cleave the DNA. Each monomer is composed of a DNA binding domain and an FokI nuclease domain. (Cermak et al. 2011; Sander et al. 2011). The lengths of the recognition sites and spacer regions are shown (nt-nucleotides).

entails assembly of three-finger arrays using N and C terminal fingers previously identified in other arrays containing a common middle finger (F2 unit) (Sander et al. 2011). With each ZF unit specifically binding to 3 base pairs, a 3-finger array ZFN monomer recognizes 9 base pairs. Sander et al. demonstrated that a large archive of N-terminal fingers (F1 units) and C-terminal fingers (F3 units) positioned adjacent to fixed F2 units could be utilised to create functionally active ZFNs (Sander et al. 2011). CoDA increases the probability of engineered ZFN activity by taking into consideration the context-dependent effects between adjacent fingers (Isalan et al. 1997; Isalan et al. 1998). This approach was used to generate a *hax1* specific ZFN expression vector and the product was then injected into single cell zebrafish embryos in order to create *hax1* mutant zebrafish lines. The ZF units were added as 5' extensions on primers used to amplify generic backbones (pCS2-Flag-ZFP-FokI-DD and pCS2-HA-ZFP-FokI-RR) containing the endonuclease FokI.

5.1.1 Generation of a zebrafish *hax1* targeting CoDA ZFN

5.1.1.1 Identification of a CoDA ZFN site in the zebrafish *hax1* gene

The zebrafish *hax1* gene sequence, deduced from the Ensembl website, was entered into the ZiFiT Targeter sequence window (http://zifit.partners.org/ZiFiT/ChoiceMenu.aspx) with exonic regions in uppercase and intronic regions in lowercase. The targeter generated five CoDA ZFN sites for the *hax1* gene, one found at the 5' of intron 1-2 and four target sites located on exon 3. It is necessary to use a CoDA target site that is most likely to disrupt the coding region of the genomic sequence of the target gene as intronic regions are likely to be spliced out and modifications of these regions would have no effect on the mRNA stability, protein structure and function. Since the first *hax1* CoDA ZFN site (ZFN-CHROMOSOME:zv8:19:7484201:7490708:1-SP-5-1) targeted intronic sequence of the gene this was not considered a suitable target site. The CoDA target site furthest from the 5' region of exon 3 was chosen (Fig. 5.2 a.). Figure 5.2 b. shows the *hax1* exon 3 target region

with the ZFN binding sites and spacer highlighted. The ZiFiT targeter also generated FASTA sequences of the left and right ZF domains. These were used to design F1 and F2F3 primers (Fig. 5.3) in order to allow addition of the ZF domains to the generic backbones. Two primers were generated for each subunit (Appendix 7.13.1). The 3' end of each primer contained 20 complementary bases to the generic backbone to ensure annealing and amplification by PCR. An F1 primer contained the F1 unit as the 5' extension whereas an F2F3 primer comprised units F2 and F3 of the ZF domain at the 5' end. Both the F1 and F2F3 primers were designed with an AgeI restriction site in order to allow digestion with AgeI following the PCR. This would then enable self-ligation of the AgeI digested plasmids into circular form with ZF units in the correct order. In addition the primers also contained 5' extensions (red) beyond the AgeI site (blue) to facilitate the AgeI restriction digest.

5.1.1.2 Preparation of the ZFN generic backbones

The left and right ZFN backbones (pCS2-Flag-ZFP-FokI-DD and pCS2-HA- ZFP-FokI-RR) (Meng et al. 2008) were kindly provided by Dr Stone Elworthy (Dept. of Biomedical Science, University of Sheffield). Briefly, Dr Elworthy prepared the plasmids by linearization with AgeI and PCR amplified the linear plasmids using primers LCS2 and goodRCS2 (Appendix 7.13) excluding the AgeI site from the amplified plasmid sequence. A 1 h restriction digest with DpnI followed in order to remove the starting plasmid. The plasmids were then gel purified and could be used as generic templates for generating CoDA ZFNs using PCR amplification with primers containing the specific F1, F2 and F3 zinc fingers, generated in section 5.1.1.1. An overview of the *hax1* targeting ZFN pair assembly is shown in Fig. 5.4.

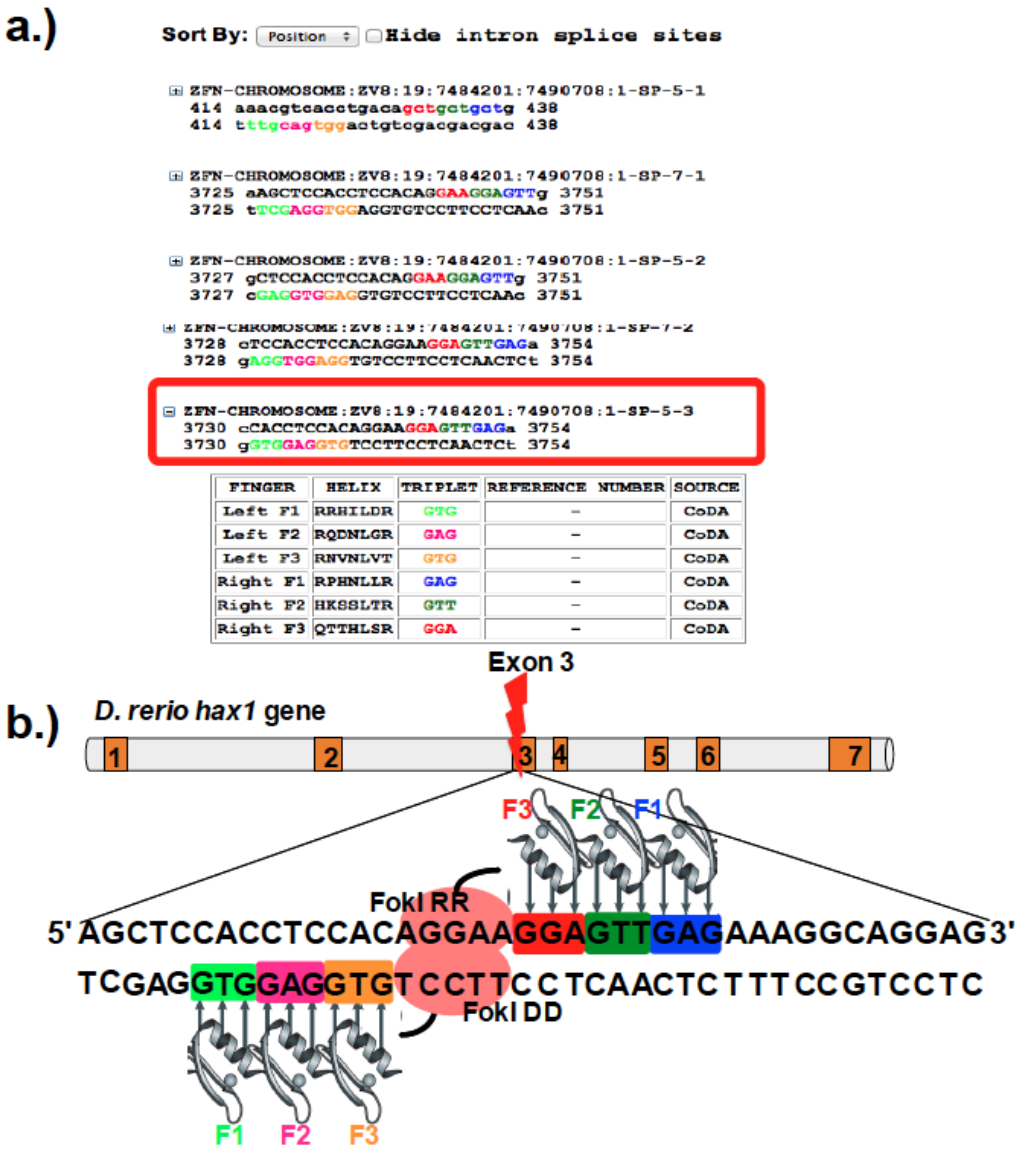

Figure 5.2 Identification of potential CoDA ZFN target sites in the zebrafish *hax1* gene

a.) *hax1* CoDA targeting output from ZiFiT version 3. The *hax1* gene sequence was entered into the ZiFiT sequence window following the instructions from the website (http://zifit.partners.org/ZiFiT/ChoiceMenu.aspx). The chosen ZFN target is indicated by the red box. The ZiFiT Targeter software summary of the CoDA zinc finger units shows the 3 bp targets of the *hax1* specific ZFN pair. **b.)** A diagram of the left and right zinc finger nuclease subunits and the target site in exon 3 of the *hax1* gene. Each nuclease consists of three zinc fingers (F1-F3) linked to the DNA-cleavage domain of FokI. Each finger binds to three consecutive basepairs of the DNA. Left and right ZFN subunit binding to this site generates a 5 bp spacer region.

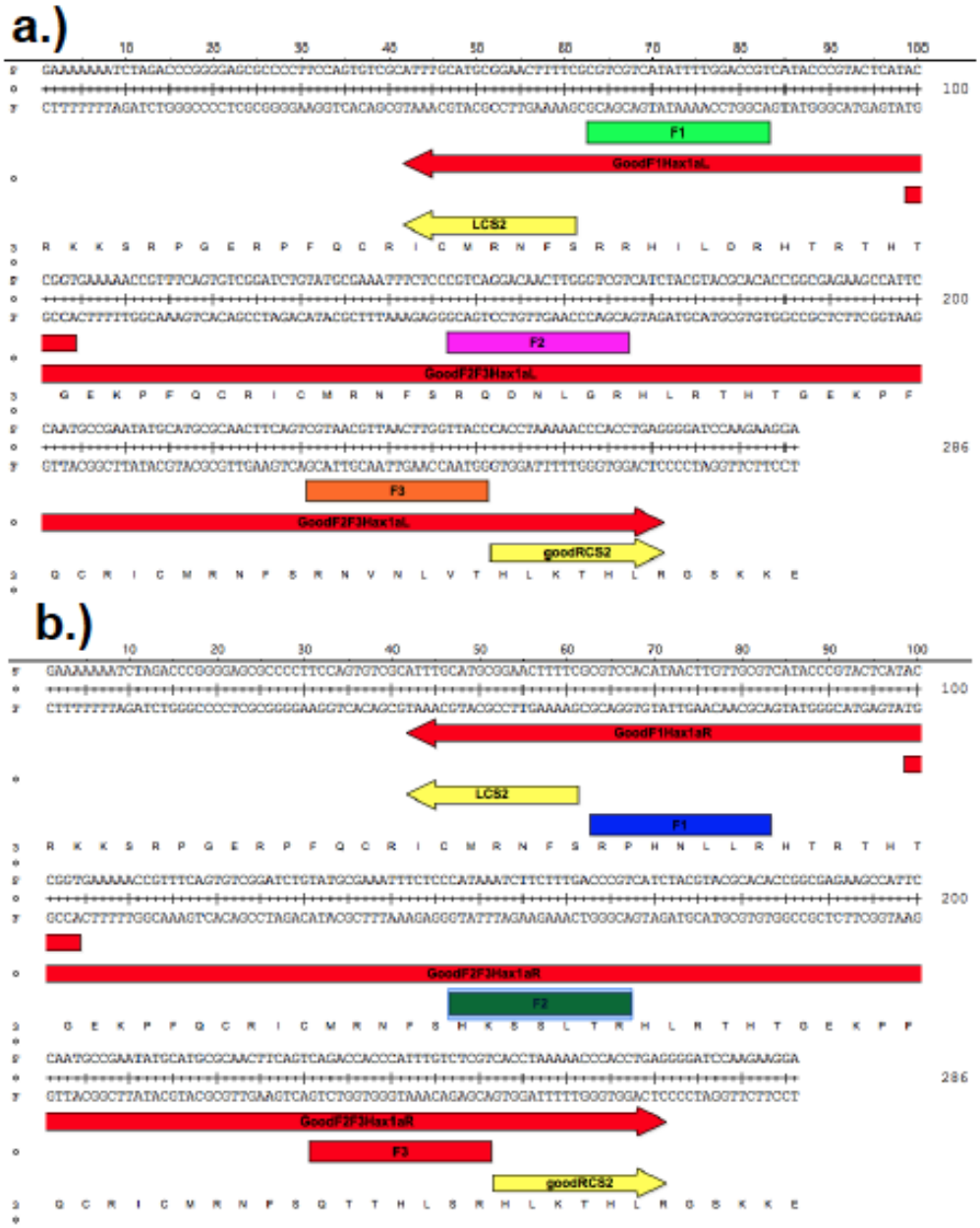

Figure 5.3 Annotation of the ZiFiT FASTA sequence output for the left and right ZFN subunits and ZFN primer design

The ZiFiT targeter sequence output for the Left (**a.**) and Right (**b.**) ZF domains. The red arrows indicate the sequence used to generate the ZFN F1 and F2F3 primers. The F1 and F2F3 units of each ZF domain are 5' extensions of the primers used to anneal and amplify the generic backbone plasmids pCS2-Flag-ZFP-FokI-DD (left ZFN subunit) and pCS2-HA-ZFP-FokI-RR (right ZFN subunit). The ZiFiT Targeter sequence output also contains an AgeI restriction site between the F1 and F2F3 fingers (overlapping region of the red arrows- ACCGGT). The F1, F2 and F3 units are annotated in colours correspond to those used in Fig. 5.2. Yellow arrows indicate primer annealing regions on the generic backbones.

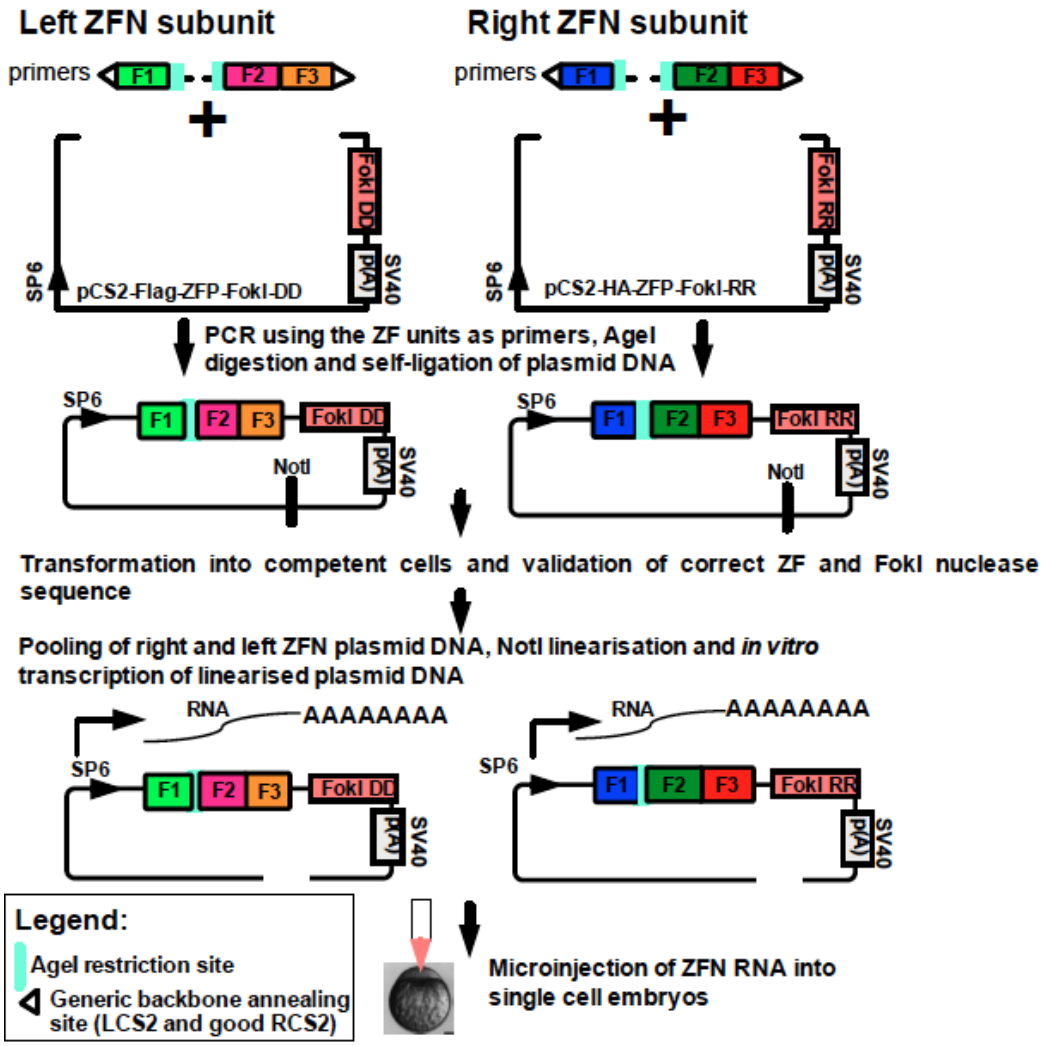

Figure 5.4 An overview of the assembly of a ZFN pair targeting the *hax1* gene

AgeI linearised left (pCS2-Flag-ZFP-FokI-DD**)** and right (pCS2-HA-ZFP-FokI-RR) ZFN generic backbones were amplified using the zinc finger units (ZFs) as primers. The F1 and F2F3 primers contained an AgeI restriction site (light blue) and a 5' extension beyond the AgeI site. Following amplification by PCR, the plasmids were subjected to an AgeI restriction digest and then allowed to self-ligate. The circular plasmids were transformed into competent cells. Purified plasmid preparations were then pooled and linearised using the unique restriction site for NotI. The NotI linearised plasmids were *in vitro* transcribed and the ZFN RNA injected into singe-cell embryos. The single-cell embryo image was adapted from the ZFIN website (http://zfin.org/zf_info/zfbook/stages/figs/fig3.html).

5.1.1.3 Addition of zinc fingers to the generic backbones

In order to verify the amplification of the ZFN generic backbones with the F1,F2 and F3 zinc fingers, the PCR products generated from the reactions assembled in section 2.2.7.1 (expected size: 5069 base pairs-bp) were subjected to agarose gel electrophoresis (Fig. 5.5 a.). A band of the expected size (~5 kb) was visible in both lanes with the PCR reaction amplifying the left ZFN producing a lower intensity band than PCR of the right ZFN construct. In order to assess the purification of the ZFN left and right plasmid following the generation of sticky ends by an AgeI, restriction digest (Section 2.2.7.2), the linearised plasmids were subjected to agarose gel electrophoresis. A band of the expected size (~5 kb) was visible for each the left and right ZFN encoding plasmids (Fig. 5.5 b.).

Following ZFN plasmid self-ligation and transformation into competent cells (Section 2.2.7.3), screening for zinc finger inserts was carried out by colony PCR of several well-separated, transformant colonies (Colony PCR- Section 2.1.20) using LseqCS2 and RseqCS2 primers (Appendix 7.13). A band of the expected ~600 bp size was visible in PCR reactions from colonies expressing both the left (L1, L8, L9, L10, L12, L14, L16) and right ZFN (R1, R3-8) subunits (Fig. 5.6). Colony PCR reactions displaying the expected PCR band size (~600 bp) were subjected to ExoI-SAP (exonuclease I- shrimp alkaline phosphatase) treatment followed by Sanger sequencing using LseqCS2 and RseqCS2 primers. Sequencing and bioinformatics analysis was carried out in order to examine whether the ZF units had inserted in the predicted order and verify the sequence. Blast analysis of the sequencing output of colony L12 and R3, which were used for in vitro transcription of the ZFN subunits, is shown in Appendix 7.14 (7.14.1 and 7.14.2).

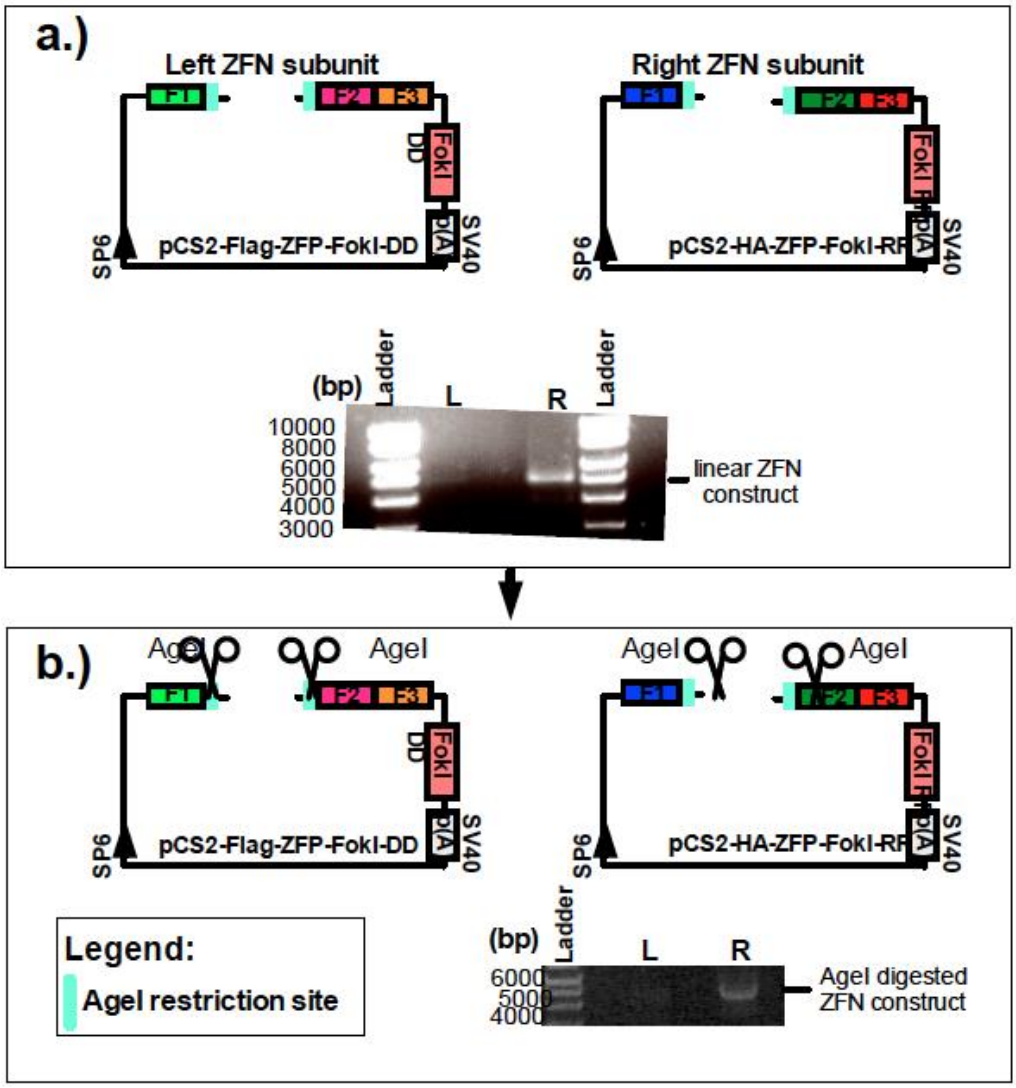

Figure 5.5 Addition of zinc fingers to the generic backbone

a.) The generic backbones were PCR amplified with the F1 and F2F3 primers. Following purification using a QIAquick PCR clean-up kit and elution into 44 µl of water , 2 µl of each PCR product was resolved on a 0.8 % SeaKem agarose gel and PCR bands were visualised using a UV transilluminator. **b.)** Following a 1 h incubation of the AgeI restriction digest, the left and right ZFN encoding plasmids were purified using a QIAquick PCR clean-up kit. Purified plasmid DNA was then subjected to agarose gel electrophoresis using a 0.8 % SeaKem agarose gel and 10 µl of the eluted DNA.

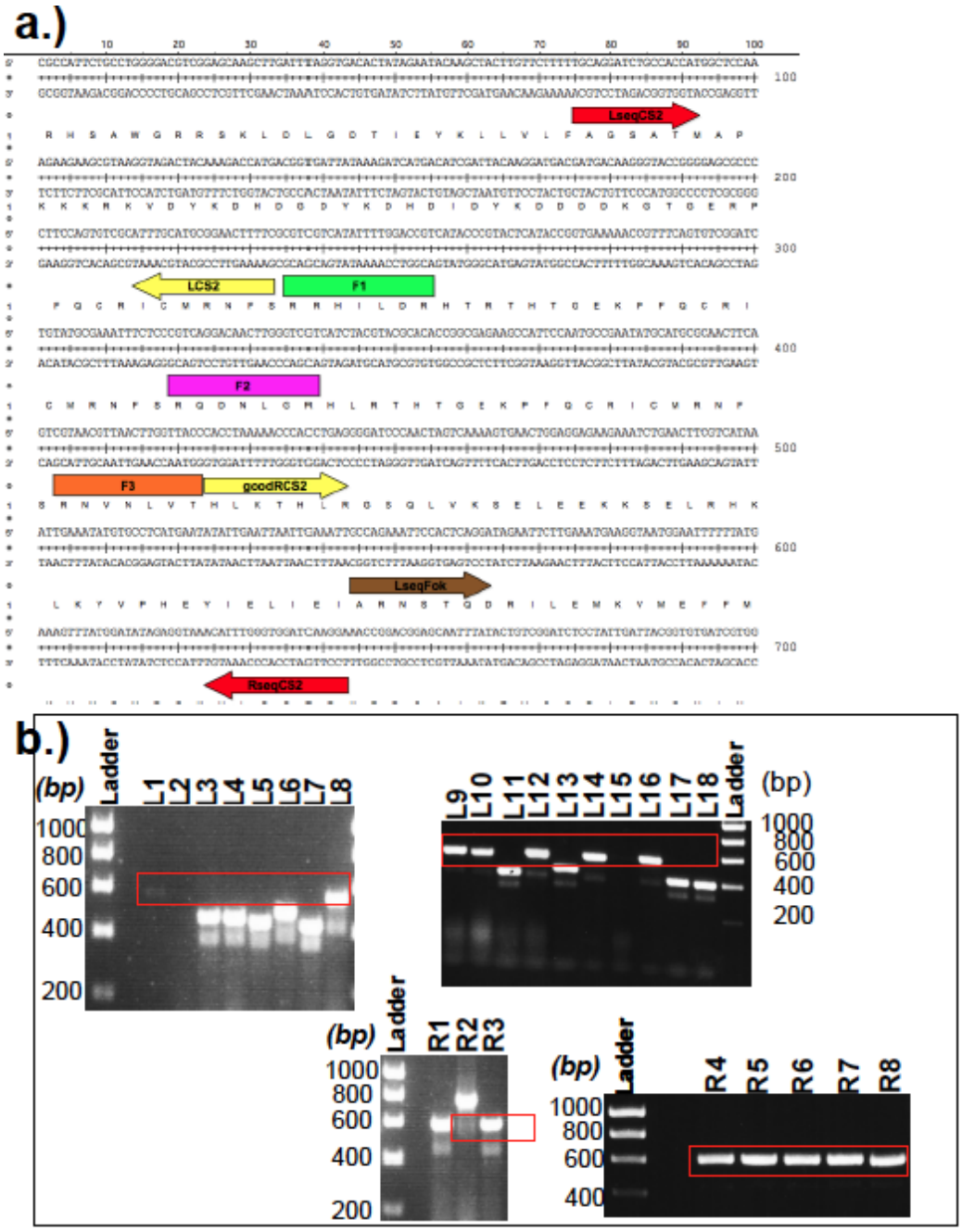

Figure 5.6 Verification of left and right ZFN subunit ZF domains by colony PCR and Sanger sequencing

a.) Left and right ZFN plasmid transformant colonies were PCR amplified using the LseqCS2 and RseqCS2 primers (red arrows). These primers flank the region containing the ZF inserts. The sequence shown is of the left ZFN subunit analysed using DNASTAR version 10.0 (Lasergene, Germany). **b.**) 5 µl of each PCR reaction was resolved on a 1.5 % SeaKem agarose gel and PCR bands were visualised using a UV transilluminator.

In order to ensure that the FokI DD (left ZFN) and FokI RR (right ZFN) nuclease domains also contain the intended sequence, clones with the verified zinc finger sequences were further examined by colony PCR and Sanger sequencing using LseqFok and RseqFok primers (Appendix 7.13) (Fig. 5.7). The PCR products were resolved by agarose gel electrophoresis. In order to validate the sequence, the colony PCR products of the correct size were Sanger sequenced using the LseqFok and RseqFok primers following ExoI-SAP treatment. Blast analysis of the FokI domain region from colonies L12 and R3, which were used for in vitro transcription of the ZFN subunits, is shown in Appendix 7.14 (7.14.3 and 7.14.4).

Once it was established that clone L12 (left ZFN subunit) and clone R3 (right ZFN subunit) contained verified sequences of the zinc finger and nuclease domains, a colony of each was used to inoculate a 50 ml carbenicillin (50 µg/ml) selective culture and grown O/N at 37 °C with shaking. The plasmid DNA was purified using a MIDI prep kit according to manufacturer's protocol (QIAGEN, Valencia, CA). The purified plasmid was quantified using a spectrophotometer. The left and right ZFN purified plasmids were linearised using NotI restriction enzyme as described in section 2.2.7.4. The left and right ZFN linear constructs were resolved by agarose gel electrophoresis alongside the circular plasmids (Fig. 5.8). The quoted DNA ladder bands were used as a comparator for quantitation

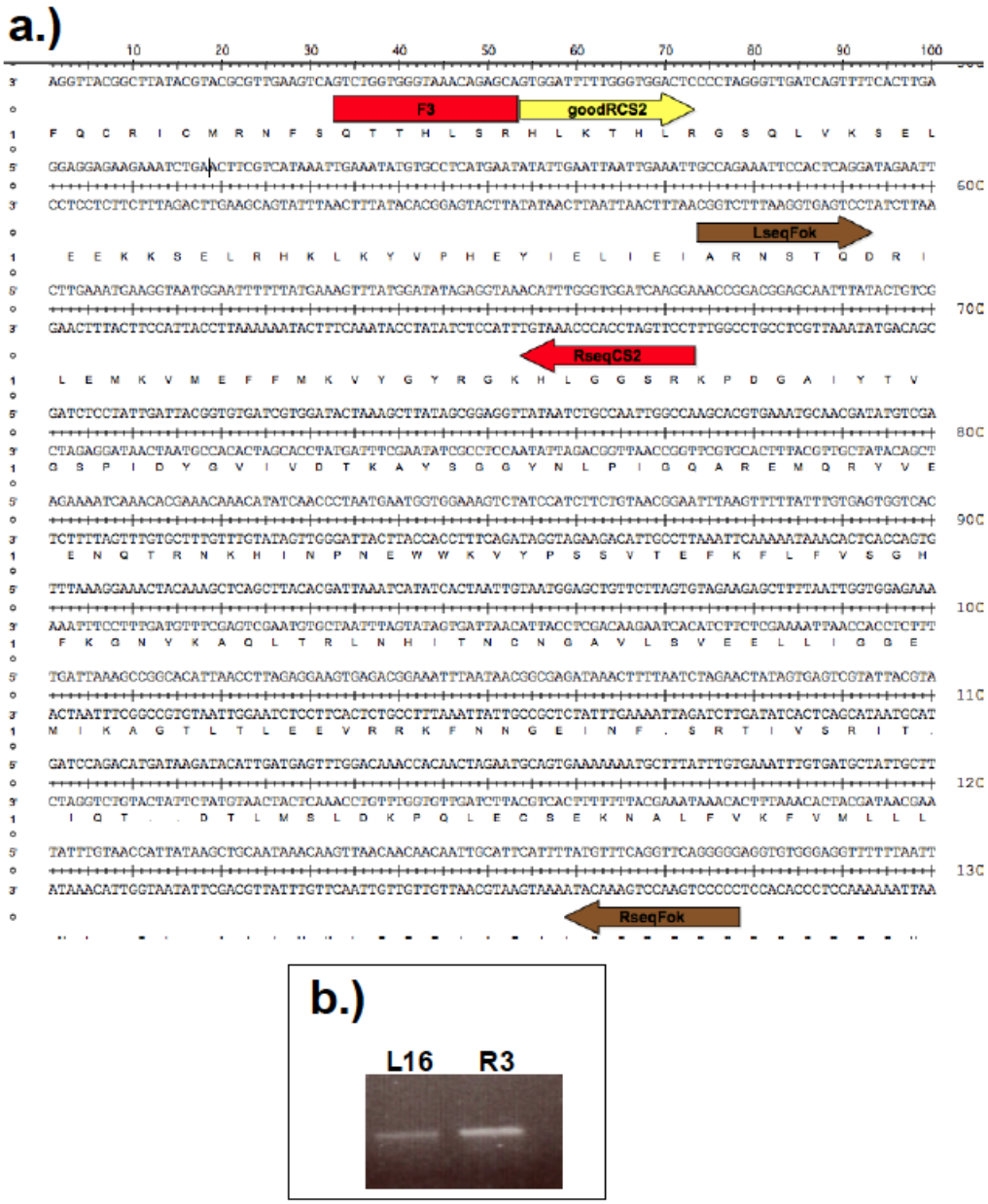

Figure 5.7 Verification of left and right *hax1* ZFN subunit ZF domains by colony PCR and Sanger sequencing

a.) Following verification of the ZF domain sequence of left ZFN expressing colony L16 and right ZFN expressing colony R3, colony PCR using the LseqFok and RseqFok primers was carried out. The L and RseqFok primers (brown arrows) flank the region of the ZFN plasmid containing the nuclease domain. The sequence shown is of the right ZFN subunit annotated using DNASTAR version 10.0 (Lasergene, Germany). **b.**) The PCR products (expected size: 705 bp) were resolved on a 1.5 % SeaKem agarose gel electrophoresis using 5 µl of the PCR reaction. PCR products were visualised using a UV transilluminator.

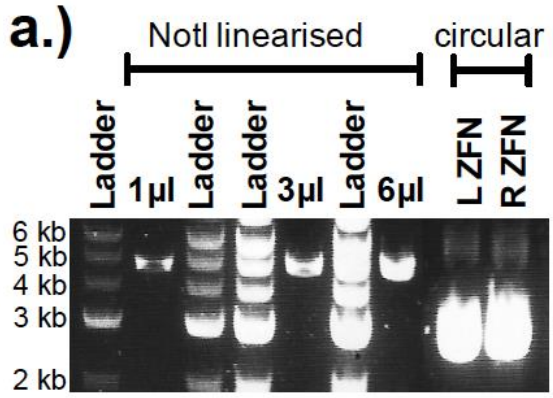

Figure 5.8 Preparation of *hax1* targeting ZFN RNA

a.) ZFN plasmids from 50 ml carbenicillin cultures were purified using a QIAGEN plasmid MIDI kit. 6 µg of each plasmid were pooled and subjected to a NotI restriction digest. Following NotI linearisation and purification of the plasmids using a QIAquick PCR clean-up kit, 0.5 µl of the left and right ZFN plasmid eluates were added to 9.5 µl of loading dye. 1 µl, 3 µl and 6 µl of this mixture were loaded alongside NEB 1 kb ladder (volumes from left 1µl, 2 µl and 5 µl) and left and right ZFN circular constructs on a 0.8 % SeaKem agarose gel.

5.1.2 Preparation of ZFN capped RNA for microinjection

In order to assess the quality and purity of the ZFN plasmid RNA generated in Section 2.2.7.4, the RNA was subjected to agarose gel electrophoresis. Figure 5.9 shows that a single RNA band was visible in the lane loaded with ZFN RNA.

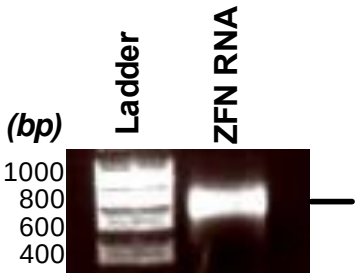

Fig. 5.9 *In vitro* transcription of *hax1* targeting ZFN expression vector
Following *in vitro* transcription and purification, 0.5 µl of the capped RNA was resolved on a 0.8 % agarose gel.

5.1.3 Microinjection of embryos with *in vitro* transcribed *hax1 targeting* ZFN mRNA

The toxicity of different ZFN RNAs varies greatly (Cornu & Cathomen 2010) and hence a range of ZFN mRNA doses were injected in order to optimize the dose in AB embryos. Single cell embryos were injected with various doses of capped RNA. Injected embryos were grown at low density (<50 per petri dish) and unfertilized or damaged embryos were removed. At 24 hpf, the embryos were inspected to determine the dose of mRNA resulting in the vast majority of embryos to be free of toxic effects. Embryos injected with ~40 pg (quantified on an agarose gel) of the capped RNA generated from section 2.2.7.4 resulted in an appropriate 30 % rate of deformity 24 hpf (data not shown).

5.1.4 *hax1* gene sequence analysis of zebrafish embryos injected with ZFN-encoding RNA

In order to analyse the zebrafish *hax1* gene sequence for somatic mutations PCR was carried out on pooled genomic DNA (gDNA) encompassing the CoDa ZFN target site. The annealing sites of the

LHax1ZFN and RHax1ZFN primers (Appendix 7.13) used for the PCR along with the ZFN binding site and spacer region are shown in Fig. 5.10 a. A restriction enzyme site for HpyAV was also identified in the spacer region in order to subsequently allow screening of mutants by restriction enzyme digest (Fig. 5.10 a.). The PCR product was then either subjected to Roche Titanium 454 sequencing or was TOPO cloned and Sanger sequenced. Analysis of the ZFN target site through TOPO cloning and colony PCR would only determine whether the mutation rate at the ZFN target site was more than ~2%.

5.1.4.1 Analysis of zebrafish *hax1* ZFN target sequence by TOPO cloning and colony PCR

Genomic DNA from 50 embryos injected with the *hax1* targeting CoDA ZFN was extracted at 24 hpf as described in section 2.1.24. A single microliter of gDNA template and Phusion HF DNA polymerase (section 2.1.17) were used in a PCR reaction amplifying the *hax1* gene region containing the exon 3 ZFN target site. In order to assess the amplification the PCR product was resolved by agarose gel electrophoresis (Fig. 5.10 b). A single ~300 bp band was visible in the PCR reaction carried out using the gDNA of ZFN injected embryos and the negative PCR control was clear. TOPO cloning was carried out using 4 µl of the PCR reaction and a Zero Blunt TOPO PCR cloning kit according to manufacturer's protocol. The cloning reaction (2 µl) was then used to transform a vial of competent One Shot TOP10 *E. coli* cells (Invitrogen Life Technologies, Carlsbad, CA) according to manufacturer's instructions. Transformed cells were streaked onto ampicillin (50 µg/ml) selective LB agar plates and grown overnight (O/N) at 37 °C. On the following morning, 96 well-separated colonies were picked from the plates and colony PCR (2.1.20) was carried out using LHax1ZFN and RHax1ZFN and a 96 well PCR plate.

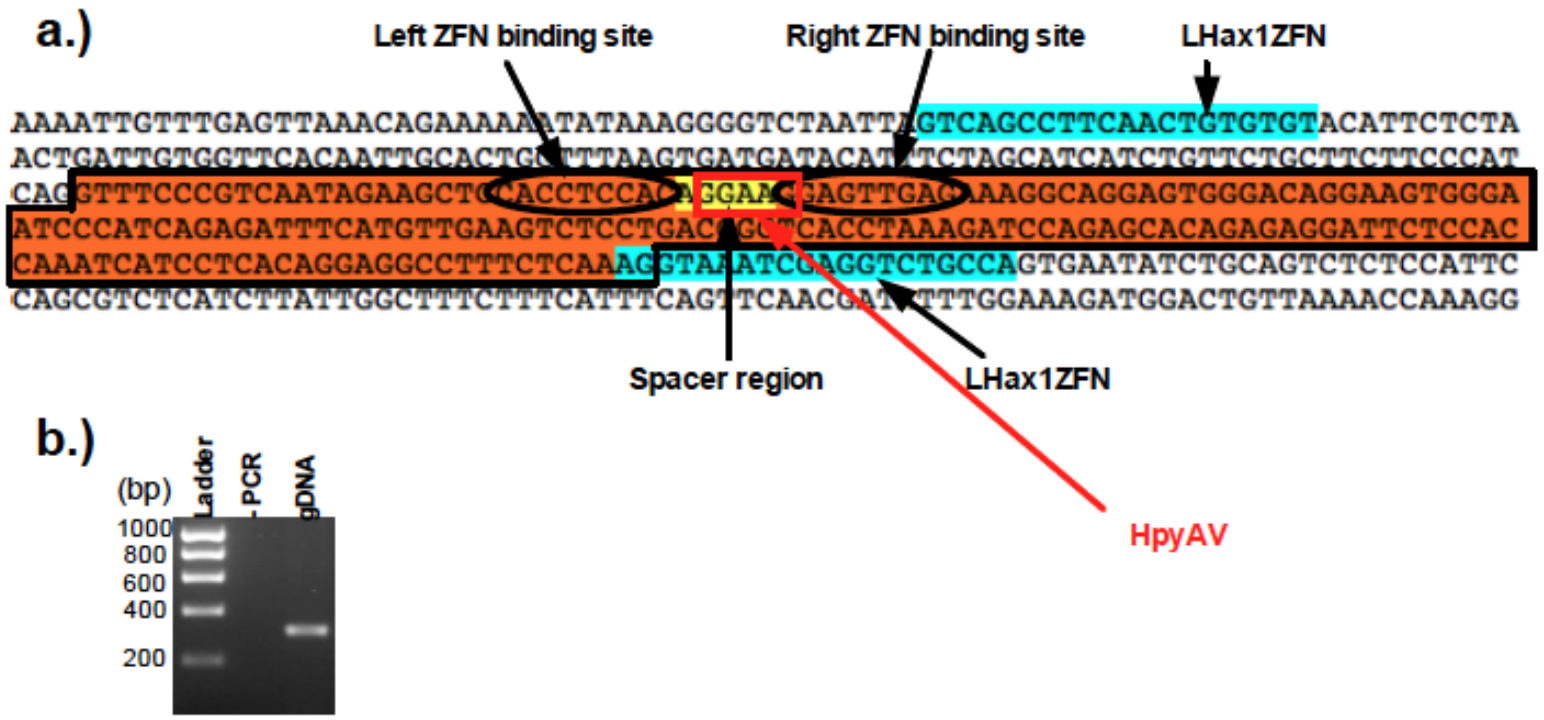

Figure 5.10 LHax1ZFN and RHax1ZFN primer binding sites

a.) The LHax1ZFN and RHax1ZFN primers (blue) were designed to span a region of 305 bp with the ZFN target spacer region (yellow) in the centre of the sequence. The left and right ZFN subunit binding sites found on exon 3 of the gene (orange) are also shown. The red box indicates the recognition site for the restriction enzyme HpyAV. **b.)** gDNA was extracted from 50 healthy *hax1* ZFN injected embryos and PCR carried out using the Hax1ZFN primers. PCR product was resolved by agarose gel electrophoresis and visualised using a UV transilluminator. A no template control for the PCR reaction (- PCR) was also included.

In order to assess the amplification, PCR products from numerous random colonies were resolved by agarose gel electrophoresis. All tested colonies contained a PCR band of the expected ~300 bp size (Fig. 5.11 a.). Following Exo-SAP treatment of the remainders of the PCR reactions, each PCR product was Sanger sequenced using LHax1ZFN and RHax1ZFN primers. The sequences of the *hax1* targeting ZFN injected embryos were then compared to the wild type (WT) reference sequence. Ape software was used to align 20 sequences at a time. An example of the output for the sequences generated from the left (b.) and right (c.) ZFN primers are shown in Fig. 5.11. The Sanger sequence analysis using both primers revealed that there were no changes detected in the site of the ZFN target or the regions flanking the site.

5.1.4.2 Analysis of zebrafish *hax1* ZFN target sequence by Roche Titanium 454 sequencing

In order to analyse the *hax1* ZFN target site by Roche Titanium 454 sequencing and detect mutations at a frequency lower than 2%, gDNA was PCR amplified using LHax1ZF454 and RHax1ZF454 primers (Appendix 7.13.2), which bind on the same region as those shown in Fig. 5.9 a but contain a 5' extension to allow Roche 454 sequencing.

The remaining PCR product was purified using a QIAquick PCR clean-up kit and the purified DNA subjected to PCR amplification using 1 µl of the eluted PCR product and the a titanium and b titanium primers (Appendix 7.13). The component and PCR cycling used were as shown above. This was again followed by purification using a QIAquick PCR clean-up kit. Following the PCR product purification, amplification of the PCR reactions each with the LHax1ZF454 and RHax1ZF454 primers (Fig. 5.12 a.) and the a titanium and b titanium primers (Fig. 5.12 b.) was assessed by agarose gel electrophoresis using a 2% 1:1 metaphor and SeaKem agarose gel. PCR analysis shows that a band of the expected ~400 bp size was clearly visible in both Fig. 5.12 a. and Fig. 5.12 b. The resulting

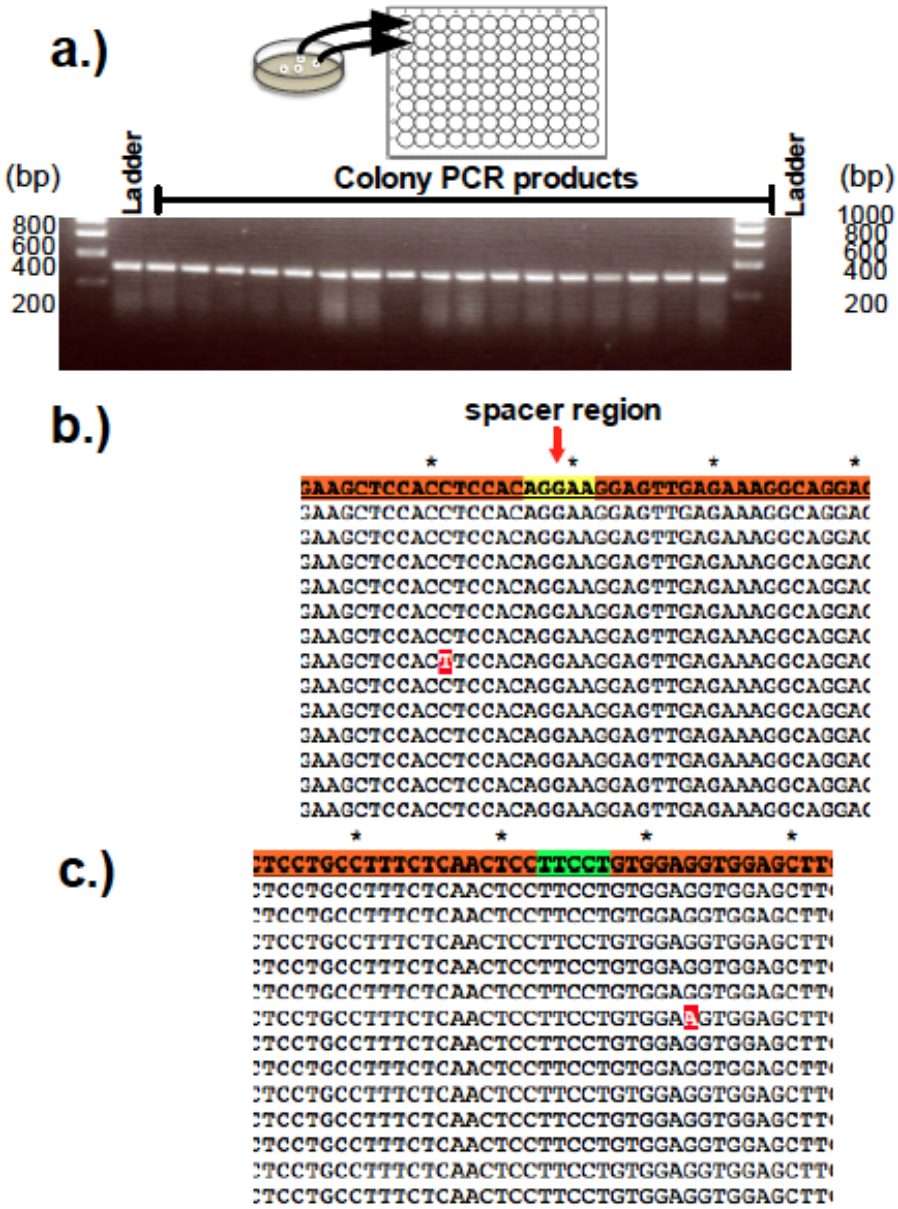

Figure 5.11 Analysis of *hax1* gDNA from embryos injected with *hax1* encoding zebrafish RNA by colony PCR and Sanger sequencing

a.) Colonies of competent cells transformed with the *hax1* fragment generated using the Hax1ZFN primers were selected and colony PCR carried out. 96 colonies were picked in total. 5 µl of PCR product from 18 randomly chosen colonies were resolved by agarose gel electrophoresis. Bands were visualised using a UV transilluminator. Following ExoI-SAP treatment, the PCR products were Sanger sequenced with LHax1ZFN (**b.**) and RHax1ZFN (**c.**) primers. Sequencing traces were analysed using Ape software. Sanger sequencing did not reveal any changes in the *hax1* ZFN target region. The top sequence in **b.** and **c.** represents the WT reference sequence. The spacer region is highlighted in yellow (**b.**) and green (**c.**).

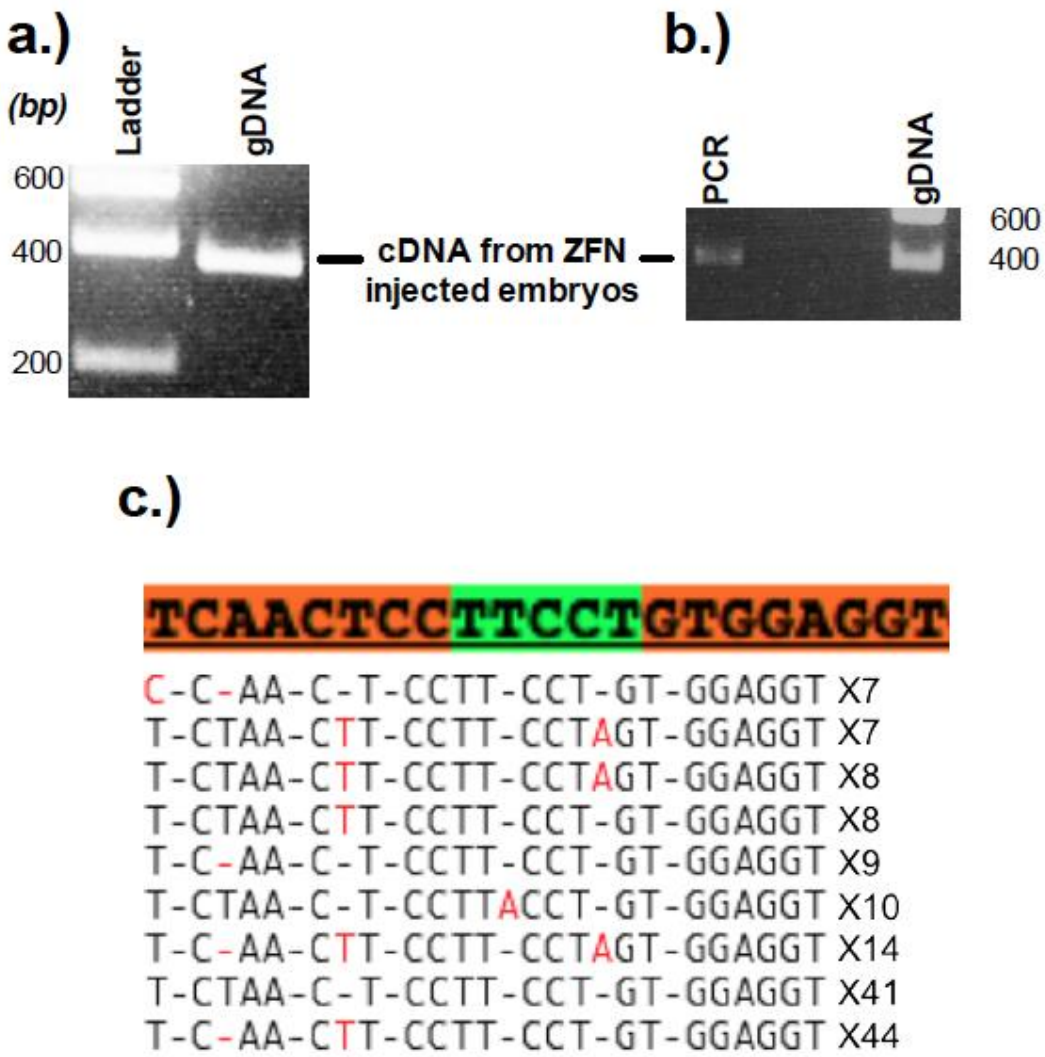

Figure 5.12 Preparation of the *hax1* ZFN target sequence and analysis by Roche Titanium 454 sequencing

a.) Genomic DNA extracted from 50 healthy *hax1* ZFN injected embryos was PCR amplified with L and RHax1ZF454 primers (gDNA). 5 µl of the PCR product were resolved on a 2% 1:1 metaphor and SeaKem agarose gel and visualised using a UV transilluminator. **b.)** The remainder of the PCR product was purified using a QIAquick PCR clean-up kit (with the guanidine HCl step) and eluted with 300 µl of water. Following PCR amplification using atitanium and btitanium primers, the PCR product was once again subjected to purification using a QIAquick PCR clean-up kit (with the guanidine HCl step) and elution into 30 µl of water. The purified PCR product (gDNA) was then subjected to agarose gel electrophoresis. **c.)** Frequencies and sequences of changes in the *hax1* ZFN target site of ZFN RNA microinjected embryos. The wild type reference sequence (orange) with the spacer region highlighted in green is also included.

amplicon from PCR using the a titanium and b titanium primers was subsequently subjected to Roche Titanium 454 sequencing. Analysis of the Roche Titanium 454 sequencing showed that out of 4938 reads received, 208 contained differences in the target sequence (Fig. 5.12 c.) resulting in a mutation frequency of 4.2%. Most of these differences were found in the region encompassing the spacer and ZF binding region. The sequence modifications were mostly single base changes and included insertion of a single A or T nucleotide and substitution of a T with C nucleotide. There were no large multiple base deletions or insertions detected by the Roche 454 sequencing. The full Roche 454 amplicon analysis is shown in Appendix 7.15. Since only a few of these mutations could be detected by Roche 454 sequencing, this method was unlikely to successfully generate knockout mutants and therefore, an alternative method using targeted transcription activator-like effector nucleases (TALENs) was utilised.

5.2 *hax1* targeted mutagenesis using a transcription activator-like effector nuclease (TALEN)

Transcription activator-like effector nucleases are a relatively new class of specific DNA binding proteins formed by a fusion between TALEN activator-like TAL effectors of the plant pathogenic bacteria of the genus *Xanthomonas spp.* to the FokI nuclease (Christian et al. 2010). The native function of TAL effectors is to directly modulate host gene expression (Bogdanove et al. 2010; Christian et al. 2010). TALEN specificity is determined by a central domain comprising 12-27 tandem repeats of 33-35 amino acids (aa) followed by a single truncated repeat of 20 amino acids (Boch & Bonas 2010). The amino acid positions 12 and 13 in each repeat known as the repeat variable di-residue (RVD) specify the target nucleotide. The Cermak et al. TALEN design is based on the use of four common RVDs HD, NI, NG and NN, which most frequently associate with nucleotides Cytosine, Adenine, Thymine and Guanine respectively (Cermak et al. 2011).

Multiple design scaffolds for TALEN assembly have been described differing in parameters including the spacer length, repeat array length and the base preference preceding the target site on the 5' end (Cermak et al. 2011; Miller et al. 2011; Li et al. 2011). TALEN assembly techniques also differ in the N and C terminus of the TALEN protein (Miller et al. 2011). The Golden Gate method described by Cermak et al. (Cermak et al. 2011) was used for the assembly of a *hax1* targeting TALE nuclease. Golden gate cloning utilises Type IIS restriction endonucleases, which cleave DNA at a defined distance from their recognition site to create unique 4 bp overhangs. This allows digestion and ligation of multiple constructs in the same reaction (Engler et al. 2009).

The set of Golden Gate TALEN assembly plasmids required for the construction of the TAL array is publicly available from the Addgene website (https://www.addgene.org). MIDI preparations of the plasmids at the desired working concentration were kindly provided by Dr Freek Van Eeden (Dept. of Biomedical Sciences). Each tandem repeat (module) containing a specific RVD is encoded by a single plasmid (Cermak et al. 2011). Cermak *et al*. utilised the TypeIIS restriction enzyme BsaI to initially excise from the plasmids and ligate to one another the first ten modules containing the RVD sequences. In the same reaction the RVD modules were cloned into an array plasmid pFUS_A (Cermak et al. 2011). Remaining modules are cloned in the same way into other specified array plasmids depending on the number of RVD repeats. This is carried out for both the left and right TALEN subunits. Esp3I digestion of the array plasmids, a plasmid containing the last repeat and the destination vector in a second reaction allows ligation of the RVD and assemble in the correct order (Cermak et al. 2011).

The following sections describe the design and construction methodology of a *hax1* targeting TALE nuclease using the pCAG-T7-TALEN(Sangamo) destination vector . To date, there are no published data describing the use of this generic TALEN backbone in successful TALEN mutagenesis approaches. Sequence analysis of the induced

mutations and preliminary results on the effects of the mutations are also included.

5.2.1 Construction of a *hax1* targeting TALE nuclease

5.2.1.1 Identification of a TALEN site in the zebrafish *hax1* gene

It has previously been shown that HAX1 human mutations affecting the 5' region of exon 2 result exclusively in a neutropenic phenotype whereas individuals harbouring mutations in the 3' region of the exon in addition to neutropenia also exhibit neurological symptoms (Germeshausen et al. 2008). Due to the TALEN technique offering more flexibility with the target site than the CoDA ZFN approach, it was possible to design a TALE nuclease targeting the 5' region of exon 2 of the zebrafish *hax1* gene. In order to allow quick and easy screening of TALEN induced mutations, the sequence of the *hax1* gene was initially deduced from the Ensembl website and inserted into the NEBcutter V2.0 (http://tools.neb.com/NEBcutter2/) for enzyme restriction analysis. A restriction site for BspHI in the 5' region of exon 2 was identified. The sequence containing the BspHI site and fifty bases upstream and downstream (Appendix 7.16) of the site was entered into the on-line tool TALEN targeter 2.0 (https://tale-nt.cac.cornell.edu/node/add/talen-old), which scanned for TALEN sites based on the TALEN design guidelines. The BspHI site is found a few bases downstream of the conserved putative acid box identified in Chapter 4, which may play a functional role. Firstly, the spacer region length was set from a minimum 16 bp to a maximum of 21 bp. Secondly, the minimum repeat array length setting was set to 15 bp and the maximum to 21 bp. Screenshots of the TALEN Targeter tool and the output for the chosen *hax1* specific TALEN pair are shown in Fig. 5.13. All of the boxes shown in Fig. 5.13 a. were un-ticked except the last box stating that a T was required at position N. The site shown in Fig 5.13 b. was used for the TALEN design described in this

a.)

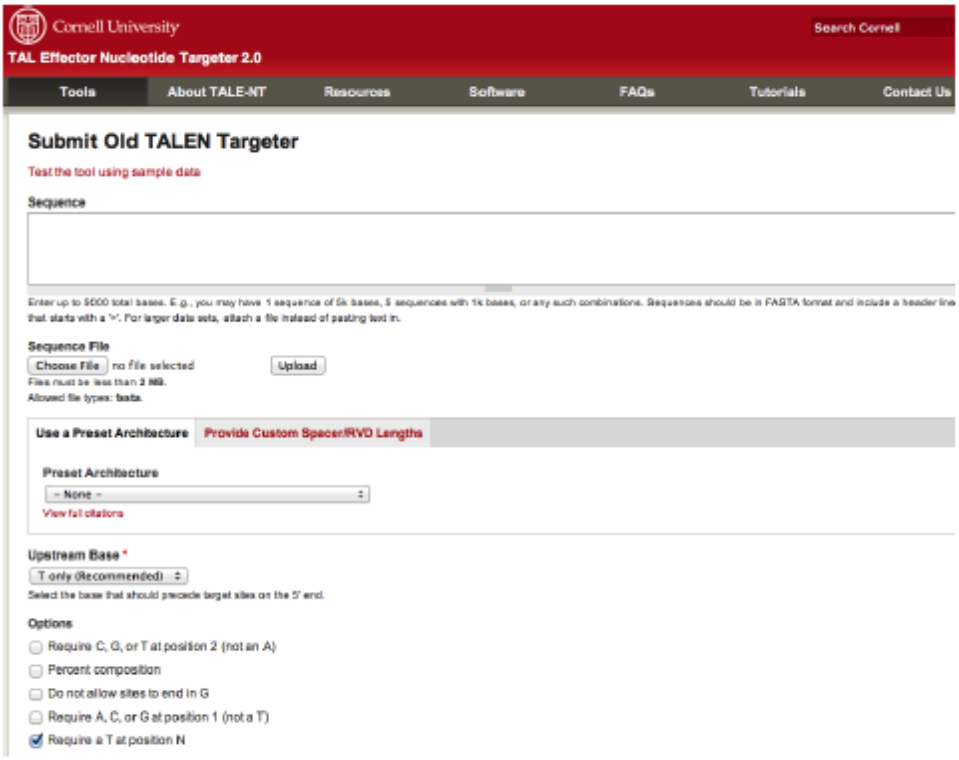

b.)

Gene	TAL1 start	TAL2 start	Spacer range	TAL1 RVDs	TAL2 RVDs	Plus strand sequence	Unique_RE_sites_in_spacer
Hax1	17	67	32-50	NI HD NI NN NN NN NI HD HD HD HD NG NG HD NG	HD NG NG HD NI NG HD NI NG HD NI NG HD NI NG HD NG	ACAGGGAC CCCTTCT TTGATGGA ATGATTCA TGA AGATGATG ATGATGAA	HinfI:GANTC BspHI:TCAT GA TfiI:GAWTC Hpy188III:TC NNGA

Figure 5.13 Identification of *hax1* TALEN site using TALEN Targeter 2.0

a.) A screenshot showing the TALEN target DNA sequence input window and the design parameters available. **b.)** A small section of the targeter output for the human *hax1* exon 2 showing the target site. The corresponding Repeat Variable Di-residues (RVDs) and the restriction sites found in the target region are also included.

chapter. The *hax1* specific TALEN pair comprises a left subunit binding to 15 base pairs and a right subunit recognising 17 base pairs. Binding of the TALEN pair to the target site produces a spacer region of 19 base pairs. The left and right RVD sequences and the recognition site of the *hax1* exon2 specific TALEN are shown in Appendix 7.16. Figure 5.13 b. shows the TALEN target site containing the BspHI within the spacer region. PCR primers were designed to amplify a sequence encompassing the spacer region, ensuring that the overlapping BspHI restriction site was unique in the amplicon (Fig. 5.14).

the TALEN pair to the target site produces a spacer region of 19 base pairs. The left and right RVD sequences and the recognition site of the *hax1* exon2 specific TALEN are shown in Appendix 7.16. Figure 5.13 b. shows the TALEN target site containing the BspHI within the spacer region. PCR primers were designed to amplify a sequence encompassing the spacer region, ensuring that the overlapping BspHI restriction site was unique in the amplicon (Fig. 5.14).

5.2.1.2 *hax1* exon 2 specific Golden Gate TALEN assembly stage I

In the first Golden Gate reaction, the left and right *hax1* TALEN subunits were each initially compiled into two halves (left TALEN part A and B, and right TALEN part A and B). The reaction components are shown in section 2.2.8.2. An outline of the whole assembly process is shown in Fig. 5.15. Following the assembly of the two parts of each TALEN, the resulting plasmids were subjected to a double restriction digest using NheI and XbaI. The digestion products of each of the four reactions carried out in section 2.2.8.2 were resolved by agarose gel electrophoresis (Fig. 5.16). The expected band sizes 266 bp, 2132 bp and 500 bp-1100 bp depending on the RVD module number were visible in all four lanes. The sizes of the left and right part B plasmids are consistent with the number of RVD modules cloned into the array plasmid (left Part B- 4 RVDs and right Part B- 6 RVDs). This indicated that the

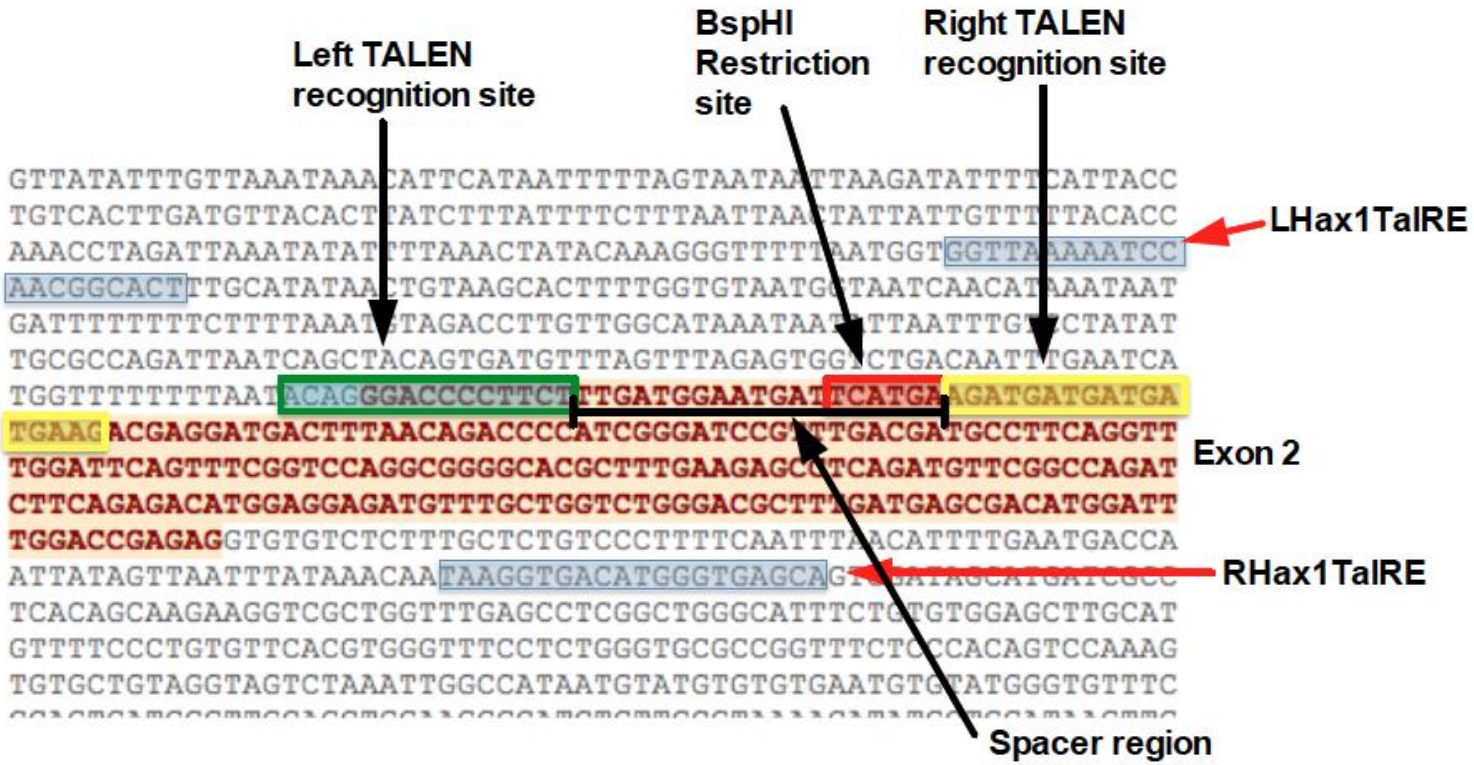

Figure 5.14 LHax1TalRE and RHax1TalRE primer binding sites

a.) The LHax1TalRE and RHax1TalRE primers (blue) were designed to span a region of 534 bp with the TALEN target spacer region in the centre of the sequence. The left (green) and right (yellow) TALEN subunit binding sites on exon 2 of the gene and the amplicon unique BspHI restriction site overlapping the spacer region are also shown. Non-highlighted region represents intronic sequence.

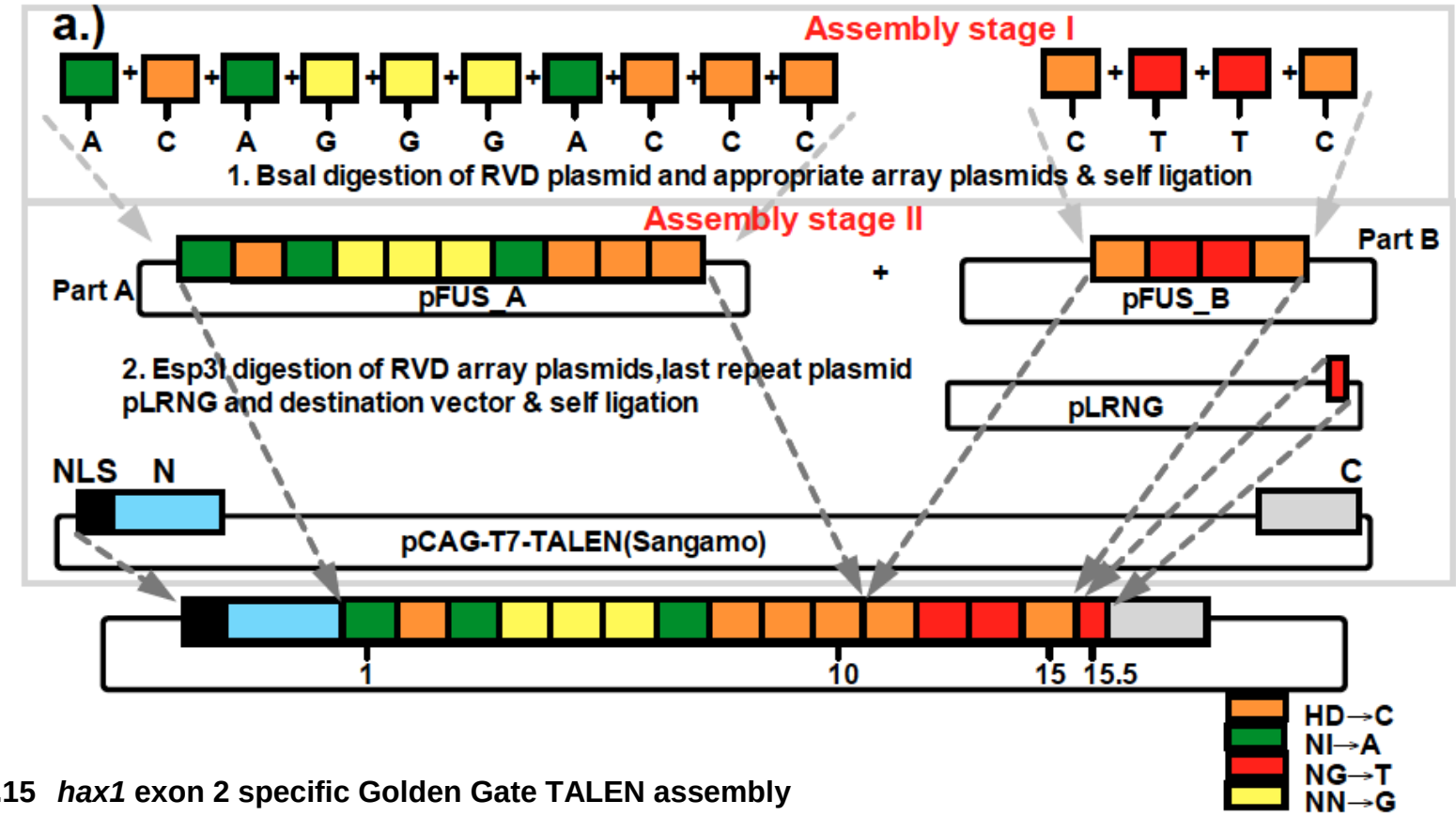

Figure 5.15 ***hax1*** **exon 2 specific Golden Gate TALEN assembly**

a.) Assembly process of the left *hax1* specific TALEN. The RVD modules (HD- orange, NI-green, NG-red, NN-yellow) required to generate the left TAL domain were initially cloned into an array plasmid using BsaI digestion and self ligation of the RVD sequences to one another and the array plasmid. The first 10 modules were inserted into pFUS_A (Part A) and the remaining 4 into pFUS_B (Part B). In the second assembly reaction, the two array plasmids and a final plasmid containing the last half repeat (LRNG) were cloned into the generic backbone pCAG-T7-TALEN (Sangamo). The generic backbone contains a nuclear localisation signal (NLS) and the FokI nuclease domain downstream of the RVD sequence (not shown). The N and C terminal of the subunit are also shown.

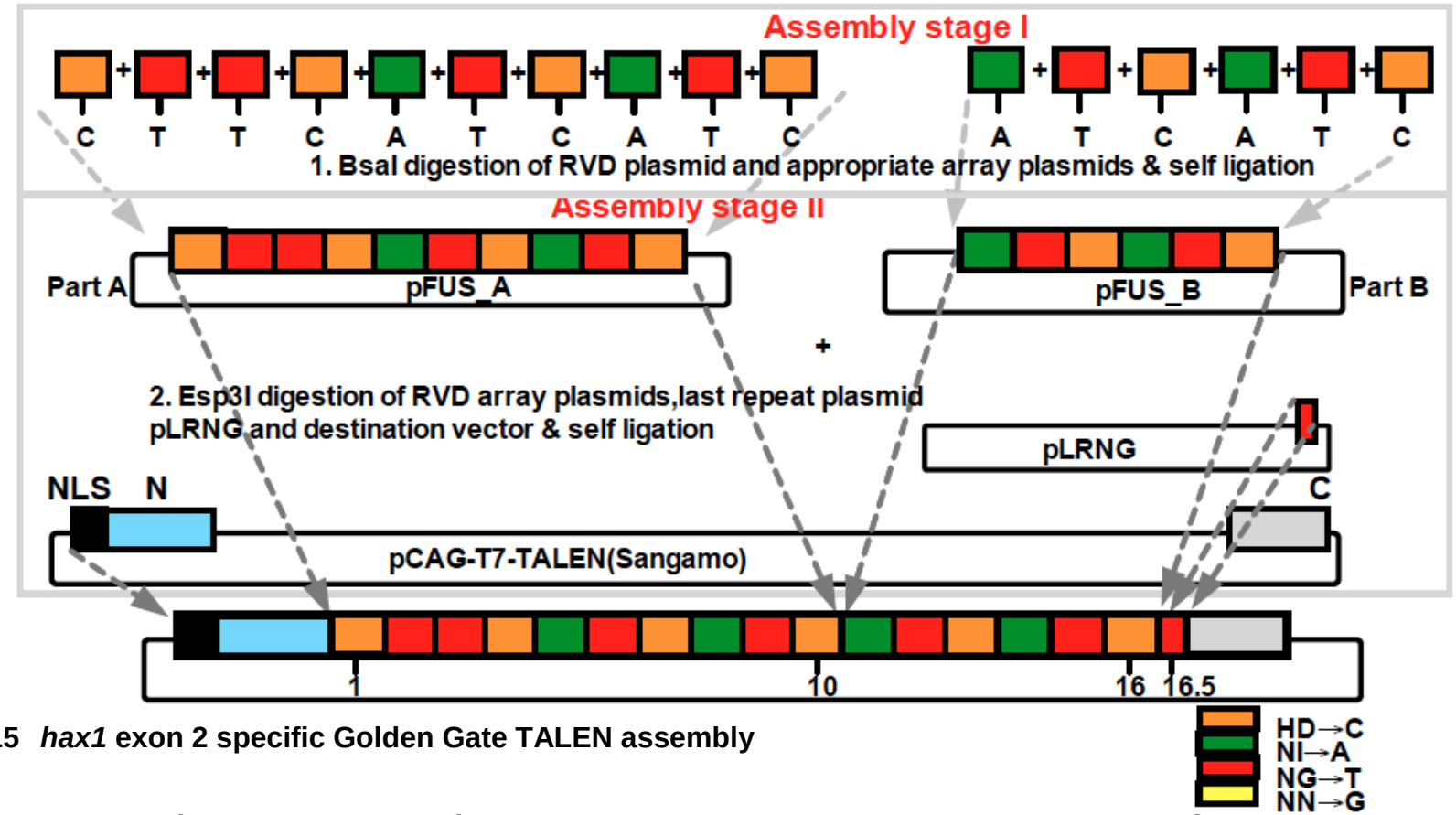

Figure 5.15 ***hax1*** **exon 2 specific Golden Gate TALEN assembly**

b.) Assembly process of the right *hax1* specific TALEN. The RVD modules (HD- orange, NI-green, NG-red, NN-yellow) required to generate the left TAL domain were initially cloned into an array plasmid using BsaI digestion and self ligation of the RVD sequences to one another and the array plasmid. The first 10 modules were inserted into pFUS_A (Part A) and the remaining 6 into pFUS_B (Part B). In the second assembly reaction, the two array plasmids and a final plasmid containing the last half repeat (LRNG) were cloned into the generic backbone pCAG-T7-TALEN (Sangamo). The generic backbone contains a nuclear localisation signal (NLS) and the FokI nuclease domain downstream of the RVD sequence (not shown). The N and C terminal of the subunit are also shown.

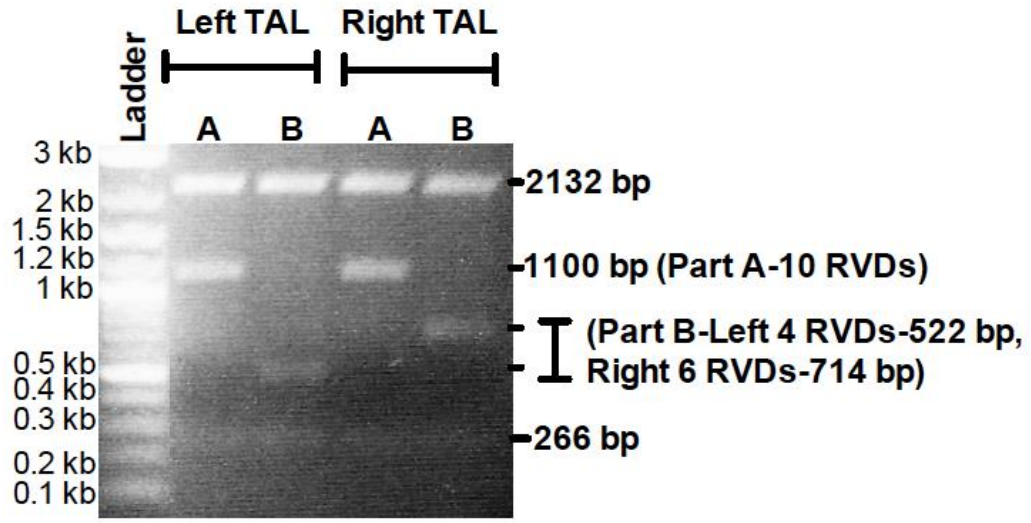

Figure 5.16 Assembly stage I: Analysis of diagnostic digests of *hax1* specific TALEN constructs

Part A and B purified plasmid DNA was subjected to an XbaI and NheI double digest. Following incubation at 37 °C, the digestion products were resolved on a 1.1 % SeaKem agarose gel and bands were visualised using a UV transilluminator. The sizes of the digestion products are indicated on the right. Note not all ladder band sizes are shown.

plasmids were very likely to have assembled correctly and therefore, were used in the next Golden Gate reaction.

5.2.1.2 *hax1* exon 2 specific Golden Gate TALEN assembly stage II

In order to assemble the RVD modules contained in part A and B of each subunit into a single plasmid containing the FokI nuclease domain, the purified array plasmids pFUS_A and pFUS_B consisting of the RVD modules were subjected to a second Golden Gate reaction. A map of the generic backbone (pCAGT7-TALEN Sangamo) is shown in Appendix 7.18.

In order to assess the second stage assembly, the *hax1* specific left and right TALEN encoding plasmids generated in section 2.2.8.3 were subjected to a diagnostic digest with BamHI and XbaI restriction enzymes. The digestion components are shown in Section 2.2.8.4. In order to assess the ligation from the second golden gate reaction and the linearization (Section 2.2.8.5), the BamHI XbaI diagnostic and purified NotI digests were subjected to agarose gel electrophoresis (Fig 5.17). Bam HI and XbaI digestion was expected to produce two bands of size 5322 bp and 2207 bp for the left TALEN subunit encoding construct and 5322 and 2411 for the right TALEN subunit encoding plasmid. The agarose gel in Fig 5.17 a. shows that the BamHI XbaI digestion reaction yielded the predicted band sizes for both subunit-encoding plasmids. Agarose gel resolution of the Not I linearization products also shows a band corresponding to the expected size (~8 kb) (Fig. 5.17 b.). The exact sizes of the plasmids containing the left and right TALEN subunits were 7529 and 7733 bp respectively. The relative ladder band intensities were used to quantify the ~8 kb plasmid DNA.

In order to analyse the sequence of the purified plasmid DNA, 20 µl of 100 ng/µl of each subunit encoding plasmid from the MIDI preparations was sent for Sanger sequencing by TAL_R2 and SeqTALEN_5.1 primers (Appendix 7.19). The sequence was analysed by SeqBuilder (Lasergene

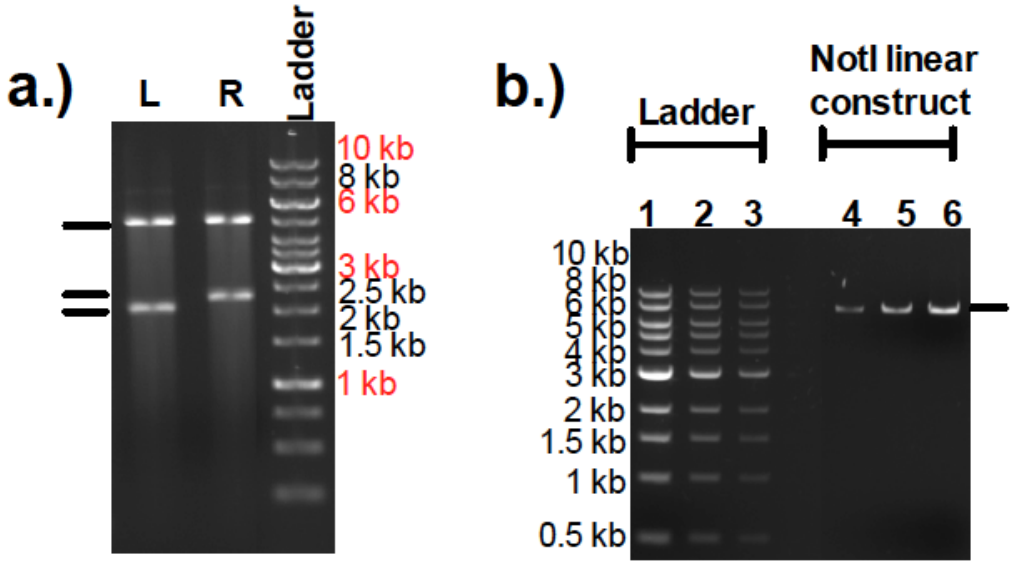

Figure 5.17 Assembly stage II: Analysis of diagnostic digests and linearisation of *hax1* specific TALEN plasmids

a.) The purified left (L) and right (R) *hax1* specific TALEN constructs were subjected to an XbaI BamHI double digest and the reaction products were resolved on a 0.7 SeaKem agarose gel alongside a Generuler 1 kb DNA ladder. Note not all ladder band sizes are shown. **b.)** The left and right TALEN subunit encoding plasmids were pooled into a linearization reaction using NotI restriction enzyme. The products were subjected to agarose gel electrophoresis using a 0.7 % agarose gel. A single µl of the reaction was added to 9 µl of loading dye. 1 µl, 3 µl and 6 µl (lanes 4-6) were then loaded onto the gel alongside 5,2 and 1 µl (lanes 1-3) of Hyperladder I. Plasmid bands were visualised using a UV transilluminator.

10, DNA Star). The Find function was used to examine whether the Sanger sequence matched the expected plasmid sequence. The TAL_R2 and SeqTALEN_5.1 primer annealing sites on the left and right *hax1* specific TALEN encoding vectors, annotated in SeqBuilder, are shown in Appendix 7.20. Sanger sequencing confirmed that the RVD repeats for the left and right subunits had assembled in the correct order and validated the sequence at these sites.

5.2.2 Preparation of *hax1* exon 2 targeting TALEN RNA for microinjection

In order to assess the transcription and purification processes described in Section 2.2.8.6, the RNA was subjected to agarose gel electrophoresis.

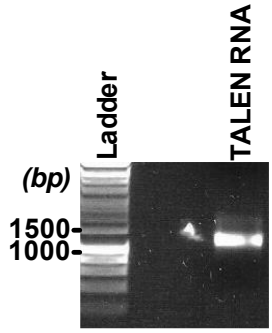

Fig. 5.18 *In vitro* transcription of *hax1* targeting left and right TALEN subunit expression vectors
Following *in vitro* transcription and purification, 0.5 µl of the capped RNA was resolved on a 0.7 % agarose gel. Note not all ladder band sizes are shown.

5.2.3 Microinjection of *Tg(mpx:GFP)i114* embryos with TALEN encoding RNA

On the morning of injection fresh injection solution was prepared by adding 3.5 µl TALEN RNA to 0.5 µl of 0.5 % phenol red. Two doses of the solution were injected at the single cell stage 0.5 nl or 1 nl per embryo in order to test the effect of the dose of the TALEN RNA on toxicity. Injected embryos were grown at low density (<50 per petri dish) and unfertilized, non-viable or damaged embryos were removed. At 24 hpf, uninjected and TALEN RNA injected embryos were inspected for toxic effects induces by the TALEN encoding RNA. At both doses, very few of the TALEN RNA injected embryos exhibited morphological defects at 24 hpf (data not shown).

5.2.4 Detection of somatic mutations in *hax1* specific TALEN mRNA microinjected *Tg(mpx:GFP)i114* embryos

In order to determine whether the *hax1* specific TALEN generated in section 5.2.1 was functionally active and thus was likely to generate indel mutations resulting in the inactivation of the zebrafish *hax1* gene, the region spanning the *hax1* TALEN target was amplified using the L and R Hax1TalRE primers (Appendix 7.19) and a BspHI restriction digest carried out on the PCR product. As described in section 5.2.1.1 the BspHI

unique restriction site in the amplicon was used to screen for any TALEN induced indel mutations as the restriction site for the enzyme overlaps the *hax1* specific TALEN spacer region. Amplicons from non-mutated embryos would contain an intact BspHI restriction site and would undergo complete digestion with the BspHI enzyme (Fig. 19 a.). TALEN induced mutation in the spacer region would result in the loss of the BspHI restriction site and therefore lead to resistance to BspHI cleavage. In order to ensure complete digestion of the *hax1* PCR products, all BspHI restriction digests were incubated at 37 °C for 6 h.

Genomic DNA was extracted from four individual control uninjected embryos, four individual *hax1* specific TALEN injected embryos (section 2.1.23), a pool of 20 uninjected and 20 TALEN injected embryos (section 2.1.24). The gDNA was subjected to PCR amplification using the L and R Hax1TalRE primers and Phusion DNA polymerase (2.1.17). BspHI digestion was carried out by adding 1 µl of BspHI enzyme to the PCR reaction. Figure 5.19 a. illustrates the expected outcome of the digest from non-mutated and mutated *hax1* target region. Pre- and post- BspHI cleavage products were subjected to agarose gel electrophoresis and visualised using a UV transilluminator (Fig. 5.19 b.). In order to test whether the TALEN mutation resulted in embryonic dysmorphism, gDNA was also extracted from three individual dysmorphic embryos and subjected to PCR analysis followed by the BspHI digest (Fig. 5.19 c.). Though the control uninjected embryo PCR products were completely cleaved by the BspHI enzyme, BspHI digestion of all TALEN injected embryos resulted in incomplete cleavage.

5.2.5 Identification of founder mutants harbouring *hax1* germline transmitted mutations

Once it was established that the *hax1* specific TALEN had successfully cleaved the *hax1* zebrafish gene, about 120 TALEN injected embryos

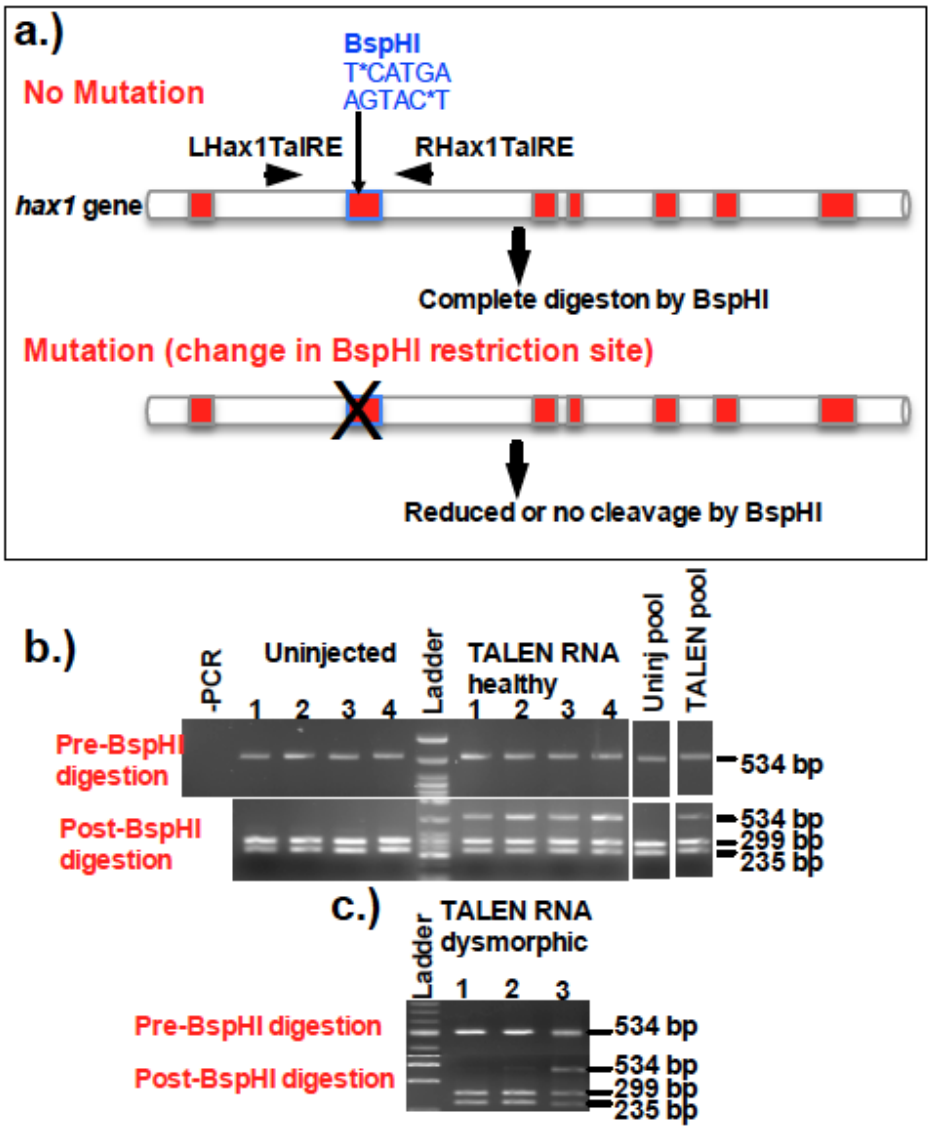

Figure 5.19 Identification of somatic mutations in *Tg(mpx:GFP)i114* embryos injected with *hax1* specific TALEN RNA

a.) Restriction digest analysis of the zebrafish *hax1* gene. The PCR product amplified using L and R Hax1TalRE primers yields an amplicon harbouring a unique BspHI restriction site. BspHI digestion of non-mutated *hax1* leads to complete digestion of the PCR product with the BspHI enzyme. Mutated *hax1* loses its BspHI restriction site resulting in reduced or no cleavage by the BspHI enzyme. **b.)** gDNA was extracted from four (lane 1-4) individual uninjected, four (1-4) *hax1* TALEN RNA injected embryos, a pool of 20 uninjected embryos (uninj pool) and a pool of 20 TALEN injected embryos (TALEN pool). PCR was carried out using L and R Hax1TalRE primers. 5 µl of the PCR reaction were subjected to agarose gel electrophoresis. The remaining PCR product was then subjected to a BspHI restriction digest. **c.)** gDNA was also extracted from three dysmorphic TALEN RNA injected embryos and subjected to PCR analysis with L and R Hax1TalRE primers followed by a BspHI digest.

were raised to adulthood. A schematic outline for generating *hax1* homozygous mutants is shown in Fig. 5.20. In order to screen for germline-transmitted mutations, potential adult *hax1* TALEN founders were out-crossed individually to WT *nacre* zebrafish. The resulting F_1 progeny embryos from each individual pair were then subjected to gDNA extraction at 48-72 hpf. Following PCR using the L and R Hax1TalRE primers and Phusion DNA polymerase, 1 µl of BspHI enzyme was added to each PCR reaction. From each potential founder, gDNA was extracted from eight pools of 3 embryos. gDNA extraction was carried out in a 96 well PCR plate and 50 µl of embryos digestion buffer (10 mM Tris Hcl pH8, 1 mM EDTA, 0.3 % Tween-20, 0.3 % NP-40) added to each pool of 3 embryos. Following a 10 min incubation at 98 °C, the embryos were transferred to ice and 4 µl of Proteinase K (25 mg/ml) were added. The embryos were then incubated for a further 3 h at 55 °C followed by a 10 min incubation at 98 °C. The gDNA was diluted with 100 µl of water and cell debris was pelleted by centrifugation at 14000 g at 4 °C for 30 min.

A Phusion DNA polymerase master mix was generated as described in section 2.1.17 and PCR carried out using 1.5 µl of the gDNA and L and R Hax1TalRE primers. Following incubation with 0.5 µl of BspHI restriction enzyme, digestion products were resolved by agarose gel electrophoresis. Representative gel images taken using a UV transilluminator are shown in Fig. 5.21. BspHI digested *hax1* PCR products from fish with no mutations or somatic mutations underwent complete digestion (Fig. 5.21a.) whereas BspHI restriction analysis of gDNA from fish with germline-transmitted mutations showed partially resistance to BspHI cleavage (Fig. 5.21 b-d). The higher the number of pools with partially digested PCR product indicated a better mutation transmission rate (e.g. Fig. 5.21 d.).

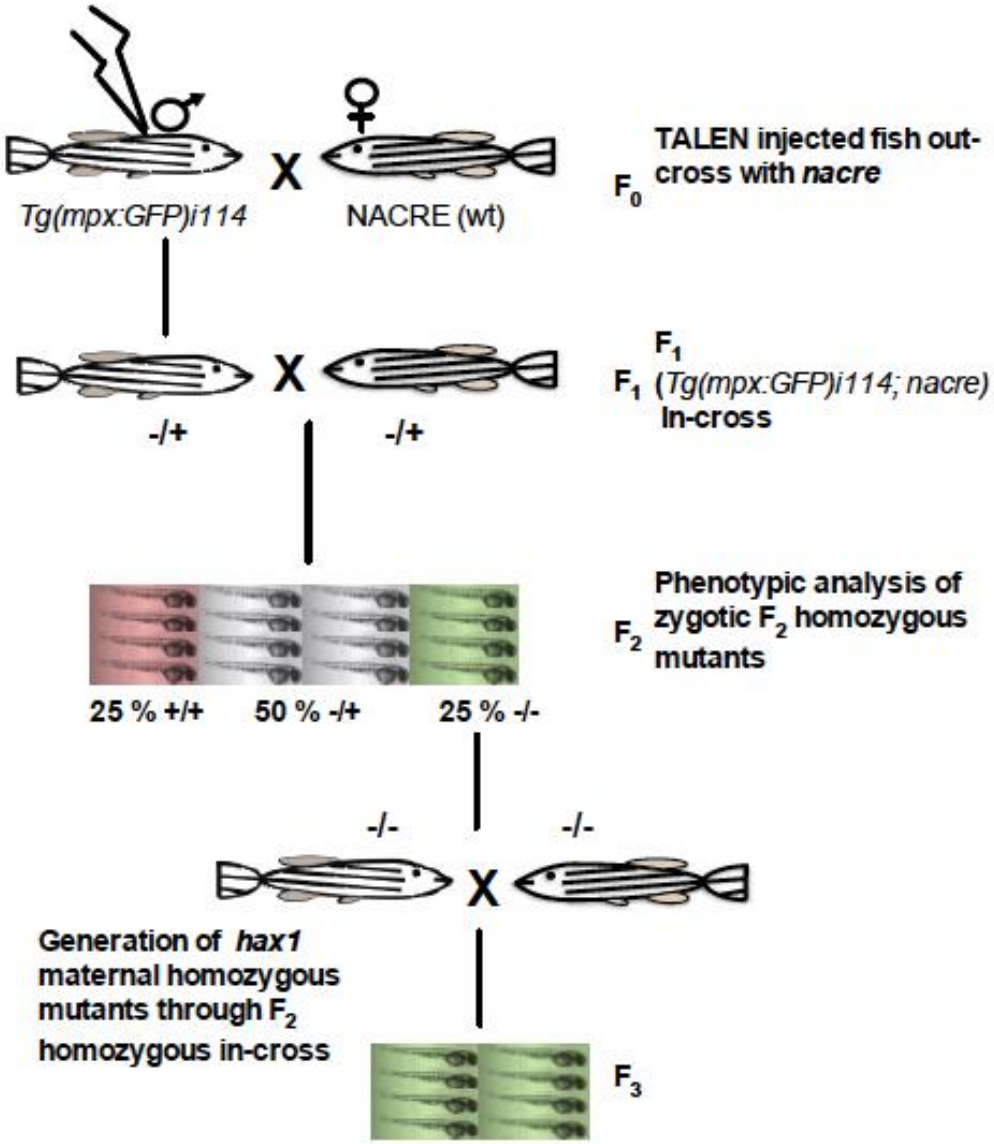

Figure 5.20 Schematic outline of zebrafish *hax1* specific TALEN mutagenesis

TALEN RNA was injected into *Tg(mpx:GFP)i114* single cell embryos. The injected embryos were raised to adulthood. The TALEN injected fish were then out-crossed with wild type *nacre* fish to generate heterozygous F_1 germline mutants. In-crossing of heterozygous siblings from the F_1 generation resulted in homozygosity in the F_2 generation. Mating of the F_2 generation would lead to an F_3 generation of mutants deprived of any maternal *hax1* mRNA (maternal mutants).

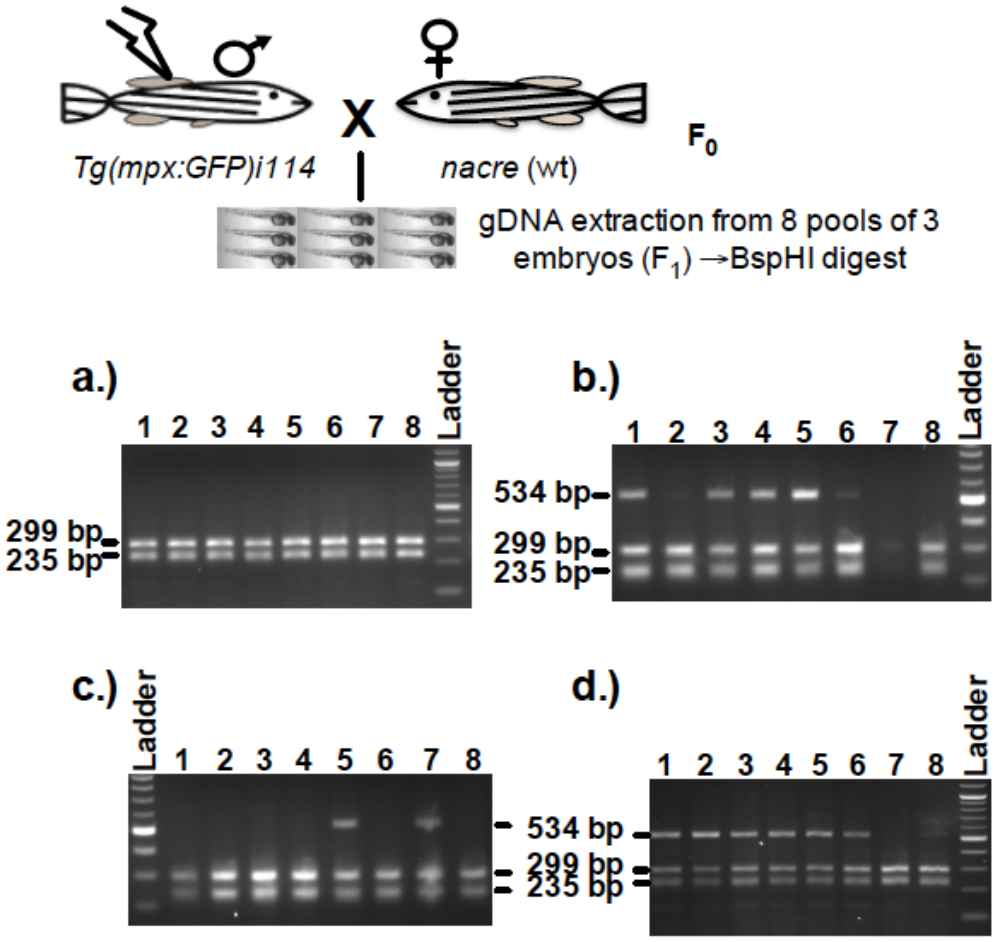

Figure 5.21 Identification of germline mutants (founders) by restriction digest analysis

Adult TALEN fish were out-crossed to the wild type *nacre* strain. Following a 72 h incubation of the offspring, gDNA was extracted from 8 pools of three embryos (lanes 1-8) from each potential founder. The gDNA was then subjected to PCR using L and R Hax1TalRE primers. The PCR product was digested using BspHI restriction enzyme and digestion products were resolved on a 1.8 % agarose gel. Representative digests from progeny of TALEN injected fish with (a.) no germline mutation and three founders (**b-d)** are shown. Also shown are lanes containing NEB 100 DNA ladder.

5.2.6 Screening for F_1 mutants by PCR and BspHI analysis

Once numerous F_0 fish that transmitted *hax1* mutations through the germline were identified, their 30-60 embryos from their F_1 progeny (section5.2.4) were raised to adulthood. In order to identify F_1 heterozygous mutants and determine the exact sequence of the mutations, anaesthetised F_1 fish were screened by isolating gDNA from caudal fin clippings at 2-3 months post fertilisation (Fig. 5.22 a.). A fin clip from each individual F_1 fish was placed in a 96 well PCR plate and residual liquid removed using a closed Pasteur pipette. gDNA was extracted by addition of 50 µl of embryos digestion buffer (10 mM Tris Hcl pH8, 1 mM EDTA, 0.3 % Tween-20, 0.3 % NP-40) followed by a 10 min incubation at 98 °C. The plate was then transferred to ice and 4 µl of Proteinase K (25 mg/ml) were added to fin clip. This was followed by incubation for a further 3 h at 55 °C followed by a 10 min incubation at 98 °C. The gDNA was diluted with 100 µl of water and cell debris was pelleted by centrifugation at 14000 g at 4 °C for 30 min. following PCR amplification as described in section 2.1.17 using 0.5 µl of the gDNA and L and R Hax1TalRE primers, 0.5 µl of BspHI restriction enzyme was added to each PCR reaction, digestion products were resolved by agarose gel electrophoresis. A representative gel image of PCR and BspHI analysis of F_1 fin clip gDNA is shown in Fig. 5.22 a.

Heterozygous *hax1* mutants were partially resistant to BspHI cleavage. Sanger sequencing of PCR products from caudal fin clips of heterozygous *hax1* mutants revealed numerous changes in the *hax1* target sequence (Fig. 5.22 b.). Regions of the sequencing traces containing double peaks were composed of WT and modified sequence. The sequencing traces from each individual heterozygous mutant were decoded. This revealed four main different TALEN induced changes in the *hax1* target sequence (Fig. 5.22). These were all deletion mutations termed Δ1-4.

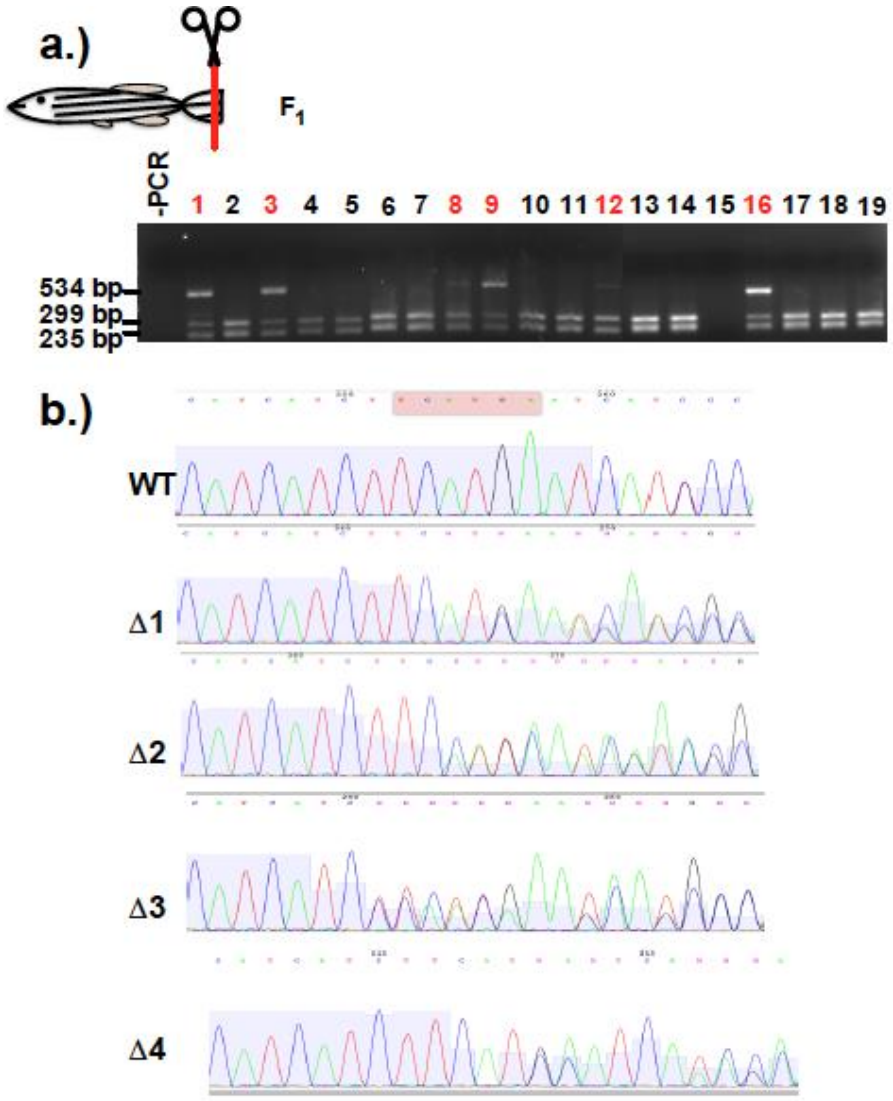

Figure 5.22 Genotyping of the F_1 generation by BspHI restriction digest and sequence analysis of TALEN induced germline transmitted mutations

a.) Adult F_1 zebrafish resulting from the *Tg(mpx:GFP)i114 nacre* outcross were fin clipped and gDNA extracted. Following PCR using L and R hax1TalRE primers, the PCR products were subjected to a BspHI restriction digest and digests analysed by agarose gel electrophoresis using a 1.8 % agarose gel. A representative gel image is shown. Each lane represents a BspHI digest of gDNA from the fin-clip of a single fish. Heterozygous mutant PCR product is indicated by red numbering of lanes. **b.)** PCR product from each individually genotyped heterozygous mutant was subjected to Sanger sequencing. Representative sequencing traces from PCR samples of a *hax1* WT fish and four mutant fish (harbouring mutations termed changes 1-4, Δ1-4) are shown. The highlighted nucleotide region (pink) on the WT sequencing trace indicates the BspHI restriction site (TCATGA).

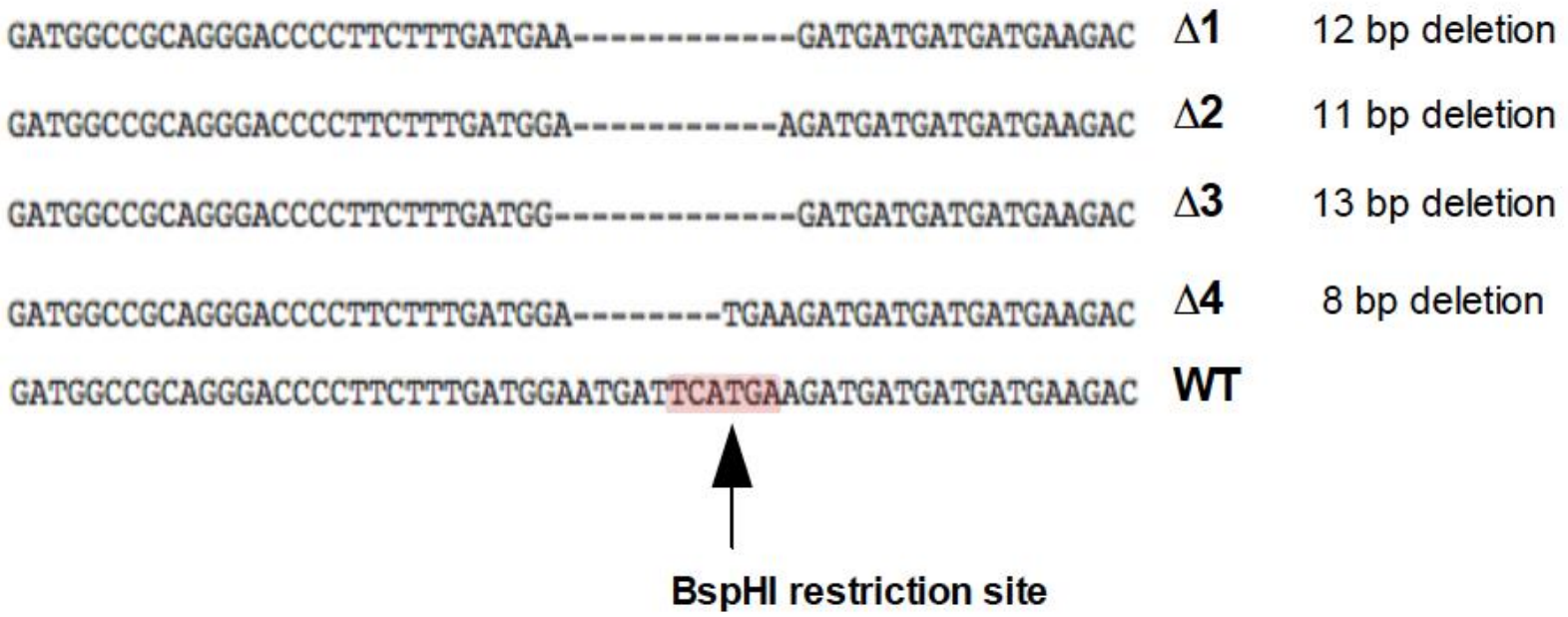

Figure 5.23 Sequence analysis *hax1* heterozygous F_1 mutants

The nucleotide sequence of each of the 1-4 different indel mutations (Δ1- Δ4) in the heterozygous F_1 mutants was deciphered by reading the nucleotides from each double peak from the sequencing traces. Mutant sequences were then compared to the WT *hax1* sequence using Clustal Omega (http://www.ebi.ac.uk/Tools/msa/clustalo/). The BspHI restriction site is also shown.

In silico expression of each mutant gene sequence using the Hax1 001 isoform ATG site (Fig. 5.24) showed that the putative protein sequences were likely to contain numerous premature stop codons with the exception of Δ1 which would result in the deletion of 4 amino acids (amino acids 30-33) but otherwise an intact protein sequence. Mutations Δ2 and Δ4 (Fig. 5.24 b. and d.) occurred in the same region of the DNA and would result in the expression of almost identical putative *hax1 001* proteins with numerous premature stop codons in the sequence.

5.2.7 Phenotypic analyses of heterozygous and homozygous F_2 mutants

In order to permit phenotypic analysis of *hax1* mutant F2 embryos generated from a t*g(mpx:GFP)i114; nacre* in-cross, F_2 embryos were subjected to gDNA extraction, PCR using L and R Hax1TalRE primers and 1 µl of gDNA followed by BspHI cleavage as described in section 2.1.23 and 2.1.17. In addition to embryos with GFP +ve PMN the in-cross would also generate embryos lacking a GFP signal in PMN cells (GFP -ve). In order to test whether the lack of GFP signal is a direct result of the in-cross or due to the lack of PMN in the embryos, gDNA was extracted from GFP +ve and GFP -ve individual embryos. Analysis of BspHI digestion product by agarose gel electrophoresis shows that the TALEN induced mutation Δ1 does not result in embryos with GFP -ve PMN as both GFP +ve and GFP -ve embryos harbour WT *hax1*, heterozygous and homozygous *hax1* Δ1 mutations (Fig. 5.25 a. and b.). Similar observations were made for *hax1* Δ2, Δ3 and Δ4 mutants (data not shown). The genotyping of the homozygous F_2 *hax1* mutants revealed that the L and R Hax1TalenRE primers occasionally produced two additional bands at ~350 bp and ~ 200 bp which could result in incorrect genotyping of embryos and adult fish. A second pair of *hax1* TALEN target region specific primers termed L and R Hax1TalenRE(01) (Appendix 7.19) was designed generating an amplicon of 367 bp. BspHI digestion of this resulted in two bands of 199 bp and 168 bp (Fig. 5.25 c.). Fig. 5.25 c. shows that amplification of the

a.)

```
Aberrant        MSVFDLFRGFFGVPGGHYREDGRRDPFFD----EDDDDEDEDDFNRPHRDPFDDAFRFGF 56
WT              MSVFDLFRGFFGVPGGHYREDGRRDPFFDGMIHEDDDDEDEDDFNRPHRDPFDDAFRFGF 60
                ****************************    *************************

Aberrant        SFGPGGARFEEPQMFGQIFRDMEEMFAGLGRFDERHGFGPRGFPSIEAPPPQEGVEKGRS 116
WT              SFGPGGARFEEPQMFGQIFRDMEEMFAGLGRFDERHGFGPRGFPSIEAPPPQEGVEKGRS 120
                ************************************************************

Aberrant        GTGSGNPIRDFMLKSPDRSPKDPEHREDSPPNHPHRRPFSKFNDIWKDGLLKPKGEDKRE 176
WT              GTGSGNPIRDFMLKSPDRSPKDPEHREDSPPNHPHRRPFSKFNDIWKDGLLKPKGEDKRE 180
                ************************************************************

Aberrant        DGDLDSQVSSGGLDQILKDPAPSQPKTRSFFKSVSVTKVVRPDGTVEERRTVRDGEGNEE 236
WT              DGDLDSQVSSGGLDQILKDPAPSQPKTRSFFKSVSVTKVVRPDGTVEERRTVRDGEGNEE 240
                ************************************************************

Aberrant        TTVTISERPGGQDRPVLDQSGPLMPGGSDMQDDFSMFSKFFRGFRSSTOP 286
WT              TTVTISERPGGQDRPVLDQSGPLMPGGSDMQDDFSMFSKFFRGFRSSTOP 290
                ************************************************
```

b.)

```
Aberrant        MSVFDLFRGFFGVPGGHYREDGRRDPFFDGR****RRG*L*QT---P-SGSV*RCLQVWI
WT              MSVFDLFRGFFGVPGGHYREDGRRDPFFDGMIHEDDDDEDEDDFNRPHRDPFDDAFRFGF
                ******************************          :    *    .  .::. :

Aberrant        QFRSRRGTL*RASDVRPDLQRHGGDVCWSG--TL**ATWIWTERFPV-----------N
WT              SFGPGGARFEE-PQMFGQIFRDME-EMFAGLGRFDERHGFGPRGFPSIEAPPPQEGVEKG
                .*    . : .  ::  :: *.     ::*   :     :  . **

Aberrant        RSSTSTGRS*ERQEWDRKWE---SHQRFHVEVS*PLT*RSRAQRGFSTKSSSQEAFLKVQ
WT              RSGTGSGNPI--RDFMLKSPDRSPKDPEHREDSPPNH-------------PHRRPFS---
                **.*.:*.    :::  *      ::  * * * *                  :. *

Aberrant        RYLERWT---VKTKGG--RQKGGW-----RSGLTGVFRWTGPDLERSSTFTAKNKVIF*V
WT              KFNDIWKDGLLKPKGEDKREDGDLDSQVSSGGLDQILKDPAPSQPKTRSFFKSVSVTK--
                :: : *.   :* **   *:.*         .**  :::  .*.  :: :*  . .*

Aberrant        CQRHQGGPTGWNCRRTANSQ------RWRR**RDDRDHLRKARWAR*ASPGS-----VWS
WT              VVRPDGTVEERRTVRDGEGNEETTVTISERPGGQDRPVLDQS---GPLMPGGSDMQDDFS
                  * :*     .  * .:.:        .*   :**  * ::       **.      :*

Aberrant
WT              FNARWF*HAG*FLHVFQVLQRLSKL
                MFSKF-------FRGFRS*------
                : :::       :: *:
```

Figure 5.24 The effect of TALEN induced *hax1* mutations on the putative *hax1 001* protein sequence

The *hax1* genomic DNA sequences generated from the sequencing traces of the mutant heterozygous fish containing Δ1 (**a.**) and Δ2 (**b.**) were *in silico* expressed using the online Expasy translate tool (http://web.expasy.org/translate/). The generated putative mutant sequences (aberrant) were compared to the wild type (WT) *hax1 001* sequence using Clustal Omega (http://www.ebi.ac.uk/Tools/msa/clustalo/). An asterisk within the amino acid sequence denotes a stop codon.

c.)

```
Aberrant    MSVFDLFRGFFGVPGGHYREDGRRDPFFDGMMMMKTRMTLTDPIGIRLTMPSGLDSVSVQ
WT          MSVFDLFRGFFGVPGGHYREDGRRDPFFDGMIHEDDDDEDEDDFNRPHRDPF--DD-AFR
            ********************************:  .      * :      *   *. :.:

Aberrant    AGHALKSLRCSARSSETWRRCLLVWDALMSDMDLD-REVSRQ*KLH-------------L
WT          FGFSFGPGGARFEEP-------QMFGQIFRDMEEMFAGLGRFDERHGFGPRGFPSIEAPP
             *.::    .  ..          ::  :: **:     :.*  : *

Aberrant    HRKELRKAGVGQEVGIPSEISC*SLLTAHLKIQSTERILHQIILTGGLSQSSTIFGKMDC
WT          PQEGVEKGRSGTGSGNPIR--D-------FMLKSPDRSPKDPEHRE---------DSPPN
             :: :.*.  *   * * .           : ::* :*  ::                .

Aberrant    *NQRGKTKGRMEIWTHRCLQVDWTRS*KIQHLHSQK--------------------QGHFL
WT          HPHRRPFSKFNDIWKDGLLKPKGEDKREDGDLDSQVSSGGLDQILKDPAPSQPKTRSFFK
              :*   .   :**..  *: .   . :  .*.**                      :..*

Aberrant    SLSASPRW-----SDRMEL*KNGEQSEME-KVMKRRP*PSQKGQVGKIGQSWISLVL*CQ
WT          SVSVTKVVRPDGTVEERRTVRDGEGNEETTVTISERPGGQDRPVLD--------------
            *:*.:          :. .  ::** .*    .:..**  .::  :

Aberrant    VVLTCRMISPCFPSSSEA---FEV-----------
WT          ------QSGPLMPGGSDMQDDFSMFSKFFRGFRS*
                  .* :*..*:    *.:
```

d.)

```
Aberrant    MSVFDLFRGFFGVPGGHYREDGRRDPFFDG*R****RRG*L*Q--TP-SGSV*RCLQVWI
WT          MSVFDLFRGFFGVPGGHYREDGRRDPFFDGMIHEDDDDEDEDDFNRPHRDPFDDAFRFGF
            ****************************          :   *    .  .::. :

Aberrant    QFRSRRGTL*RASDVRPDLQRHGGDVCWSG--TL**ATWIWTERFPV-----------N
WT          SFGPGGARFEE-PQMFGQIFRDME-EMFAGLGRFDERHGFGPRGFPSIEAPPPQEGVEKG
            .*    . : .  ::  :: *.     ::*   :     :  . **

Aberrant    RSSTSTGRS*ERQEWDRKWE---SHQRFHVEVS*PLT*RSRAQRGFSTKSSSQEAFLKVQ
WT          RSGTGSGNPI--RDFMLKSPDRSPKDPEHREDSPPNH-------------PHRRPFS---
            **.*.:*.    :::  *      ::  * * * *                  :. *

Aberrant    RYLERWT---VKTKGG--RQKGGW-----RSGLTGVFRWTGPDLERSSTFTAKNKVIF*V
WT          KFNDIWKDGLLKPKGEDKREDGDLDSQVSSGGLDQILKDPAPSQPKTRSFFKSVSVTK--
            :: : *.   :* **   *:.*        .**  :::  .*.  :: :*  . .*

Aberrant    CQRHQGGPTGWNCRRTANSQ------RWRR**RDDRDHLRKARWAR*ASPGS-----VWS
WT          VVRPDGTVEERRTVRDGEGNEETTVTISERPGGQDRPVLDQS---GPLMPGGSDMQDDFS
              * :*     .  * .:.:        .*   :**  * ::       **.      :*

Aberrant    FNARWF*HAG*FLHVFQVLQRLSKL
WT          MFSKF-------FRGFRS-------
            : :::       :: *:
```

Figure 5.24 The effect of TALEN induced *hax1* mutations on the putative *hax1 001* protein sequence

The *hax1* genomic DNA sequences generated from the sequencing traces of the mutant heterozygous fish containing Δ3 (**c.**) and Δ4 (**d.**) were *in silico* expressed using the online Expasy translate tool (http://web.expasy.org/translate/). The generated putative mutant sequences (aberrant) were compared to the wild type (WT) *hax1 001* sequence using Clustal Omega (http://www.ebi.ac.uk/Tools/msa/clustalo/). An asterisk within the amino acid sequence denotes a stop codon.

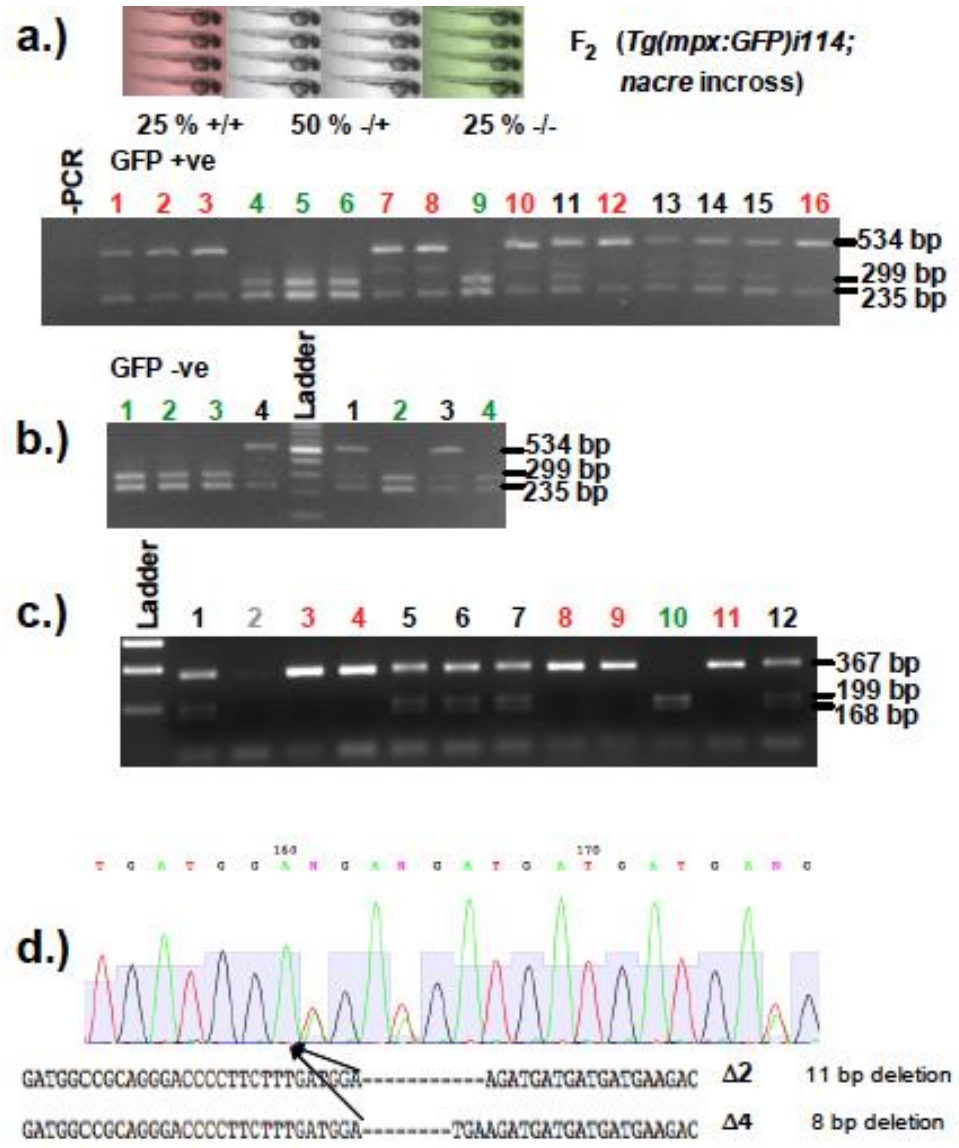

Figure 5.25 Analysis of F_2 embryos generated from *hax1* heterozygous mutant incrosses using PCR and BspHI restriction digestion

Heterozygous F_1 mutants were incrossed. Each F_2 embryo was lysed and gDNA extracted at 72 hpf. PCR was carried out using L and R Hax1TalRE primers and PCR products were subjected to a BspHI digest. The digestion products were resolved by agarose gel electrophoresis. Representative gel images are shown. Lanes containing homozygous (red), heterozygous (black) and WT (green) embryo PCR products are colour coded. Restriction digest analysis was carried out in GFP +ve (**a.)** and GFP -ve PMN embryos (**b.**). Note not all NEB 100 bp ladder band sizes are shown. **c.)** PCR and BspHI restriction digest analysis using L and R Hax1TalRE(2) primers. gDNA was extracted from single embryos at 72 hpf. Following BspHI digestion of the amplicon, digestion products were resolved by agarose gel (1.8 %) electrophoresis. **d.)** Analysis of *hax1* F_2 *hax1* Δ2/ Δ4 mutants fin clip *hax1* gDNA by Sanger sequencing. The arrow indicates the location of the A nucleotide.

hax1 gene using the L and R Hax1TalenRE(1) primers did not result in the appearance of any additional bands. From hereon, genotyping was carried out using the L and R Hax1TalenRE(1). Sequencing of the homozygous adult zebrafish fin clip gDNA using these primers validated the homozygous mutant sequences (Fig. 5.25 d.).

5.2.7.1 The effect of the *hax1* Δ1 mutation on PMN number

In order to investigate the effect of the *hax1* Δ1 mutation on total embryo PMN number, a pair of heterozygous *hax1* Δ1 t*g(mpx:GFP)i114; nacre* fish were in-crossed and the resulting F_2 progeny visualised under a 2x objective on a Nikon Eclipse TE2000U inverted microscope. Micrographs of embryos with GFP labeled PMN were taken at 48 and 72 hpf and PMN counted at the relevant time point (Fig. 5.26 a. and b.). In comparison to the WT control and heterozygous Δ1 mutants, homozygous Δ1 mutations did not appear to have the expected negative effect on the PMN number at either 48 and 72 hpf. There also does not appear to be a major difference between the groups in the increase in PMN number from 48 to 72 hpf (Fig. 5.26 c.).

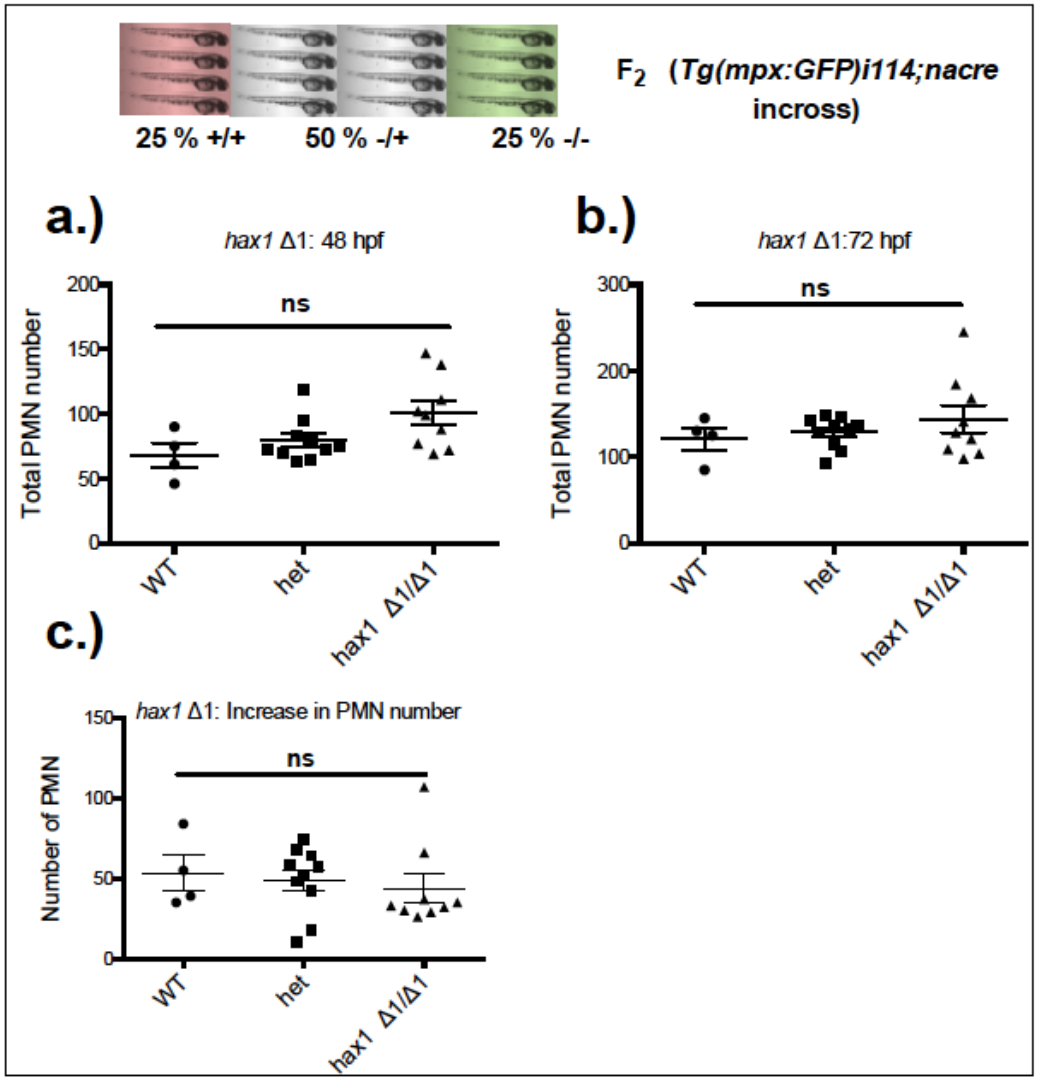

Figure 5.26 The effect of the homozygous *hax1* Δ1 mutation on PMN number

F_2 embryos generated from a single incross of a pair of heterozygous *hax1 Δ1* mutants were sorted into GFP +ve and GFP -ve groups. Micrographs of GFP +ve embryos were taken using a 2x objective on a Nikon Eclipse TE2000U inverted microscope. Total PMN counts were carried out on images taken using the GFP channel. PMN were counted from 23 embryos at 48 (**a.**) and 72 (**b.**) hpf. The increase in PMN number from 48 to 72 hpf was also calculated and is shown (**c.**). Bars represent mean number of PMN. Following this, each individual embryo was genotyped by PCR and BspHI restriction digest as shown in Fig. 5.25. PMN counts from WT: n=4, het: n=10, *hax1 Δ1/ Δ1*: n=9, performed as a single experiment, were analysed using a one way ANOVA with Bonferroni's post test (ns- indicates not significant).

5.2.7.2 The effect of the homozygous *hax1* Δ2/Δ4 mutation on PMN number

In order to assess the effect of the *hax1* Δ2/ Δ4 mutation on total embryo PMN number, a heterozygous *hax1* Δ2 t*g(mpx:GFP)i114; nacre* fish was crossed with a heterozygous Δ4 t*g(mpx:GFP)i114; nacre*. During the course of these studies, it was not possible to generate true Δ2 and Δ4 mutants a result of a gender skew in the Δ2 and Δ4 heterozygous F_1 mutant populations however, the two mutations differed only by three nucleotides and were located in the same region. The *hax1* Δ2/Δ4 F_2 progeny embryos were visualised under a 2x objective on a Nikon Eclipse TE2000U inverted microscope (Fig. 5.27 a.). Homozygous *hax1* Δ2/Δ4 had normal morphology when compared to *hax1* WT t*g(mpx:GFP)i114* embryos. The total number of PMN was counted from GFP +ve embryos at 48 and 72 hpf. Although the number of WT embryos was low there appeared to be no major differences in the total PMN numbers between any of the WT embryos, heterozygous (*hax1* Δ2 or *hax1* Δ4) and *hax1* Δ2/ Δ4 homozygous mutants (Fig. 5.27 b.). No major differences were visible in the increase in PMN number from 48 to 72 hpf (Fig. 5.27 c.) and the number of PMN at the caudal hematopoietic tissue (CHT) (Fig. 5.27 d.).

The F_2 *hax1* Δ2/ Δ4 homozygous mutants were generated from heterozygous F_1 parents, which contain a copy of WT *hax1*. In order to test whether maternal *hax1* mRNA protects the early embryos from harbouring a specific phenotype, *hax1* splice MO and ATG MO was co-injected into WT embryos, heterozygous and homozygous *hax1* Δ2/Δ4 embryos at the single cell stage. The MO co-injection resulted in a decrease in total PMN number in WT, heterozygous and homozygous *hax1* mutant embryos in comparison to the uninjected group at 48 and 72 hpf (Fig. 5.28 a. and b.). At 48 and 72 hpf, MO co-injected the heterozygous and homozygous *hax1* mutant embryos contained a slightly higher total PMN number than the MO co-injected WT embryos. It is important to note that the genotyping of the F_2 embryos showed that there

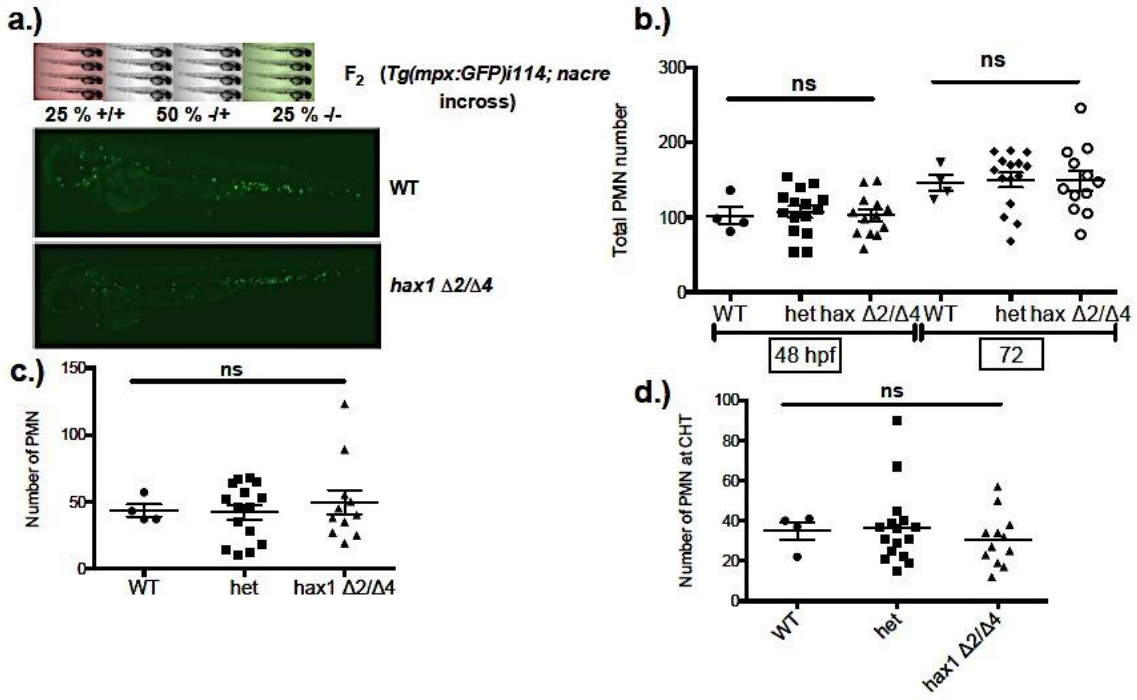

Figure 5.27 The effect of the homozygous *hax1* Δ2/ Δ4 mutation on PMN number

F_2 embryos generated from heterozygous *hax1* TALEN mutants were sorted into GFP +ve and GFP -ve groups. **a.)** Representative micrographs of a WT *Tg(mpx:GFP)i114* and homozygous *hax1* Δ2*/* Δ4 embryos. PMN were counted at 48 hpf (WT: n=4, het =15, *hax1 Δ2/ Δ4*: n=13) and 72 hpf from 33 embryos generated from a heterozygous *Δ2/ Δ4* mutant cross (WT: n=4, het =15, *hax1 Δ2/ Δ4*: n=12) (**b.**).**c.)** Increase in PMN number from 48 hpf and 72 hpf was calculated. **d.)** The number of PMN present at the CHT at 48 hpf was also counted. Following this, each individual embryo was genotyped by PCR and BspHI restriction digest. Images and counts are representative of a single experiment. Bars represent the mean ±SEM PMN number. PMN counts performed in single experiments were analysed using a one way ANOVA with Bonferroni's post test (ns- indicates not significant).

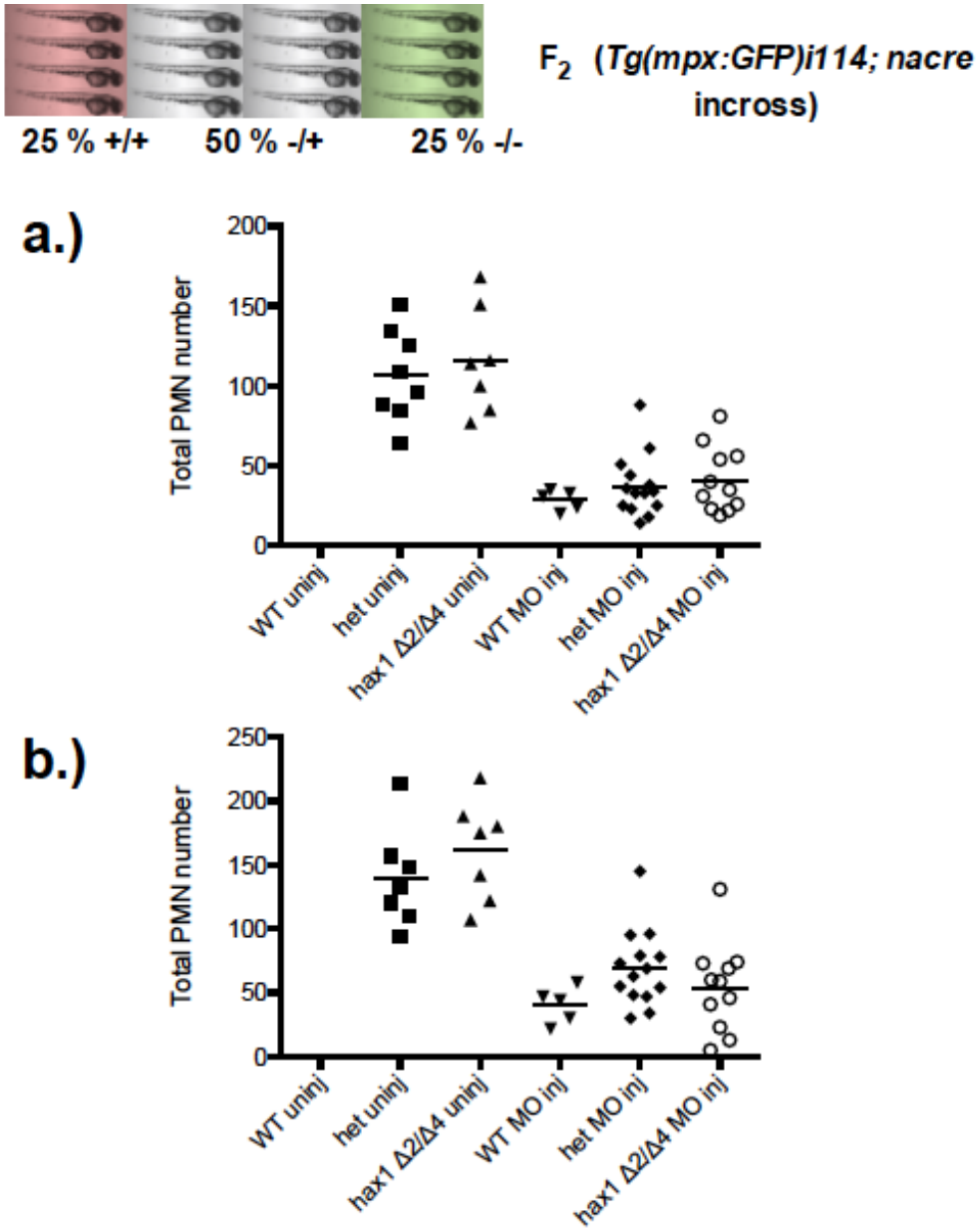

Figure 5.28 The effect of *hax1* MO microinjection in F_2 *hax1* Δ 2/ Δ4 mutants on total PMN number

F_2 embryos were co-injected with 1 nl of 0.5 mM splice 0.2 mM ATG MOs at the single cell stage. Control uninjected (uninj-15) and MO injected (MO inj) embryos (30) were visualised using a 2x objective on a Nikon Eclipse TE2000U inverted microscope. Micrographs of each embryo were taken using the GFP channel at 48 (**a.**) and 72 (**b.**) hpf. Total PMN numbers were then counted from each embryo. Each individual embryo was then genotyped by PCR and BspHI restriction digest of the gDNA. Note the uninjected group of 15 did not contain any WT embryos.

were no WT control embryos in the uninjected group and only 4 *hax1* WT embryos in the MO injected embryos.

5.2.8 Phenotypic analyses of heterozygous and homozygous F_3 *hax1* Δ2/Δ4 mutants

In order to generate *hax1* Δ2/Δ4 mutant embryos lacking maternal mRNA, the GFP +ve F_2 embryos were genotyped by caudal fin clipping at 3 dpf and grouped into heterozygous Δ2 or Δ4 embryos and homozygous *hax1* Δ2/Δ4.

5.2.8.1 Genotyping of F_2 embryos by Caudal fin clipping at 3 dpf, PCR and BspHI restriction digest analysis

Fin clipping at 3 dpf was carried out by adding 3 µl of 25 % Tween-20 to anaesthetised embryos in a petri dish. The embryos were fin-clipped using a scalpel and the fin clip transferred to a 96 well PCR plate. Excess media was removed and the fin clip lysed in 15 µl of digestion buffer (10 mM Tris Hcl pH8, 1 mM EDTA, 0.3 % Tween-20, 0.3 % NP-40) followed by a 10 min incubation at 98 °C. The plate was then transferred to ice and 2 µl of Proteinase K (25 mg/ml) were added to fin clip. This was followed by incubation for a further 1.5 h at 55 °C followed by a 10 min incubation at 98 °C. The *hax1* target region was amplified using the L and R Hax1TalRE primers with 2 µl of the 3 dpf fin clip gDNA. The amplicon was then subjected to BspHI digestion followed by agarose gel electrophoresis (data not shown).

5.2.8.2 The effect of Genotyping of maternal *hax1* Δ2/Δ4 mutations on PMN number and chemotaxis

Adult F_2 embryos were in-crossed and the total PMN number of progeny embryos analysed at 48 (Fig. 5.29 a.). Micrographs of 12 embryos from a single heterozygous and homozygous Δ2/Δ4 in-cross each were taken at 48 h 2x objective on a Nikon Eclipse TE2000U inverted microscope. The graph in Fig. 2.29 a. appears to show that there was no difference in the

total number of PMN between the progeny of the *hax1* heterozygous and homozygous *hax1* Δ2/Δ4 in-crosses. In order to test the effect of the *hax1* Δ2/Δ4 mutation in PMN migration during recruitment and resolution towards a wound site, tail fin transections were carried out on embryos at 2 dpf. The PMN number at the site of injury was then counted at 6 (recruitment- Fig. 5.29 b.) and 24 h (resolution- Fig. 5.29 c.) post injury. There were no significant differences in the percentages of PMN at the site of injury between the progeny of the *hax1* Δ2/Δ4 homozygous in-cross and that of the het in-cross, at both the recruitment and resolution phases. In order to visualise the PMN cell migration over time, average PMN track speed and meandering index (displacement divided by path length) plots were generated by tracking PMN movement for 3 h. The micrographs in Fig. 5.30 a. show the tail end of the zebrafish embryos with each PMN path indicated in a different coloured line. Mean calculations of meandering index and track velocity (mean neutrophil speed/time, μ/s) did not reveal any expected differences in the PMN of maternal homozygous F_3 Δ2/Δ4 mutants in comparison to the progeny of the F_2 heterozygous (*hax1* Δ2/+ x *hax1* Δ4/+) in-cross during the recruitment phase as indicated by Fig. 5.30. In order to quantify the directionality or the ability of PMN to migrate towards the site of injury, a bearing angle was calculated for each PMN cell using Volocity®. Fig. 5.31 demonstrates that the bearing plots showing PMN from the maternal homozygous F_3 Δ2/Δ4 mutants were comparable to those of F_2 heterozygous (*hax1* Δ2/+ x *hax1* Δ4/+) where most PMN migrated towards the site of injury (right hand side) within the first 3 h post injury.

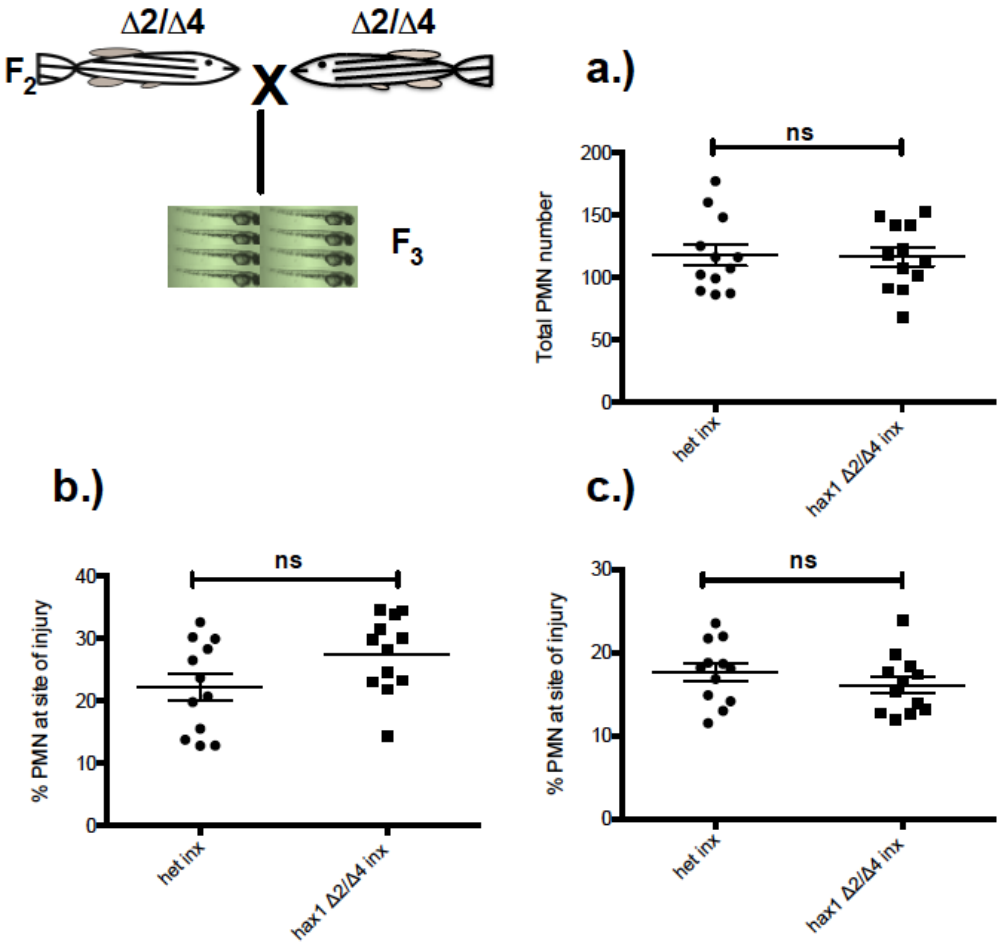

Figure 5.29 The Δ2/ Δ4 mutation does not affect PMN number
Heterozygous and homozygous F2 embryos generated from a Δ2 Δ4 cross were raised to adulthood. A pair of heterozygous (het inx) and homozygous (hax1 Δ2/ Δ4 inx) F2 fish was in-crossed. Micrographs of the embryos were taken at 48 and 72 hpf using a 2x objective on a Nikon Eclipse TE2000U inverted microscope. Total PMN numbers of F3 generation were then counted from each embryo at 48 hpf (a.). b.) Embryos were injured at 2 dpf and PMN number at site of injury at 6 h post injury (recruitment phase) was counted. c.) F3 generation embryos were injured at 2 dpf and PMN number at site of injury at 24 h post injury (resolution phase) was counted. Bars represent mean PMN number ±SEM or mean % ±SEM PMN at the site of injury. PMN counts and calculated percentages (n=12) generated from a single experiment were analysed using an unpaired student's t-test.

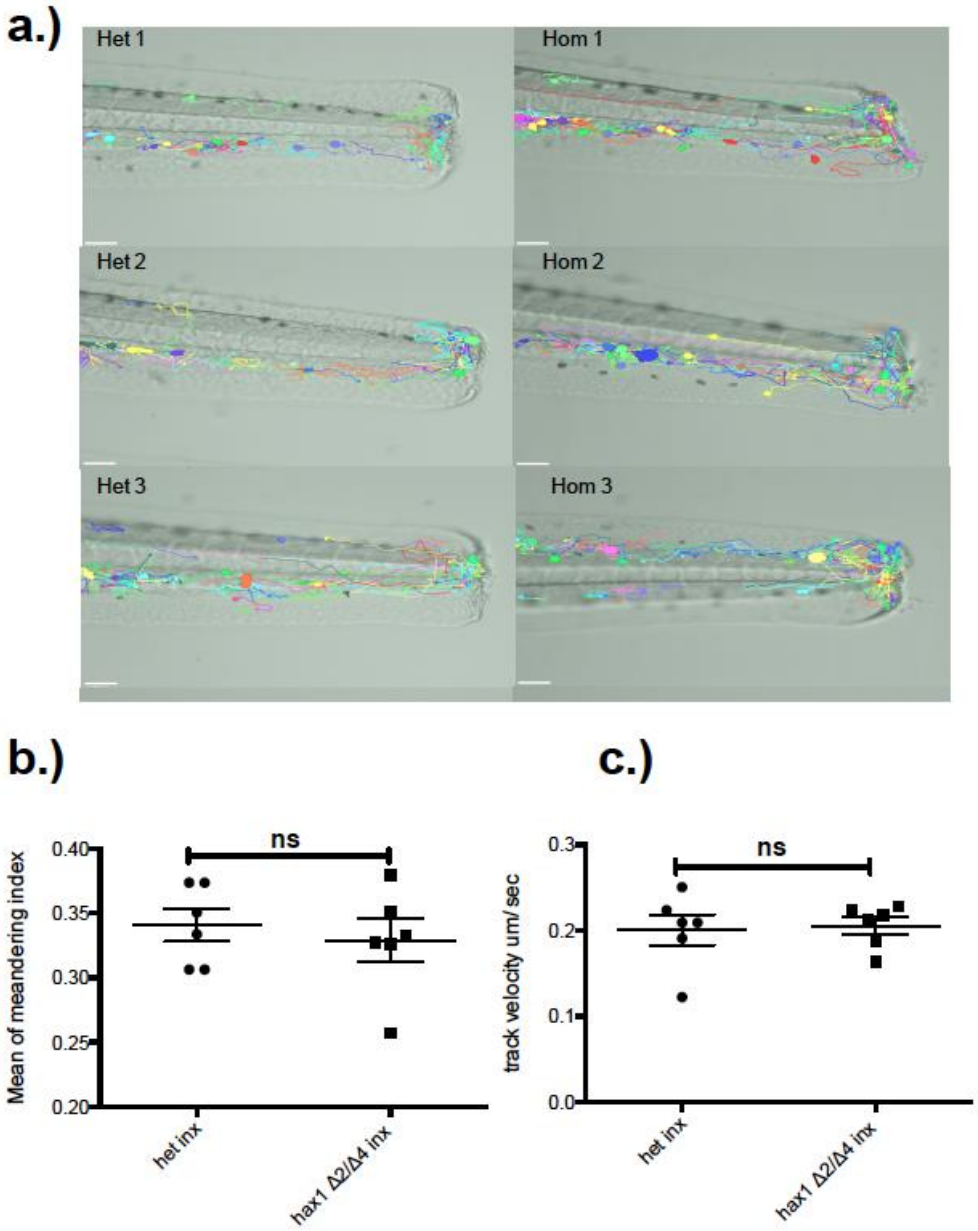

Figure 5.30 The effect of *hax1* Δ2/ Δ4 homozygous mutations on PMN chemotaxis

a.) Embryos generated from a single F_2 heterozygous (*hax1 Δ*2/+ x *hax1 Δ*4/+) and a homozygous (*hax1* Δ2*/* Δ4 x *hax1* Δ2*/* Δ4) incross were injured at 2 dpf and a time-lapse sequence taken for 3 h and analysis of PMN chemotaxis performed using Volocity® software. Representative PMN tracks over the course of the 3 h period are shown in different colours. The mean meandering index (**b.**) and the track velocity (**c.**) of six embryos in each group is shown. The bars represent the mean value ±SEM for each group of embryos. Values (n=6 performed in a single experiment) were analysed using an unpaired student's t-test.

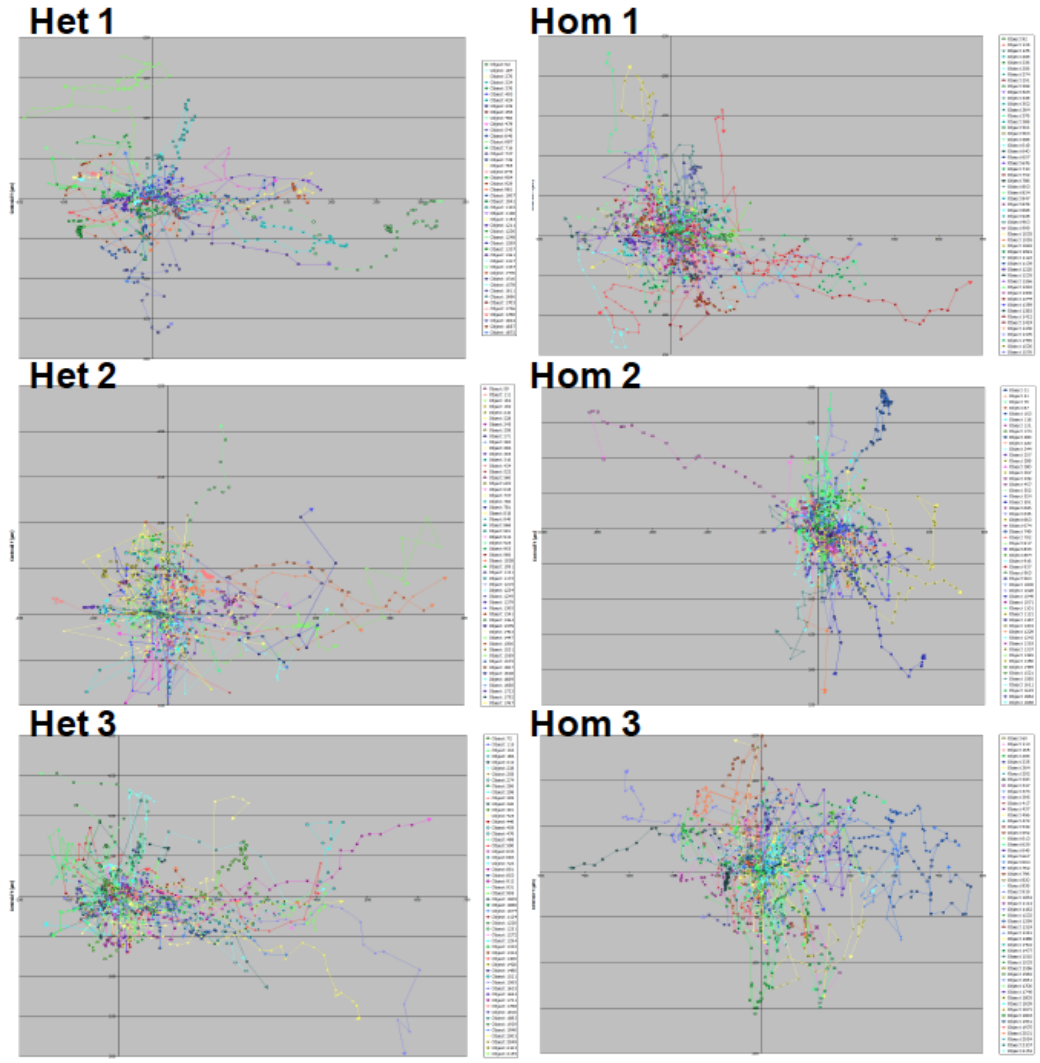

Figure 5.31 The effect of *hax1* Δ2/ Δ4 homozygous mutations on PMN chemotaxis

Embryos generated from a single F_2 heterozygous (*hax1* Δ2/+ x *hax1* Δ4/+) and a homozygous (*hax1* Δ2/ Δ4 x *hax1* Δ2/ Δ4) incross were injured at 2 dpf and a time-lapse sequence taken for 3 h and analysis of PMN chemotaxis performed using Volocity® software. The direction of PMN movement is shown in the form of bearing plots. Representative images are shown from three embryos in each condition.

5.2.9 Summary

The aim of this chapter was to generate stable zebrafish *hax1* knockout lines using zinc finger and TALEN nuclease technology. I have demonstrated targeted *hax1* gene disruption in the zebrafish using both ZFN and TALEN nucleases. A zinc finger nuclease targeting exon 3 of the *hax1* gene was engineered and injected into single cell zebrafish embryos. I have shown that the injected zing finger nuclease mRNA induced single base changes in the *hax1* gene, which would not permit screening of mutants by restriction digest. Embryos injected with a TALE nuclease targeting exon 2 of the *hax1* gene carried a number of different deletions at the target site. Furthermore, the TALEN induced germline mutations were transmitted to progeny. Preliminary phenotypic analysis of heterozygous and homozygous *hax1* mutants generated using the TALEN technology demonstrate that the *hax1* exon 2 deletion mutations did not appear to have an effect on PMN number and chemotaxis.

5.3 Discussion

5.3.1 Targeting zebrafish *hax1* using ZFN technology

Injection of ZFN mRNA into zebrafish embryos is a well-established technique shown to result in efficient ZFN-induced mutagenesis of numerous genes in several model organisms (Doyon et al. 2008; Meng et al. 2008; Foley et al. 2009). The CoDA ZFN approach is one of numerous methods described in the literature for engineering ZFNs (Maeder et al. 2008; Doyon et al. 2008; Kim et al. 2010; Lee et al. 2010; Sander et al. 2011). This approach has been described as the least labour intensive and simple to practice with a high success rate of ZFN activity when compared to selection based methods such as oligomerized pool engineering (OPEN) (Sander et al. 2011).

However, there are also several disadvantages of using the ZFN CoDA approach. Firstly, in comparison to existing methods, CoDA limits the number of target sites within a gene (Kim et al. 2009; Lee et al. 2010;

Sander et al. 2011). Sander *et al* reported that a CoDA site is found approximately every 500 bp of random sequence with a potential increase in target range depending on genomic sequence (Handel et al. 2009). Secondly, although the approach is context-dependent, the identity of the F2 unit in the three-finger array is constrained which could imbalance the affinity of the finger array and have a negative effect on the overall specificity (Bibikova et al. 2001).

Although the *hax1* targeting ZFN generated did not appear to be completely inactive, it was only able to induce single nucleotide changes in the *hax1* DNA sequence. Sanger sequencing did not detect these changes. The limitations of Sanger sequencing to assess nuclease activity have been noted in a study by Moore et al. who found that Sanger sequencing could not detect somatic DNA mutations in zebrafish targeted at three different loci previously reported to induce mutation rates ranging from 0.9- 3.3%. The single nucleotide changes did not appear to be Roche Titanium 454 sequencing errors since they do not relate to homopolymers (consecutive occurrences of the same base), a major limitation of 454 sequencing (Shendure & Ji 2008). In addition, due to the lack of flexibility in the *hax1* CoDA target sites, only a single restriction enzyme (HpyAV) was identified which could be used for mutation screening. It in turn only partially spanned the spacer region. This would render mutant screening difficult and was likely to omit most mutations affecting the central spacer region.

It has been reported that injection of highly concentrated ZFN mRNA into the zebrafish and other model systems can cause non-specific developmental abnormalities likely to occur as a result of cleavage at off-target sites (Bibikova et al. 2002; Beumer et al. 2006; Miller et al. 2007; Meng et al. 2008). This suggests that ZFNs exhibit imperfect target site recognition. In this chapter, the embryos that were injected with high doses of *hax1* ZFN mRNA displayed lethality at 1 dpf. This limited the amount of ZFN to be injected per single embryo to ~40 pg. The lowered

ZFN dose could have had a negative effect on the success of the *hax1* mutation rate. In a study carried out by Cathomen et al., it was shown that for a given target DNA site, ZFNs with higher binding specificity exhibit higher activity, which in turn correlates with lower ZFN-induced cytotoxicity (Cornu et al. 2008). This may suggest that the ZFN generated in this chapter did not have a high DNA-binding specificity for the zebrafish *hax1* gene. A low *hax1* binding specificity of the ZFN could also support our finding of lack of multiple base deletions and insertions in the *hax1* target sequence.

ZFN toxicity may be partly due to the lack of regulation of the DNA cleavage by the ZFN (Szczepek et al. 2007). In addition to the expected FokI heterodimer formation, uncontrolled ZFN cleavage has been shown to result in generation of FokI nuclease homodimers due to the monomers binding at appropriately spaced off-target sites. This in turn leads to cleavage at off-target sites (Szczepek et al. 2007). In this chapter I have indicated that the DD-RR FokI variant was utilised in the construction of the *hax1* targeting ZFN. Using computer analysis and a chromosomal homologous recombination assay, Szczepek et al. demonstrated that the DD-RR performed better than the EE-QK FokI variant due to less favourable homodimerisation of the DD and RR domains (Szczepek et al. 2007). This appears to have not been the case for the *hax1* targeting ZFN.

The length of the spacer region is another factor likely to have affected the *hax1* targeting ZFN nuclease activity. In this chapter, I have shown that binding of the *hax1* ZFN to the target sequence would generate a 5 bp spacer region. Numerous studies have demonstrated that a ZFN arrangement producing a short spacer region (5-7 bp) between the two binding sites of the left and right subunits results in increased ZFN function (Bibikova et al. 2001; Handel et al. 2009; Shimizu et al. 2009). This did not appear to apply to the *hax1* targeting ZFN described in this chapter. It is important to note that each ZFN is likely to have a different affinity and specificity for the intended target site. Therefore, the activity of

one ZFN cannot directly be compared to the activities of existing ZFNs. Some ZFNs have been shown to remain inactive and it has been suggested that this is due to an unfavourable chromatin environment at the target site (Bhakta et al. 2013).

The lack of deletion and insertion mutations comparative to published data (Foley et al. 2009) combined with the relatively low single nucleotide change frequency (4.2 %) of the generated *hax1* ZFN was likely to result in unsuccessful mutant screening by restriction digest analysis. To circumvent this, I next went on to utilise a new approach using TALEN technology in an attempt to induce high frequency *hax1* mutations and in turn generate a *hax1* knockout line.

5.3.2 Targeting zebrafish *hax1* using TALEN technology

The injection of *hax1* Golden Gate TALEN mRNA into single cell zebrafish embryos generated a high enough mutation rate allowing screening by BspHI restriction digest. Although incomparable to the *hax1* ZFN generated due to the use of a different target site, this finding is in agreement with published literature, which has demonstrated a higher success rate of TALEN mutagenesis in multiple model systems (Cermak et al. 2011; Miller et al. 2011; Moore et al. 2012; Cade et al. 2012).

One of the limitations of using ZFNs and TALENs to induce mutations in the zebrafish is that the indel mutations are random and cannot be pre-determined. In comparison to the ZFN mutagenesis approach, the TALEN technology is a faster, cost-effective simpler technique. One of the main advantages of TALENs is their increased flexibility in targeting range. This is a due to their utilisation of a simple binding code whereby each individual RVD recognises a single nucleotide at the target locus. In addition, the longer TALEN recognition sites may play a role in the increased specificity and in turn reduced toxicity in comparison to ZFN. Guidelines based on natural occurring TAL effectors have been published by Cermak et al. who demonstrated that when applying these guidelines

a candidate cleavage site was found on average every 35 bp (Cermak et al. 2011). The lack of detectable TALEN induced toxicity in the *hax1* TALEN injected embryos supports previous findings showing that most TALE nucleases cause no detectable cytotoxicity (Li et al. 2011).

Multiple TALEN scaffolds have been described differing in the N and C terminal length, FokI nuclease linker as well as nuclear localisation sequences (Cermak et al. 2011; Mussolino et al. 2011; Miller et al. 2011). In agreement with published data, the *hax1* left and right TALEN constructs containing the 147 bp long N-terminal region, a wild type homodimeric FokI nuclease domain and the +63 bp long C-terminal successfully cleaved the *hax1* target site although it has been demonstrated that both hetero- and homodimeric nuclease domains induce mutation with comparable efficiency (Cade et al. 2012). Miller et al have demonstrated that a 19 bp spacer generated ~15 % of endogenous human CCR5 modification activity using the +63 bp C-terminal domain compared to a 2% of a TALEN containing a truncated C-terminus (+28 bp) targeting the same region (Miller et al. 2011). Increased understanding of these parameters can lead to elevated target specificity and affinity in turn increasing the mutation frequencies for a specified gene.

5.3.3 Validation of *hax1* TALEN induced mutant sequences

In this chapter, the sequence analysis of the TALEN induced mutations from the heterozygous and homozygous zebrafish provides considerable evidence for the generation of premature Hax1 protein. However, it should be noted that in order to fully validate the mutant sequence, genomic DNA from mutant embryos should first be amplified using *hax1* specific primers. Following this, the PCR product could be TOPO cloned into competent *E. coli* cells and colony PCR carried out. Each colony would then contain a single allele which would be Sanger sequenced and compared to the wild type *hax1* sequence. Therefore, caution should be

taken when interpreting the preliminary phenotypic data generated in this chapter.

5.3.4 The effects of *hax1* exon 2 TALEN induced deletion mutations on zebrafish PMN number and chemotaxis

The TALEN mutagenesis data generated in this chapter suggest that mutation in the exon 2 of the zebrafish *hax1* gene do not affect PMN number. Furthermore, analysis of migration during recruitment and resolution from a wound site indicated that there was no difference between wild type and homozygous knockout mutants in PMN chemotaxis. This does not support previous findings demonstrated from human patient samples and mammalian cell culture models (Klein et al. 2007; Cavnar et al. 2011; Morishima et al. 2013). These results raise interesting questions as to how disruption of the 5' site of *hax1* exon 2 does not recapitulate the human phenotype. There are a number of reasons, which could explain this phenomenon. Firstly, the genetic organisation of the HAX1 gene is extremely complex due to its differential splicing pattern. The TALEN only targeted exon 2 of the zebrafish gene, however, in chapter 4 I have demonstrated the expression of multiple *hax1* variants. Splicing out of exon 2 could occur to generate alternative functional *hax1* isoforms. The evidence for alternative splicing in the zebrafish may also support my findings on co-injected *hax1* TALEN embryos with the *hax1* start MO and *hax1* splice MO where PMN levels were reduced but not abolished.

Secondly, the mechanisms of *hax1* function in the zebrafish are unknown and may differ to the human counterpart. In light of this, it is important to note that in humans, PMN are produced in the bone marrow, a tissue type which zebrafish lack (Charbord et al. 1996). The mechanisms of PMN onset in the bone marrow are not understood. In the zebrafish, PMN are first produced at ~30 h in the posterior intermediate cell mass and anterior yolk sack (Bennett et al. 2001). During later stages of zebrafish development and adulthood, most of the haematopoiesis occurs in kidney

(Bennett et al. 2001). In a single study, it has been shown that the bone marrow is likely to play a crucial role in PMN clearance under homeostatic conditions. This difference between human and the zebrafish model in the PMN 'niche' may represent dissimilar functions of HAX1 in the two organisms and could lead to the lack of recapitulation of the human phenotype. Lastly, the loss of the multifunctional Hax1 protein may be detrimental to the zebrafish embryos and consequently the zebrafish may have a compensatory switch utilizing unknown factor/s to counteract the lack of Hax1 expression.

5.5 Conclusion

In conclusion, I provide novel evidence for *hax1* gene disruption in the zebrafish. In addition, I have shown that TALEN induced *hax1* mutations were maintained in the germline up to F_3. Homozygous knockout mutations predicted to result in premature truncation of the Hax1 protein did not appear to have an effect on PMN number and chemotaxis. The lack of recapitulation of the human phenotype was discussed and the differences in PMN sites of production in human and zebrafish were highlighted.

6 Final Discussion

6.1 Aims of the study

The aim of this thesis was to investigate the function of HAX1 in regulating PMN function during inflammation. To this end I studied expression patterns and regulation of HAX1 in human PMN and the myeloid cell line PLB-985. In addition, in order to generate an *in vivo* working model for *hax1* study, I aimed to explore *hax1* expression in zebrafish embryos and the effects of its mutagenesis in the context of PMN biology.

6.2 Discussion and future work

PMN survival and homeostasis play an important role in inflammation and defence against host pathogens. Defects in the apoptotic pathway of PMN result in numerous chronic inflammatory diseases (Kotecha et al. 2003; Brown et al. 2009; Moriceau et al. 2010). The finding by Klein *et al* revealing that *HAX1* deficiency in human results in SCN implicated a role for this gene in PMN survival and homeostasis (Klein et al. 2007). To date, the molecular mechanism underlying neutropenia in HAX1 deficiency is unknown. Elucidation of the pathways in which HAX1 is involved is essential for our understanding of how HAX1 regulates PMN survival and homeostasis and could allow identification of novel therapeutic targets for chronic inflammatory diseases where dysregulated PMN survival is central to pathogenesis.

I began my research with an investigation into *HAX1* expression at the transcript and protein level in primary human PMN and a number of cell lines including PLB-985. I have shown that although numerous transcript variants are expressed in PMN, based on the expression of previously identified variants these cells did not appear to have a specific *hax1* transcription profile. Several other unidentified *hax1* variants were visible in the PMN PCRs amplified using *hax1* specific primers and have also been described in other cell types (Lees et al. 2008). Identification through 3’ and 5’ rapid amplification of cDNA ends (RACE) and sequencing of *hax1* transcript variants may result in the detection of novel cell specific isoforms. qPCR is more quantitative than the RT-PCR

used in this thesis, which only detects dramatic changes in transcript levels. Further analysis therefore, by qPCR of previously and newly identified variants could also indicate whether *hax1* is transcriptionally regulated and allow complete characterisation of the *hax1* transcript expression patterns in PMN in both health and disease.

Numerous studies have highlighted the anti-apoptotic properties of HAX1. Overexpression of HAX1 in cardiac myocytes, HeLa and HEK293 cells was shown to suppress apoptosis (Yedavalli et al. 2005; Han et al. 2006; Vafiadaki et al. 2007). In cardiac myocytes, the anti-apoptotic effects of HAX1 are exerted through caspase-9 inhibition (Han et al. 2006). Other studies have also linked HAX1 to the mitochondrial apoptotic machinery. To date it is not known whether HAX1 is also regulated in this way in the PMN. I have shown that full-length HAX1 protein levels (isoform 001) are degraded over time in PMN. The HAX1 degradation is likely to correspond to breakdown by caspase activity during apoptosis since inhibition of caspases by qVD-OPh resulted in an increase in HAX1 levels. However, in order to fully establish the link between HAX1 degradation and caspase activity, HAX1 levels of freshly isolated PMN could be compared to those of cells treated with different stimuli and analysed by western blotting. If HAX1 levels were upregulated in response to the stimuli then this would suggest that HAX1 is an upstream regulator of the PMN apoptotic pathway. Attempts during my studies to identify HAX1 protein binding partners and in turn potentially shed light into HAX1 anti-apoptotic effects through co-immunoprecipitation assays were unsuccessful.

A recent study claims that HAX1 splicing in the rat heart results in the expression of anti- and pro-apoptotic isoforms (Koontz & Kontrogianni-Konstantopoulos 2014). The anti- and pro-apoptotic HAX1 forms in the rat were shown to modulate apoptosis through the formation of homo- and heterodimers (Koontz & Kontrogianni-Konstantopoulos 2014). In PMN, in addition to the full-length isoform (001) several immunoreactive bands were detected using both HAX1 antibodies. Although full-length HAX1 levels decreased during PMN ageing, I have shown that the expression of some of the HAX1 specific bands

remained unchanged and, although speculative, these may represent novel pro-apoptotic forms of the protein.

In PLB-985 cells CHX and STSP induced the expression of several HAX1 specific species <30 kDa in size. This work raises interesting questions as to whether the additional bands detected in my studies are a result of HAX1 cleavage or pro-apoptotic forms of the protein, although the use of CHX indicates are unlikely to be newly expressed isoforms. Further work in this field could involve characterisation of HAX1 specific bands by protein sequencing and investigation into the dimerization states of HAX1 isoforms in healthy and aged PMN.

I hypothesised that HAX1 plays a role in the mitochondrial stability of myeloid cells. My work on the PLB-985 cell line using siRNA to knockdown the *HAX1* gene does not support this hypothesis. *HAX1* knockdown in PLB-985 cells had no effect on basal mitochondrial membrane stability or cell death. These results are in disagreement with previous literature of HAX1 involvement in the regulation of apoptosis. Conversely, a very recent study found that *Hax1* deficiency did not increase cytokine deprivation-induced apoptosis in primary murine bone marrow-derived mast cells but that HAX1 does in part, mediate calcium-dependent survival (Trebinska et al. 2014). These data provide further support for HAX1 cell type- and stimulus specific roles and highlight that careful consideration should be taken into the type of stimulus utilised when devising HAX1 studies. Canvar *et al* showed that HAX1 deficiency using siRNA had no significant effect on PLB-985 apoptosis induced by hydrogen peroxide, but instead affected cell adhesion and chemotaxis (Cavnar et al. 2011). Perhaps these results would have differed in calcium-dependent triggered apoptosis.

One of the main problems of working with primary PMN is that they are short-lived in culture and genetically intractable. Attempts to knockdown *HAX1* using novel polymerosome technology in PMN and test the effects on PMN survival were unsuccessful, as shown in Chapter 3. The use of the PLB-985 cell line as a model is also not ideal since these cells differ to PMN in many ways. In

addition, although the *HAX1* knockdown efficiency using siRNA in PLB-985 was high, it should be noted that it is only a transient change and some HAX1 protein remained in the *HAX1* siRNA transfected cells at both of the timepoints tested. The small pool of HAX1 protein may have been sufficient for its functional purpose. These limitations in combination with the lethality of the *Hax1* homozygous knockout mutation in mice resulted in a search for an alternative *in vivo* model.

The genetic tractability of the zebrafish makes it an ideal model system for the study of monogenic disease. The utilisation of recently developed nuclease-targeted mutagenesis techniques can provide insight into the molecular pathophysiology of human mutations. In addition, the generated knockout zebrafish lines can be utilised to validate MO knockdown data. My research revealed that zebrafish express the *hax1* gene and, similarly to the human gene, the zebrafish gene is also alternatively spliced resulting in multiple splice-variants. Disruption of the *hax1* gene using MOs resulted in reduced PMN number, which may be due either to the loss of Hax1 in the embryo or the concomitant developmental delay. The reduction in PMN numbers following MO induced knockdown supports a role for Hax1 in PMN homeostasis and cell survival and shows resemblance to the human phenotype of HAX1 deficiency. However, the effects of the MOs should be interpreted with caution due to potential off-target effects (Robu et al. 2007). Attempts to reduce or overcome any off-target effects using a p53 MO, and to rescue the MO phenotype using full-length *hax1* were unsuccessful. This reduces our confidence in the MO data.

In this thesis, I have shown that a *hax1* targeting ZFN did not result in the effective mutagenesis of the *hax1* gene. Conversely, a *hax1* exon 2 targeting TALEN efficiently modified the gene and the mutations were successfully transmitted through the germline. This further demonstrates that TALENs are a simple, robust and efficient technology to perform heritable targeted gene mutations in the zebrafish. Contrary to our expectations, the *hax1* homozygous

knockout mutation in exon 2 did not have an effect on zebrafish PMN number. Preliminary data also showed that it did not appear to affect PMN chemotaxis.

The recent findings suggesting *HAX1* exists in pro- and anti- apoptotic forms, could help to justify the lack of a PMN specific phenotype of the *hax1* TALEN targeting exon 2. As shown in the zebrafish *hax1* variant expression profile in Chapter 4, exon 2 is likely to be expressed in numerous *hax1* variants and so may be found in both pro- and anti-apoptotic isoforms. Targeting of this region could therefore, have resulted in the deficiency of both pro- and anti-apoptotic forms that in turn could have lead to a neutralisation of the phenotype. It may be that unidentified PMN specific isoforms exist that were not affected by the siRNA in PLB-985 and the TALEN in zebrafish, respectively.

It is important to note that our understanding of PMN development in the zebrafish is very limited and species differences could reflect differences in the HAX1 deficiency PMN specific phenotypes. One could speculate that the lack of a *hax1* knockout phenotype in the zebrafish could reflect the differences in the PMN production and/or PMN differentiation niches. The data generated on PLB-985 in this thesis suggest that HAX1 may not be playing a role in apoptosis. It may be that the protein is involved in PMN mobilisation out of the bone marrow and since this tissue is absent in the zebrafish, this difference could have resulted in a lack of phenotype. This could explain the lack of differences in PMN number between the wild type and the *hax1* knockout zebrafish embryos. Genetic redundancy of *hax1* with other pathway members in the zebrafish could also have accounted for the absence of a phenotype. The presence of an unsuspected *hax1* paralogue in zebrafish that could have concealed the effects of the *hax1* exon 2 TALEN induced mutation should not be disregarded. Conversely, the TALEN induced *hax1* exon 2 mutation could have resulted in the synthesis of a functionally active splice form that restored the phenotype.

In order to verify the MO data, the same *hax1* region targeted by the splice site MO could be targeted by a nuclease to investigate whether the effects on PMN number and development are recapitulated. Novel technology using a bacterial

type II CRISPR (clustered, regularly interspaced, short palindromic repeats) system and Cas9 endonuclease has been shown to exert even more flexibility with the target site than the TALENs and could be used to induce mutations in the *hax1* exon 3 region targeted by the splice site MO (Hwang et al. 2013). TALEN or CRISPR/Cas9 technology could also be used to induce mutations in other regions of the gene and test whether the effects of this on PMN survival and chemotaxis differ from the exon 2 homozygous mutation.

Following further characterization of the zebrafish *hax1* variants, the different *hax1* transcripts could be overexpressed in PMN and tagged with fluorescent protein in order to determine their subcellular localisation and effects on PMN survival. PMN specific promoters and the viral 2A peptide could be used to allow cell-specific expression (Provost et al. 2007). If the findings of the recent study suggesting the presence of pro-apoptotic *HAX1* isoforms were to be true for PMN, then the overexpression of certain isoforms in PMN would be expected to result in increased apoptosis (Koontz & Kontrogianni-Konstantopoulos 2014). This would allow investigation into the possible mechanisms of *hax1* function *in vivo*. Known published interactions of HAX1 in other cell types could then be explored in zebrafish PMN.

6.3 HAX1 as a potential therapeutic target

In chronic inflammatory disease, PMN are recruited to sites of lesions resulting in uncontrolled amplification of inflammation. Airway diseases such as asthma and COPD are characterised by systemic and chronic localised inflammation. They are among the world's most prevalent diseases and studies show they are on the increase. To date, strategies for selective targeting of persistent neutrophilic inflammation are lacking. Many of the prescribed drug treatments for these diseases lack efficacy and have adverse effects highlighting a need for the identification of novel therapeutic targets.

The PMN specific phenotype of HAX1 deficiency in humans highlights a cell specific role for this protein and suggests that treatment of inflammatory disease by targeting of HAX1 would be selective for PMN and result in reduced adverse

effects. My research has highlighted that an understanding of the *HAX1* isoform specific functions will be key for selective drug target generation. A better understanding of HAX1 function may also prove valuable in the treatment of other disorders since HAX1 overexpression has also been implicated in numerous other diseases including melanoma, psoriasis, lung and breast cancer (Mirmohammadsadegh et al. 2003; Trebinska et al. 2010).

6.4 Summary

This thesis has explored the expression and roles of HAX1 in human PMN and the zebrafish. This is the first description of HAX1 transcript variant characterisation in human PMN and PLB-985 showing that PMN do not appear to have a distinct transcriptional profile from other cell types. HAX1 levels were shown to be degraded during apoptotic cell death and the use of pro- and anti-apoptotic stimuli demonstrated that HAX1 is modulated in PMN. Further work is required to determine whether this was a result of caspase inhibition or if HAX1 acts upstream of caspase activation. In zebrafish, I have shown that multiple isoforms of *hax1* are expressed, providing novel evidence for the expression and alternative splicing of *hax1* in the model organism. These data enabled me to use MO and TALEN technology in order to investigate the effects of *hax1* mutagenesis in zebrafish embryos. To our knowledge, this is the first study describing *hax1* mutagenesis through the use of both MO and TALEN technologies. The reduction of PMN following MO induced knockdown of *hax1* supports a role for *hax1* in PMN homeostasis and/or cell survival. Contrary to our expectations however, preliminary data generated utilising a *hax1* deficient zebrafish line created using TALEN technology showed that the *hax1* exon 2 mutation did not affect PMN number and chemotaxis. These findings along with previously generated data suggest that HAX1 isoforms are likely to exert their pro- and/or anti-apoptotic functions in a cell and stimulus specific manner. Collectively my data highlight the complexity of the *HAX1* genetic organization in human and zebrafish and a need for further study of *HAX1*. Understanding the function of *HAX1* in the regulation of PMN survival and homeostasis may offer a potential therapeutic opportunity for the treatment of inflammatory diseases.

7 Appendices

7.1 Appendix 1: Buffers for whole cell lysate preparation and western blotting

7.1.1 SDS-PAGE loading buffer (10 ml)

Reagent	Concentration in buffer	Volume
1 M Dithiothreitol (DTT)	0.1 M	1 ml
10 % SDS	4 %	4 ml
Glycerol	20 %	2 ml
1 M Tris HCl (pH 6.8)	0.0625 M	625 µl
0.2 % Bromophenol Blue	0.004 %	200 µl
dH_2O		2.175

7.1.2 Resolving Gels (1.5 mm gel plates)

% Resolving gel:	12%		15%	
	1 gel	2 gels	1 gel	2 gels
dH_2O	6.6 ml	9.9 ml	5.4 ml	8.1 ml
40 % Acrylamide	4.4 ml	6.8 ml	5.6 ml	8.4 ml
1.5 M Tris pH 8	3.8 ml	5.7 ml	3.8 ml	5.7 ml
20 % SDS	75 µl	112.5 µl	75 µl	112.5 µl
20 % APS	150 µl	225 µl	150 µl	225 µl
TEMED	6 µl	9 µ	9 µl	9 µl

7.1.3 Stacking Gels (1.5 mm gel plates)

Reagent	**1 gel**	**2 gels**
dH_2O	3 ml	6 ml
40 % Acrylamide	620 µl	1240 µl
0.5 M Tris pH 6.8	1260 µl	2520 µl
20 % SDS	25 µl	50 µl
20 % APS	50 µl	100 µl
TEMED	5 µl	10 µl

7.1.4 10X Running Buffer (1 l)

10X stock solution (1 l)	Mass
Reagent	
Tris/Trizma base	30.3 g
Glycine	144 g
SDS	10 g

1 l of 10X stock solution was made up by adding 1 l of dH_2O to the above reagents. For 1 working buffer (pH ~ 8.3), 100 ml of 10X stock was diluted with 900 ml of dH_2O.

7.1.5 10X Transfer Buffer (1 l)

10X stock solution (800 ml)	Volume/Mass
Tris/Trizma base	29 g
Glycine	145 g
dH_2O	800 ml

For 1X working buffer (1 l) 80 ml of 10X stock were added to 200 ml of methanol and 720 ml of dH_2O.

7.1.6 10 X Tris Buffered Saline (TBS) (1 l)

Reagent	Volume/Mass
Tris-HCl 1M pH 8.0	100 ml
NaCl	97.3 g
dH_2O	to 1000 ml

For 1X working buffer (1 l) 100 ml of 10X stock were added to 900 of dH_2O.

7.1.7 10X Tris Buffered Saline (TBS) -Tween (1 l)

Reagent	Volume/Mass
Tris-HCl 1M pH 8.0	M 100 ml
NaCl	97.3 g
Tween-20	5 ml
dH_2O	to 1000 ml

For 1X working buffer (1 l) 100 ml of 10X stock were added to 900 of dH_2O.

7.2 Appendix 2: Primary and Secondary Antibodies

7.2.1 Primary Antibodies

Protein target	Size of target protein	Conc. (µg/ml)	Required working dilution	Required Secondary Antibody (IgG)
β- actin (Sigma)	40 kDa	400	1:4000	Goat anti-rabbit HRP
HAX1 (BD) (Cat ♯: 610824)	35 kDa	250	1:800	Goat anti-mouse HRP
HAX1 (GenTex) (Cat ♯: GTX101992)	35 kDa	250	1:1500	Goat anti-rabbit HRP
Mcl-1(Santa Cruz) (Cat ♯: Sc818)	40 kDa	200	1:1000	Goat anti-rabbit HRP

7.2.2 Secondary Antibodies

Secondary Antibody	Conc. (µg/ml)	Required working dilution
Goat anti- Mouse (Dako)	200	1:2000
Goat anti-Rabbit HRP conjugate (Dako)	200	1:2000

7.3 Appendix 3:

7.3.1 RT-PCR primers for amplification and sequencing of *D. rerio hax1* isoforms

Target	Sequence	Expected size (bp)	Annealing temp. (°C)
hax1 001	Forward 5'-ATGGTGGCATTTTGTGAAGG-3' Reverse 5'-ATTGTGATCGTGGTGGGTTT-3'	964	60
hax1 002	Forward 5'-GAGTGGTCTGACAATTTGAATC-3' Reverse 5'-CAATTCATGAGACCGTAAGGCAGAC-3'	1150	58
hax1 003 & 005	Forward 5'-GGCACGCTTTGAAGAGCCTCAG-3' Reverse 5'-CGGGAAACCTGATGGGAAGAAGC-3'	*003* - 1625 *005* -130	58
hax1 007	Forward 5'-CCTACTTAACGAAGGATAGCGCGC-3' Reverse 5'-CAATTCATGAGACCGTAAGGCAGAC-3'	907	58
hax1 008	Forward 5'-CAGGCTGTAAATATGCTCTGC-3' Reverse 5'-CAATTCATGAGACCGTAAGGCAGAC-3'	592	58
hax1	Forward 5'-GGCACGCTTTGAAGAGCCTCAG-3' Reverse 5'-CAATTCATGAGACCGTAAGGCAGAC-3'	984	60
hax1 x	Forward 5'-GTTCCCGGAGGTCATTATCGAG-3' Reverse 5'-CGAAAGCCTCTGAAGAACTTGG-3'	818 (full length *hax1*)	60
hax1 MO intron 3-4 R	Reverse 5'- CTGGCAGACCTCGATTTACC-3'	-	Sequencing primer
EF1-α	Forward 5' TACGCCTGGGTGTTGGACAAA 3' Reverse 5' TCTTCTTGATGTATCCGCTGAC 3'	470	60

7.3.2 RT-PCR primers for amplification of human *HAX1* isoforms

Target	Sequence	Expected product size (bp)	Annealing temp. (°C)
HAX1 001	Forward 5'-AGGAATTTGGCTTCGGCTTC-3' Reverse 5'-CTGGAAGTTCAGGAGGATGG-3'	151	60
HAX1 002	Forward 5'-GAGCTGAGGTCTGACTTTGA-3' Reverse 5'-TGAGGGTTAACAAGGCTACC-3'	1009	60
HAX1 003 & 005	Forward 5'-AGGAATTTGGCTTCGGCTTC-3' Reverse 5'-TGAGGGTTAACAAGGCTACC-3'	*003*- 316 *005*- 165	60
HAX1 004	Forward 5'-ACCTCGGAGCTTCAGCCCAGGA-3' Reverse 5'-TGAGGGTTAACAAGGCTACC-3'	667	60
HAX1 006	Forward 5'-GATGACCTAAACTTCCAGGTC-3' Reverse 5'-TGAGGGTTAACAAGGCTACC-3'	548	60
HAX1 007	Forward 5'-ATGGTAAGTCTGGAGGAAGG-3' Reverse 5'-TGAGGGTTAACAAGGCTACC-3'	454	58
HAX1 008	Forward 5'-AGTATGGCCAGGGAACGAAT-3' Reverse 5'-TGAGGGTTAACAAGGCTACC-3'	297	60
HAX1	Forward 5'-TGGAGGGGTTCAAAGGTTCG-3' Reverse 5'-AAGTTCAGGAGGATGGGAAGGC-3'	356	57.8
GAPDH	Forward 5'-ACTTTGGTATCGTGGAAGGAC-3' Reverse 5'-TGGTCGTTGAGGGCAATG-3'	420	50

7.4 Appendix 4: D. Rerio Hax1 genetic sequence indicating primer binding regions

Gene: zgc:92196 (ENSDARG00000036764), HCLS1 associated protein X-1 [Source:RefSeqpeptide;Acc:NP_001002337] (Exons: orange)

KEY:

AAA – Forward primer for isoforms *hax1, 003* & *005*
AAA – Forward primer for isoform *002*
AAA – Forward primer for isoform *007*
AAA – Forward primer for isoform *008*

Forward primer for isoform *001*
Reverse primer for isoform *001*

AAA – Reverse primer for isoforms *hax1*, *002*, *007* & *008*
AAA – Reverse primer for isoforms *003* & *005*.
AAA – Forward primer for any additional isoform (*hax1 x*)
CCA -– Reverse primer for any additional isoform (*hax1 x*)

ATG -Start codon
TAA - Stop codon

>Chromosome: Zv8:19:7484201:7490708:1
GATAAACTTCCGGTAAAACGTGTATGTAATCGTTTTAAATTTCATAAGGTTCATTTTACAGTATCGATACTTTATGTAACTAAATATAATCCAA
CTTAATTGACTTAAGCATTTGTTTAGAAAGAAAGCGTTAAAAGATAACAGACGCAAGAAGGAACACATCATGCCGTGTGGGACTTTAATTTT
GAAACTTGTGCGGAAGCAGGTGGAAAGCTCTAGTAGGTTTCCTCACTGTTCTTCCTGCGCTAATCTCTGATGCAACTCTGTTTGTTATGGT
GGCATTTTGTGAAGGTCTCAGGATTCTGTCCATAAATGAGCGTTTTTGATCTGTTTCGTGGGTTTTTCGGGGTTCCCGGAGGTCATTATC
GAGAAGATGGCCGCAGGTGAiliGTTTGTCAAATTGTTAAAATAAGTTCAAACGTCACCTGACAGCTGCTGCTGTTAAACAGATAATGTTTAA
ATATATAACCACGTGTATTTTGTGTTGTTCTGTGCGTTATGTACTTAATTTATATTTTATCTGCAAATATTACGGTTTGTAACTTGTGAATTGC
ATCCTTTGTGTTAAGTTAATAGCATAATGGTTAAAGCAAAACGATGATCGTTTAAATGGTAATCTTGTGTGTAGAAGTTATGTAATCTAATAT
AATTCATCTCGCTTTCTTGAGGTTTTTGTATCGTTAATGGTTTTAATACAAGTAACATTTAAACATTTTTAAATAAACAAAAGCGTTTATATATT
GAAATTAAATTATGTTCGTGTCATTATAAGTTTTAATATATATGTTAGATAGACAATAACTTTGCAAGTACACAGATTATTTGGTCCAGTTTTA
TTTTCGAGTAAGTAACAGCTGAGATGTAGAGATGTGAAGCCATATGGAACATTCTTTCACTTTTATTTTGACACACCAGAACATGAAATGGT
AAACACCGTGTTGCTCCTTGAAACATTAACACACACCTCTTCATAAGTACTTTAATTAAATGAGACTTAATTATTGCGGTTTCACATTTTAAA
GTAGTAATAAGTATGAAAAATTCAGCAACAGATGACATCAGAATATCCTAATATAAAGAGAAGAAATATGAAAGAAAAGATAAAAGAATATT
AATTTTCTTTTCGGCTTAGTCCCTTTAGTAATCAGTGGTCACCACAGCCGAATAAACCGCCAACTCATCCAGCATATGTTGTACGCAGCGG
ATGACCTTCCAGCTGCAATCCAACTCTGGGAAGCACGCATACACTATGGCCAATTTAGCTTCAATTCACCTGTTCCACATGTCTTTGGAAT
ATGGGGGAAACCCACGCCAACACAGGGAGAACATGCAAACTCCACACAGAAATGCCAACTGACCCAGCCGAGACTCTGCGACCTTCCTG
CTGTGAGGCGATCTTGCTACCCACTGCACCACCGTGATGCCCTGTACAAATATGTACACTGGATGTAGTTTTATGAACCCCCCCACCCAA
AAAAAAAGCAGAGCAACAGAATATAAGCAGCATATTTTTTGACCCAAGAATATTTATCTTAAAATCATGCTTAGACTTGCATGCTAAAATGTT
ATATTTGTTAAATAAACATTCATAATTTTTAGTAATAATTAAGATATTTTCATTACCTGTCACTTGATGTTACACTTATCTTTATTTTCTTTAATT
AACTATTATTGTTTTTACACCAAACCTAGATTAAATATATTTTAAACTATACAAAGGGTTTTTAATGGTGGTTAAAAATCCAACGGCACTTTGC
ATATAACTGTAAGCACTTTTGGTGTAATGGTAATCAACATAAATAATGATTTTTTTTCTTTTAAATGTAGACCTTGTTGGCATAAATAATATTA
ATTTGTCCTATATTGCGCCAGATTAATCAGCTACAGTGATGTTTAGTTTAGAGTGGTCTGACAATTTGAATCATGGTTTTTTTTAATACAGGG
ACCCCTTCTTTGATGGAATGATTCATGAAGATGATGATGATGAAGACGAGGATGACTTTAACAGACCCCATCGGGATCCGTTTGACGAT
GCCTTCAGGTTTGGATTCAGTTTCGGTCCAGGCGGGCCACGCTTTCAAGAGCCTCACATGTTCGGCCAGATCTTCAGAGACATGGAGG
AGATGTTTGCTGGTCTGGGACGCTTTGATGAGCGACATGGATTTGGACCGAGAGGTGTGTCTCTTTGCTCTGTCCCTTTTCAATTTAACA
TTTTGAATGACCAATTATAGTTAATTTATAAACAATAAGGTGACATGGGTGAGCAGTGGATAGCATGATCGCCTCACAGCAAGAAGGTCGC

7.4 Appendix 4: D. Rerio Hax1 genetic sequence indicating primer binding regions

TGGTTTGAGCCTCGGCTGGGCATTTCTGTGTGGAGCTTGCATGTTTTCCCTGTGTTCACGTGGGTTTCCTCTGGGTGCGCCGGTTTCTCC
CACAGTCCAAAGTGTGCTGTAGGTAGTCTAAATTGGCCATAATGTATGTGTGTGAATGTGTATGGGTGTTTCCCAGTGATGGGTTGCAGCT
GGAAGGGCATCTGTTGCGTAAAACATATGCTGGATAAGTTGGCGGTTCACACCGCTGTGTTGACCCCTGATGAAAAAAGGGGCTAAGCC
GAAAAGAAAATAAATGACTGACTGAATGAATGAAGATGTTATAATAATAAAGAATACTTATGAGAAGAGCAACATGAGTGTTGACATTACAA
AGTATTCAATTTCTTTCCTTTTTTGGTACTAAATGACCCCAAATTACTGAAAAAATACCCCAAGATAAAAATTTCTAAACTGTCCATACCTTAG
CCGAATACACAATGACAGGCTTGTCATAATTTTACAAATTGTCTTACAATGTCAGAACAGGGTAATAATTTACAGTTTGTTGTGAAATAAGCT
AATTGATGATGGTTAGATCAGCTCATTGCACAATTTATTGTATTACTTTCCCCCTCAGATTTGGTCAAAACAAAAGTGGCCGATGTATTTTA
TTGCTTGTTCAGATGACATTCTCCAGTTAAAATTACTAATTGAGTGAAAGTGTCTAGGCCAGTATCTACACCAGTGCAAATAACCACAATCG
CGCATTTTCAAACTGAGACAGAACTCGCGGACTGCTGCTTTACAACTGACCTTATTGAGTTCAAATACAGTTGAAGTCAAAATTATTCGGC
CTTCTGTGAATTTTTTTTAGTATTTTTTTTAAAAAATCTTTCCCAAATGATGTTTAACAGAGCAAGGAAATTATCATAGTATTACCTATAATATT
CTTTCTTCTGGTGAAAATCTTATTTATTTATTTTTCCAGCTAGAATAAAAGCAGTTTGAATTTTATTTATAGTATTTTACGGTCAATATTATTAT
CCCCCTTAATCAATTTTTTTTTTTTTCAGTATGTCTACAGAACAAACCATCGTTATACAGTGCCTTGCCTAATTACCCTAACCTGCCTAGGTAA
CCTAGTTAAGCCTCTAAATGTCACTTTAAGCTGTATAGAAGGGTAGAAATATCTAGTAAAACATTGTTTACTGTCATCATGGCAAAGATAAA
ATAAATCAGTTATAAGAAATGAGTTATTAAAACTAATATGATTAGATATGTGTTGAAAAAAATTGTTTGAGTTAAACAGAAAAAATATAAAGG
GGTCTAATTAGTCAGCCTTCAACTGTGTGTACATTCTCTAACTGATTGTGGTTCACAATTGCACTGGTTTAAGTGATGATACATTTCTAGCA
TCATCTGTTCTCCTTCTTCCCATCACCTTTCCCGTCAATAGAAGCTCCACCTCCACAGGAAGGAGTTGAGAAAGGCAGGAGTGGGACA
GGAAGTGGGAATCCCATCAGAGATTTCATGTTGAAGTCTCCTGACCGCTCACCTAAAGATCCAGAGCACAGAGAGGATTCTCCACCAA
ATCATCCTCACAGGAGGCCTTTCTCAAAGGTAAATCGAGGTCTGCCAGTGAATATCTGCAGTCTCTCCATTCCAGCGTCTCATCTTATTG
GCTTTCTTTCATTTCAGTTCAACGATATTTGGAAAGATGGACTGTTAAAACCAAAGGGGGAAGACAAAAGGGAGGATGGAGGTAATGC
ATCTTGTGCAGGTTTTCACAACAATTATACAAGTCTGAGAGCAGATATAGTTCTCAAAACCATTCAGTAGGTTTCCATTTAATTTTTTGTTA
CAGATAAAGCTGATGGATTTGCTAATTATTGATTCAATTAAGCTAATTTGACAACCTTTTTCTTTAGCGGGGGATCTCTGTATATACTAAATA
TTCTAGATTACCTACTTAACGAAGGATAGCGCGCTACTTAACAAAGGGTAAATGCAAATTTAATTTAATAATGGGAAAATATAACATCTAATT
TATGTTTATTTATATTGTATTATAAATAGTTTTTAAATATCATAAGATGATGAATGTCACATAAAAACGTAAATTAGCAGAAATTAATTTACAAA
CACTCTAATTTACATAAGGTAATCATCTGAGCATTGCTGTTATCATCTTACAGATGTTCCTTCAACAAATCTTTTGTTTTCTTGTTCTTGCCTC
AGATCTGGACTCACAGGTGTCTTCAGGTGGACTGGACCAGATCTTGAAAGATCCAGCACCTTCACAGCCAAAAACAAGGTCATTTTTTA
AGTCTGTCAGCGTCACCAAGGTGGTCCGACCGGATGGAGTGAGTGGATCATTTTGTCTTCAATACTATTTCTAAATACAATCATTGTAGAA
TTATATTTCAGGCTGTAAATATGCTCTGCATTTATGCTTATAATAACGGAGAGTGTGTGTGTCTCTGTCTGTCTGTCTGTCTGTCTGTGTAG
ACTGTAGAAGAACGGCGAACAGTCAGAGATGGAGAAGGTAATGAAGAGACGACCGTGACCATCTCAGAAAGGCCAGGTGGGCAAGA
TAGGCCAGTCCTGGATCAGTCTGGTCCTTTAATGCCAGGTTAGTGGTTTAATAATCTTTTTTTCTGTAAATAAAGATTATTAAGCTATAGAT
TATGTTTATTGTACTTTACTTAAACTCTATCCAATGTATTTATTTAATGTATGTTTATATAAAAATTTCATAAAAACAAAAAACAAAAAATGAAT
AGTTATAATTAGATGTGCAATGTTTGCATACATGTTTGCATACAGTTTATTATTTGAGTGTGGATTATTAAAATTATATATATATATATATATAT
ATATATATATATATATATACAACAGTTCTGTCTGGTTCTCAAATCTGATTGGCTGATAGCCGTGCGATATTCTGCAATATCAGAACTCCTACA
GCCTCTTTACCCTTTGTGTATTACTCCGCCCACATACAGCCAGCAAAAAGCAGACACTACAGATCTAAAGTTTAAAAGATGCACGCTCAAC
TGTTTAACTGTCAGCTTATGATTTGAATCCAGAAGAAAGTAGTTCCTCATACAAAAGGGTTTTTGAGACTCTCCTTGTTTGATTTTGTTTTTA
TATACACAATTATGCTGTCAAACTGTTGTATAAACGCAATATCACACTCGTAGCAGTGTGATATGGCTGTATATCGGCAGTGGTGTGGGCA
CAACGCACGGCTCCCACCAGTGCCGATATACAGCCATATCGCACTGCTACTCGTGTGATATTGCTCATATATATATATATATATATAATATA
TATATTTAAAAATATTTATTGTAATTGTAAAAATATTGTAATTTAAAGAAAGACAGAGACACAATTTAAGTAAACTGCTACTTAATAAAAAACA
AGCAATTTTATGATTAGTTTTCTCCACCGCTGTTCCCCAAAAAGCTAAGATCTCAAAACCAAGGATCTTACTAAAAGTTATCTATGCGTATCA
TCCCCCCTTAGCATTAATGTTAATAAAATGTCTTCACATTTACATAAAGTCTTTTGCATTTACAGTATTTGTACATTAGACATATTTATTTGTA
ATCATTCAGTGATGTGTTTTTCTGCATCTTTCAGGTGGTTCTGACATGCAGGATGATTTCTCCATGTTTTCCAAGTTCTTCAGAGGCTTTCG
AAGTTAAAAGAGTTTTGGAACCAAAACCGAAGGACAATCTCTTTCCCGGCATTTCATTCTTAAGTATATTTGTGGAGATCCACAACATC
AACATTGATCAAATATCACACAATGAACCTCAAAACTCTGCTGACTTTTTCATTTTTTATATAATTTCCATTAAAGATATGCAAATAATTA
TATAGACCGAACTTTGGGTTAGTTGGGTTTTGTTCAGAAATGACACTTTAATATATTTAAACATTTTATTTCAATAGGTGTAAATAAAAAAA
CTAAATGAAGTCTGCCTTACGGTCTCATGAATTGTTTTCAGGAACATCTAAATGTGGAAGCTGGCATATTTTCTGTATCTGAAGAGCACTAA
TTTAAGCAAACAGCTCTTTTTATTGGATAAATAGAGCAAACGCAGTACATTGTATTTTTAAGTGATTCTAAATGTAAGAGAGCTGCTCGTTTT
GACAGCTGCTTAGCATTCTGAGGTCAAGTCAGTAGTAGCAGCTCATCAAAATTT

7.5 Appendix 5: PCR gel electrophoresis

7.5.1 50X TAE buffer (1 l)

Reagent	M **Volume/mass**
Tris Base	242 g
EDTA	37.2 g
Acetic acid	57.1 ml
dH_2O	to 1000 ml

For 1X TAE 200 ml of 50 X buffer were added to 800 ml of dH_2O.

7.6 Appendix 6: pCR-Blunt II- TOPO vector and pCS2+ plasmid vector maps

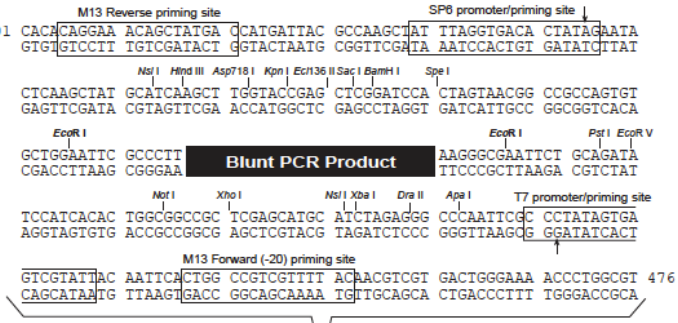

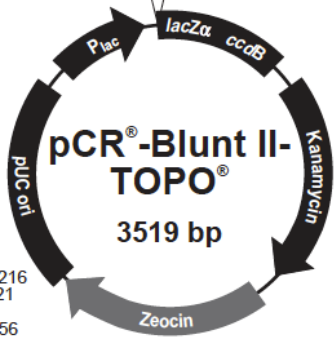

Comments for pCR®-Blunt II-TOPO®
3519 nucleotides

lac promoter/operator region: bases 95-216
M13 Reverse priming site: bases 205-221
LacZ-alpha ORF: bases 217-576
SP6 promoter priming site: bases 239-256
Multiple Cloning Site: bases 269-399
TOPO®-Cloning site: bases 336-337
T7 promoter priming site: bases 406-425
M13 (-20) Forward priming site: bases 433-448
Fusion joint: bases 577-585
ccdB lethal gene ORF: bases 586-888
kan gene: bases 1099-2031
kan promoter: bases 1099-1236
Kanamycin resistance gene ORF: bases 1237-2031
Zeocin resistance ORF: bases 2238-2612
pUC origin: bases 2724-3397

pCS2+ (http://www.xenbase.org/reagents/vectorAction.do?method=displayVectorSummary&vectorId=1221270)

Antibiotic resistance: Ampicillin

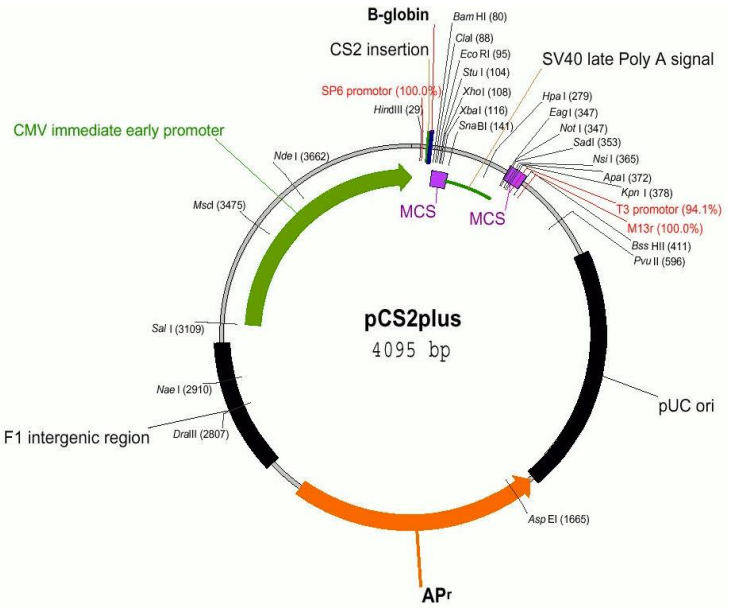

7.7 Appendix 7: Whole mount *in situ* Hybridization (WISH) buffers

7.7.1 Pre-Hybridization buffer (50 ml)

Reagent	M **Volume/mass required to make 50 ml of buffer**
50 % Formamide	25 ml
5X SSC	12.5 ml of 20X
0.1 % Tween 20	50 µl
Citric Acid to pH6	460 µl of 1M
50 µg/ml heparin	50 ul of 500 mg/ml stock
500 µg tRNA	20 µl of 24.75 µg/ µl stock
dH_2O	12 ml

7.7.2 20X Saline-sodium citrate (SSC) buffer (200 ml)

Reagent	M **Volume/mass required to make 200 ml of buffer**
NaCl	35.06 g
Sodium citrate	17.64 g
Adjust to pH 7 using citric acid	
dH_2O	to 200 ml

7.7.3 HybWash buffer (50 ml)

Reagent	M **Volume/mass required to make 50 ml of buffer**
50 % Formamide	25 ml
5 x SSC	12.5 of 20X stock
0.1 % Tween	50 µl
Adjust to pH 6 using citric acid	460 µl
dH_2O	12 ml

7.7.4 Staining wash (50 ml)

Reagent	M **Volume/mass required to make 50 ml of buffer**
100 mM Tris HCl pH9.5	to 50 ml
50 mM MgCl2	0.51 g
100 mM NaCl	0.292
0.1 % Tween	50 µl

To make up the staining solution 112.5 µl of NBT (50 mg/ml) and 175 µl of BCIP (50 mg/ml) were added to 50 ml of staining wash.

7.8 Appendix 8: Egg medium for zebrafish embryos (E3)

7.8.1 60X E3 medium (2 l)

Reagent	M **Volume/mass required to make 2 l of buffer**
NaCl	34.8 g
KCl	1.6 g
$CaCl_2$	5.8 g
$MgCl_4$	9.78 g
dH_2O	to 2000 ml

7.8.2 1X E3 medium (1 l)

Reagent	M **Volume/mass required to make 1l of buffer**
60 X E3	16.7 ml
1% Methylene Blue	100 µl
dH_2O	to 1000 ml

7.9 Appendix 9: Sanger sequencing analysis of *D. rerio hax1 008*

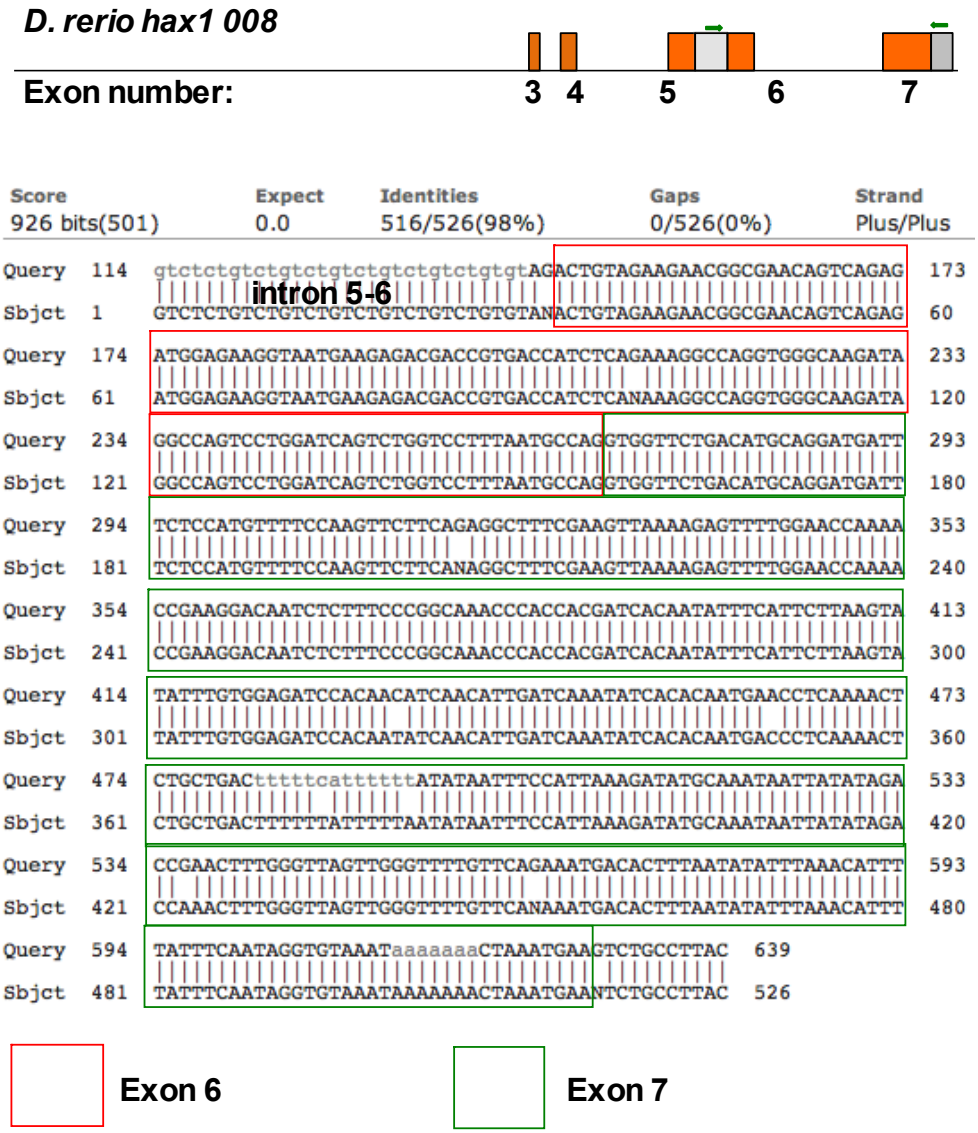

Query- expected *hax1 008* sequence amplified using primers for isoform *008*
Subject- Sanger sequencing output using *hax1 008* forward primer

Green arrows indicate *hax1 008* primer annealing sites.

7.10 Appendix 10: Sanger sequencing analysis of PCR band amplified using the *D. rerio hax1 x* primer pair reveals the band is *hax1 001*

D. rerio hax1 001

Score	Expect	Identities	Gaps	Strand
1033 bits(559)	0.0	586/608(96%)	2/608(0%)	Plus/Plus

```
Query  230  TGAAGATGATGATGATGAAGACGAGGATGACTTTAACAGACCCCATCGGGATCCGTTTGA  289
Exon 2
Sbjct  12   TGAAGANGATGATGATGNAGACGAGGATGACTTTAACAGACCCCATCGGGATCCGTTTGA  71

Query  290  CGATGCCTTCAGGTTTGGATTCAGTTTCGGTCCAGGCGGGGCACGCTTTGAAGAGCCTCA  349
Exon 2
Sbjct  72   CGATGCCTTCAGGTTTGGATTCAGTTTCGGTCCAGGCGGGGCACGCTTTGAAGAGCCTCA  131

Query  350  GATGTTCGGCCAGATCTTCAGAGACATGGAGGAGATGTTTGCTGGTCTGGGACGCTTTGA  409
Exon 2
Sbjct  132  GATGTTCGGCCAGATCTTCAGAGACATGGAGGAGATGTTTGCTGGTCTGGGACGCTTTGA  191

Query  410  TGAGCGACATGGATTTGGACCGAGAGGTTTCCCGTCAATAGAAGCTCCACCTCCACAGGA  469
Exon 2                                                          Exon 3
Sbjct  192  TGAGCGACATGGATTTGGACCGAGAGGTTTCCCGTCAATAGAAGCTCCACCTCCACAGGA  251

Query  470  AGGAGTTGAGAAAGGCAGGAGTGGGACAGGAAGTGGGAATCCCATCAGAGATTTCATGTT  529
Exon 3
Sbjct  252  AGGAGTTGAGAAAGGCAGGAGTGGAACAGGAAGTGGGAATCCCATCAGAGATTTCATGTT  311

Query  530  GAAGTCTCCTGACCGCTCACCTAAAGATCCAGAGCACAGAGAGGATTCTCCACCAAATCA  589
Exon 3
Sbjct  312  GAAGTCTCCTGACCGCTCACCTAAAGATCCAGAGCACAGAGAAGATTCTCCACCAAATCA  371

Query  590  TCCTCACAGGAGGCCTTTCTCAAAGTTCAACGATATTTGGAAAGATGGACTGTTAAAACC  649
Exon 3                                                          Exon 4
Sbjct  372  TCCTCACAGGAGGCCTTTCTCAAAGTTCAACGATATTTGGAAAGATGGACTGTTAAAACC  431

Query  650  AAAGGGGGAAGACAAAAGGGAGGATGGAGATCTGGACTCACAGGTGTCTTCAGGTGGACT  709
Exon 4                                                          Exon 5
Sbjct  432  AAAGGGGGAAGACAAAAGGGAGGATGGAGATCTGGACTCACAGGTGTCTTCAGGTGGACT  491

Query  710  GGACCAGATCTTGAAAGATCCAGCACCTTCACAGCCAAAAACAAGGTCATTTTTTAAGTC  769
Exon 5
Sbjct  492  GGACCAGATCTTGAAAGATCCANCACCTTCACAGCCNAAAACAAGGTCATTTTTTAANTC  551

Query  770  TGTCAGCGTCACCAAG-GTGGTCCGACCGGATGGAACTGTAGAAGAACGGCGAA-CAGTC  827
Exon 5                                                          Exon 6
Sbjct  552  TGTCAGCGTCNNNNNNNGTGGTCCGACCNNATGGAACTGTANAANAACGGCNAANCANTC  611

Query  828  AGAGATGG  835
Exon 6
Sbjct  612  AGANATGG  619
```

Red arrows indicate *hax1 x* primer annealing sites
Query- *hax1 001* sequence deduced from the Ensebl sequencing data
Subject- Sanger sequencing output using *hax1 x* forward primer

7.11 Appendix 11: Sanger sequencing analysis of TOPO cloned *hax1* MO induced 2.5 kb PCR band pair

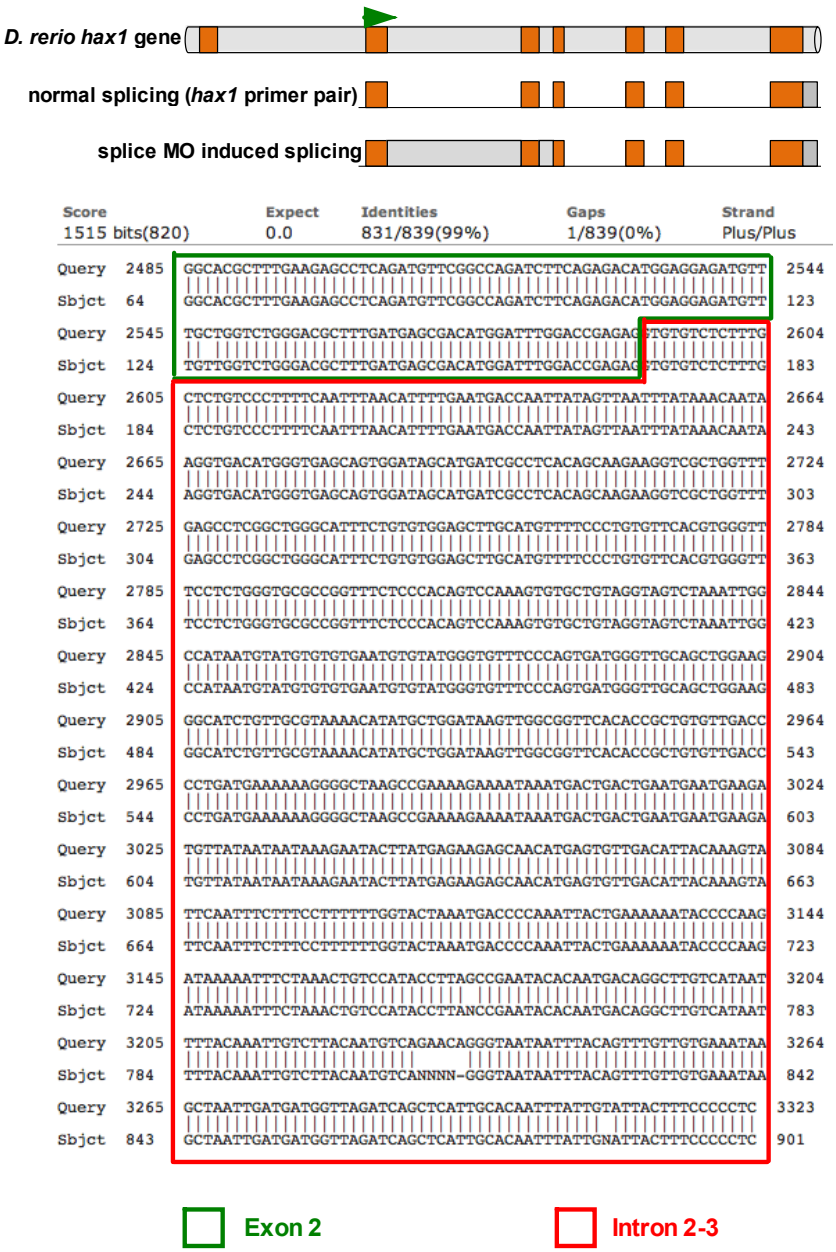

The 2.5 kb PCR band induced by splice MO injection and amplified using the *hax1* primer pair was TOPO cloned into the pCR-BLUNT II-TOPO vector. Sanger sequencing of the PCR band using an M13 Forward primer (green arrow) resulted in sequence identical to the 3' of exon 2 and most of intron 2-3 (from the 5' end). Query: *D. rerio hax1* gene sequence deduced from the Ensembl website. Subject: Sanger sequencing output.

7.11 Appendix 11: Sanger sequencing analysis of cloned *hax1* MO induced 2.5 kb band amplified using the *D. rerio hax1* primer pair (cont.)

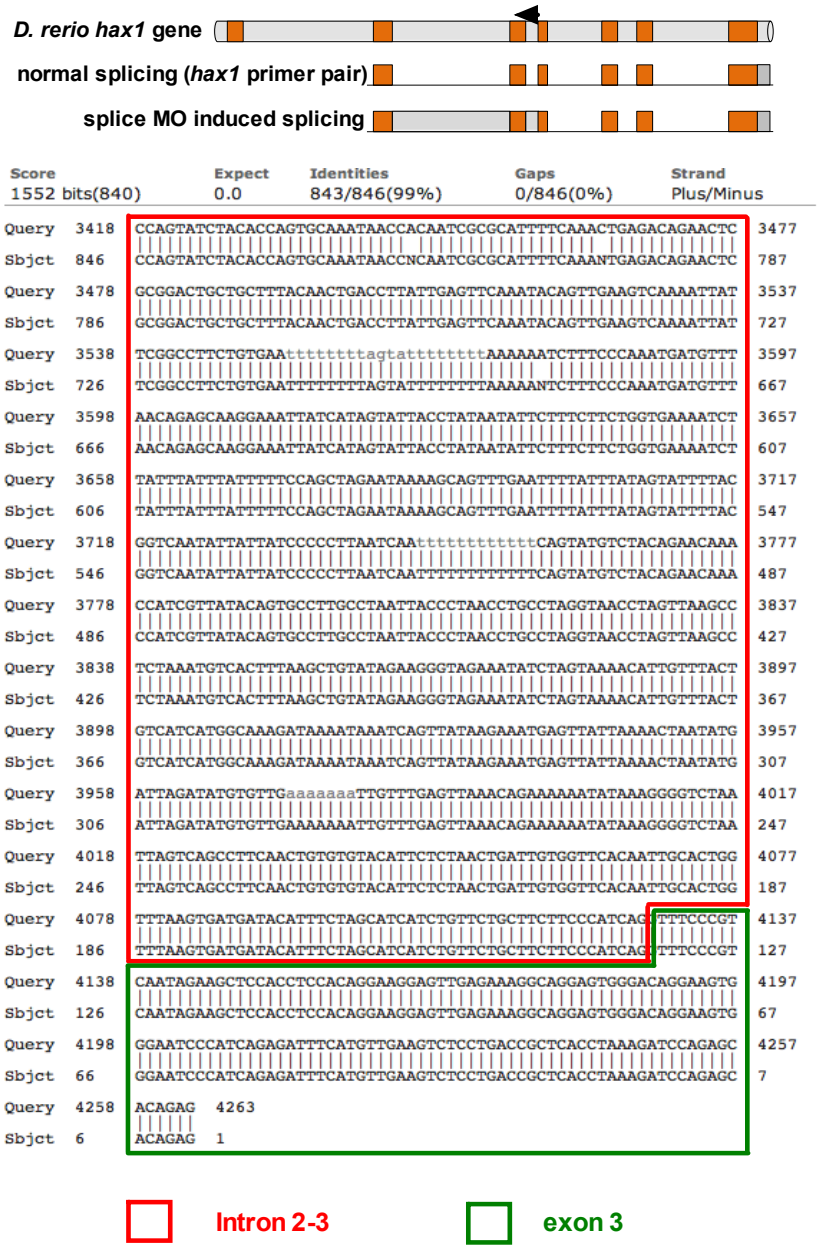

Sanger sequencing of PCR band using the *hax1* MO intron 3-4 R primer (black arrow) resulted in sequence identical to most of intron 2-3 (from the 3 ‘ end) and most of exon 3 (from the 5 ‘ end). Query: *D. rerio hax1* gene sequence deduced from the Ensembl website. Subject: Sanger sequencing output.

7.11 Appendix 11: Sanger sequencing analysis of cloned *hax1* MO induced 2.5 kb band amplified using the *D. rerio hax1* primer pair (cont.)

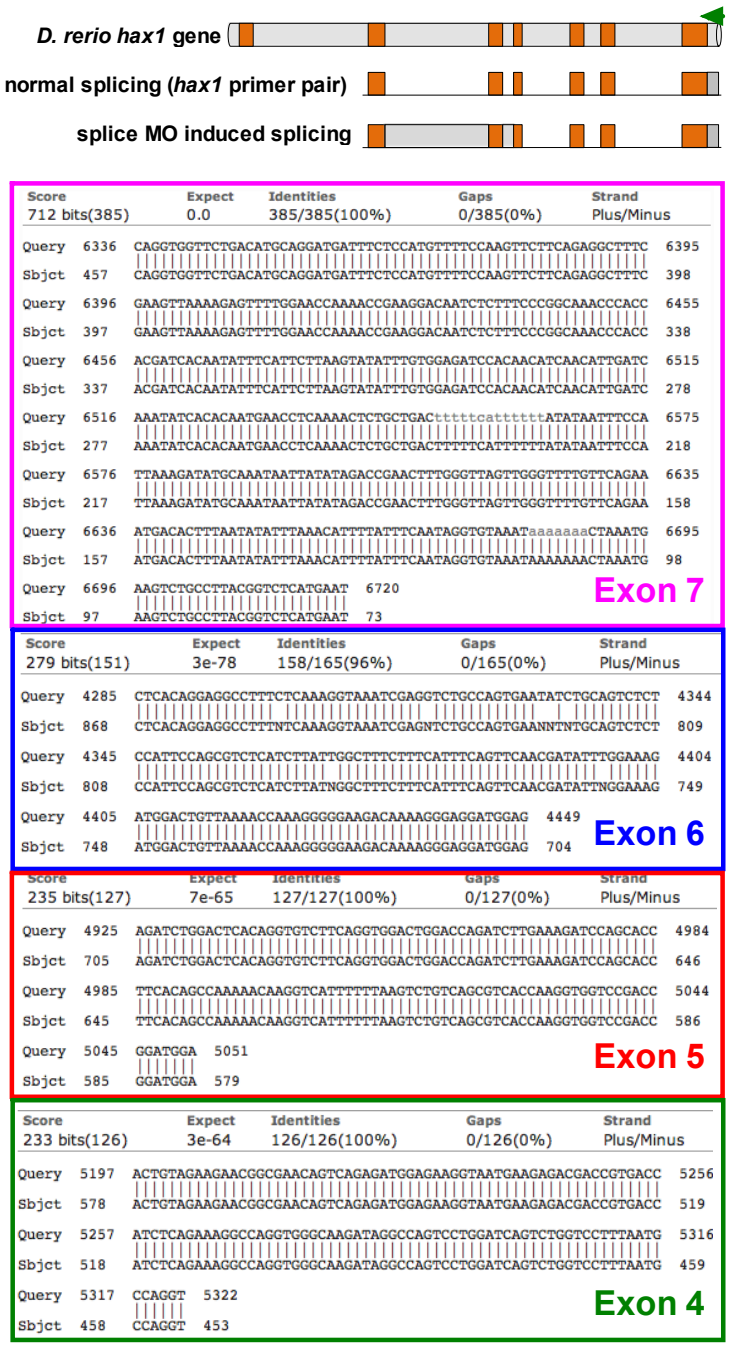

Sanger sequencing of PCR band using an M13 Reverse primer (green arrow) resulted in sequence identical to exons 4-7. Query: *D. rerio hax1* gene sequence deduced from the Ensembl website. Subject: Sanger sequencing output.

7.12 Appendix 12: Determining the insert orientation by Sanger sequencing of the cloned *hax1* 001 cds in pCS2+

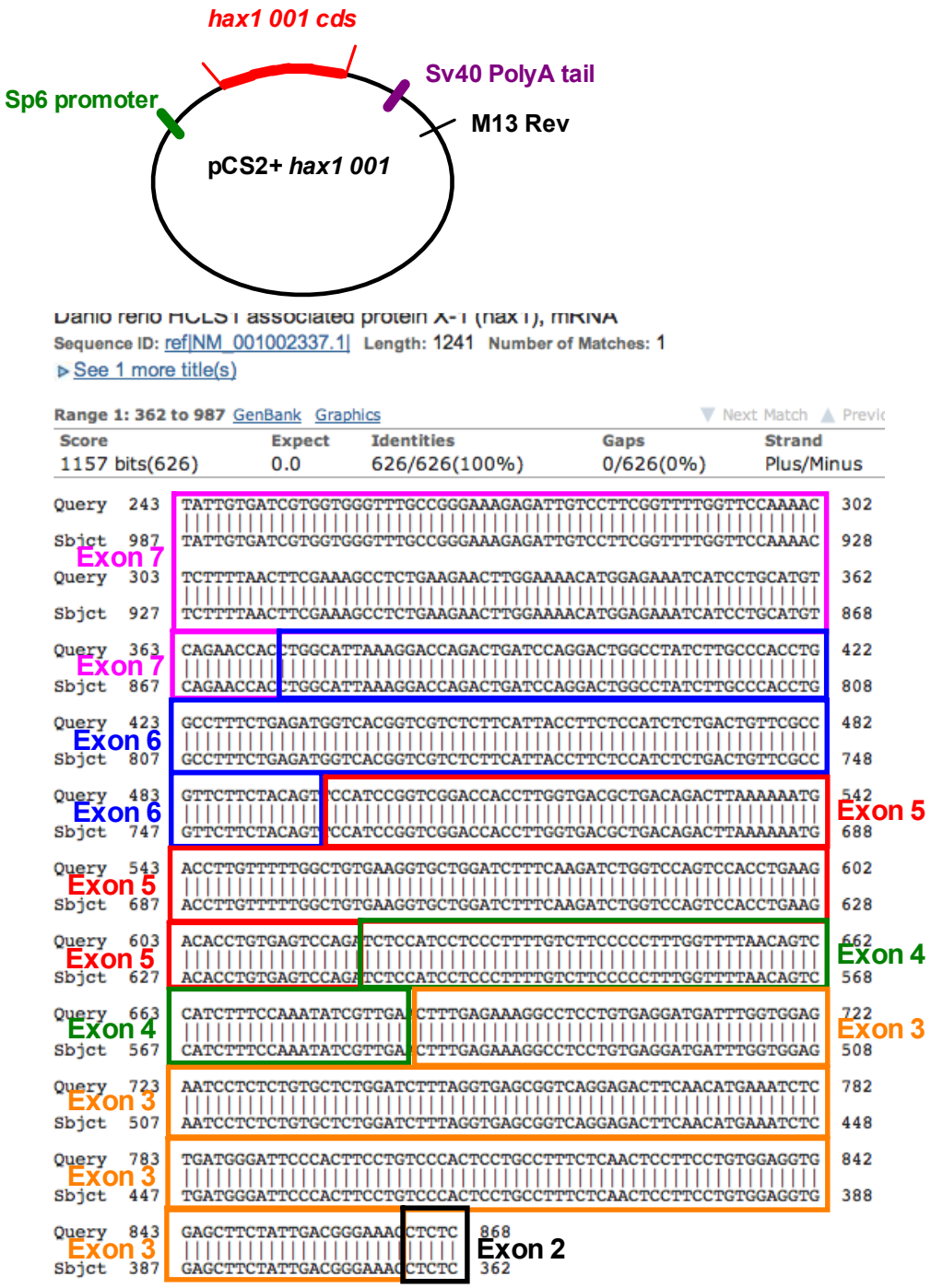

Sequencing of pCS2+ *hax1 001* using the M13 Reverse primer revealed that the full length cds insert is in the 5'-3' direction. Therefore, the *hax1* coding sequence is in the correct orientation for *in vitro* transcription to generate full length *hax1* capped RNA for injection into single cell zebrafish embryos.

7.13 Appendix 13: PCR primers for generation, amplification and sequencing of ZFN constructs

7.13.1 Left ZFN subunit F1 and F2F3 primers:

GoodF1Hax1aL

5'-ggccACCGGTATGAGTACGGGTATGACGGTCCAAAATATGACGACGCGA
AAAGTTCCGCATGCAAAT-3'

GoodF2F3Hax1aL

5'-ggccACCGGTGAAAAACCGTTTCAGTGTCGGATCTGTATGCGAAATTTCT
CCCGTCAGGACAACTTGGGTCGTCATCTACGTACGCACACCGGCGAGAAG
CCATTCCAATGCCGAATATGCATGCGCAACTTCAGTCGTAACGTTAACTTG
GTTACCCACCTAAAAACCCACCTGAG-3'

Right ZFN subunit F1 and F2F3 primers:

GoodF1Hax1aR

5'-ggccACCGGTATGAGTACGGGTATGACGCAACAAGTTATGTGGACGCGA
AAAGTTCCGCATGCAAAT-3'

GoodF2F3Hax1aR

5'-ggccACCGGTGAAAAACCGTTTCAGTGTCGGATCTGTATGCGAAATTTCT
CCCATAAATCTTCTTTGACCCGTCATCTACGTACGCACACCGGCGAGAAGC
CATTCCAATGCCGAATATGCATGCGCAACTTCAGTCAGACCACCCATTTGT
CTCGTCACCTAAAAACCCACCTGAG-3'

The F1 and F2F3 primers (4 nmole ultramer synthesis) for each the left and right subunits were purchased from Integrated DNA Technologies, Coraville, IA.

7.13.2 PCR primers for ZFN construct amplification and sequencing

	Sequence	Product size (bp)	Annealing temp. (°C)
LCS2 goodRCS2	5'-GAAAAGTTCCGCATGCAAAT-3' 5'-CACCTAAAAACCCACCTGAG-3'	4867	50
LseqC2 RseqCS2	5'-TGCAGGATCTGCCACCAT-3' 5'-TCCTTGATCCACCCAAATGT-3'	602	50-60
LseqFok RseqFok	5'-GCCAGAAATTCCACTCAGGA-3' 5'-CCCCCTGAACCTGAAACATA-3'	705	50-60
LHax1ZFN RHax1ZFN	5'-AGTCAGCCTTCAACTGTGTGT -3' 5'-TGGCAGACCTCGATTTACCT-3'	305	50-60
LHax1ZF454 RHax1ZF454	5'-CGTATCGCCTCCCTCGCGCCATCAG acgagtgcgtAGTCAGCCTTCAACTGTGTGT-3' 5'-CTATGCGCCTTGCCAGCCCGCTCAG cgagagatacTGGCAGACCTCGATTTACCT-3'	375	
atitanium btitanium	5'- CGTATCGCCTCCCTCGCGCCATCAG -3' 5'- CTATGCGCCTTGCCAGCCCGCTCAG -3'	375	

7.14 Appendix 14: Validation of the ZF (F1-F3 array) and nuclease domain sequences of the left and right *hax1* targeting ZFN expression vectors

7.14.1 Validation of the Left ZFN ZF sequence (Colony L12)

a.)

Score	Expect	Identities	Gaps	Strand
915 bits(495)	0.0	496/497(99%)	0/497(0%)	Plus/Plus

```
Query  58   TGACGGTGATTATAAAGATCATGACATCGATTACAAGGATGACGATGACAAGGGTACCGG  117
            ||||||||| ||||||||||||||||||||||||||||||||||||||||||||||||||
Sbjct  21   TGACGGTGANTATAAAGATCATGACATCGATTACAAGGATGACGATGACAAGGGTACCGG  80

Query  118  GGAGCGCCCCTTCCAGTGTCGCATTTGCATGCGGAACTTTTCGCGTCGTCATATTTTGGA  177
            ||||||||||||||||||||||||||||||||||||||||||||||||||||||||||||
Sbjct  81   GGAGCGCCCCTTCCAGTGTCGCATTTGCATGCGGAACTTTTCGCGTCGTCATATTTTGGA  140

Query  178  CCGTCATACCCGTACTCATACCGGTGAAAAACCGTTTCAGTGTCGGATCTGTATGCGAAA  237
            ||||||||||||||||||||||||||||||||||||||||||||||||||||||||||||
Sbjct  141  CCGTCATACCCGTACTCATACCGGTGAAAAACCGTTTCAGTGTCGGATCTGTATGCGAAA  200

Query  238  TTTCTCCCGTCAGGACAACTTGGGTCGTCATCTACGTACGCACACCGGCGAGAAGCCATT  297
            ||||||||||||||||||||||||||||||||||||||||||||||||||||||||||||
Sbjct  201  TTTCTCCCGTCAGGACAACTTGGGTCGTCATCTACGTACGCACACCGGCGAGAAGCCATT  260

Query  298  CCAATGCCGAATATGCATGCGCAACTTCAGTCGTAACGTTAACTTGGTTACCCACCTAAA  357
            ||||||||||||||||||||||||||||||||||||||||||||||||||||||||||||
Sbjct  261  CCAATGCCGAATATGCATGCGCAACTTCAGTCGTAACGTTAACTTGGTTACCCACCTAAA  320

Query  358  AACCCACCTGAGGGGATCCCAACTAGTCAAAAGTGAACTGGAGGAGAAGAAATCTGAACT  417
            ||||||||||||||||||||||||||||||||||||||||||||||||||||||||||||
Sbjct  321  AACCCACCTGAGGGGATCCCAACTAGTCAAAAGTGAACTGGAGGAGAAGAAATCTGAACT  380
```

b.)

Score	Expect	Identities	Gaps	Strand
909 bits(492)	0.0	492/492(100%)	0/492(0%)	Plus/Minus

```
Query  19   GGCTCCAAAGAAGAAGCGTAAGGTAGACTACAAAGACCATGACGGTGATTATAAAGATCA  78
            ||||||||||||||||||||||||||||||||||||||||||||||||||||||||||||
Sbjct  512  GGCTCCAAAGAAGAAGCGTAAGGTAGACTACAAAGACCATGACGGTGATTATAAAGATCA  453

Query  79   TGACATCGATTACAAGGATGACGATGACAAGGGTACCGGGGAGCGCCCCTTCCAGTGTCG  138
            ||||||||||||||||||||||||||||||||||||||||||||||||||||||||||||
Sbjct  452  TGACATCGATTACAAGGATGACGATGACAAGGGTACCGGGGAGCGCCCCTTCCAGTGTCG  393

Query  139  CATTTGCATGCGGAACTTTTCGCGTCGTCATATTTTGGACCGTCATACCCGTACTCATAC  198
            ||||||||||||||||||||||||||||||||||||||||||||||||||||||||||||
Sbjct  392  CATTTGCATGCGGAACTTTTCGCGTCGTCATATTTTGGACCGTCATACCCGTACTCATAC  333

Query  199  CGGTGAAAAACCGTTTCAGTGTCGGATCTGTATGCGAAATTTCTCCCGTCAGGACAACTT  258
            ||||||||||||||||||||||||||||||||||||||||||||||||||||||||||||
Sbjct  332  CGGTGAAAAACCGTTTCAGTGTCGGATCTGTATGCGAAATTTCTCCCGTCAGGACAACTT  273

Query  259  GGGTCGTCATCTACGTACGCACACCGGCGAGAAGCCATTCCAATGCCGAATATGCATGCG  318
            ||||||||||||||||||||||||||||||||||||||||||||||||||||||||||||
Sbjct  272  GGGTCGTCATCTACGTACGCACACCGGCGAGAAGCCATTCCAATGCCGAATATGCATGCG  213

Query  319  CAACTTCAGTCGTAACGTTAACTTGGTTACCCACCTAAAAACCCACCTGAGGGGATCCCA  378
            ||||||||||||||||||||||||||||||||||||||||||||||||||||||||||||
Sbjct  212  CAACTTCAGTCGTAACGTTAACTTGGTTACCCACCTAAAAACCCACCTGAGGGGATCCCA  153

Query  379  ACTAGTCAAAAGTGAACTGGAGGAGAAGAAATCTGAACTTCGTCATAAATTGAAATATGT  438
            ||||||||||||||||||||||||||||||||||||||||||||||||||||||||||||
Sbjct  152  ACTAGTCAAAAGTGAACTGGAGGAGAAGAAATCTGAACTTCGTCATAAATTGAAATATGT  93

Query  439  GCCTCATGAATATATTGAATTAATTGAAATTGCCAGAAATTCCACTCAGGATAGAATTCT  498
            ||||||||||||||||||||||||||||||||||||||||||||||||||||||||||||
Sbjct  92   GCCTCATGAATATATTGAATTAATTGAAATTGCCAGAAATTCCACTCAGGATAGAATTCT  33

Query  499  TGAAATGAAGGT  510
            ||||||||||||
Sbjct  32   TGAAATGAAGGT  21
```

Sanger sequence of the Left ZFN subunit expressing colony L12 using LseqCS2 (a.) and RseqCS2 (b.). Query: Expected 569 bp PCR product. Subject: Sanger sequencing output.

7.14.2 Validation of the Right ZFN ZF sequence (Colony R3)

a.)

Score	Expect	Identities	Gaps	Strand
989 bits(535)	0.0	535/535(100%)	0/535(0%)	Plus/Plus

```
Query  52   CGATGTTCCTGACTATGCGGGCTATCCCTATGACGTCCCGGACTATGCAGGATCGTATCC  111
            ||||||||||||||||||||||||||||||||||||||||||||||||||||||||||||
Sbjct  16   CGATGTTCCTGACTATGCGGGCTATCCCTATGACGTCCCGGACTATGCAGGATCGTATCC  75

Query  112  ATATGACGTTCCAGATTACGCTGCTCATGGTACCGGGGAGCGCCCCTTCCAGTGTCGCAT  171
            ||||||||||||||||||||||||||||||||||||||||||||||||||||||||||||
Sbjct  76   ATATGACGTTCCAGATTACGCTGCTCATGGTACCGGGGAGCGCCCCTTCCAGTGTCGCAT  135

Query  172  TTGCATGCGGAACTTTTCGCGTCCACATAACTTGTTGCGTCATACCCGTACTCATACCGG  231
            ||||||||||||||||||||||||||||||||||||||||||||||||||||||||||||
Sbjct  136  TTGCATGCGGAACTTTTCGCGTCCACATAACTTGTTGCGTCATACCCGTACTCATACCGG  195

Query  232  TGAAAAACCGTTTCAGTGTCGGATCTGTATGCGAAATTTCTCCCATAAATCTTCTTTGAC  291
            ||||||||||||||||||||||||||||||||||||||||||||||||||||||||||||
Sbjct  196  TGAAAAACCGTTTCAGTGTCGGATCTGTATGCGAAATTTCTCCCATAAATCTTCTTTGAC  255

Query  292  CCGTCATCTACGTACGCACACCGGCGAGAAGCCATTCCAATGCCGAATATGCATGCGCAA  351
            ||||||||||||||||||||||||||||||||||||||||||||||||||||||||||||
Sbjct  256  CCGTCATCTACGTACGCACACCGGCGAGAAGCCATTCCAATGCCGAATATGCATGCGCAA  315
```

b.)

Score	Expect	Identities	Gaps	Strand
918 bits(497)	0.0	497/497(100%)	0/497(0%)	Plus/Minus

```
Query  18   TGGCTCCAAAGAAGAAGCGTAAGGTATACCCATACGATGTTCCTGACTATGCGGGCTATC  77
            ||||||||||||||||||||||||||||||||||||||||||||||||||||||||||||
Sbjct  518  TGGCTCCAAAGAAGAAGCGTAAGGTATACCCATACGATGTTCCTGACTATGCGGGCTATC  459

Query  78   CCTATGACGTCCCGGACTATGCAGGATCGTATCCATATGACGTTCCAGATTACGCTGCTC  137
            ||||||||||||||||||||||||||||||||||||||||||||||||||||||||||||
Sbjct  458  CCTATGACGTCCCGGACTATGCAGGATCGTATCCATATGACGTTCCAGATTACGCTGCTC  399

Query  138  ATGGTACCGGGGAGCGCCCCTTCCAGTGTCGCATTTGCATGCGGAACTTTTCGCGTCCAC  197
            ||||||||||||||||||||||||||||||||||||||||||||||||||||||||||||
Sbjct  398  ATGGTACCGGGGAGCGCCCCTTCCAGTGTCGCATTTGCATGCGGAACTTTTCGCGTCCAC  339

Query  198  ATAACTTGTTGCGTCATACCCGTACTCATACCGGTGAAAAACCGTTTCAGTGTCGGATCT  257
            ||||||||||||||||||||||||||||||||||||||||||||||||||||||||||||
Sbjct  338  ATAACTTGTTGCGTCATACCCGTACTCATACCGGTGAAAAACCGTTTCAGTGTCGGATCT  279

Query  258  GTATGCGAAATTTCTCCCATAAATCTTCTTTGACCCGTCATCTACGTACGCACACCGGCG  317
            ||||||||||||||||||||||||||||||||||||||||||||||||||||||||||||
Sbjct  278  GTATGCGAAATTTCTCCCATAAATCTTCTTTGACCCGTCATCTACGTACGCACACCGGCG  219

Query  318  AGAAGCCATTCCAATGCCGAATATGCATGCGCAACTTCAGTCAGACCACCCATTTGTCTC  377
            ||||||||||||||||||||||||||||||||||||||||||||||||||||||||||||
Sbjct  218  AGAAGCCATTCCAATGCCGAATATGCATGCGCAACTTCAGTCAGACCACCCATTTGTCTC  159

Query  378  GTCACCTAAAAACCCACCTGAGGGGATCCCAACTAGTCAAAAGTGAACTGGAGGAGAAGA  437
            ||||||||||||||||||||||||||||||||||||||||||||||||||||||||||||
Sbjct  158  GTCACCTAAAAACCCACCTGAGGGGATCCCAACTAGTCAAAAGTGAACTGGAGGAGAAGA  99

Query  438  AATCTGAACTTCGTCATAAATTGAAATATGTGCCTCATGAATATATTGAATTAATTGAAA  497
            ||||||||||||||||||||||||||||||||||||||||||||||||||||||||||||
Sbjct  98   AATCTGAACTTCGTCATAAATTGAAATATGTGCCTCATGAATATATTGAATTAATTGAAA  39

Query  498  TTGCCAGAAATTCCACT  514
            |||||||||||||||||
Sbjct  38   TTGCCAGAAATTCCACT  22
```

Sanger sequence of the Right ZFN subunit expressing colony R3 using LseqCS2 (a.) and RseqCS2 (b.). Query: Expected 599 bp PCR product. Subject: Sanger sequencing output.

7.14.3 Validation of the Left ZFN FokI sequence (Colony L12)

a.)

Score	Expect	Identities	Gaps	Strand
1186 bits(642)	0.0	643/644(99%)	0/644(0%)	Plus/Plus

```
Query  62   TTTATGGATATAGAGGTAAACATTTGGGTGGATCAAGGAAACCGGACGGAGCAATTTATA  121
            ||||||||||||||||||||||||||||||||||||||||||||||||||||||||||||
Sbjct  35   TTTATGGATATAGAGGTAAACATTTGGGTGGATCAAGGAAACCGGACGGAGCAATTTATA  94

Query  122  CTGTCGGATCTCCTATTGATTACGGTGTGATCGTGGATACTAAAGCTTATAGCGGAGGTT  181
            ||||||||||||||||||||||||||||||||||||||||||||||||||||||||||||
Sbjct  95   CTGTCGGATCTCCTATTGATTACGGTGTGATCGTGGATACTAAAGCTTATAGCGGAGGTT  154

Query  182  ATAATCTGCCAATTGGCCAAGCAGATGAAATGCAAGACTATGTCGAAGAAAATCAAACAC  241
            ||||||||||||||||||||||||||||||||||||||||||||||||||||||||||||
Sbjct  155  ATAATCTGCCAATTGGCCAAGCAGATGAAATGCAAGACTATGTCGAAGAAAATCAAACAC  214

Query  242  GAAACAAACATATCAACCCTAATGAATGGTGGAAAGTCTATCCATCTTCTGTAACGGAAT  301
            ||||||||||||||||||||||||||||||||||||||||||||||||||||||||||||
Sbjct  215  GAAACAAACATATCAACCCTAATGAATGGTGGAAAGTCTATCCATCTTCTGTAACGGAAT  274

Query  302  TTAAGTTTTTATTTGTGAGTGGTCACTTTAAAGGAAACTACAAAGCTCAGCTTACACGAT  361
            ||||||||||||||||||||||||||||||||||||||||||||||||||||||||||||
Sbjct  275  TTAAGTTTTTATTTGTGAGTGGTCACTTTAAAGGAAACTACAAAGCTCAGCTTACACGAT  334

Query  362  TAAATCATATCACTAATTGTAATGGAGCTGTTCTTAGTGTAGAAGAGCTTTTAATTGGTG  421
            ||||||||||||||||||||||||||||||||||||||||||||||||||||||||||||
Sbjct  335  TAAATCATATCACTAATTGTAATGGAGCTGTTCTTAGTGTAGAAGAGCTTTTAATTGGTG  394

Query  422  GAGAAATGATTAAAGCCGGCACATTAACCTTAGAGGAAGTGAGACGGAAATTTAATAACG  481
            ||||||||||||||||||||||||||||||||||||||||||||||||||||||||||||
Sbjct  395  GAGAAATGATTAAAGCCGGCACATTAACCTTAGAGGAAGTGAGACGGAAATTTAATAACG  454

Query  482  GCGAGATAAACTTTTAATCTAGAACTATAGTGAGTCGTATTACGTAGATCCAGACATGAT  541
            ||||||||||||||||||||||||||||||||||||||||||||||||||||||||||||
Sbjct  455  GCGAGATAAACTTTTAATCTAGAACTATAGTGAGTCGTATTACGTAGATCCAGACATGAT  514

Query  542  AAGATACATTGATGAGTTTGGACAAACCACAACTAGAATGCAGTGaaaaaaaTGCTTTAT  601
            ||||||||||||||||||||||||||||||||||||||||||||||||||||||||||||
Sbjct  515  AAGATACATTGATGAGTTTGGACAAACCACAACTAGAATGCAGTGAAAAAAAATGCTTTAT  574

Query  602  TTGTGAAATTTGTGATGCTATTGCTTTATTTGTAACCATTATAAGCTGCAATAAACAAGT  661
            ||||||||||||||||||||||||||||||||||||||||||||||||||||||||||||
Sbjct  575  TTGTGAAATTTGTGATGCTATTGCTTTATTTGTAACCATTATAAGCTGCAATAAACAAGT  634

Query  662  TAACAACAACAATTGCATTCATTTTATGTTTCAGGTTCAGGGGG  705
            |||||||||||||||||||||||||||||||||||| ||||
Sbjct  635  TAACAACAACAATTGCATTCATTTTATGTTTCAGGTTCANGGGG  678

            ||||||||||||||||||||||||||||||||||||||||||||||||||||||||||||
Sbjct  488  AATTGGCCAAGCAGATGAAATGCAAGANTATGTCGAAGAAAATCAAACACGAAACAAACA  429

Query  252  TATCAACCCTAATGAATGGTGGAAAGTCTATCCATCTTCTGTAACGGAATTTAAGTTTTT  311
            ||||||||||||||||||||||||||||||||||||||||||||||||||||||||||||
Sbjct  428  TATCAACCCTAATGAATGGTGGAAAGTCTATCCATCTTCTGTAACGGAATTTAAGTTTTT  369

Query  312  ATTTGTGAGTGGTCACTTTAAAGGAAACTACAAAGCTCAGCTTACACGATTAAATCATAT  371
            ||||||||||||||||||||||||||||||||||||||||||||||||||||||||||||
Sbjct  368  ATTTGTGAGTGGTCACTTTAAAGGAAACTACAAAGCTCAGCTTACACGATTAAATCATAT  309

Query  372  CACTAATTGTAATGGAGCTGTTCTTAGTGTAGAAGAGCTTTTAATTGGTGGAGAAATGAT  431
            ||||||||||||||||||||||||||||||||||||||||||||||||||||||||||||
Sbjct  308  CACTAATTGTAATGGAGCTGTTCTTAGTGTAGAAGAGCTTTTAATTGGTGGAGAAATGAT  249

Query  432  TAAAGCCGGCACATTAACCTTAGAGGAAGTGAGACGGAAATTTAATAACGGCGAGATAAA  491
            ||||||||||||||||||||||||||||||||||||||||||||||||||||||||||||
Sbjct  248  TAAAGCCGGCACATTAACCTTAGAGGAAGTGAGACGGAAATTTAATAACGGCGAGATAAA  189

Query  492  CTTTTAATCTAGAACTATAGTGAGTCGTATTACGTAGATCCAGACATGATAAGATACATT  551
            ||||||||||||||||||||||||||||||||||||||||||||||||||||||||||||
Sbjct  188  CTTTTAATCTAGAACTATAGTGAGTCGTATTACGTAGATCCAGACATGATAAGATACATT  129

Query  552  GATGAGTTTGGACAAACCACAACTAGAATGCAGTGaaaaaaaTGCTTTATTTGTGAAATT  611
            ||||||||||||||||||||||||||||||||||||||||||||||||||||||||||||
Sbjct  128  GATGAGTTTGGACAAACCACAACTAGAATGCAGTGAAAAAAATGCTTTATTTGTGAAATT  69

Query  612  TGTGATGCTATTGCTTTATTTGTAACCATTATAAGCTGCAA  652
            |||||||||||||||||| |||||||||||||| |||
Sbjct  68   TGTGATGCTATTGCTTTATTNGTAACCATTATAAGCTNCAA  28
```

b.)

Sanger sequence of the Left ZFN subunit expressing colony L12 using LseqFok (a.) and RseqFok (b.). Query: Expected 705 bp PCR product. Subject: Sanger sequencing output.

7.14.4 Validation of the Right ZFN FokI sequence (Colony R3)

a.)

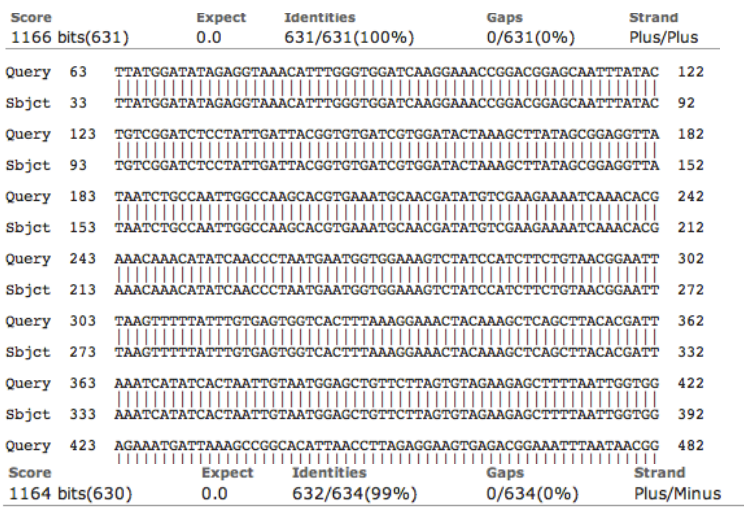

Score	Expect	Identities	Gaps	Strand
1166 bits(631)	0.0	631/631(100%)	0/631(0%)	Plus/Plus

```
Query  63   TTATGGATATAGAGGTAAACATTTGGGTGGATCAAGGAAACCGGACGGAGCAATTTATAC  122
            ||||||||||||||||||||||||||||||||||||||||||||||||||||||||||||
Sbjct  33   TTATGGATATAGAGGTAAACATTTGGGTGGATCAAGGAAACCGGACGGAGCAATTTATAC  92

Query  123  TGTCGGATCTCCTATTGATTACGGTGTGATCGTGGATACTAAAGCTTATAGCGGAGGTTA  182
            ||||||||||||||||||||||||||||||||||||||||||||||||||||||||||||
Sbjct  93   TGTCGGATCTCCTATTGATTACGGTGTGATCGTGGATACTAAAGCTTATAGCGGAGGTTA  152

Query  183  TAATCTGCCAATTGGCCAAGCACGTGAAATGCAACGATATGTCGAAGAAAATCAAACACG  242
            ||||||||||||||||||||||||||||||||||||||||||||||||||||||||||||
Sbjct  153  TAATCTGCCAATTGGCCAAGCACGTGAAATGCAACGATATGTCGAAGAAAATCAAACACG  212

Query  243  AAACAAACATATCAACCCTAATGAATGGTGGAAAGTCTATCCATCTTCTGTAACGGAATT  302
            ||||||||||||||||||||||||||||||||||||||||||||||||||||||||||||
Sbjct  213  AAACAAACATATCAACCCTAATGAATGGTGGAAAGTCTATCCATCTTCTGTAACGGAATT  272

Query  303  TAAGTTTTTATTTGTGAGTGGTCACTTTAAAGGAAACTACAAAGCTCAGCTTACACGATT  362
            ||||||||||||||||||||||||||||||||||||||||||||||||||||||||||||
Sbjct  273  TAAGTTTTTATTTGTGAGTGGTCACTTTAAAGGAAACTACAAAGCTCAGCTTACACGATT  332

Query  363  AAATCATATCACTAATTGTAATGGAGCTGTTCTTAGTGTAGAAGAGCTTTTAATTGGTGG  422
            ||||||||||||||||||||||||||||||||||||||||||||||||||||||||||||
Sbjct  333  AAATCATATCACTAATTGTAATGGAGCTGTTCTTAGTGTAGAAGAGCTTTTAATTGGTGG  392

Query  423  AGAAATGATTAAAGCCGGCACATTAACCTTAGAGGAAGTGAGACGGAAATTTAATAACGG  482
            ||||||||||||||||||||||||||||||||||||||||||||||||||||||||||||
```

Score	Expect	Identities	Gaps	Strand
1164 bits(630)	0.0	632/634(99%)	0/634(0%)	Plus/Minus

b.)

```
Query  15   TCAGGATAGAATTCTTGAAATGAAGGTAATGGAATTTTTTATGAAAGTTTATGGATATAG  74
            ||||||||||||||||||||||||||||||||||||||||||||||||||||||||||||
Sbjct  665  TCAGGATAGAATTCTTGAAATGAAGGTAATGGAATTTTTTATGAAAGTTTATGGATATAG  606

Query  75   AGGTAAACATTTGGGTGGATCAAGGAAACCGGACGGAGCAATTTATACTGTCGGATCTCC  134
            ||||||||||||||||||||||||||||||||||||||||||||||||||||||||||||
Sbjct  605  AGGTAAACATTTGGGTGGATCAAGGAAACCGGACGGAGCAATTTATACTGTCGGATCTCC  546

Query  135  TATTGATTACGGTGTGATCGTGGATACTAAAGCTTATAGCGGAGGTTATAATCTGCCAAT  194
            ||||||||||||||||||||||||||||||||||||||||||||||||||||||||||||
Sbjct  545  TATTGATTACGGTGTGATCGTGGATACTAAAGCTTATAGCGGAGGTTATAATCTGCCAAT  486

Query  195  TGGCCAAGCACGTGAAATGCAACGATATGTCGAAGAAAATCAAACACGAAACAAACATAT  254
            ||||||||||||||||||||||||||||||||||||||||||||||||||||||||||||
Sbjct  485  TGGCCAAGCACGTGAAATGCAACGATATGTCGAAGAAAATCAAACACGAAACAAACATAT  426

Query  255  CAACCCTAATGAATGGTGGAAAGTCTATCCATCTTCTGTAACGGAATTTAAGTTTTTATT  314
            ||||||||||||||||||||||||||||||||||||||||||||||||||||||||||||
Sbjct  425  CAACCCTAATGAATGGTGGAAAGTCTATCCATCTTCTGTAACGGAATTTAAGTTTTTATT  366

Query  315  TGTGAGTGGTCACTTTAAAGGAAACTACAAAGCTCAGCTTACACGATTAAATCATATCAC  374
            ||||||||||||||||||||||||||||||||||||||||||||||||||||||||||||
Sbjct  365  TGTGAGTGGTCACTTTAAAGGAAACTACAAAGCTCAGCTTACACGATTAAATCATATCAC  306

Query  375  TAATTGTAATGGAGCTGTTCTTAGTGTAGAAGAGCTTTTAATTGGTGGAGAAATGATTAA  434
            ||||||||||||||||||||||||||||||||||||||||||||||||||||||||||||
Sbjct  305  TAATTGTAATGGAGCTGTTCTTAGTGTAGAAGAGCTTTTAATTGGTGGAGAAATGATTAA  246

Query  435  AGCCGGCACATTAACCTTAGAGGAAGTGAGACGGAAATTTAATAACGGCGAGATAAACTT  494
            ||||||||||||||||||||||||||||||||||||||||||||||||||||||||||||
Sbjct  245  AGCCGGCACATTAACCTTAGAGGAAGTGAGACGGAAATTTAATAACGGCGAGATAAACTT  186

Query  495  TTAATCTAGAACTATAGTGAGTCGTATTACGTAGATCCAGACATGATAAGATACATTGAT  554
            ||||||||||||||||||||||||||||||||||||||||||||||||||||||||||||
Sbjct  185  TTAATCTAGAACTATAGTGAGTCGTATTACGTAGATCCAGACATGATAAGATACATTGAT  126

Query  555  GAGTTTGGACAAACCACAACTAGAATGCAGTGaaaaaaaTGCTTTATTTGTGAAATTTGT  614
            ||||||||||||||||||||||||||||||||||||||||||||||||||||||||||||
Sbjct  125  GAGTTTGGACAAACCACAACTAGAATGCAGTGAAAAAAATGCTTTATTTGTGAAATTTGT  66

Query  615  GATGCTATTGCTTTATTTGTAACCATTATAAGCT  648
            |||||||||||||||||||||||||  |||||||
Sbjct  65   GATGCTATTGCTTTATTTGTAACCNNTATAAGCT  32
```

Sanger sequence of the Right ZFN subunit expressing colony R3 using LseqFok (a.) and RseqFok (b.). Query: Expected 705 bp PCR product. Subject: Sanger sequencing output.

7.15 Appendix 15: Roche Titanium 454 sequence comparison analysis of the *hax1* amplicon generated from gDNA of *hax1* ZFN injected embryos

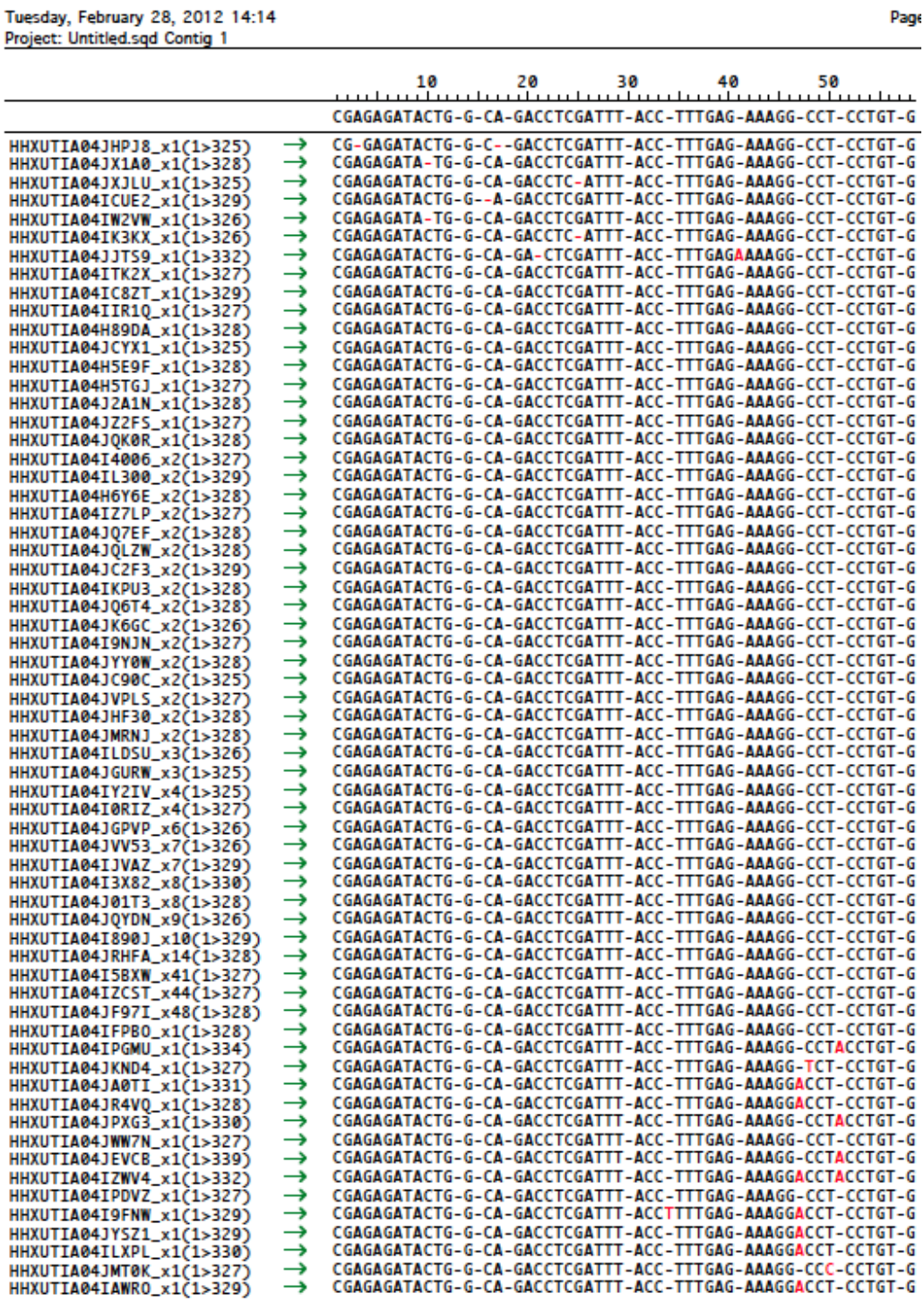

Amplicon identity- x (number of occurrences) (sequence size). Red letters denote changes in the sequence. ZFN spacer region:218-222.

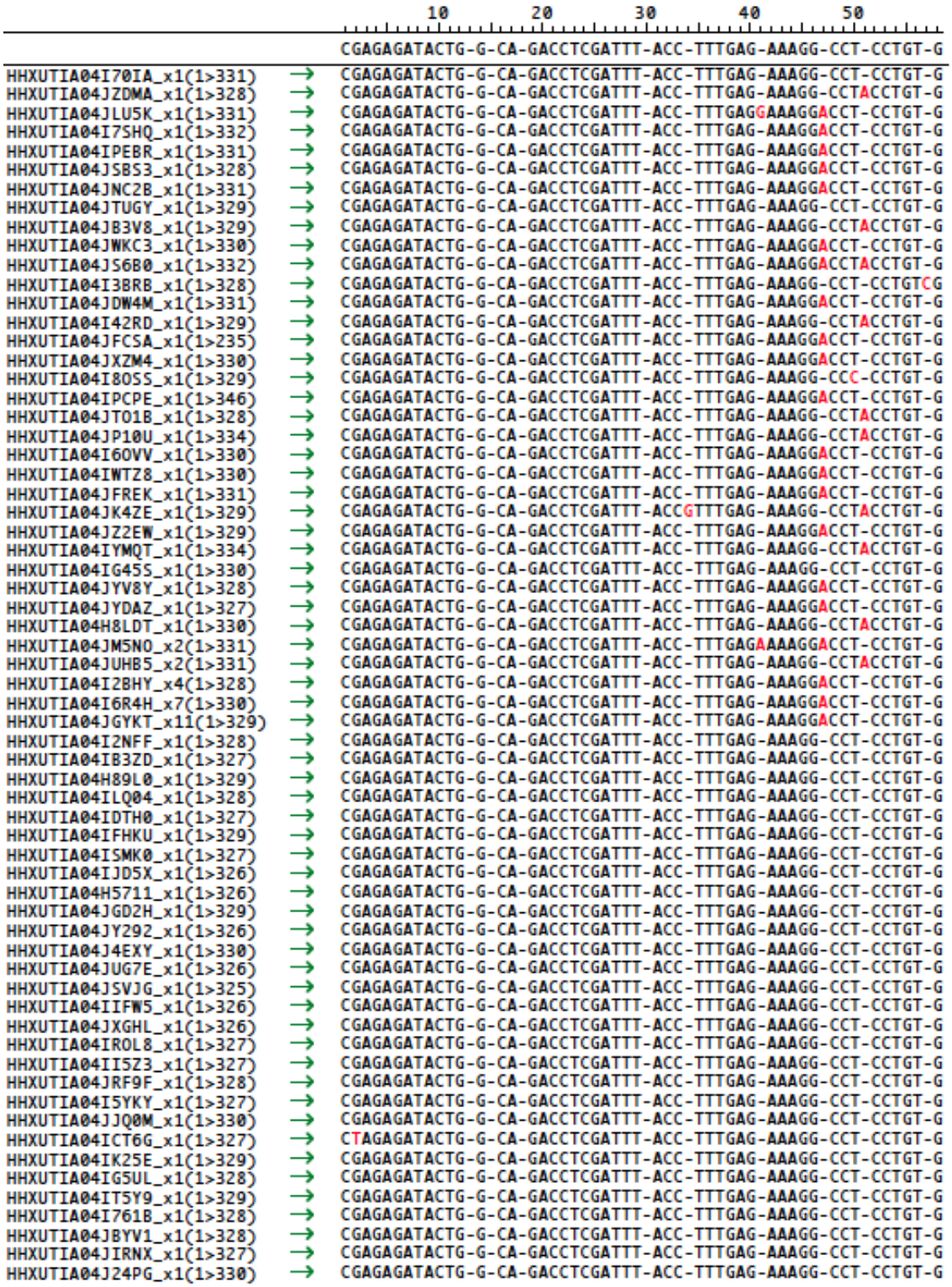

Amplicon identity- x (number of occurrences) (sequence size). Red letters denote changes in the sequence. ZFN spacer region:218-222.

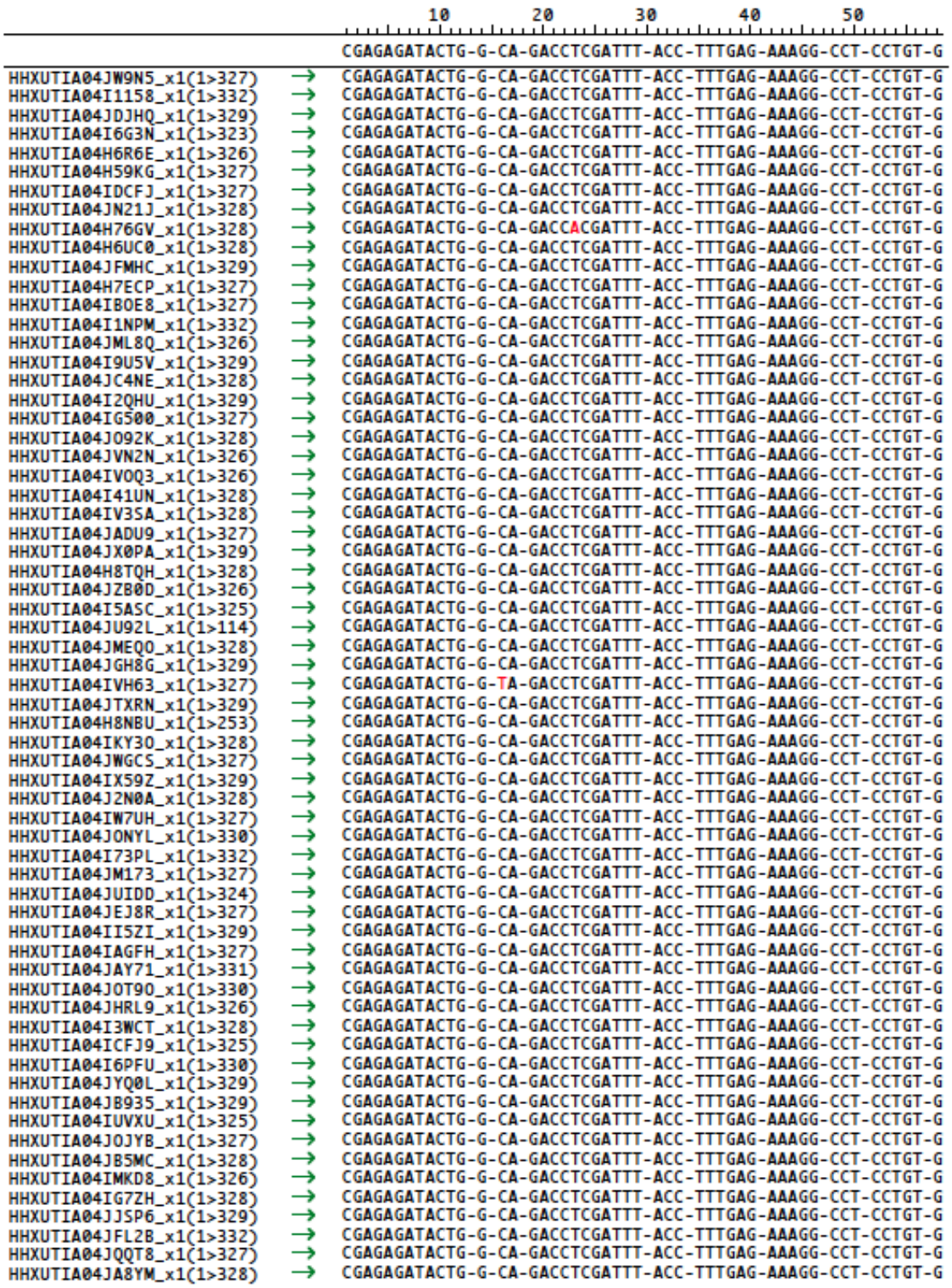

Amplicon identity- x (number of occurrences) (sequence size). Red letters denote changes in the sequence. ZFN spacer region:218-222.

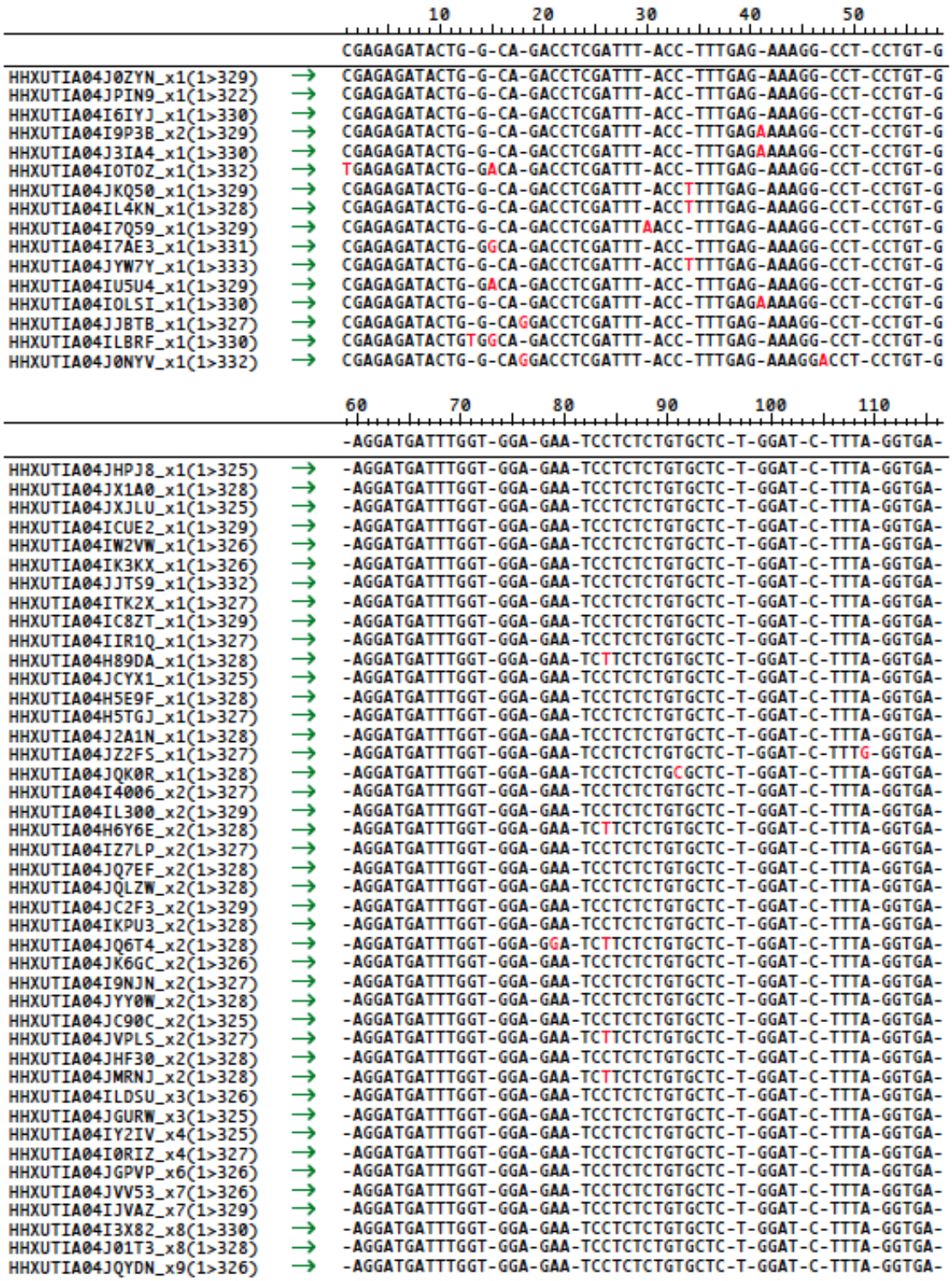

Amplicon identity- x (number of occurrences) (sequence size). Red letters denote changes in the sequence. ZFN spacer region:218-222.

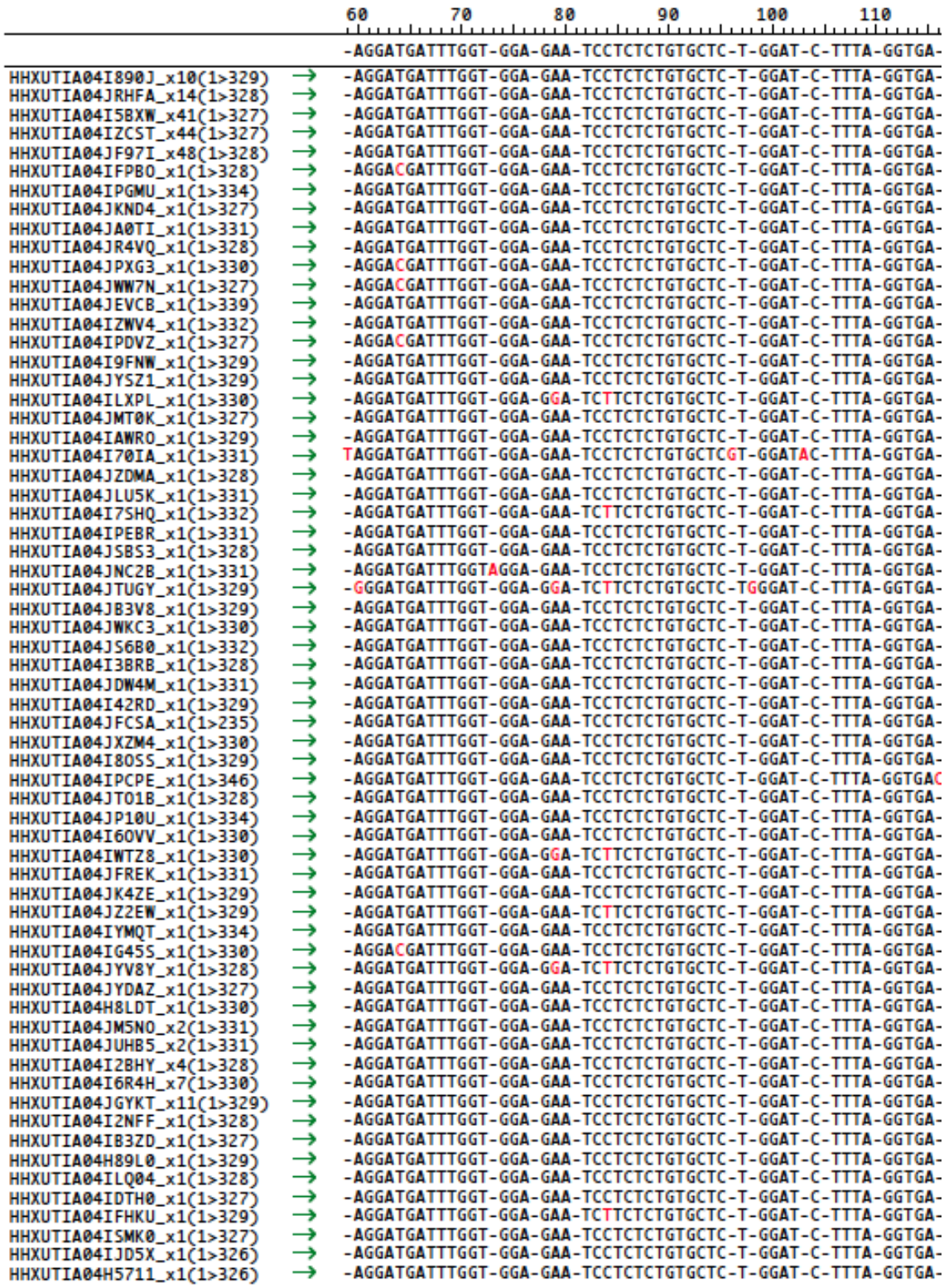

Amplicon identity- x (number of occurrences) (sequence size). Red letters denote changes in the sequence. ZFN spacer region:218-222.

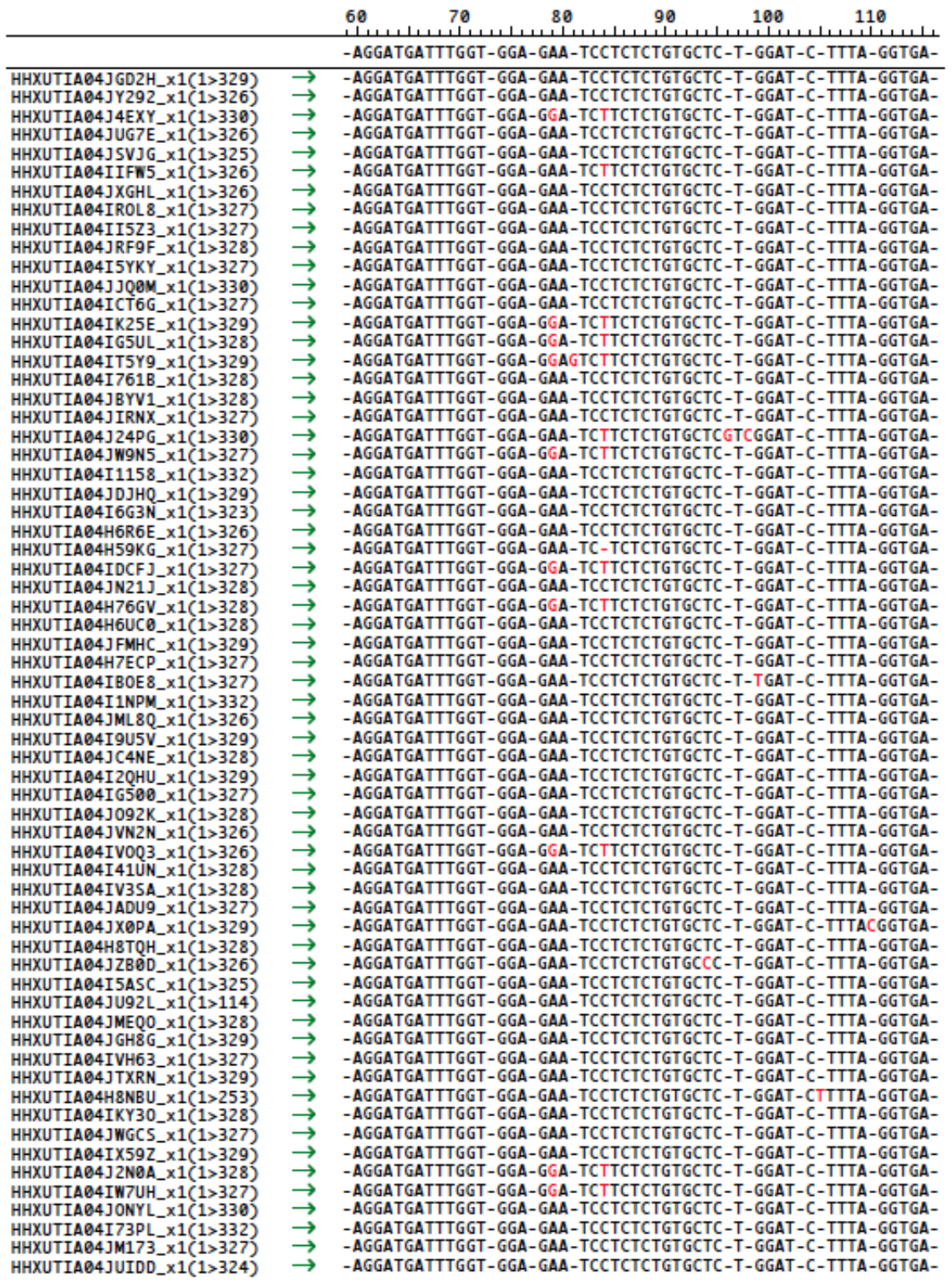

Amplicon identity- x (number of occurrences) (sequence size). Red letters denote changes in the sequence. ZFN spacer region:218-222.

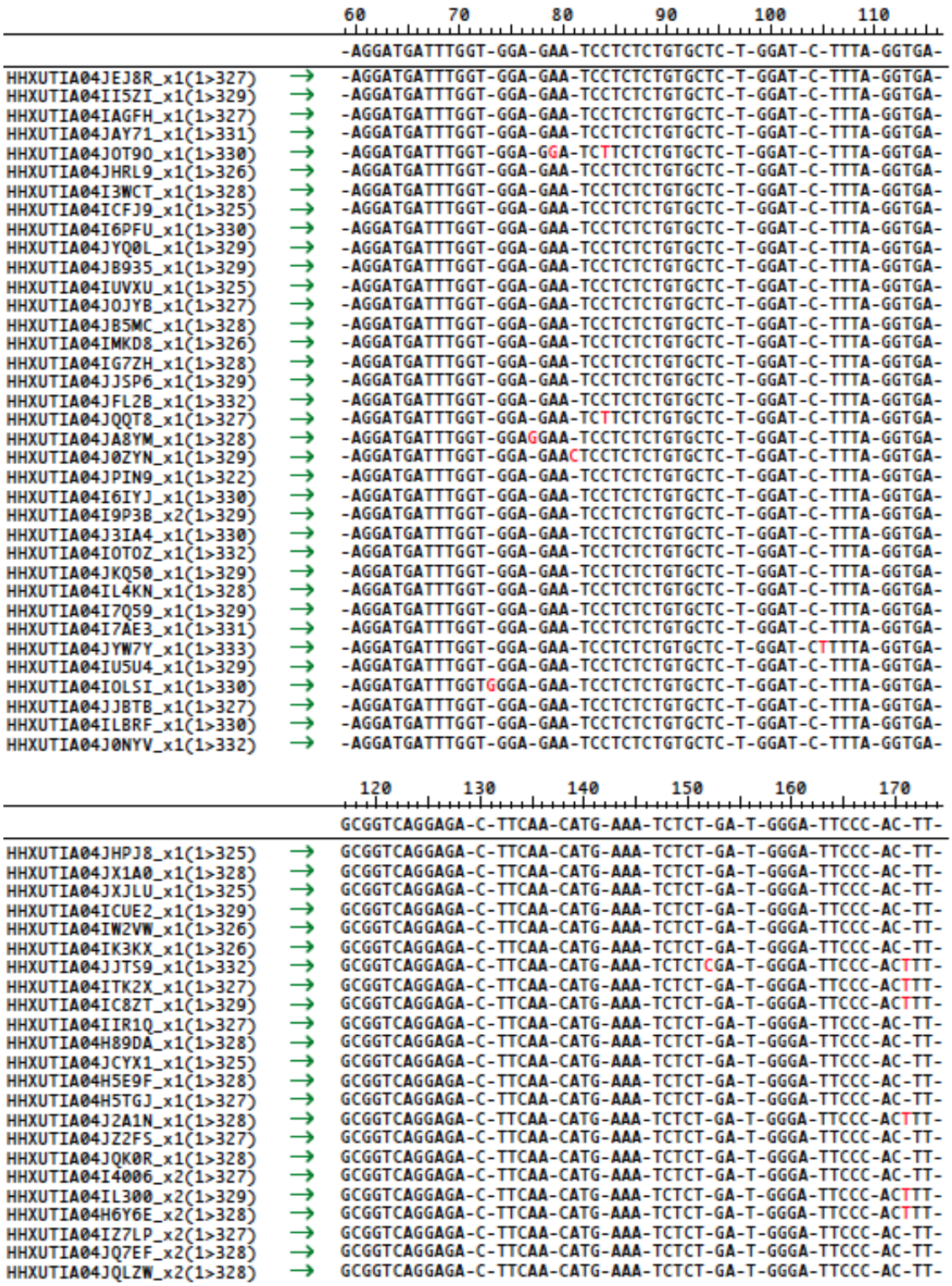

Amplicon identity- x (number of occurrences) (sequence size). Red letters denote changes in the sequence. ZFN spacer region:218-222.

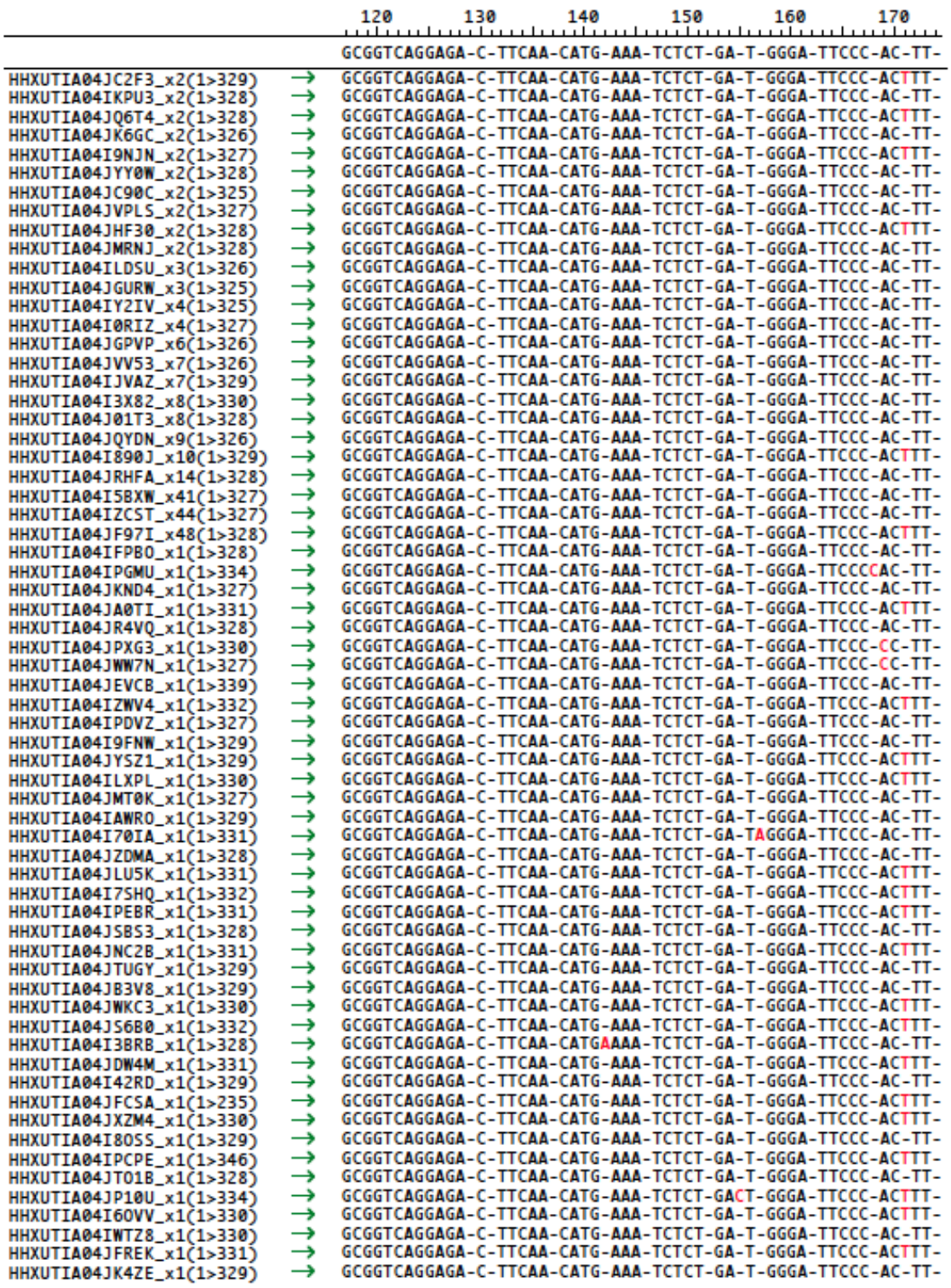

Amplicon identity- x (number of occurrences) (sequence size). Red letters denote changes in the sequence. ZFN spacer region:218-222.

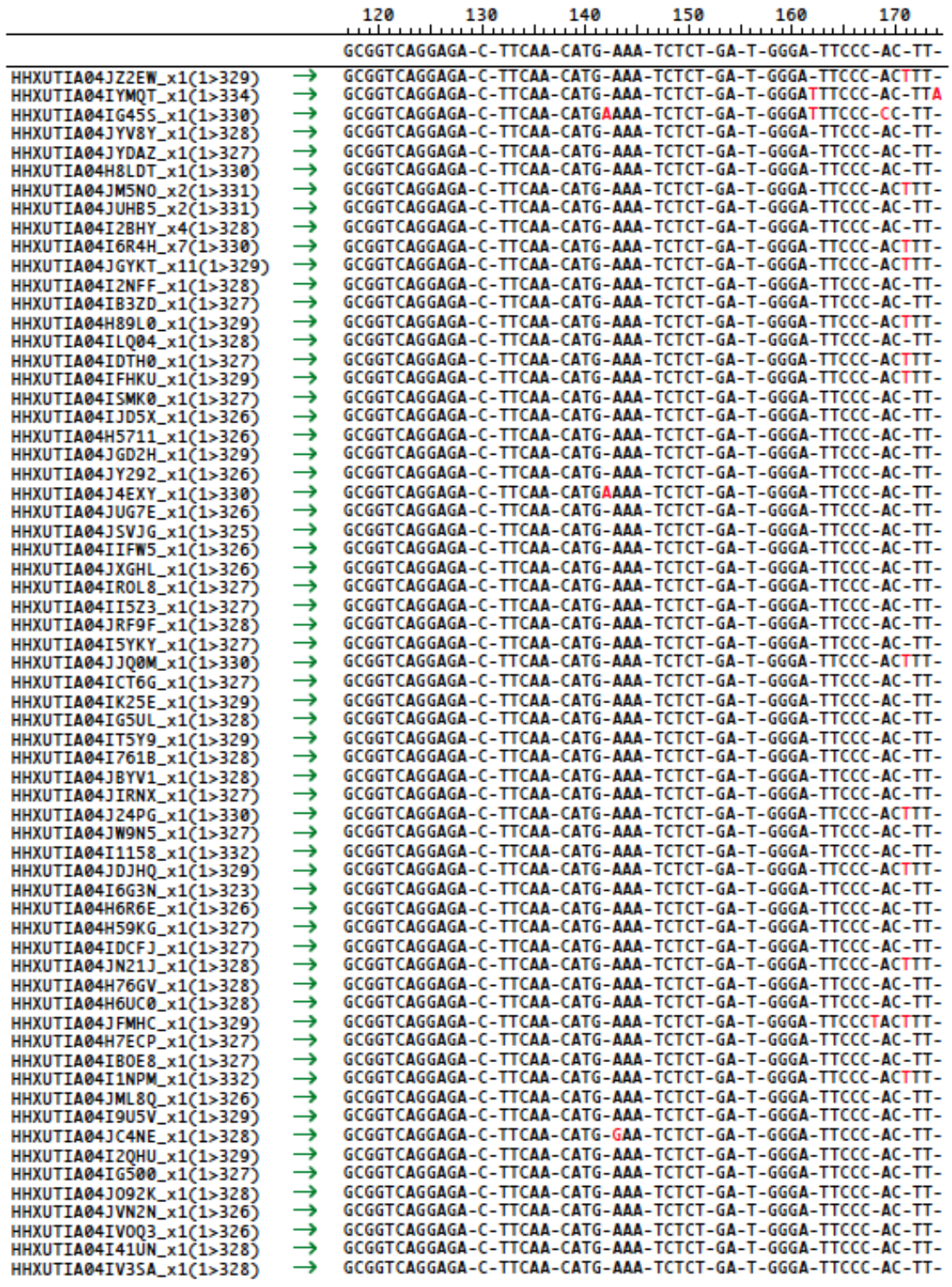

Amplicon identity- x (number of occurrences) (sequence size). Red letters denote changes in the sequence. ZFN spacer region:218-222.

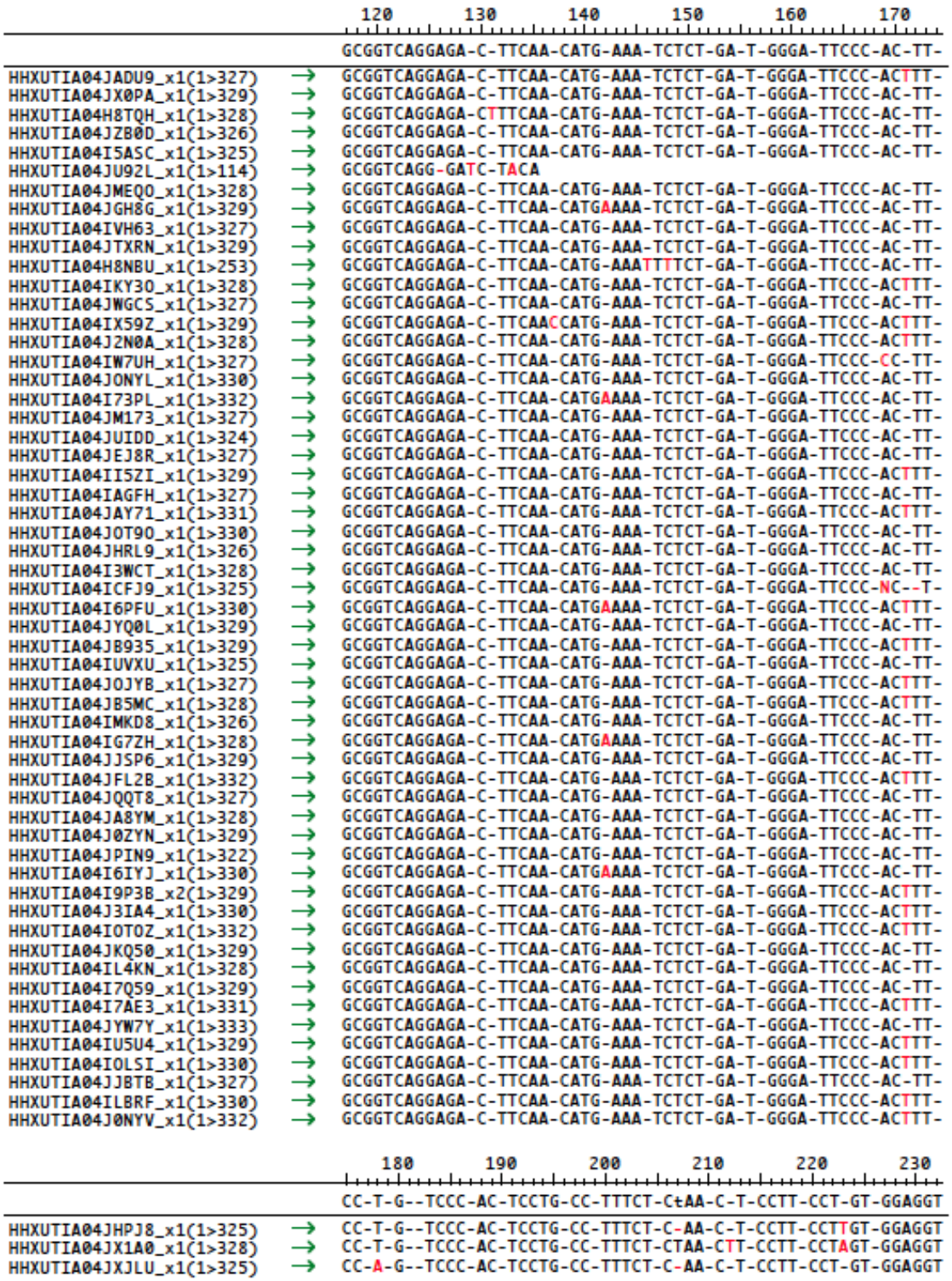

Amplicon identity- x (number of occurrences) (sequence size). Red letters denote changes in the sequence. ZFN spacer region:218-222.

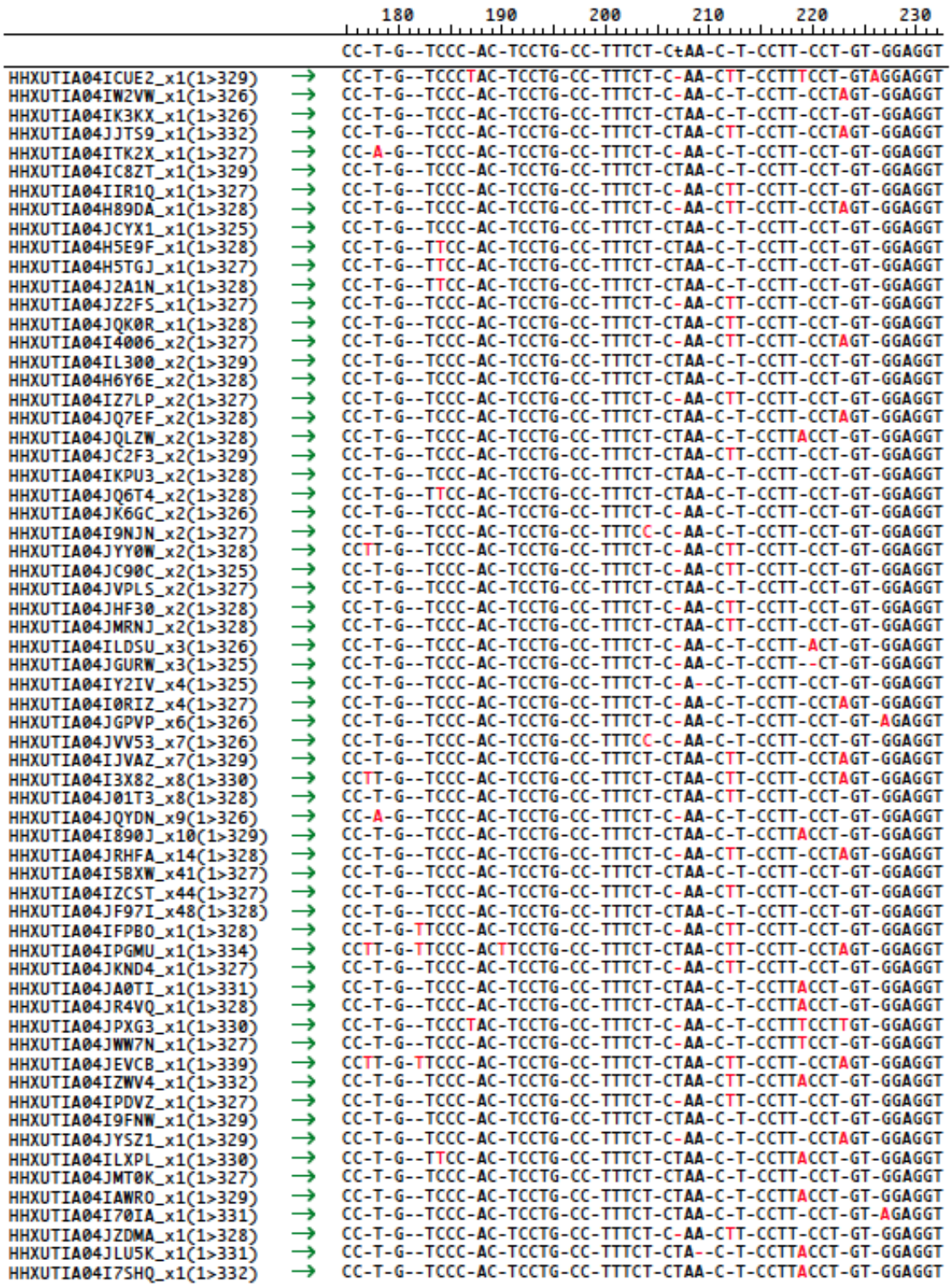

Amplicon identity- x (number of occurrences) (sequence size). Red letters denote changes in the sequence. ZFN spacer region:218-222.

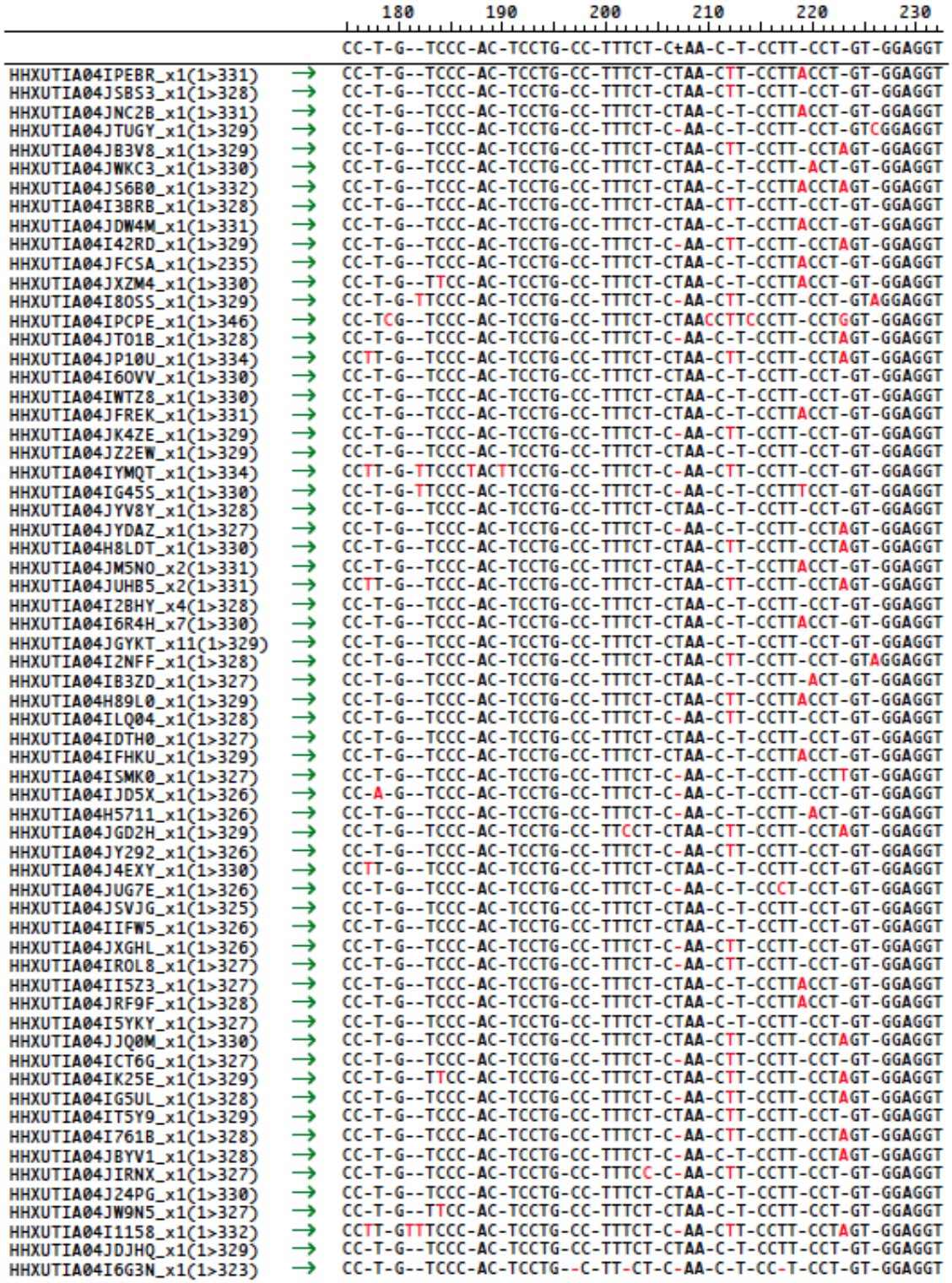

Amplicon identity- x (number of occurrences) (sequence size). Red letters denote changes in the sequence. ZFN spacer region:218-222.

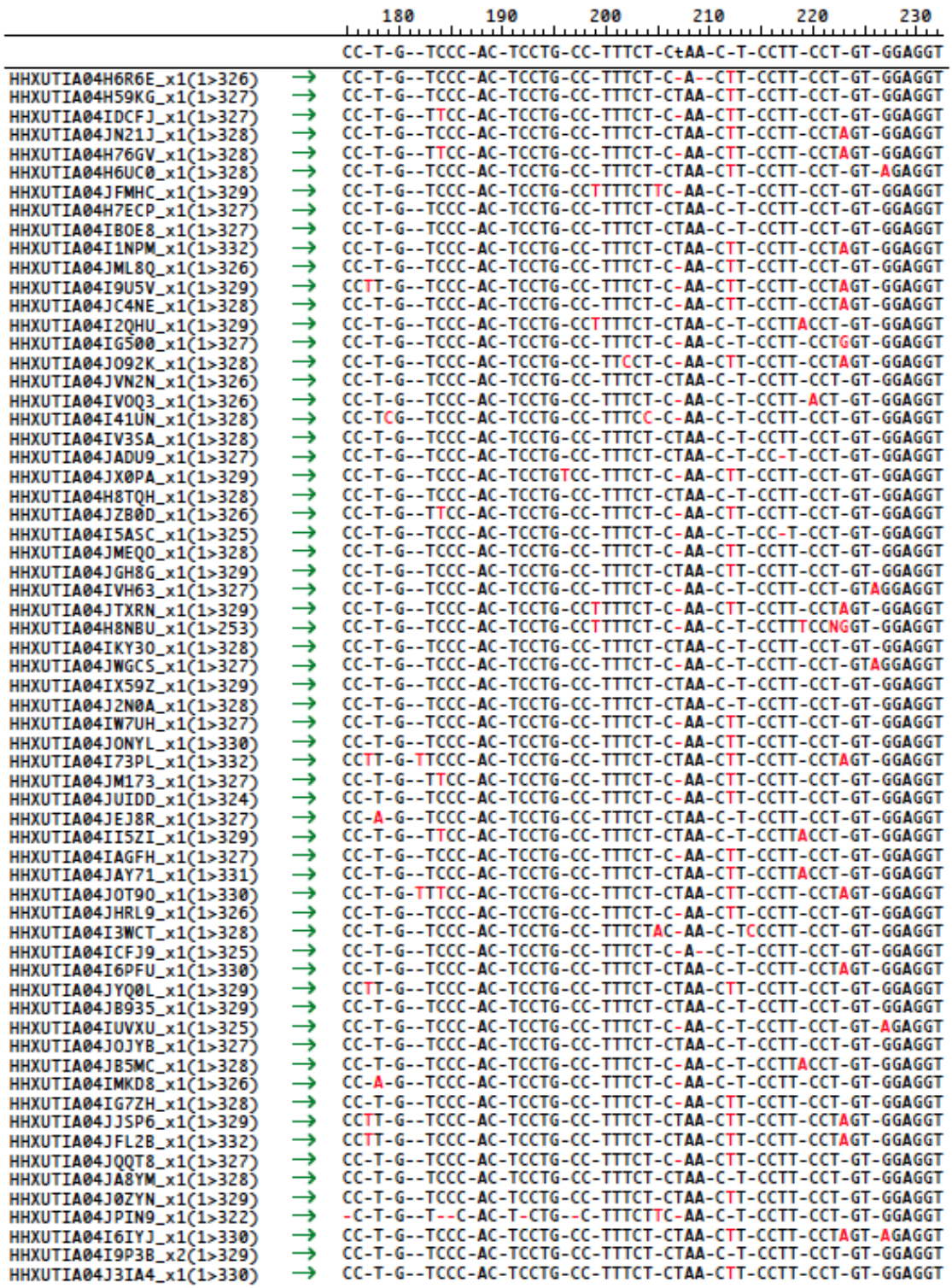

Amplicon identity- x (number of occurrences) (sequence size). Red letters denote changes in the sequence. ZFN spacer region:218-222.

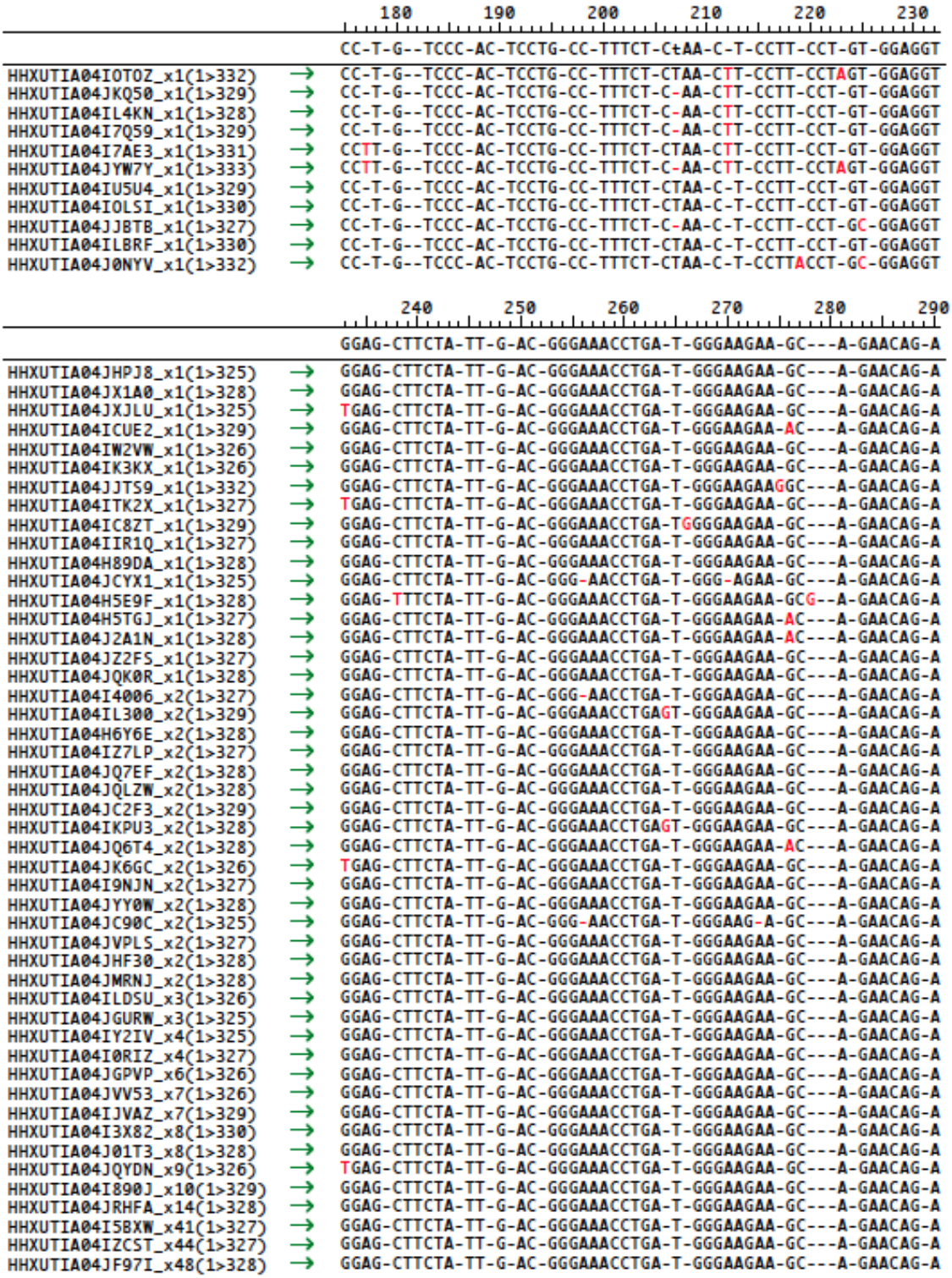

Amplicon identity- x (number of occurrences) (sequence size). Red letters denote changes in the sequence. ZFN spacer region:218-222.

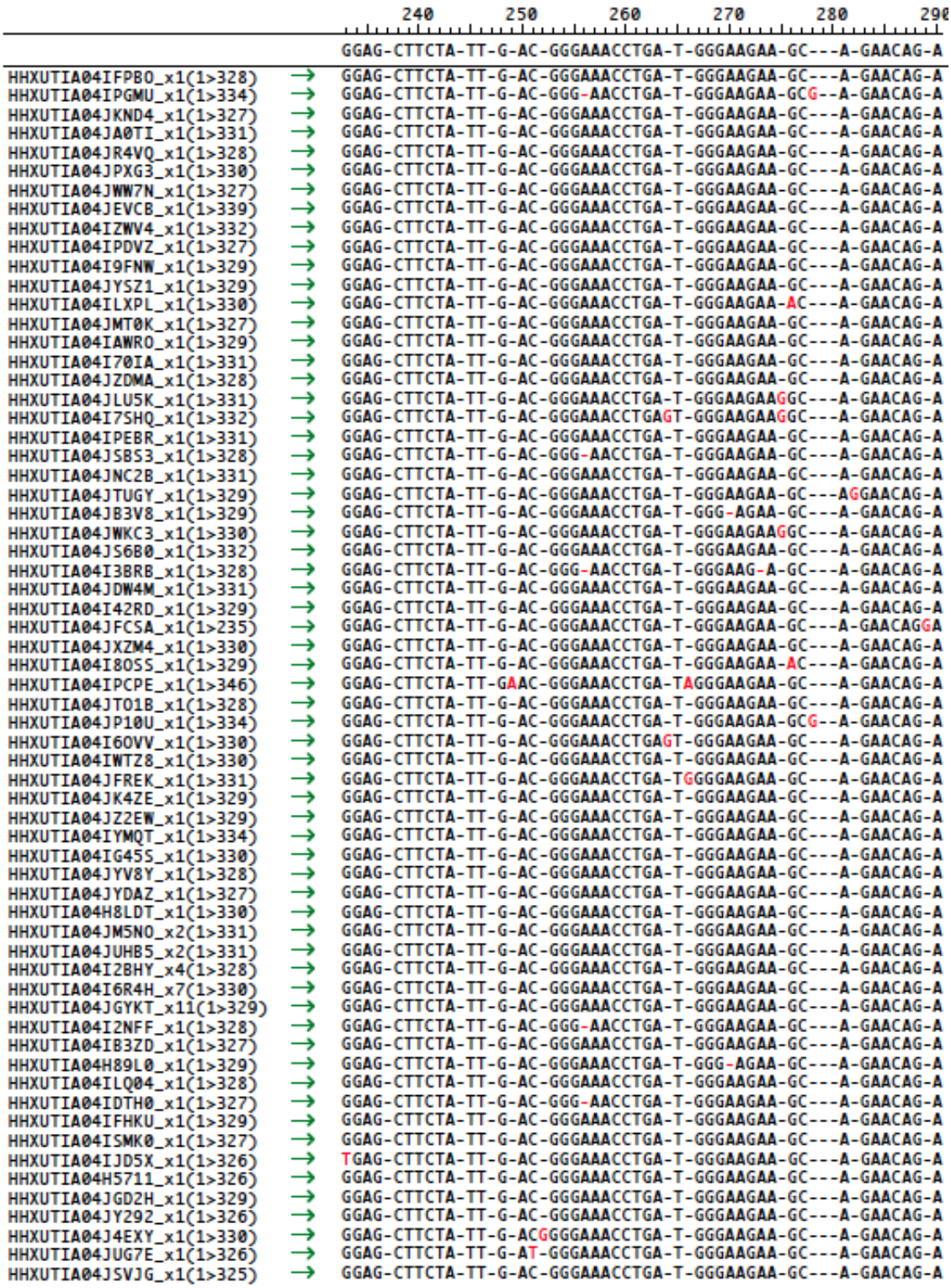

Amplicon identity- x (number of occurrences) (sequence size). Red letters denote changes in the sequence. ZFN spacer region:218-222.

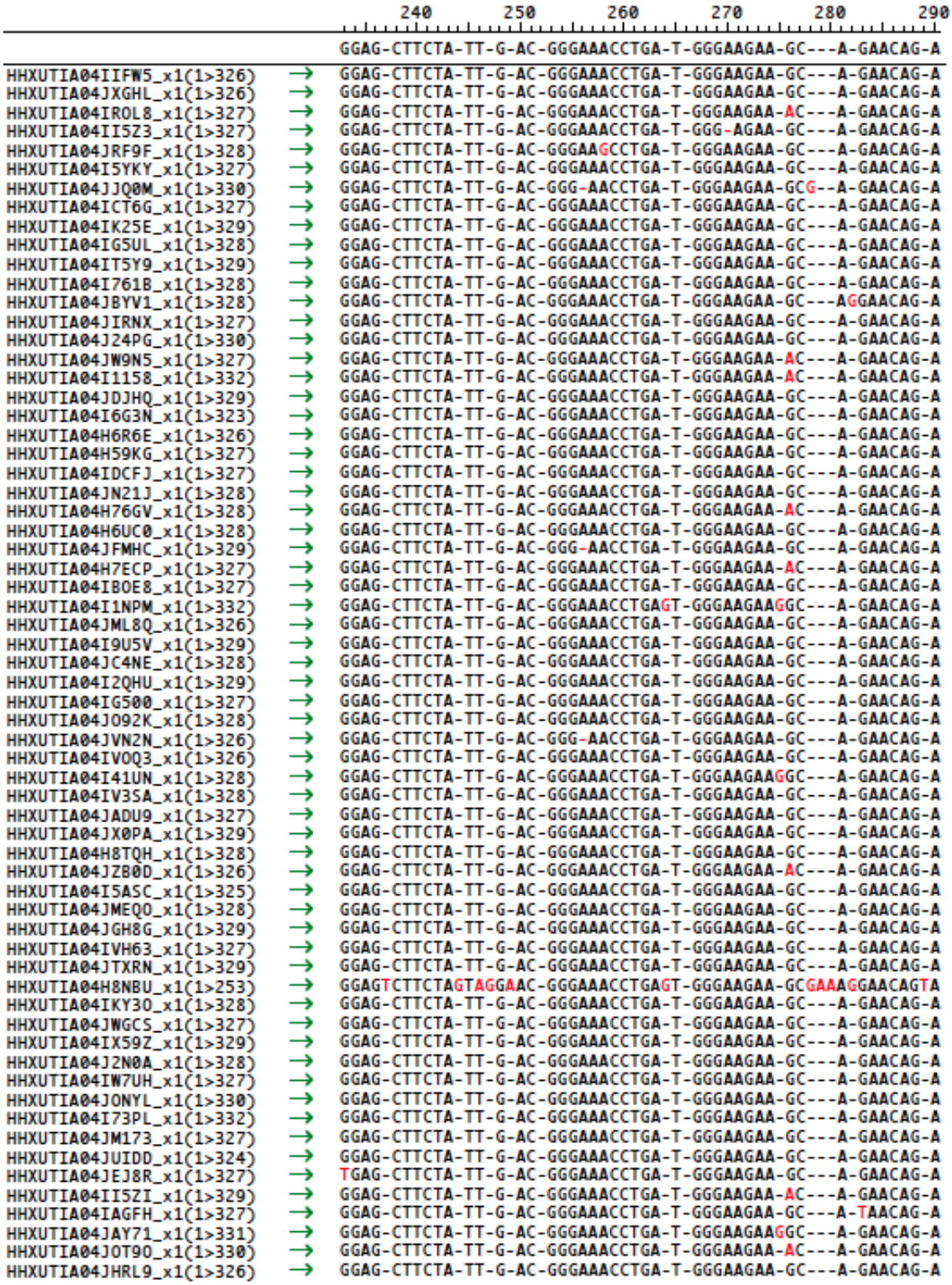

Amplicon identity- x (number of occurrences) (sequence size). Red letters denote changes in the sequence. ZFN spacer region:218-222.

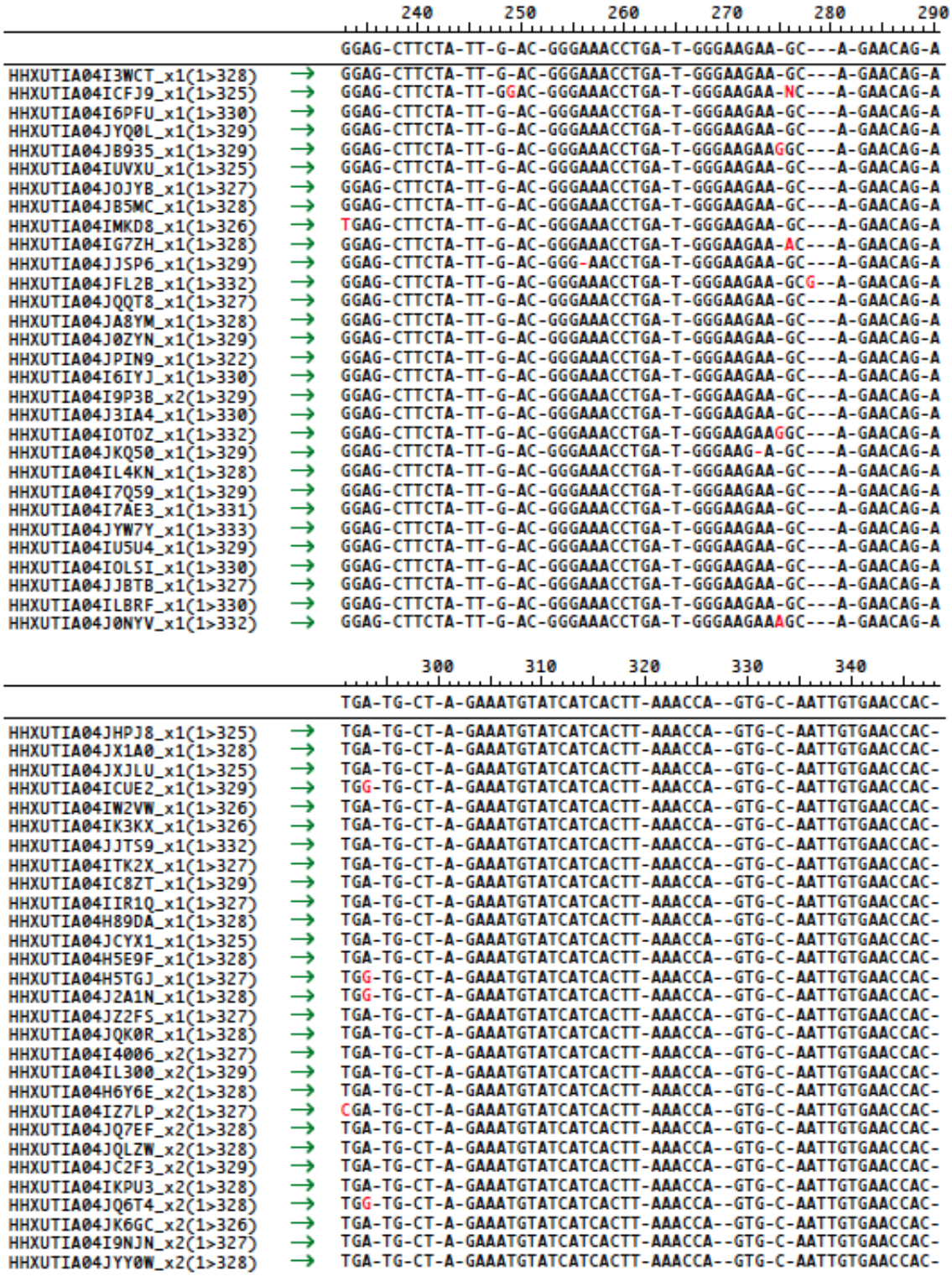

Amplicon identity- x (number of occurrences) (sequence size). Red letters denote changes in the sequence. ZFN spacer region:218-222.

7.16 *hax1* gene sequence input into the TALEN Targeter 2.0 tool for identification of TALEN sites and *hax1* exon 2 specific TALEN RVD sequences

aatcatggtttttttaatacag**GGACCCCTTCTTTGATGGAATGATTCATGAAGATG**
ATGATGATGAAGACGAGGATGACTTTAACAGACCCCATCGGG

50 bp of DNA sequence 5' and 3' of the BspHI site (highlighted yellow) were inserted into the online tool. Lower and upper case sequences denote intronic region and exonic regions, respectively.

LEFT TALEN RVD Sequence: NI, HD, NI, NN, NN, NN, NI, HD, HD, HD, HD, NG, NG, HD, NG, **DNA sequence recognised**: ACAGGGACCCCTTCT.

RIGHT TALEN RVD Sequence: HD, NG, NG, HD, NI, NG, HD, NI, NG, HD, NI, NG, HD, NI, NG, HD, NG, **DNA sequence recognised**: AGATGATGATGATGA AG).

Spacer region sequence: TTGATGGAATGATTCATGA.

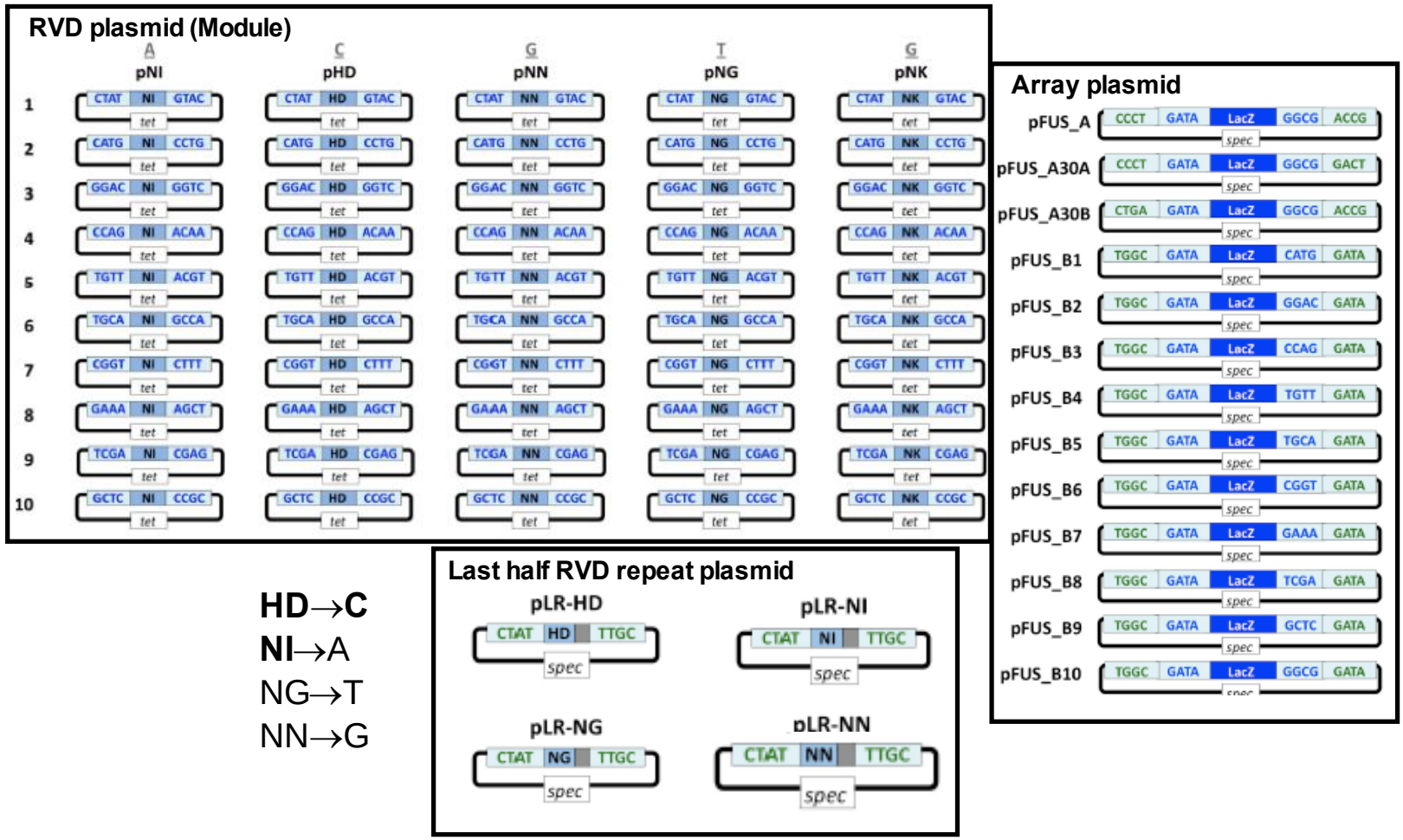

7.17 Appendix 17: Golden Gate TALEN assembly plasmids

Adapted from (Cermak et al. 2011). Note not all of the available plasmids are shown.

7.18 Appendix 18: A map of the Golden Gate TALEN assembly generic backbone

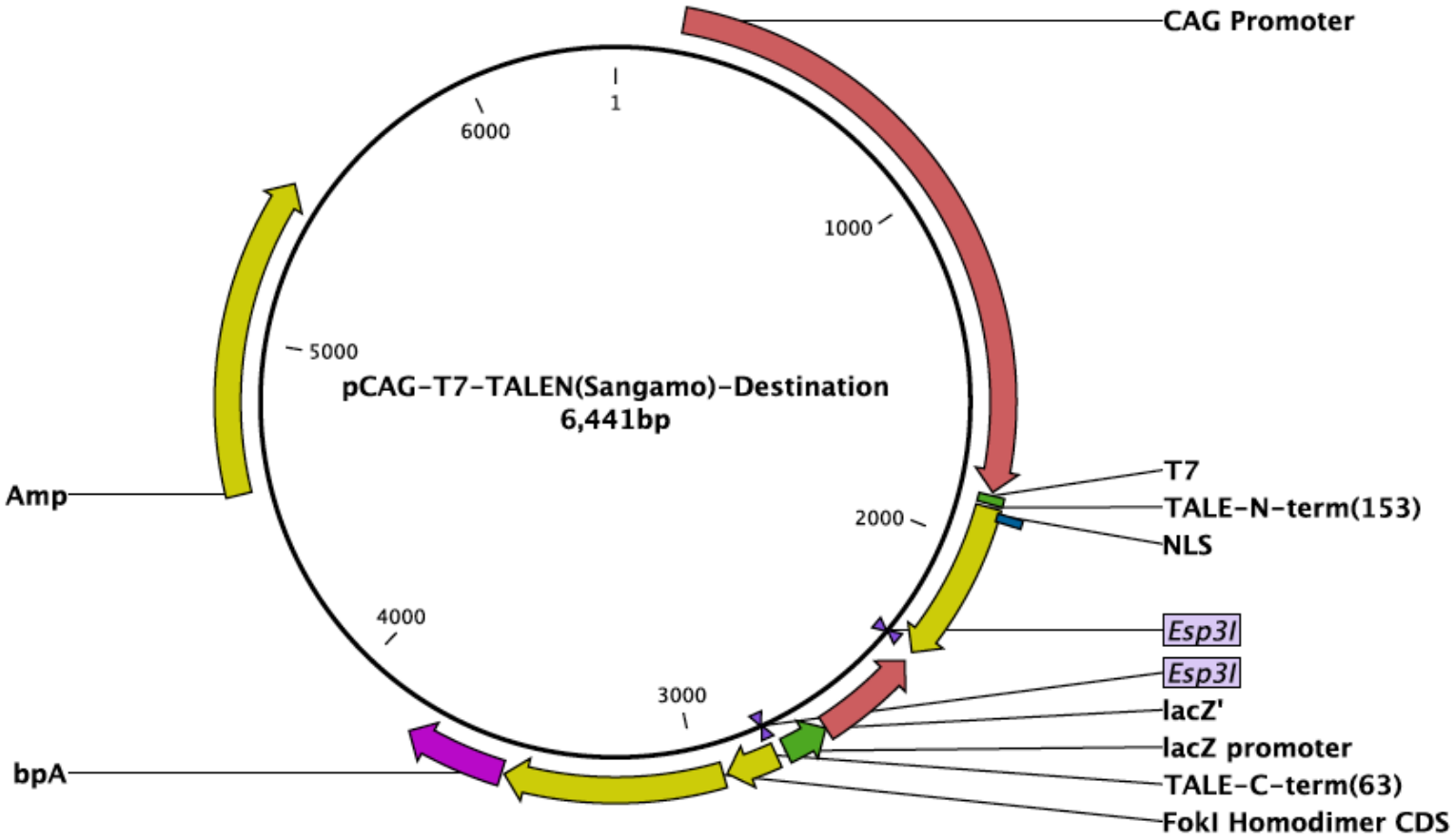

7.19 Appendix 19: Primers required for amplification and sequencing of the TALEN constructs and *hax1* specific TALEN target site

Target	Sequence	Expected size (bp)	Annealing temp. (°C)
TAL_R2	**Forward** 5'- ggcgacgaggtggtcgttgg -3'	-	-
SeqTALEN_5-1	**Forward** 5'- catcgcgcaatgcactgac -3'	-	-
Hax1TalRE	**Forward** 5'-GGTTAAAAATCCAACGGCACT -3' **Reverse** 5'-TGCTTCACCCATGTCACCTTA-3'	534 bp	55
Hax1TalRE (1)	**Forward** 5'-AAGCACTTTTGGTGTAATGGTAATC-3' **Reverse** 5'-CCAGCAAACATCTCCTCCATGTCTC-3'	367 bp	55

7.20 Annotation of left and right *hax1* specific left and right TALEN encoding vector sequences

7.20.1 Left TALEN subunit ((L*hax1*pCAGT7-TALEN(Sangamo))

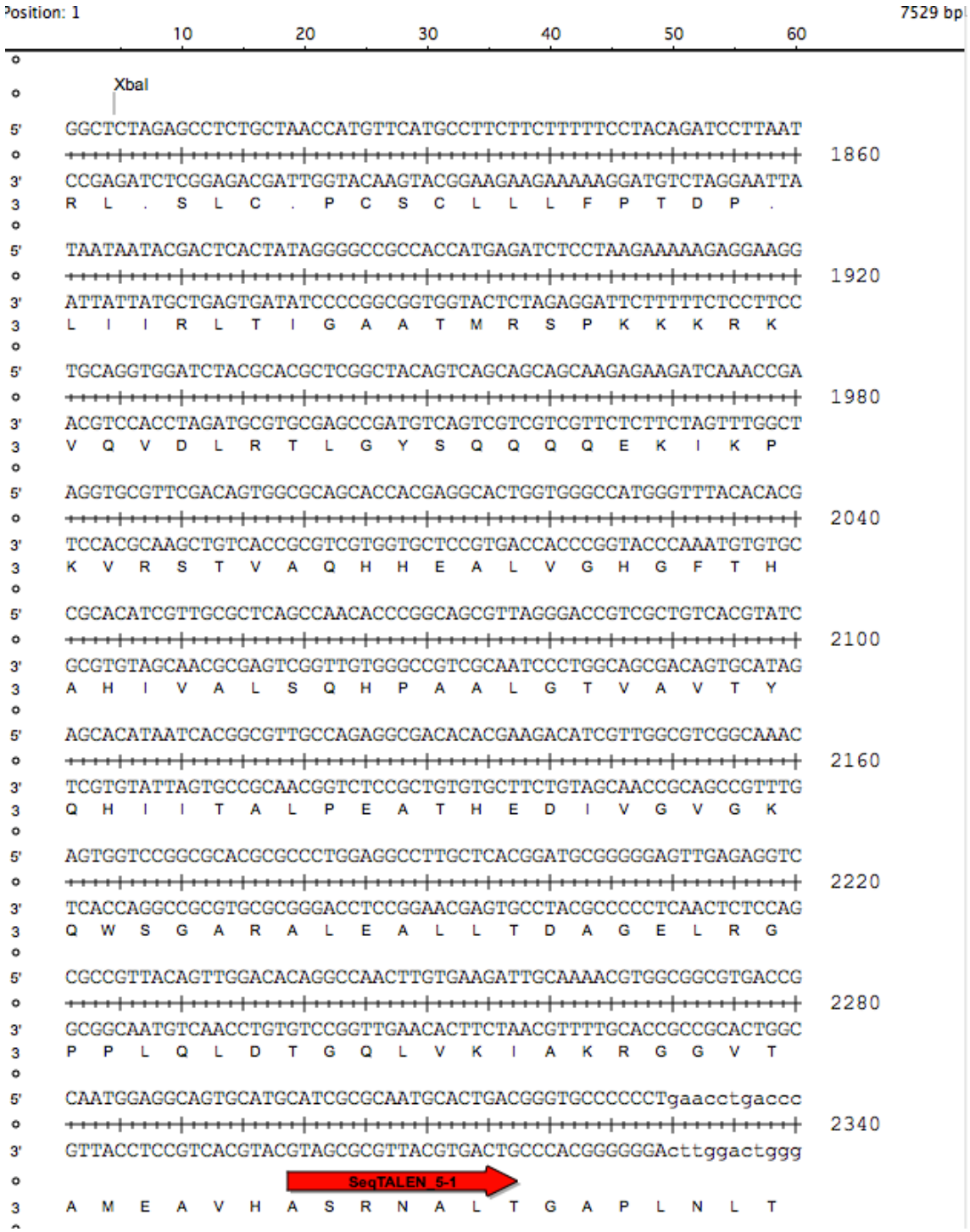

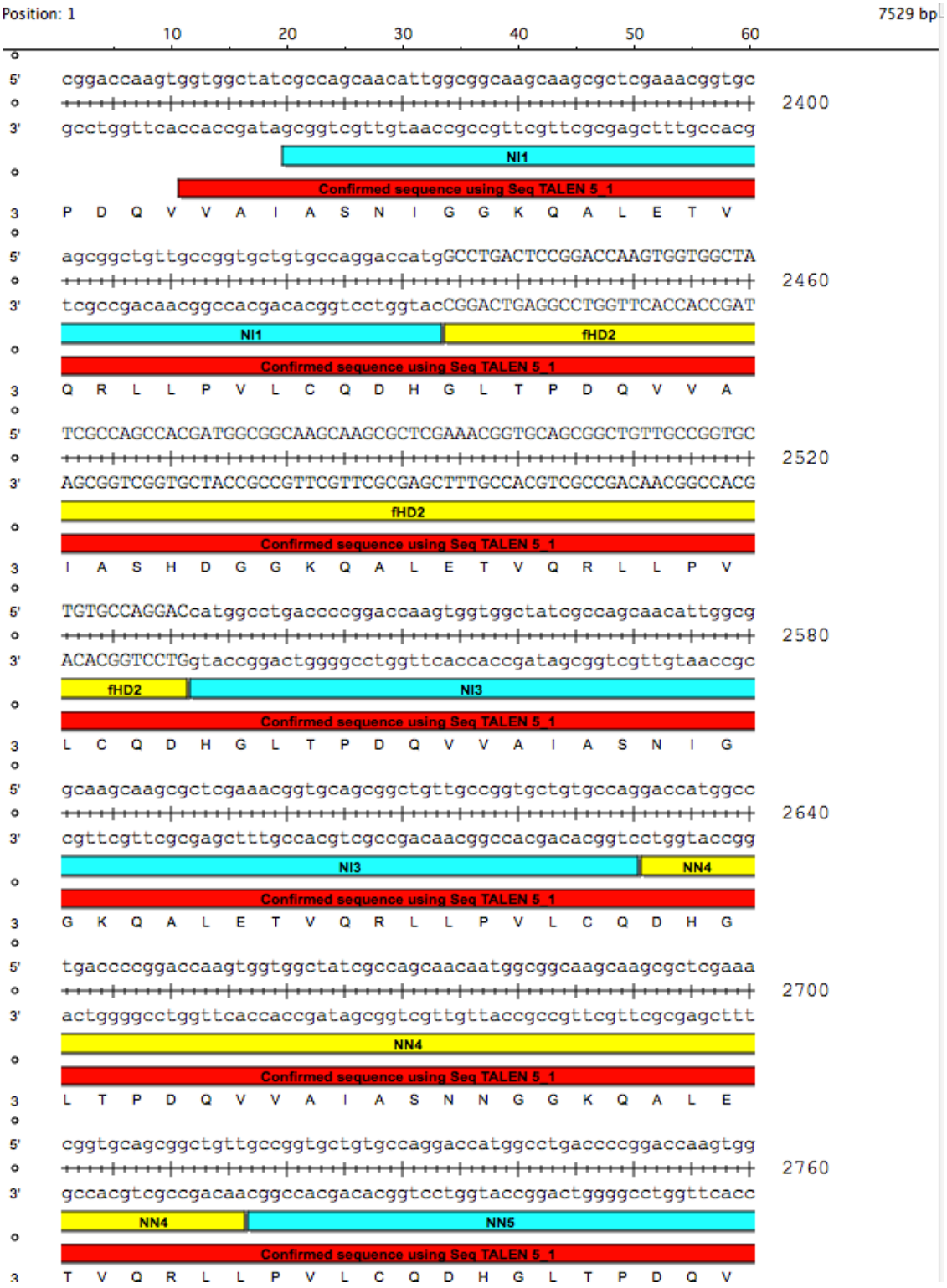
Position: 1
7529 bp
10
20
30
40
50
60
5'
cggaccaagtggtggctatcgccagcaacattggcggcaagcaagcgctcgaaacggtgc
2400
3'
gcctggttcaccaccgatagcggtcgttgtaaccgccgttcgttcgcgagctttgccacg
NI1
Confirmed sequence using Seq TALEN 5_1
P D Q V V A I A S N I G G K Q A L E T V
5'
agcggctgttgccggtgctgtgccaggaccatgGCCTGACTCCGGACCAAGTGGTGGCTA
2460
3'
tcgccgacaacggccacgacacggtcctggtacCGGACTGAGGCCTGGTTCACCACCGAT
NI1
fHD2
Confirmed sequence using Seq TALEN 5_1
Q R L L P V L C Q D H G L T P D Q V V A
5'
TCGCCAGCCACGATGGCGGCAAGCAAGCGCTCGAAACGGTGCAGCGGCTGTTGCCGGTGC
2520
3'
AGCGGTCGGTGCTACCGCCGTTCGTTCGCGAGCTTTGCCACGTCGCCGACAACGGCCACG
fHD2
Confirmed sequence using Seq TALEN 5_1
I A S H D G G K Q A L E T V Q R L L P V
5'
TGTGCCAGGACcatggcctgaccccggaccaagtggtggctatcgccagcaacattggcg
2580
3'
ACACGGTCCTGgtaccggactggggcctggttcaccaccgatagcggtcgttgtaaccgc
fHD2
NI3
Confirmed sequence using Seq TALEN 5_1
L C Q D H G L T P D Q V V A I A S N I G
5'
gcaagcaagcgctcgaaacggtgcagcggctgttgccggtgctgtgccaggaccatggcc
2640
3'
cgttcgttcgcgagctttgccacgtcgccgacaacggccacgacacggtcctggtaccgg
NI3
NN4
Confirmed sequence using Seq TALEN 5_1
G K Q A L E T V Q R L L P V L C Q D H G
5'
tgaccccggaccaagtggtggctatcgccagcaacaatggcggcaagcaagcgctcgaaa
2700
3'
actggggcctggttcaccaccgatagcggtcgttgttaccgccgttcgttcgcgagcttt
NN4
Confirmed sequence using Seq TALEN 5_1
L T P D Q V V A I A S N N G G K Q A L E
5'
cggtgcagcggctgttgccggtgctgtgccaggaccatggcctgaccccggaccaagtgg
2760
3'
gccacgtcgccgacaacggccacgacacggtcctggtaccggactggggcctggttcacc
NN4
NN5
Confirmed sequence using Seq TALEN 5_1
T V Q R L L P V L C Q D H G L T P D Q V

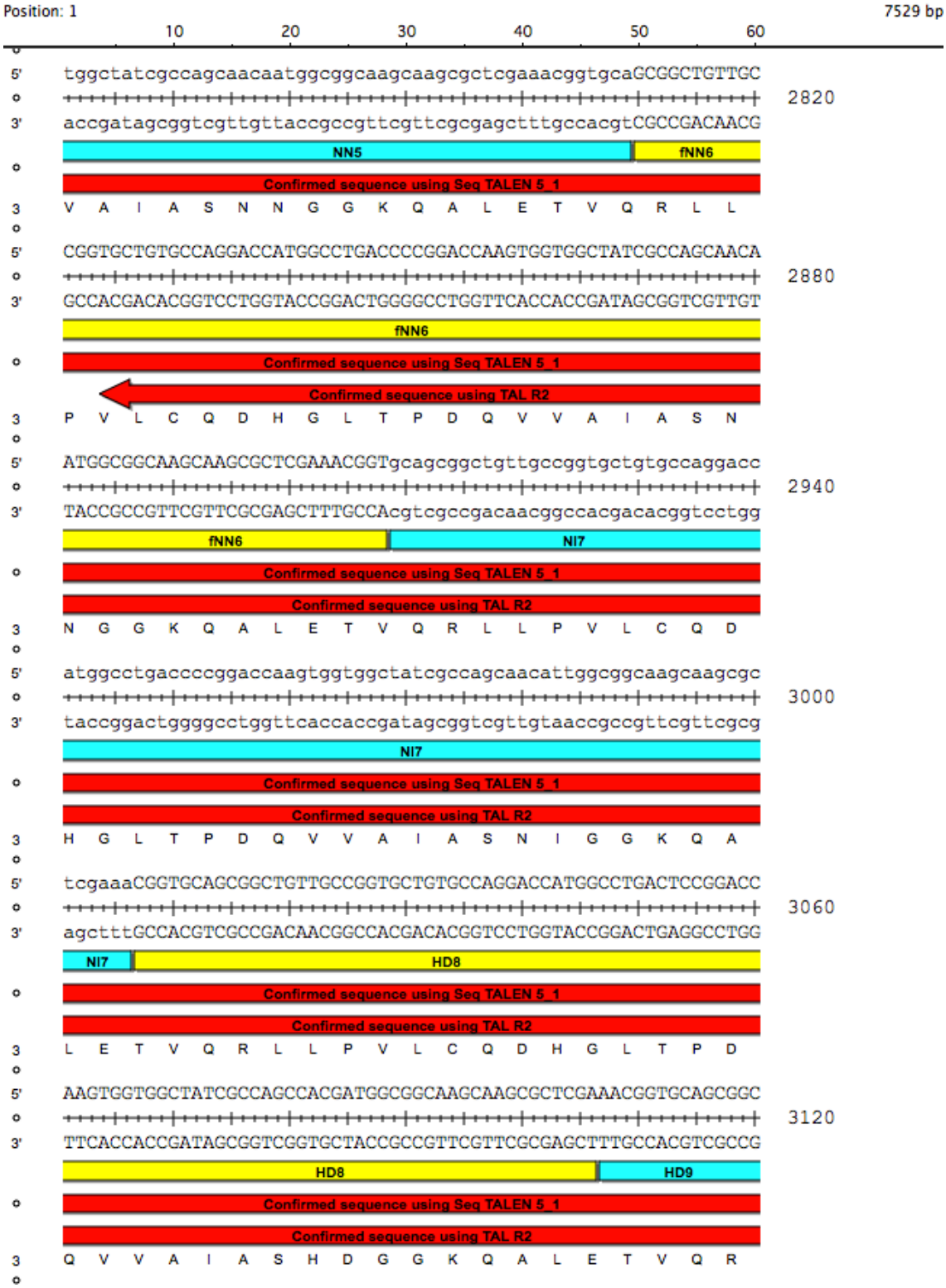
Position: 1
7529 bp
10
20
30
40
50
60
5'
tggctatcgccagcaacaatggcggcaagcaagcgctcgaaacggtgcaGCGGCTGTTGC
2820
3'
accgatagcggtcgttgttaccgccgttcgttcgcgagctttgccacgtCGCCGACAACG
NN5
fNN6
Confirmed sequence using Seq TALEN 5_1
3
V A I A S N N G G K Q A L E T V Q R L L
5'
CGGTGCTGTGCCAGGACCATGGCCTGACCCCGGACCAAGTGGTGGCTATCGCCAGCAACA
2880
3'
GCCACGACACGGTCCTGGTACCGGACTGGGGCCTGGTTCACCACCGATAGCGGTCGTTGT
fNN6
Confirmed sequence using Seq TALEN 5_1
Confirmed sequence using TAL R2
3
P V L C Q D H G L T P D Q V V A I A S N
5'
ATGGCGGCAAGCAAGCGCTCGAAACGGTgcagcggctgttgccggtgctgtgccaggacc
2940
3'
TACCGCCGTTCGTTCGCGAGCTTTGCCAcgtcgccgacaacggccacgacacggtcctgg
fNN6
NI7
Confirmed sequence using Seq TALEN 5_1
Confirmed sequence using TAL R2
3
N G G K Q A L E T V Q R L L P V L C Q D
5'
atggcctgaccccggaccaagtggtggctatcgccagcaacattggcggcaagcaagcgc
3000
3'
taccggactggggcctggttcaccaccgatagcggtcgttgtaaccgccgttcgttcgcg
NI7
Confirmed sequence using Seq TALEN 5_1
Confirmed sequence using TAL R2
3
H G L T P D Q V V A I A S N I G G K Q A
5'
tcgaaaCGGTGCAGCGGCTGTTGCCGGTGCTGTGCCAGGACCATGGCCTGACTCCGGACC
3060
3'
agctttGCCACGTCGCCGACAACGGCCACGACACGGTCCTGGTACCGGACTGAGGCCTGG
NI7
HD8
Confirmed sequence using Seq TALEN 5_1
Confirmed sequence using TAL R2
3
L E T V Q R L L P V L C Q D H G L T P D
5'
AAGTGGTGGCTATCGCCAGCCACGATGGCGGCAAGCAAGCGCTCGAAACGGTGCAGCGGC
3120
3'
TTCACCACCGATAGCGGTCGGTGCTACCGCCGTTCGTTCGCGAGCTTTGCCACGTCGCCG
HD8
HD9
Confirmed sequence using Seq TALEN 5_1
Confirmed sequence using TAL R2
3
Q V V A I A S H D G G K Q A L E T V Q R

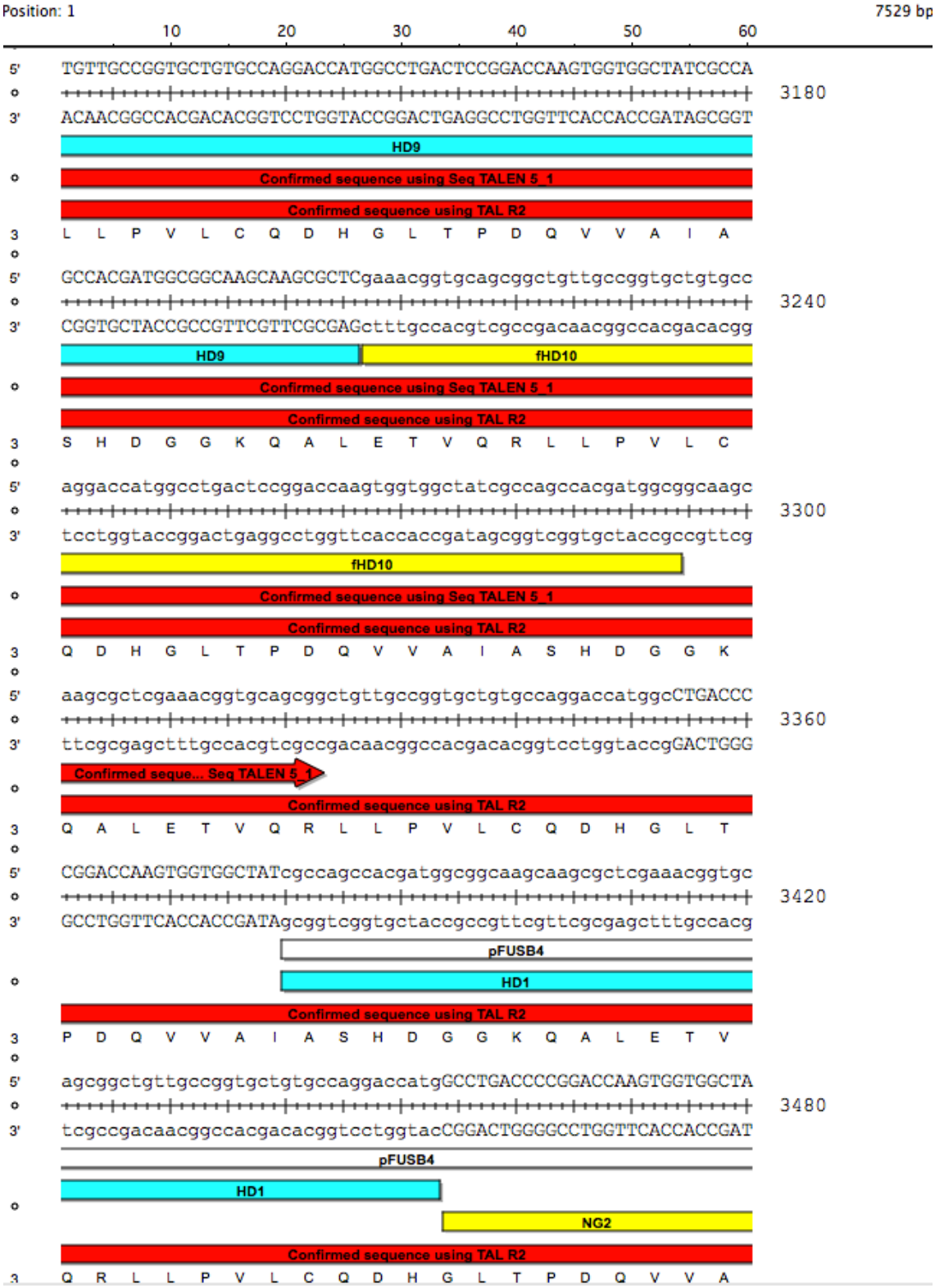
Position: 1
7529 bp
10
20
30
40
50
60
5' TGTTGCCGGTGCTGTGCCAGGACCATGGCCTGACTCCGGACCAAGTGGTGGCTATCGCCA
3180
3' ACAACGGCCACGACACGGTCCTGGTACCGGACTGAGGCCTGGTTCACCACCGATAGCGGT
HD9
Confirmed sequence using Seq TALEN 5_1
Confirmed sequence using TAL R2
3 L L P V L C Q D H G L T P D Q V V A I A
5' GCCACGATGGCGGCAAGCAAGCGCTCgaaacggtgcagcggctgttgccggtgctgtgcc
3240
3' CGGTGCTACCGCCGTTCGTTCGCGAGctttgccacgtcgccgacaacggccacgacacgg
HD9
fHD10
Confirmed sequence using Seq TALEN 5_1
Confirmed sequence using TAL R2
3 S H D G G K Q A L E T V Q R L L P V L C
5' aggaccatggcctgactccggaccaagtggtggctatcgccagccacgatggcggcaagc
3300
3' tcctggtaccggactgaggcctggttcaccaccgatagcggtcggtgctaccgccgttcg
fHD10
Confirmed sequence using Seq TALEN 5_1
Confirmed sequence using TAL R2
3 Q D H G L T P D Q V V A I A S H D G G K
5' aagcgctcgaaacggtgcagcggctgttgccggtgctgtgccaggaccatggcCTGACCC
3360
3' ttcgcgagctttgccacgtcgccgacaacggccacgacacggtcctggtaccgGACTGGG
Confirmed seque... Seq TALEN 5_1
Confirmed sequence using TAL R2
3 Q A L E T V Q R L L P V L C Q D H G L T
5' CGGACCAAGTGGTGGCTATcgccagccacgatggcggcaagcaagcgctcgaaacggtgc
3420
3' GCCTGGTTCACCACCGATAgcggtcggtgctaccgccgttcgttcgcgagctttgccacg
pFUSB4
HD1
Confirmed sequence using TAL R2
3 P D Q V V A I A S H D G G K Q A L E T V
5' agcggctgttgccggtgctgtgccaggaccatgGCCTGACCCCGGACCAAGTGGTGGCTA
3480
3' tcgccgacaacggccacgacacggtcctggtacCGGACTGGGGCCTGGTTCACCACCGAT
pFUSB4
HD1
NG2
Confirmed sequence using TAL R2
3 Q R L L P V L C Q D H G L T P D Q V V A

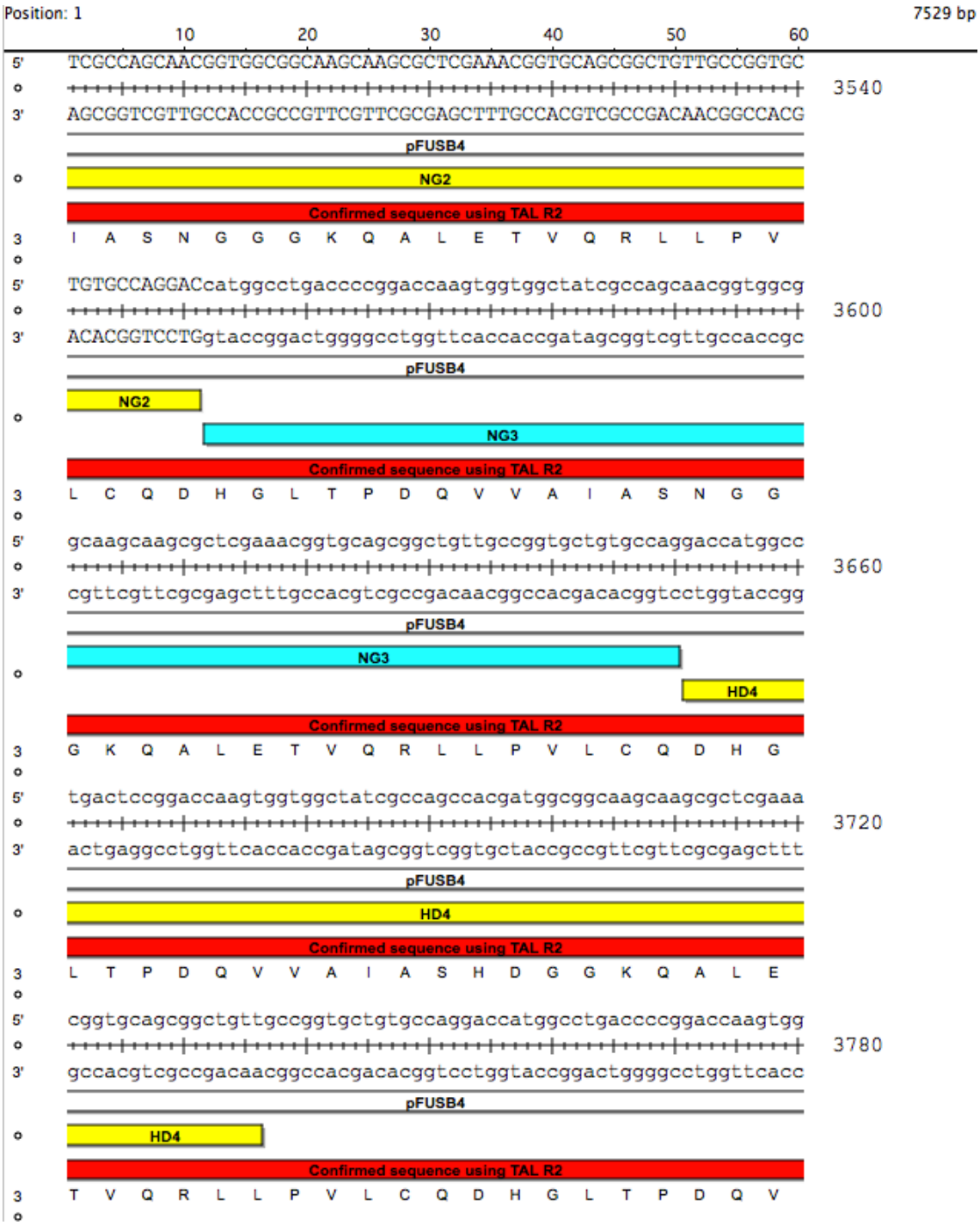
Position: 1
7529 bp
10
20
30
40
50
60
5'
TCGCCAGCAACGGTGGCGGCAAGCAAGCGCTCGAAACGGTGCAGCGGCTGTTGCCGGTGC
3540
3'
AGCGGTCGTTGCCACCGCCGTTCGTTCGCGAGCTTTGCCACGTCGCCGACAACGGCCACG
pFUSB4
NG2
Confirmed sequence using TAL R2
3
I A S N G G G K Q A L E T V Q R L L P V
5'
TGTGCCAGGACcatggcctgaccccggaccaagtggtggctatcgccagcaacggtggcg
3600
3'
ACACGGTCCTGgtaccggactggggcctggttcaccaccgatagcggtcgttgccaccgc
pFUSB4
NG2
NG3
Confirmed sequence using TAL R2
3
L C Q D H G L T P D Q V V A I A S N G G
5'
gcaagcaagcgctcgaaacggtgcagcggctgttgccggtgctgtgccaggaccatggcc
3660
3'
cgttcgttcgcgagctttgccacgtcgccgacaacggccacgacacggtcctggtaccgg
pFUSB4
NG3
HD4
Confirmed sequence using TAL R2
3
G K Q A L E T V Q R L L P V L C Q D H G
5'
tgactccggaccaagtggtggctatcgccagccacgatggcggcaagcaagcgctcgaaa
3720
3'
actgaggcctggttcaccaccgatagcggtcggtgctaccgccgttcgttcgcgagcttt
pFUSB4
HD4
Confirmed sequence using TAL R2
3
L T P D Q V V A I A S H D G G K Q A L E
5'
cggtgcagcggctgttgccggtgctgtgccaggaccatggcctgaccccggaccaagtgg
3780
3'
gccacgtcgccgacaacggccacgacacggtcctggtaccggactggggcctggttcacc
pFUSB4
HD4
Confirmed sequence using TAL R2
3
T V Q R L L P V L C Q D H G L T P D Q V

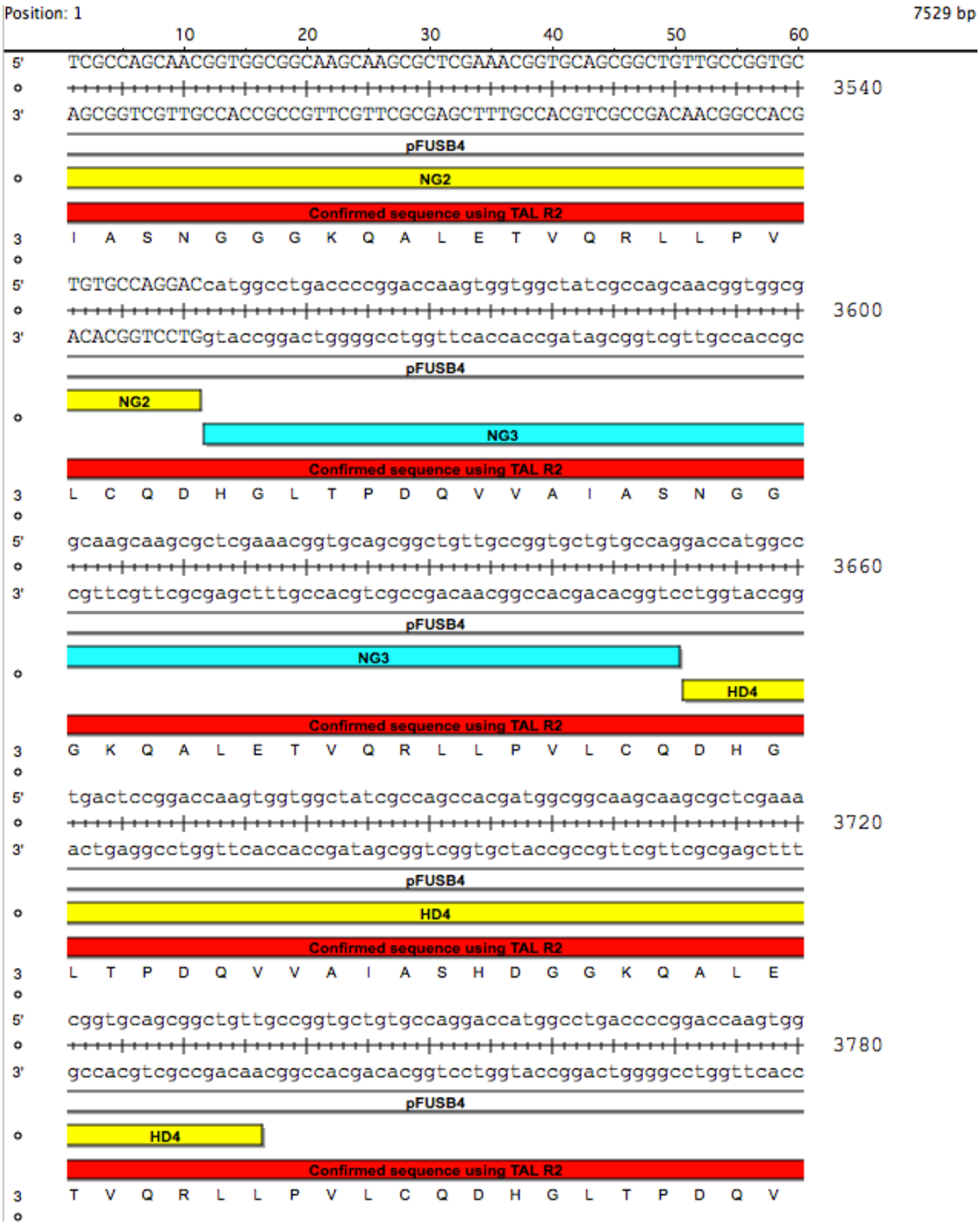
Position: 1
7529 bp
10
20
30
40
50
60
5'
TCGCCAGCAACGGTGGCGGCAAGCAAGCGCTCGAAACGGTGCAGCGGCTGTTGCCGGTGC
3540
3'
AGCGGTCGTTGCCACCGCCGTTCGTTCGCGAGCTTTGCCACGTCGCCGACAACGGCCACG
pFUSB4
NG2
Confirmed sequence using TAL R2
3
I A S N G G G K Q A L E T V Q R L L P V
5'
TGTGCCAGGACcatggcctgaccccggaccaagtggtggctatcgccagcaacggtggcg
3600
3'
ACACGGTCCTGgtaccggactggggcctggttcaccaccgatagcggtcgttgccaccgc
pFUSB4
NG2
NG3
Confirmed sequence using TAL R2
3
L C Q D H G L T P D Q V V A I A S N G G
5'
gcaagcaagcgctcgaaacggtgcagcggctgttgccggtgctgtgccaggaccatggcc
3660
3'
cgttcgttcgcgagctttgccacgtcgccgacaacggccacgacacggtcctggtaccgg
pFUSB4
NG3
HD4
Confirmed sequence using TAL R2
3
G K Q A L E T V Q R L L P V L C Q D H G
5'
tgactccggaccaagtggtggctatcgccagccacgatggcggcaagcaagcgctcgaaa
3720
3'
actgaggcctggttcaccaccgatagcggtcggtgctaccgccgttcgttcgcgagcttt
pFUSB4
HD4
Confirmed sequence using TAL R2
3
L T P D Q V V A I A S H D G G K Q A L E
5'
cggtgcagcggctgttgccggtgctgtgccaggaccatggcctgaccccggaccaagtgg
3780
3'
gccacgtcgccgacaacggccacgacacggtcctggtaccggactggggcctggttcacc
pFUSB4
HD4
Confirmed sequence using TAL R2
3
T V Q R L L P V L C Q D H G L T P D Q V

7.20.2 Right TALEN subunit (R*hax1*pCAGT7-TALEN(Sangamo))

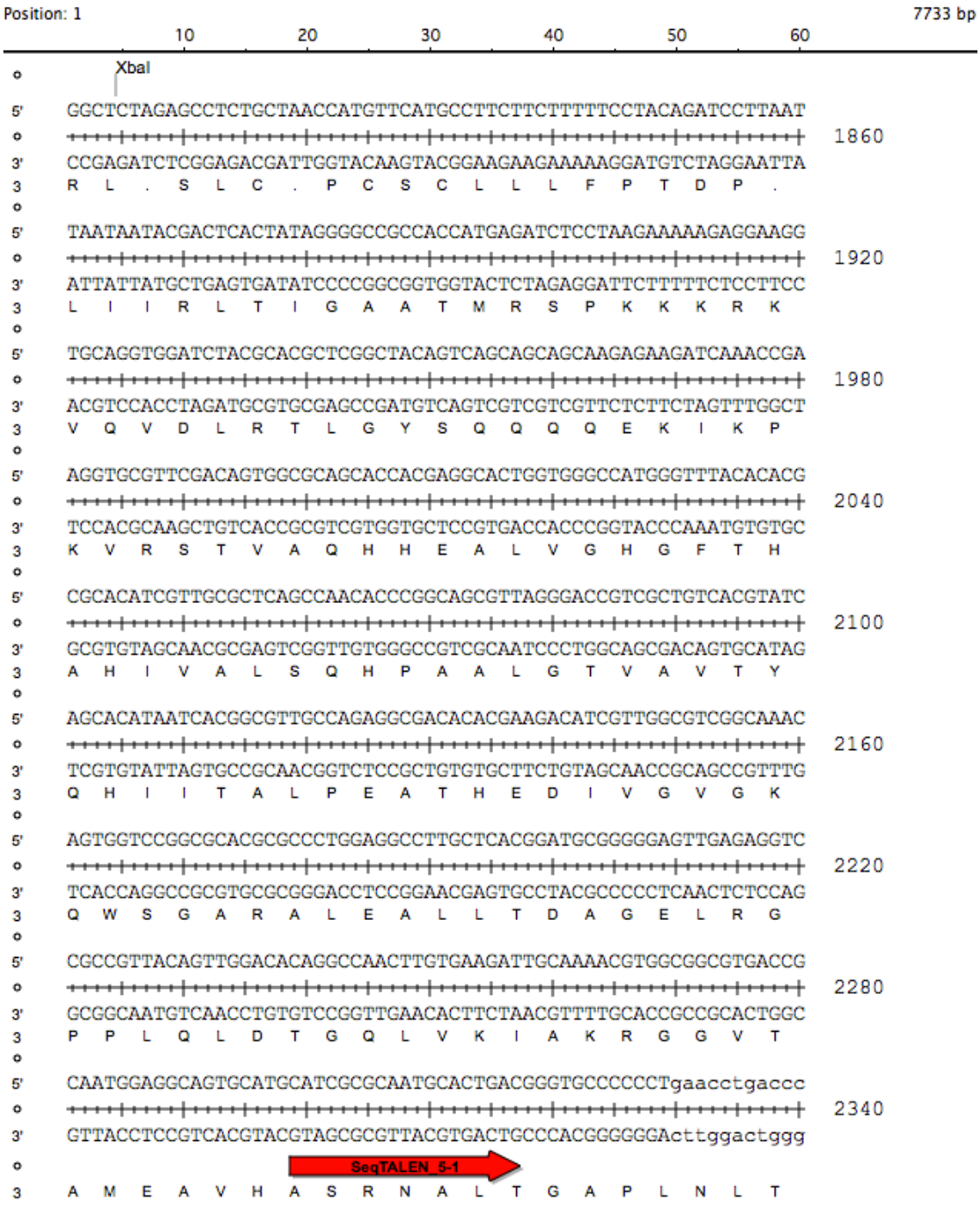

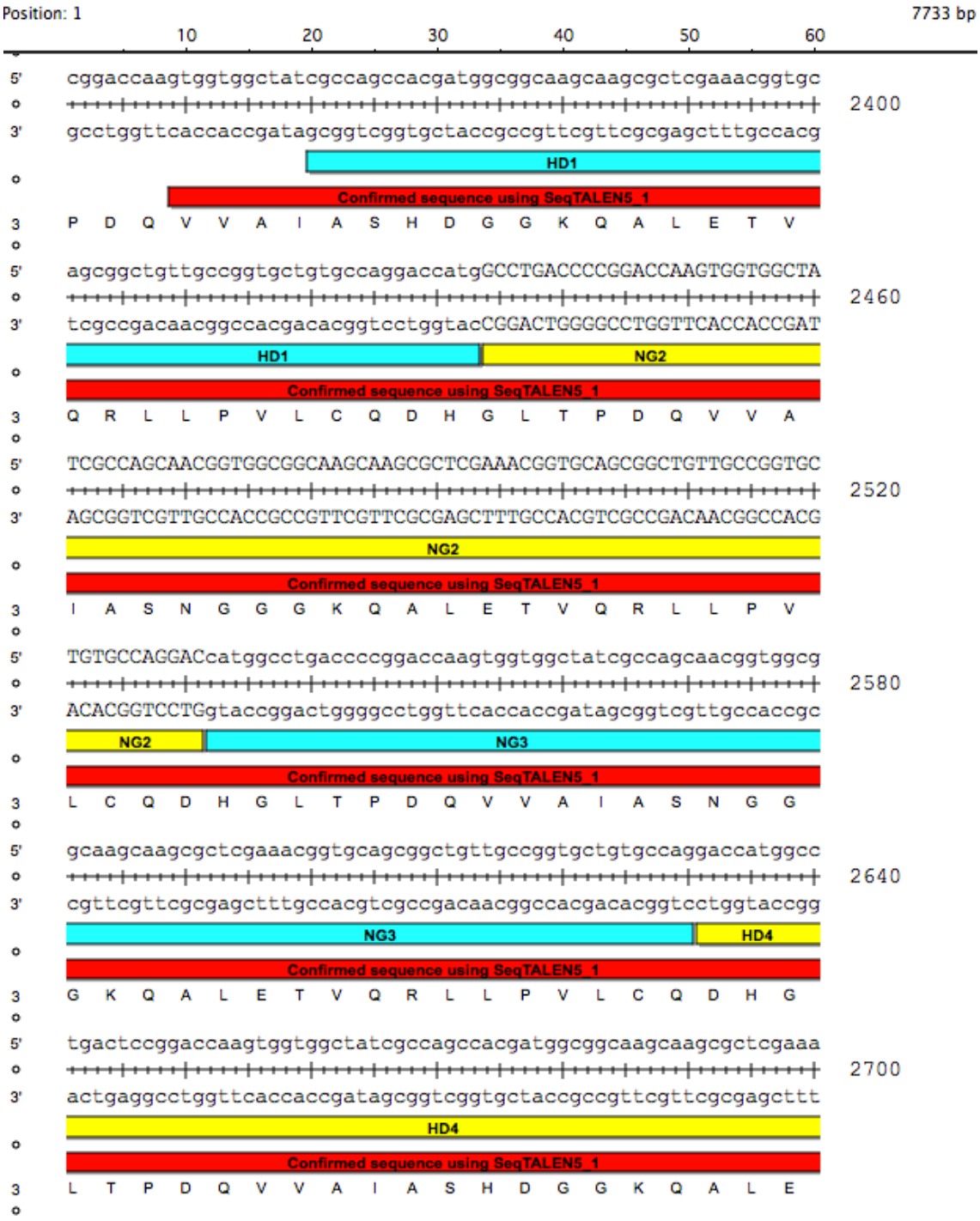
Position: 1
7733 bp
10
20
30
40
50
60
5'
cggaccaagtggtggctatcgccagccacgatggcggcaagcaagcgctcgaaacggtgc
2400
3'
gcctggttcaccaccgatagcggtcggtgctaccgccgttcgttcgcgagctttgccacg
HD1
Confirmed sequence using SeqTALEN5_1
3
P D Q V V A I A S H D G G K Q A L E T V
5'
agcggctgttgccggtgctgtgccaggaccatgGCCTGACCCCGGACCAAGTGGTGGCTA
2460
3'
tcgccgacaacggccacgacacggtcctggtacCGGACTGGGGCCTGGTTCACCACCGAT
HD1
NG2
Confirmed sequence using SeqTALEN5_1
3
Q R L L P V L C Q D H G L T P D Q V V A
5'
TCGCCAGCAACGGTGGCGGCAAGCAAGCGCTCGAAACGGTGCAGCGGCTGTTGCCGGTGC
2520
3'
AGCGGTCGTTGCCACCGCCGTTCGTTCGCGAGCTTTGCCACGTCGCCGACAACGGCCACG
NG2
Confirmed sequence using SeqTALEN5_1
3
I A S N G G G K Q A L E T V Q R L L P V
5'
TGTGCCAGGACcatggcctgaccccggaccaagtggtggctatcgccagcaacggtggcg
2580
3'
ACACGGTCCTGgtaccggactggggcctggttcaccaccgatagcggtcgttgccaccgc
NG2
NG3
Confirmed sequence using SeqTALEN5_1
3
L C Q D H G L T P D Q V V A I A S N G G
5'
gcaagcaagcgctcgaaacggtgcagcggctgttgccggtgctgtgccaggaccatggcc
2640
3'
cgttcgttcgcgagctttgccacgtcgccgacaacggccacgacacggtcctggtaccgg
NG3
HD4
Confirmed sequence using SeqTALEN5_1
3
G K Q A L E T V Q R L L P V L C Q D H G
5'
tgactccggaccaagtggtggctatcgccagccacgatggcggcaagcaagcgctcgaaa
2700
3'
actgaggcctggttcaccaccgatagcggtcggtgctaccgccgttcgttcgcgagcttt
HD4
Confirmed sequence using SeqTALEN5_1
3
L T P D Q V V A I A S H D G G K Q A L E

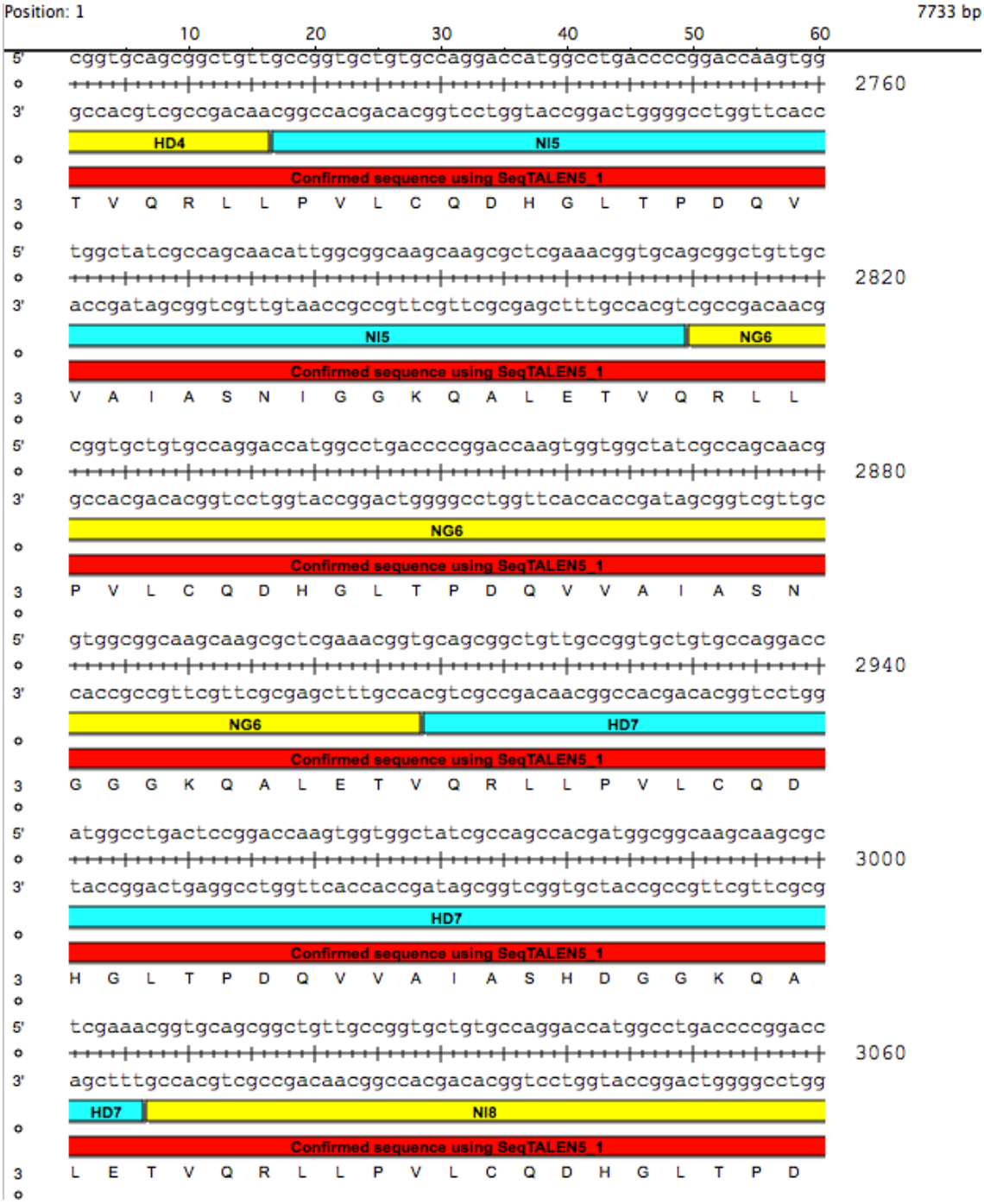
Position: 1
7733 bp
10
20
30
40
50
60
5'
cggtgcagcggctgttgccggtgctgtgccaggaccatggcctgaccccggaccaagtgg
2760
3'
gccacgtcgccgacaacggccacgacacggtcctggtaccggactggggcctggttcacc
HD4
NI5
Confirmed sequence using SeqTALEN5_1
T V Q R L L P V L C Q D H G L T P D Q V
5'
tggctatcgccagcaacattggcggcaagcaagcgctcgaaacggtgcagcggctgttgc
2820
3'
accgatagcggtcgttgtaaccgccgttcgttcgcgagctttgccacgtcgccgacaacg
NI5
NG6
Confirmed sequence using SeqTALEN5_1
V A I A S N I G G K Q A L E T V Q R L L
5'
cggtgctgtgccaggaccatggcctgaccccggaccaagtggtggctatcgccagcaacg
2880
3'
gccacgacacggtcctggtaccggactggggcctggttcaccaccgatagcggtcgttgc
NG6
Confirmed sequence using SeqTALEN5_1
P V L C Q D H G L T P D Q V V A I A S N
5'
gtggcggcaagcaagcgctcgaaacggtgcagcggctgttgccggtgctgtgccaggacc
2940
3'
caccgccgttcgttcgcgagctttgccacgtcgccgacaacggccacgacacggtcctgg
NG6
HD7
Confirmed sequence using SeqTALEN5_1
G G G K Q A L E T V Q R L L P V L C Q D
5'
atggcctgactccggaccaagtggtggctatcgccagccacgatggcggcaagcaagcgc
3000
3'
taccggactgaggcctggttcaccaccgatagcggtcggtgctaccgccgttcgttcgcg
HD7
Confirmed sequence using SeqTALEN5_1
H G L T P D Q V V A I A S H D G G K Q A
5'
tcgaaacggtgcagcggctgttgccggtgctgtgccaggaccatggcctgaccccggacc
3060
3'
agctttgccacgtcgccgacaacggccacgacacggtcctggtaccggactggggcctgg
HD7
NI8
Confirmed sequence using SeqTALEN5_1
L E T V Q R L L P V L C Q D H G L T P D

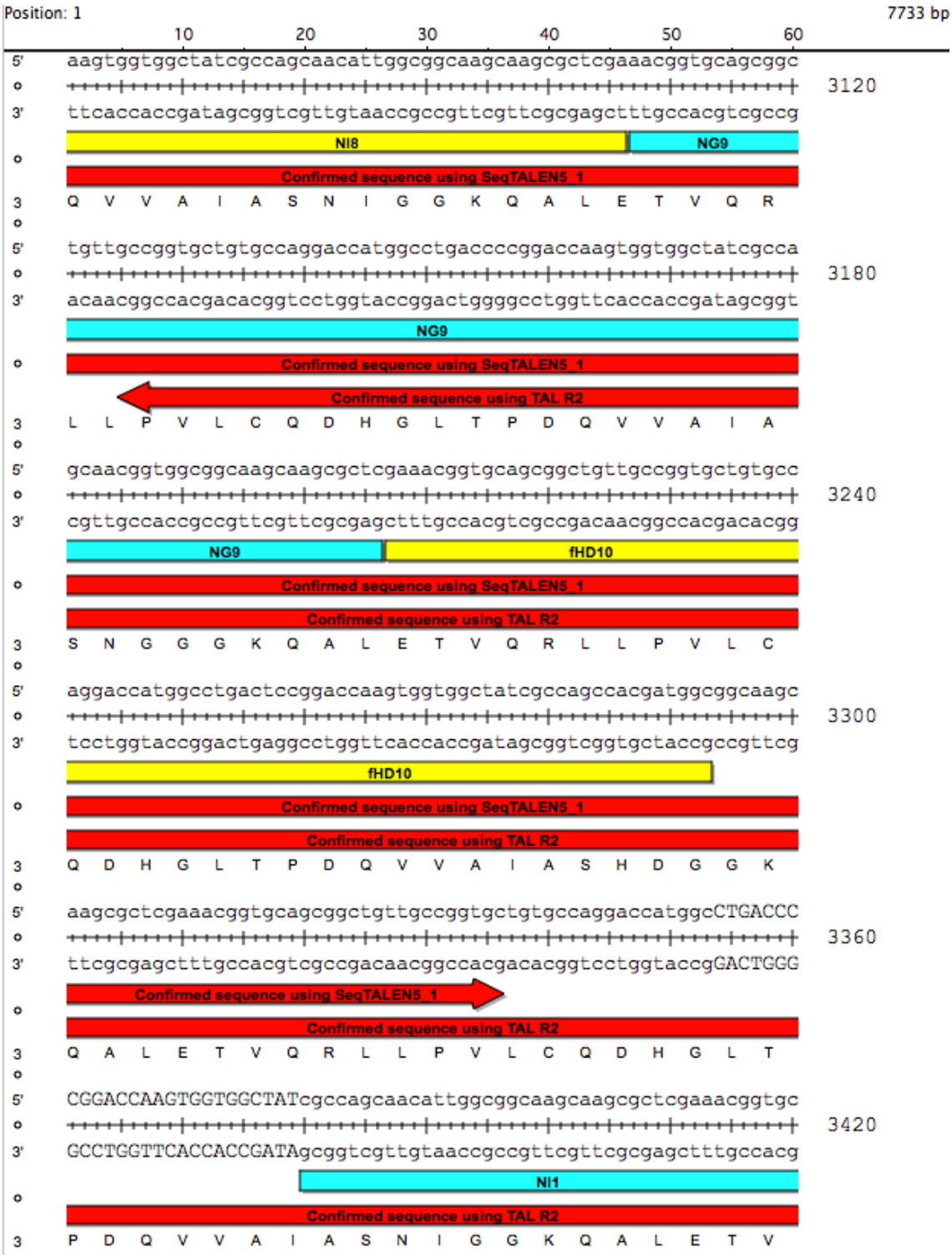
Position: 1
7733 bp
10
20
30
40
50
60
5' aagtggtggctatcgccagcaacattggcggcaagcaagcgctcgaaacggtgcagcggc
3120
3' ttcaccaccgatagcggtcgttgtaaccgccgttcgttcgcgagctttgccacgtcgccg
NI8
NG9
Confirmed sequence using SeqTALEN5_1
3 Q V V A I A S N I G G K Q A L E T V Q R
5' tgttgccggtgctgtgccaggaccatggcctgaccccggaccaagtggtggctatcgcca
3180
3' acaacggccacgacacggtcctggtaccggactggggcctggttcaccaccgatagcggt
NG9
Confirmed sequence using SeqTALEN5_1
Confirmed sequence using TAL R2
3 L L P V L C Q D H G L T P D Q V V A I A
5' gcaacggtggcggcaagcaagcgctcgaaacggtgcagcggctgttgccggtgctgtgcc
3240
3' cgttgccaccgccgttcgttcgcgagctttgccacgtcgccgacaacggccacgacacgg
NG9
fHD10
Confirmed sequence using SeqTALEN5_1
Confirmed sequence using TAL R2
3 S N G G G K Q A L E T V Q R L L P V L C
5' aggaccatggcctgactccggaccaagtggtggctatcgccagccacgatggcggcaagc
3300
3' tcctggtaccggactgaggcctggttcaccaccgatagcggtcggtgctaccgccgttcg
fHD10
Confirmed sequence using SeqTALEN5_1
Confirmed sequence using TAL R2
3 Q D H G L T P D Q V V A I A S H D G G K
5' aagcgctcgaaacggtgcagcggctgttgccggtgctgtgccaggaccatggcCTGACCC
3360
3' ttcgcgagctttgccacgtcgccgacaacggccacgacacggtcctggtaccgGACTGGG
Confirmed sequence using SeqTALEN5_1
Confirmed sequence using TAL R2
3 Q A L E T V Q R L L P V L C Q D H G L T
5' CGGACCAAGTGGTGGCTATcgccagcaacattggcggcaagcaagcgctcgaaacggtgc
3420
3' GCCTGGTTCACCACCGATAgcggtcgttgtaaccgccgttcgttcgcgagctttgccacg
NI1
Confirmed sequence using TAL R2
3 P D Q V V A I A S N I G G K Q A L E T V

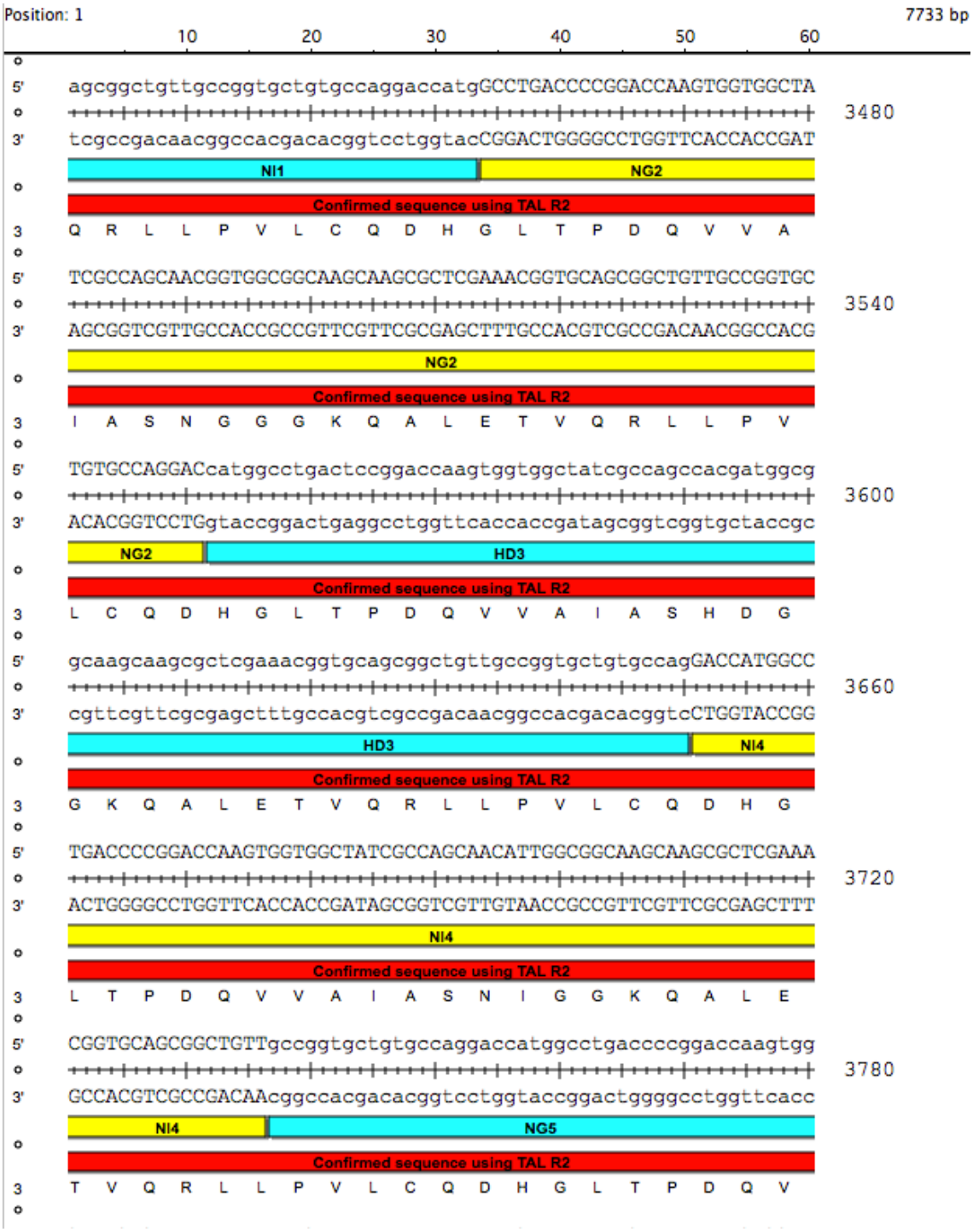
Position: 1
7733 bp
10
20
30
40
50
60
5' agcggctgttgccggtgctgtgccaggaccatgGCCTGACCCCGGACCAAGTGGTGGCTA
3480
3' tcgccgacaacggccacgacacggtcctggtacCGGACTGGGGCCTGGTTCACCACCGAT
NI1
NG2
Confirmed sequence using TAL R2
3 Q R L L P V L C Q D H G L T P D Q V V A
5' TCGCCAGCAACGGTGGCGGCAAGCAAGCGCTCGAAACGGTGCAGCGGCTGTTGCCGGTGC
3540
3' AGCGGTCGTTGCCACCGCCGTTCGTTCGCGAGCTTTGCCACGTCGCCGACAACGGCCACG
NG2
Confirmed sequence using TAL R2
3 I A S N G G G K Q A L E T V Q R L L P V
5' TGTGCCAGGACcatggcctgactccggaccaagtggtggctatcgccagccacgatggcg
3600
3' ACACGGTCCTGgtaccggactgaggcctggttcaccaccgatagcggtcggtgctaccgc
NG2
HD3
Confirmed sequence using TAL R2
3 L C Q D H G L T P D Q V V A I A S H D G
5' gcaagcaagcgctcgaaacggtgcagcggctgttgccggtgctgtgccagGACCATGGCC
3660
3' cgttcgttcgcgagctttgccacgtcgccgacaacggccacgacacggtcCTGGTACCGG
HD3
NI4
Confirmed sequence using TAL R2
3 G K Q A L E T V Q R L L P V L C Q D H G
5' TGACCCCGGACCAAGTGGTGGCTATCGCCAGCAACATTGGCGGCAAGCAAGCGCTCGAAA
3720
3' ACTGGGGCCTGGTTCACCACCGATAGCGGTCGTTGTAACCGCCGTTCGTTCGCGAGCTTT
NI4
Confirmed sequence using TAL R2
3 L T P D Q V V A I A S N I G G K Q A L E
5' CGGTGCAGCGGCTGTTgccggtgctgtgccaggaccatggcctgaccccggaccaagtgg
3780
3' GCCACGTCGCCGACAAcggccacgacacggtcctggtaccggactggggcctggttcacc
NI4
NG5
Confirmed sequence using TAL R2
3 T V Q R L L P V L C Q D H G L T P D Q V

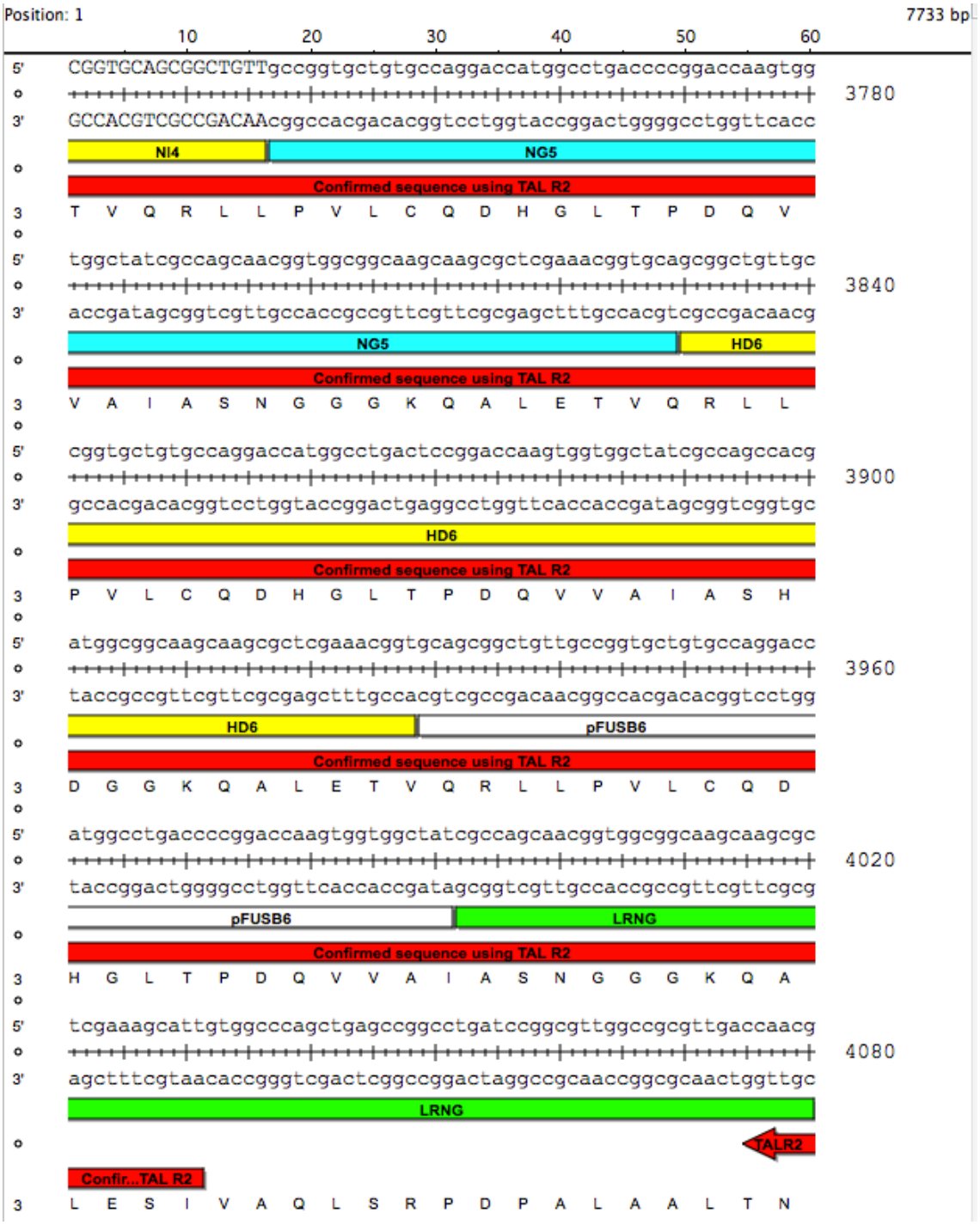
Position: 1
7733 bp
10
20
30
40
50
60
5'
CGGTGCAGCGGCTGTTgccggtgctgtgccaggaccatggcctgaccccggaccaagtgg
3780
3'
GCCACGTCGCCGACAAcggccacgacacggtcctggtaccggactggggcctggttcacc
NI4
NG5
Confirmed sequence using TAL R2
3
T V Q R L L P V L C Q D H G L T P D Q V
5'
tggctatcgccagcaacggtggcggcaagcaagcgctcgaaacggtgcagcggctgttgc
3840
3'
accgatagcggtcgttgccaccgccgttcgttcgcgagctttgccacgtcgccgacaacg
NG5
HD6
Confirmed sequence using TAL R2
3
V A I A S N G G G K Q A L E T V Q R L L
5'
cggtgctgtgccaggaccatggcctgactccggaccaagtggtggctatcgccagccacg
3900
3'
gccacgacacggtcctggtaccggactgaggcctggttcaccaccgatagcggtcggtgc
HD6
Confirmed sequence using TAL R2
3
P V L C Q D H G L T P D Q V V A I A S H
5'
atggcggcaagcaagcgctcgaaacggtgcagcggctgttgccggtgctgtgccaggacc
3960
3'
taccgccgttcgttcgcgagctttgccacgtcgccgacaacggccacgacacggtcctgg
HD6
pFUSB6
Confirmed sequence using TAL R2
3
D G G K Q A L E T V Q R L L P V L C Q D
5'
atggcctgaccccggaccaagtggtggctatcgccagcaacggtggcggcaagcaagcgc
4020
3'
taccggactggggcctggttcaccaccgatagcggtcgttgccaccgccgttcgttcgcg
pFUSB6
LRNG
Confirmed sequence using TAL R2
3
H G L T P D Q V V A I A S N G G G K Q A
5'
tcgaaagcattgtggcccagctgagccggcctgatccggcgttggccgcgttgaccaacg
4080
3'
agctttcgtaacaccgggtcgactcggccggactaggccgcaaccggcgcaactggttgc
LRNG
TALR2
Confir...TAL R2
3
L E S I V A Q L S R P D P A L A A L T N

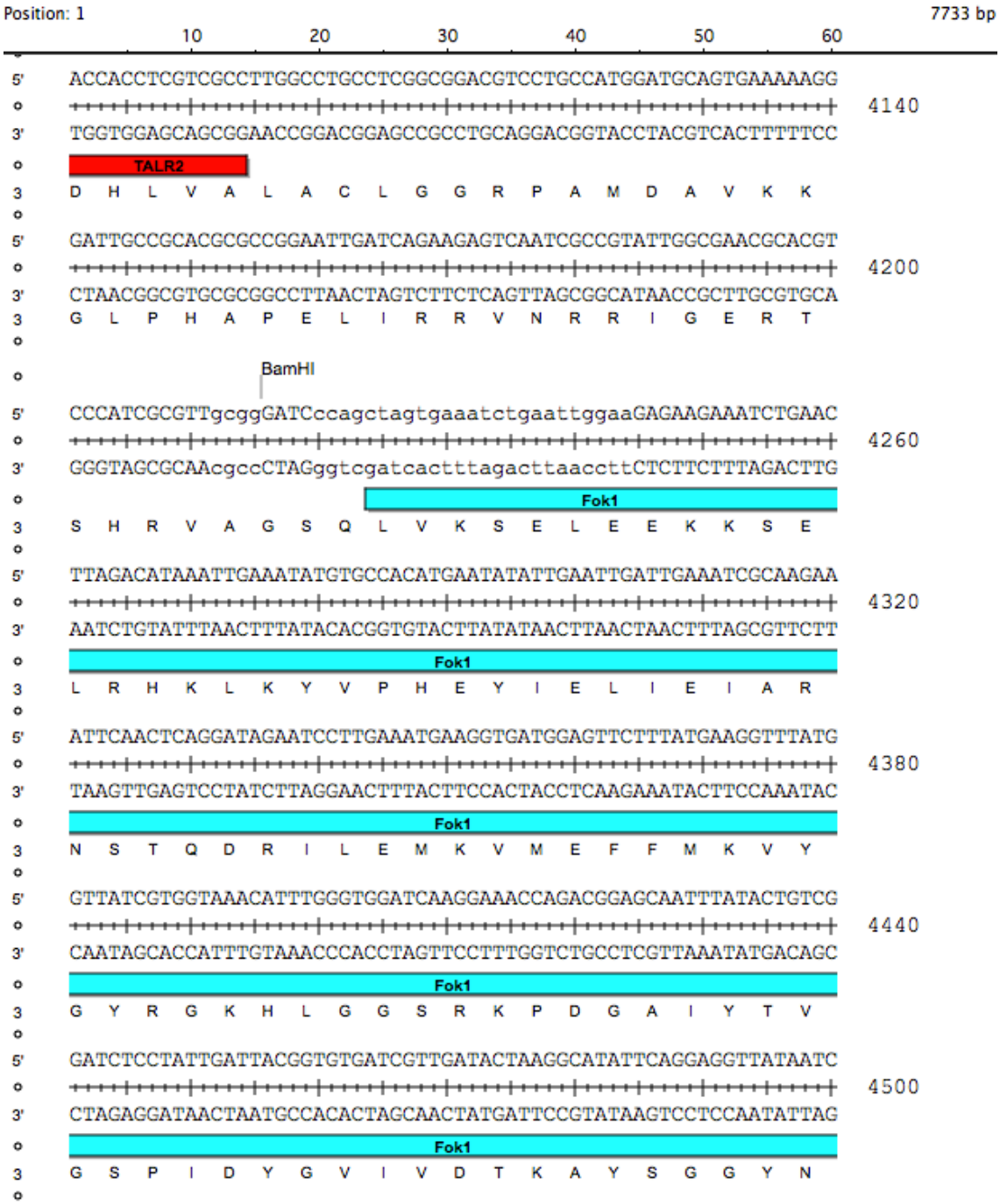
Position: 1
7733 bp
10
20
30
40
50
60
5' ACCACCTCGTCGCCTTGGCCTGCCTCGGCGGACGTCCTGCCATGGATGCAGTGAAAAAGG
4140
3' TGGTGGAGCAGCGGAACCGGACGGAGCCGCCTGCAGGACGGTACCTACGTCACTTTTTCC
TALR2
3 D H L V A L A C L G G R P A M D A V K K
5' GATTGCCGCACGCGCCGGAATTGATCAGAAGAGTCAATCGCCGTATTGGCGAACGCACGT
4200
3' CTAACGGCGTGCGCGGCCTTAACTAGTCTTCTCAGTTAGCGGCATAACCGCTTGCGTGCA
3 G L P H A P E L I R R V N R R I G E R T
BamHI
5' CCCATCGCGTTgcggGATCccagctagtgaaatctgaattggaaGAGAAGAAATCTGAAC
4260
3' GGGTAGCGCAAcgccCTAGggtcgatcactttagacttaaccttCTCTTCTTTAGACTTG
Fok1
3 S H R V A G S Q L V K S E L E E K K S E
5' TTAGACATAAATTGAAATATGTGCCACATGAATATATTGAATTGATTGAAATCGCAAGAA
4320
3' AATCTGTATTTAACTTTATACACGGTGTACTTATATAACTTAACTAACTTTAGCGTTCTT
Fok1
3 L R H K L K Y V P H E Y I E L I E I A R
5' ATTCAACTCAGGATAGAATCCTTGAAATGAAGGTGATGGAGTTCTTTATGAAGGTTTATG
4380
3' TAAGTTGAGTCCTATCTTAGGAACTTTACTTCCACTACCTCAAGAAATACTTCCAAATAC
Fok1
3 N S T Q D R I L E M K V M E F F M K V Y
5' GTTATCGTGGTAAACATTTGGGTGGATCAAGGAAACCAGACGGAGCAATTTATACTGTCG
4440
3' CAATAGCACCATTTGTAAACCCACCTAGTTCCTTTGGTCTGCCTCGTTAAATATGACAGC
Fok1
3 G Y R G K H L G G S R K P D G A I Y T V
5' GATCTCCTATTGATTACGGTGTGATCGTTGATACTAAGGCATATTCAGGAGGTTATAATC
4500
3' CTAGAGGATAACTAATGCCACACTAGCAACTATGATTCCGTATAAGTCCTCCAATATTAG
Fok1
3 G S P I D Y G V I V D T K A Y S G G Y N

References

Adams, D.H. & Shaw, S., 1994. Leucocyte-endothelial interactions and regulation of leucocyte migration. *Lancet*, 343(8901), pp.831–836.

Adams, J.M., 2003. Ways of dying: multiple pathways to apoptosis. *Genes & Development*, 17(20), pp.2481–2495.

Adams, J.M. & Cory, S., 1998. The Bcl-2 protein family: arbiters of cell survival. *Science*, 281(5381), pp.1322–1326.

Al-Maghrebi, M. et al., 2002. The 3' untranslated region of human vimentin mRNA interacts with protein complexes containing eEF-1gamma and HAX-1. *Nucleic Acids Research*, 30(23), pp.5017–5028.

Alexa, K. et al., 2009. Maternal and zygotic aldh1a2 activity is required for pancreas development in zebrafish. *PloS one*, 4(12), p.e8261.

Allen, L. et al., 2005. Pyocyanin production by Pseudomonas aeruginosa induces neutrophil apoptosis and impairs neutrophil-mediated host defenses in vivo. *Journal of Immunology*, 174(6), pp.3643–3649.

Ashkenazi, A. & Dixit, V.M., 1998. Death receptors: signaling and modulation. *Science*, 281(5381), pp.1305–1308.

Babior, B.M., 1984. The respiratory burst of phagocytes. *The Journal of Clinical Investigation*, 73(3), pp.599–601.

Baden, K.N. et al., 2007. Early developmental pathology due to cytochrome c oxidase deficiency is revealed by a new zebrafish model. *The Journal of Biological Chemistry*, 282(48), pp.34839–34849.

Bae, J. et al., 2000. MCL-1S, a splicing variant of the antiapoptotic BCL-2 family member MCL-1, encodes a proapoptotic protein possessing only the BH3 domain. *Journal of Biological Chemistry*, 275, pp.25255–25261.

Baines, K.J. et al., 2010. Differential gene expression and cytokine production from neutrophils in asthma phenotypes. *The European Respiratory Journal*, 35(3), pp.522–531.

Bainton, D.F., Ullyot, J.L. & Farquhar, M.G., 1971. The development of neutrophilic polymorphonuclear leukocytes in human bone marrow. *The Journal of Experimental Medicine*, 134(4), pp.907–934.

Baldwin Jr., A.S., 1996. The NF-kappa B and I kappa B proteins: new discoveries and insights. *Annual Review of Immunology*, 14, pp.649–683.

Banerjee, A. et al., 2009. Hepatitis C virus core protein and cellular protein HAX-1 promote 5-fluorouracil-mediated hepatocyte growth inhibition. *Journal of Virology*, 83(19), pp.9663–9671.

Bannenberg, G. & Serhan, C.N., 2010. Specialized pro-resolving lipid mediators in the inflammatory response: An update. *Biochimica et Biophysica Acta*, 1801(12), pp.1260–1273.

Baran, J. et al., 1996. Apoptosis of monocytes and prolonged survival of granulocytes as a result of phagocytosis of bacteria. *Infection and Immunity*, 64, pp.4242–4248.

Belaaouaj, A. et al., 1998. Mice lacking neutrophil elastase reveal impaired host defense against gram negative bacterial sepsis. *Nature Medicine*, 4(5), pp.615–618.

Bellocchio, S. et al., 2004. TLRs govern neutrophil activity in aspergillosis. *Journal of Immunology*, 173(12), pp.7406–7415.

Bennett, C.M. et al., 2001. Myelopoiesis in the zebrafish, Danio rerio. *Blood*, 98(3), pp.643–651.

Bennett, J.T. et al., 2007. Maternal nodal and zebrafish embryogenesis. *Nature*, 450(7167), pp.E1–2; discussion E2–4.
Beumer, K. et al., 2006. Efficient gene targeting in Drosophila with zinc-finger nucleases. *Genetics*, 172(4), pp.2391–2403.
Bhakta, M.S. et al., 2013. Highly active zinc-finger nucleases by extended modular assembly. *Genome Research*, 23(3), pp.530–538.
Bianchi, S.M. et al., 2006. Granulocyte apoptosis in the pathogenesis and resolution of lung disease. *Clinical Science*, 110(3), pp.293–304.
Bibikova, M. et al., 2001. Stimulation of homologous recombination through targeted cleavage by chimeric nucleases. *Molecular and Cellular Biology*, 21(1), pp.289–297.
Bibikova, M. et al., 2002. Targeted chromosomal cleavage and mutagenesis in Drosophila using zinc-finger nucleases. *Genetics*, 161(3), pp.1169–1175.
Boch, J. & Bonas, U., 2010. Xanthomonas AvrBs3 family-type III effectors: discovery and function. *Annual Review of Phytopathology*, 48, pp.419–436.
Bogdanove, A.J., Schornack, S. & Lahaye, T., 2010. TAL effectors: finding plant genes for disease and defense. *Current Opinion in Plant Biology*, 13(4), pp.394–401.
Borregaard, N. et al., 1993. Human neutrophil granules and secretory vesicles. *European Journal of Haematology*, 51(4), pp.187–198.
Borregaard, N. & Cowland, J.B., 1997. Granules of the human neutrophilic polymorphonuclear leukocyte. *Blood*, 89(10), pp.3503–3521.
Borregaard, N. & Herlin, T., 1982. Energy metabolism of human neutrophils during phagocytosis. *The Journal of Clinical Investigation*, 70(3), pp.550–557.
Bouillet, P. et al., 1999. Proapoptotic Bcl-2 relative Bim required for certain apoptotic responses, leukocyte homeostasis, and to preclude autoimmunity. *Science*, 286(5445), pp.1735–1738.
Boztug, K. et al., 2009. A syndrome with congenital neutropenia and mutations in G6PC3. *The New England Journal of Medicine*, 360, pp.32–43.
Boztug, K. & Klein, C., 2011. Genetic etiologies of severe congenital neutropenia. *Current Opinion in Pediatrics*, 23, pp.21–26.
Brach, M.A. et al., 1992. Prolongation of survival of human polymorphonuclear neutrophils by granulocyte-macrophage colony-stimulating factor is caused by inhibition of programmed cell death. *Blood*, 80, pp.2920–2924.
Brinkmann, V. et al., 2004. Neutrophil extracellular traps kill bacteria. *Science*, 303(5663), pp.1532–1535.
Brown, S.B. & Savill, J., 1999. Phagocytosis triggers macrophage release of Fas ligand and induces apoptosis of bystander leukocytes. *Journal of Immunology*, 162(1), pp.480–485.
Brown, V. et al., 2009. Dysregulated apoptosis and NFkappaB expression in COPD subjects. *Respiratory Research*, 10, p.24.
Buckley, C.D. et al., 2006. Identification of a phenotypically and functionally distinct population of long-lived neutrophils in a model of reverse endothelial migration. *Journal of Leukocyte Biology*, 79(2), pp.303–311.
Burnicka-Turek, O. et al., 2010. Pelota interacts with HAX1, EIF3G and SRPX and the resulting protein complexes are associated with the actin cytoskeleton. *BMC Cell Biology*, 11, p.28.
Cade, L. et al., 2012. Highly efficient generation of heritable zebrafish gene mutations using homo- and heterodimeric TALENs. *Nucleic Acids Research*, 40(16), pp.8001–8010.

Cannistra, S.A. & Griffin, J.D., 1988. Regulation of the production and function of granulocytes and monocytes. *Seminars in Hematology*, 25(3), pp.173–188.
Canton, I. et al., 2013. Fully synthetic polymer vesicles for intracellular delivery of antibodies in live cells. *Federation of American Societies for Experimental Biology Journal*, 27(1), pp.98–108.
Carlsson, G. et al., 2004. Kostmann syndrome: severe congenital neutropenia associated with defective expression of Bcl-2, constitutive mitochondrial release of cytochrome c, and excessive apoptosis of myeloid progenitor cells. *Blood*, 103(9), pp.3355–3361.
Caserta, T.M. et al., 2003. Q-VD-OPh, a broad spectrum caspase inhibitor with potent antiapoptotic properties. *Apoptosis*, 8, pp.345–352.
Cathomen, T. & Joung, J.K., 2008. Zinc-finger nucleases: the next generation emerges. *Molecular therapy : The Journal of the American Society of Gene Therapy*, 16(7), pp.1200–1207.
Cavaillon, J.-M., 2011. The historical milestones in the understanding of leukocyte biology initiated by Elie Metchnikoff. *Journal of Leukocyte Biology*, 90, pp.413–424.
Cavnar, P.J. et al., 2011. Hax1 regulates neutrophil adhesion and motility through RhoA. *Journal of Cell Biology*, 193(3), pp.465–473.
Cermak, T. et al., 2011. Efficient design and assembly of custom TALEN and other TAL effector-based constructs for DNA targeting. *Nucleic Acids Research*, 39(12), p.e82.
Chao, J.R. et al., 2008. Hax1-mediated processing of HtrA2 by Parl allows survival of lymphocytes and neurons. *Nature*, 452(7183), pp.98–102.
Chapple, D.S. et al., 1998. Structure-function relationship of antibacterial synthetic peptides homologous to a helical surface region on human lactoferrin against Escherichia coli serotype O111. *Infection and Immunity*, 66(6), pp.2434–2440.
Charbord, P. et al., 1996. Early ontogeny of the human marrow from long bones: an immunohistochemical study of hematopoiesis and its microenvironment. *Blood*, 87(10), pp.4109–4119.
Chen, J. et al., 2007. Characterization of a mutation in the Phox homology domain of the NADPH oxidase component p40phox identifies a mechanism for negative regulation of superoxide production. *Journal of Biological Chemistry*, 282, pp.30273–30284.
Christian, M. et al., 2010. Targeting DNA double-strand breaks with TAL effector nucleases. *Genetics*, 186(2), pp.757–761.
Cilenti, L. et al., 2004. Regulation of HAX-1 anti-apoptotic protein by Omi/HtrA2 protease during cell death. *The Journal of Biological Chemistry*, 279(48), pp.50295–50301.
Colamussi, M.L. et al., 1999. Influenza A virus accelerates neutrophil apoptosis and markedly potentiates apoptotic effects of bacteria. *Blood*, 93(7), pp.2395–2403.
Colucci-Guyon, E. et al., 2011. Strategies of professional phagocytes in vivo: unlike macrophages, neutrophils engulf only surface-associated microbes. *Journal of Cell Science*, 124(Pt 18), pp.3053–3059.
Cornu, T.I. et al., 2008. DNA-binding specificity is a major determinant of the activity and toxicity of zinc-finger nucleases. *Molecular therapy : the Journal of the American Society of Gene Therapy*, 16(2), pp.352–358.

Cornu, T.I. & Cathomen, T., 2010. Quantification of zinc finger nuclease-associated toxicity. *Methods in Molecular Biology*, 649, pp.237–245.

Cowland, J.B., Johnsen, A.H. & Borregaard, N., 1995. hCAP-18, a cathelin/pro-bactenecin-like protein of human neutrophil specific granules. *Federation of European Biochemical Societies Letters*, 368(1), pp.173–176.

Cox, D. et al., 1997. Requirements for both Rac1 and Cdc42 in membrane ruffling and phagocytosis in leukocytes. *The Journal of Experimental Medicine*, 186(9), pp.1487–1494.

Cramer, E. et al., 1985. Ultrastructural localization of lactoferrin and myeloperoxidase in human neutrophils by immunogold. *Blood*, 65(2), pp.423–432.

DeLeo, F.R. & Quinn, M.T., 1996. Assembly of the phagocyte NADPH oxidase: molecular interaction of oxidase proteins. *Journal of Leukocyte Biology*, 60(6), pp.677–691.

Deng, Q. et al., 2011. Dual roles for Rac2 in neutrophil motility and active retention in zebrafish hematopoietic tissue. *Developmental Cell*, 21(4), pp.735–745.

Derouet, M. et al., 2004. Granulocyte macrophage colony-stimulating factor signaling and proteasome inhibition delay neutrophil apoptosis by increasing the stability of Mcl-1. *The Journal of Biological Chemistry*, 279(26), pp.26915–26921.

Diamond, M.S. et al., 1990. ICAM-1 (CD54): a counter-receptor for Mac-1 (CD11b/CD18). *Journal of Cell Biology*, 111(6 Pt 2), pp.3129–3139.

Diamond, P. et al., 1999. Regulation of leukocyte trafficking by lipoxins. *Clinical chemistry and laboratory medicine*, 37(3), pp.293–297.

Dixon, G. et al., 2012. A Method for the In Vivo Measurement of Zebrafish Tissue Neutrophil Lifespan. *International Scholarly Research Notices: Hematology*, 2012, pp.1–6.

Dosch, R. et al., 2004. Maternal control of vertebrate development before the midblastula transition: mutants from the zebrafish I. *Developmental Cell*, 6(6), pp.771–780.

Downey, G.P. et al., 1993. Neutrophil sequestration and migration in localized pulmonary inflammation. Capillary localization and migration across the interalveolar septum. *The American Review of Respiratory Disease*, 147(1), pp.168–176.

Doyon, Y. et al., 2008. Heritable targeted gene disruption in zebrafish using designed zinc-finger nucleases. *Nature Biotechnology*, 26(6), pp.702–708.

Dransfield, I. & Rossi, A.G., 2004. Granulocyte apoptosis: who would work with a “real” inflammatory cell? *Biochemical Society transactions*, 32(Pt3), pp.447–451.

Dufva, M., Olsson, M. & Rymo, L., 2001. Epstein-Barr virus nuclear antigen 5 interacts with HAX-1, a possible component of the B-cell receptor signalling pathway. *Journal of General Virology*, 82(Pt 7), pp.1581–1587.

Van Dyke, T.E. & Kornman, K.S., 2008. Inflammation and factors that may regulate inflammatory response. *Journal of Periodontology*, 79(8 Suppl), pp.1503–1507.

Eimon, P.M. et al., 2006. Delineation of the cell-extrinsic apoptosis pathway in the zebrafish. *Cell Death and Differentiation*, 13, pp.1619–1630.

Eisen, J.S. & Smith, J.C., 2008. Controlling morpholino experiments: don’t stop making antisense. *Development*, 135(10), pp.1735–1743.

Ekker, S.C. & Larson, J.D., 2001. Morphant technology in model developmental systems. *Genesis*, 30(3), pp.89–93.
Elbim, C. & Estaquier, J., 2010. Cytokines modulate neutrophil death. *European Cytokine Network*, 21(1), pp.1–6.
Elbim, C., Katsikis, P.D. & Estaquier, J., 2009. Neutrophil apoptosis during viral infections. *The Open Virology Journal*, 3, pp.52–59.
Elks, P.M. et al., 2011. Activation of hypoxia-inducible factor-1alpha (Hif-1alpha) delays inflammation resolution by reducing neutrophil apoptosis and reverse migration in a zebrafish inflammation model. *Blood*, 118(3), pp.712–722.
Ellett, F. et al., 2011. mpeg1 promoter transgenes direct macrophage-lineage expression in zebrafish. *Blood*, 117(4), pp.e49–56.
Engler, C. et al., 2009. Golden gate shuffling: a one-pot DNA shuffling method based on type IIs restriction enzymes. *PloS One*, 4(5), p.e5553.
Fadeel, B. & Grzybowska, E., 2009. HAX-1: a multifunctional protein with emerging roles in human disease. *Biochimica et Biophysica Acta*, 1790(10), pp.1139–1148.
Fadok, V.A. et al., 1998. Macrophages that have ingested apoptotic cells in vitro inhibit proinflammatory cytokine production through autocrine/paracrine mechanisms involving TGF-beta, PGE2, and PAF. *The Journal of Clinical Investigation*, 101(4), pp.890–898.
Fecho, K. & Cohen, P.L., 1998. Fas ligand (gld)- and Fas (lpr)-deficient mice do not show alterations in the extravasation or apoptosis of inflammatory neutrophils. *Journal of Leukocyte Biology*, 64(3), pp.373–383.
Filep, J.G. & El Kebir, D., 2009. Neutrophil apoptosis: a target for enhancing the resolution of inflammation. *Journal of Cellular Biochemistry*, 108(5), pp.1039–1046.
Foley, J.E. et al., 2009. Rapid mutation of endogenous zebrafish genes using zinc finger nucleases made by Oligomerized Pool ENgineering (OPEN). *PloS One*, 4(2), p.e4348.
Fossati, G. et al., 2003. The mitochondrial network of human neutrophils: role in chemotaxis, phagocytosis, respiratory burst activation, and commitment to apoptosis. *Journal of Immunology*, 170(4), pp.1964–1972.
Fouret, P. et al., 1989. Expression of the neutrophil elastase gene during human bone marrow cell differentiation. *The Journal of Experimental Medicine*, 169(3), pp.833–845.
Foxman, E.F., Kunkel, E.J. & Butcher, E.C., 1999. Integrating conflicting chemotactic signals. The role of memory in leukocyte navigation. *Journal of Cell Biology*, 147(3), pp.577–588.
Franklin, W. et al., 1956. Chronic obstructive pulmonary emphysema; a disease of smokers. *Annals of Internal Medicine*, 45(2), pp.268–274.
Fuentes-Prior, P. & Salvesen, G.S., 2004. The protein structures that shape caspase activity, specificity, activation and inhibition. *The Biochemical Journal*, 384(Pt 2), pp.201–232.
Furmanski, P. & Li, Z.P., 1990. Multiple forms of lactoferrin in normal and leukemic human granulocytes. *Experimental Hematology*, 18(8), pp.932–935.
Furze, R.C. & Rankin, S.M., 2008. The role of the bone marrow in neutrophil clearance under homeostatic conditions in the mouse. *Federation of American Societies for Experimental Biology Journal*, 22(9), pp.3111–3119.

Gallagher, A.R. et al., 2000. The polycystic kidney disease protein PKD2 interacts with Hax-1, a protein associated with the actin cytoskeleton. *Proceedings of the National Academy of Sciences of the United States of America*, 97(8), pp.4017–4022.

Gallin, J.I., 1984. Human neutrophil heterogeneity exists, but is it meaningful? *Blood*, 63(5), pp.977–983.

Gallucci, S. & Matzinger, P., 2001. Danger signals: SOS to the immune system. *Current Opinion in Immunology*, 13(1), pp.114–119.

Gerber, J.S. & Mosser, D.M., 2001. Reversing lipopolysaccharide toxicity by ligating the macrophage Fc gamma receptors. *Journal of Immunology*, 166(11), pp.6861–6868.

Germeshausen, M. et al., 2008. Novel HAX1 mutations in patients with severe congenital neutropenia reveal isoform-dependent genotype-phenotype associations. *Blood*, 111(10), pp.4954–4957.

Giacomello, M. et al., 2007. Mitochondrial Ca2+ as a key regulator of cell life and death. *Cell Death and Differentiation*, 14(7), pp.1267–1274.

Gilroy, D.W. et al., 2004. Inflammatory resolution: new opportunities for drug discovery. *Nature Reviews Drug Discovery*, 3(5), pp.401–416.

Glasser, L. & Fiederlein, R.L., 1987. Functional differentiation of normal human neutrophils. *Blood*, 69(3), pp.937–944.

Gong, J., Li, X. & Darzynkiewicz, Z., 1993. Different patterns of apoptosis of HL-60 cells induced by cycloheximide and camptothecin. *Journal of Cellular Physiology*, 157, pp.263–270.

Green, D.R. & Kroemer, G., 2004. The pathophysiology of mitochondrial cell death. *Science*, 305(5684), pp.626–629.

Grenda, D.S. et al., 2002. Mice expressing a neutrophil elastase mutation derived from patients with severe congenital neutropenia have normal granulopoiesis. *Blood*, 100(9), pp.3221–3228.

Grzybowska, E.A. et al., 2006. Identification and expression analysis of alternative splice variants of the rat Hax-1 gene. *Gene*, 371(1), pp.84–92.

Haddy, T.B., Rana, S.R. & Castro, O., 1999. Benign ethnic neutropenia: what is a normal absolute neutrophil count? *The Journal of Laboratory and Clinical Medicine*, 133(1), pp.15–22.

Hakem, R. et al., 1998. Differential requirement for caspase 9 in apoptotic pathways in vivo. *Cell*, 94(3), pp.339–352.

Hamasaki, A. et al., 1998. Accelerated neutrophil apoptosis in mice lacking A1-a, a subtype of the bcl-2-related A1 gene. *The Journal of Experimental Medicine*, 188(11), pp.1985–1992.

Hammerschmidt, M., Blader, P. & Strahle, U., 1999. Strategies to perturb zebrafish development. *Methods in Cell Biology*, 59, pp.87–115.

Han, J. et al., 2010. Deregulation of mitochondrial membrane potential by mitochondrial insertion of granzyme B and direct Hax-1 cleavage. *The Journal of Biological Chemistry*, 285(29), pp.22461–22472.

Han, Y. et al., 2006. Overexpression of HAX-1 protects cardiac myocytes from apoptosis through caspase-9 inhibition. *Circulation Research*, 99(4), pp.415–423.

Handel, E.M., Alwin, S. & Cathomen, T., 2009. Expanding or restricting the target site repertoire of zinc-finger nucleases: the inter-domain linker as a major determinant of target site selectivity. *Molecular therapy : the Journal of the American Society of Gene Therapy*, 17(1), pp.104–111.

Harlin, H. et al., 2001. Characterization of XIAP-deficient mice. *Molecular and Cellular Biology*, 21(10), pp.3604–3608.
Haslett, C. et al., 1994. Granulocyte apoptosis and the control of inflammation. *Philosophical Transactions of the Royal Society of London. Series B, Biological Sciences*, 345(1313), pp.327–333.
Haylock, D.N. et al., 1992. Ex vivo expansion and maturation of peripheral blood CD34+ cells into the myeloid lineage. *Blood*, 80(6), pp.1405–1412.
Hippe, A. et al., 2006. Expression and tissue distribution of mouse Hax1. *Gene*, 379, pp.116–126.
Homburg, C.H. et al., 1995. Human neutrophils lose their surface Fc gamma RIII and acquire Annexin V binding sites during apoptosis in vitro. *Blood*, 85(2), pp.532–540.
Huynh, M.L., Fadok, V.A. & Henson, P.M., 2002. Phosphatidylserine-dependent ingestion of apoptotic cells promotes TGF-beta1 secretion and the resolution of inflammation. *The Journal of Clinical Investigation*, 109(1), pp.41–50.
Hwang, W.Y. et al., 2013. Efficient genome editing in zebrafish using a CRISPR-Cas system. *Nature Biotechnology*, 31(3), pp.227–229.
Imai, Y. & Talbot, W.S., 2001. Morpholino phenocopies of the bmp2b/swirl and bmp7/snailhouse mutations. *Genesis*, 30(3), pp.160–163.
Isalan, M., Choo, Y. & Klug, A., 1997. Synergy between adjacent zinc fingers in sequence-specific DNA recognition. *Proceedings of the National Academy of Sciences of the United States of America*, 94(11), pp.5617–5621.
Isalan, M., Klug, A. & Choo, Y., 1998. Comprehensive DNA recognition through concerted interactions from adjacent zinc fingers. *Biochemistry*, 37(35), pp.12026–12033.
Janeway Jr., C.A. & Medzhitov, R., 2002. Innate immune recognition. *Annual Review of Immunology*, 20, pp.197–216.
Jeyaraju, D. V et al., 2009. Hax1 lacks BH modules and is peripherally associated to heavy membranes: implications for Omi/HtrA2 and PARL activity in the regulation of mitochondrial stress and apoptosis. *Cell death and differentiation*, 16(12), pp.1622–1629.
Jitkaew, S. et al., 2009. N(alpha)-tosyl-L-phenylalanine chloromethyl ketone induces caspase-dependent apoptosis in transformed human B cell lines with transcriptional down-regulation of anti-apoptotic HS1-associated protein X-1. *The Journal of Biological Chemistry*, 284(41), pp.27827–27837.
Jones, J.M. et al., 2003. Loss of Omi mitochondrial protease activity causes the neuromuscular disorder of mnd2 mutant mice. *Nature*, 425(6959), pp.721–727.
Kane, D.A. & Kimmel, C.B., 1993. The zebrafish midblastula transition. *Development*, 119(2), pp.447–456.
Kang, Y.J. et al., 2010. Molecular interaction between HAX-1 and XIAP inhibits apoptosis. *Biochemical and Biophysical Research Communications*, 393(4), pp.794–799.
Kariko, K. et al., 2004. mRNA is an endogenous ligand for Toll-like receptor 3. *The Journal of Biological Chemistry*, 279(13), pp.12542–12550.
Kawaguchi, Y. et al., 2000. Interaction of Epstein-Barr virus nuclear antigen leader protein (EBNA-LP) with HS1-associated protein X-1: implication of

cytoplasmic function of EBNA-LP. *Journal of Virology*, 74(21), pp.10104–10111.
Kawai, T. & Akira, S., 2007. Antiviral signaling through pattern recognition receptors. *Journal of Biochemistry*, 141(2), pp.137–145.
El Kebir, D. & Filep, J.G., 2010. Role of neutrophil apoptosis in the resolution of inflammation. *The Scientific World Journal*, 10, pp.1731–1748.
Kerr, J.F., Wyllie, A.H. & Currie, A.R., 1972. Apoptosis: a basic biological phenomenon with wide-ranging implications in tissue kinetics. *BrItish Journal of Cancer*, 26(4), pp.239–257.
Kim, H.J. et al., 2009. Targeted genome editing in human cells with zinc finger nucleases constructed via modular assembly. *Genome Research*, 19(7), pp.1279–1288.
Kim, J.S., Lee, H.J. & Carroll, D., 2010. Genome editing with modularly assembled zinc-finger nucleases. *Nature Methods*, 7(2), p.91; author reply 91–2.
Kim, Y.G., Cha, J. & Chandrasegaran, S., 1996. Hybrid restriction enzymes: zinc finger fusions to Fok I cleavage domain. *Proceedings of the National Academy of Sciences of the United States of America*, 93(3), pp.1156–1160.
Kischkel, F.C. et al., 1995. Cytotoxicity-dependent APO-1 (Fas/CD95)-associated proteins form a death-inducing signaling complex (DISC) with the receptor. *The European Molecular Biology Organization Journal*, 14(22), pp.5579–5588.
Kjeldsen, L. et al., 1992. Subcellular localization and release of human neutrophil gelatinase, confirming the existence of separate gelatinase-containing granules. *The Biochemical Journal*, 287 (Pt 2, pp.603–610.
Klebanoff, S.J., 1968. Myeloperoxidase-halide-hydrogen peroxide antibacterial system. *Journal of Bacteriology*, 95(6), pp.2131–2138.
Klein, C. et al., 2007. HAX1 deficiency causes autosomal recessive severe congenital neutropenia (Kostmann disease). *Nature Genetics*, 39(1), pp.86–92.
Klein, J.B. et al., 2000. Granulocyte-macrophage colony-stimulating factor delays neutrophil constitutive apoptosis through phosphoinositide 3-kinase and extracellular signal-regulated kinase pathways. *Journal of Immunology*, 164, pp.4286–4291.
Kluck, R.M. et al., 1997. The release of cytochrome c from mitochondria: a primary site for Bcl-2 regulation of apoptosis. *Science*, 275(5303), pp.1132–1136.
Kobayashi, K.S. et al., 2005. Nod2-dependent regulation of innate and adaptive immunity in the intestinal tract. *Science*, 307(5710), pp.731–734.
Kobayashi, S.D. et al., 2003. Bacterial pathogens modulate an apoptosis differentiation program in human neutrophils. *Proceedings of the National Academy of Sciences of the United States of America*, 100(19), pp.10948–10953.
Kobayashi, S.D. et al., 2005. Spontaneous neutrophil apoptosis and regulation of cell survival by granulocyte macrophage-colony stimulating factor. *Journal of Leukocyte Biology*, 78(6), pp.1408–1418.
Koenderman, L. et al., 2000. Monitoring of neutrophil priming in whole blood by antibodies isolated from a synthetic phage antibody library. *Journal of Leukocyte Biology*, 68(1), pp.58–64.

Kokoszynska, K., Rychlewski, L. & Wyrwicz, L.S., 2010. Distant homologs of anti-apoptotic factor HAX1 encode parvalbumin-like calcium binding proteins. *BioMed Central Research Notes*, 3, p.197.

Koontz, J. & Kontrogianni-Konstantopoulos, A., 2014. Competition through dimerization between antiapoptotic and proapoptotic HS-1-associated protein X-1 (Hax-1). *The Journal of Biological Chemistry*, 289(6), pp.3468–3477.

Korchak, H.M. et al., 1983. Granulocytes without degranulation: neutrophil function in granule-depleted cytoplasts. *Proceedings of the National Academy of Sciences of the United States of America*, 80(16), pp.4968–4972.

Kotecha, S. et al., 2003. The role of neutrophil apoptosis in the resolution of acute lung injury in newborn infants. *Thorax*, 58(11), pp.961–967.

Kotz, K.T. et al., 2010. Clinical microfluidics for neutrophil genomics and proteomics. *Nature Medicine*, 16, pp.1042–1047.

Kratz, E. et al., 2006. Functional characterization of the Bcl-2 gene family in the zebrafish. *Cell Death and Differentiation*, 13(10), pp.1631–1640.

Kroemer, G. et al., 2005. Classification of cell death: recommendations of the Nomenclature Committee on Cell Death. *Cell Death and Differentiation*, 12 Suppl 2, pp.1463–1467.

Kumar, V. & Sharma, A., 2010. Neutrophils: Cinderella of innate immune system. *International Immunopharmacology*, 10, pp.1325–1334.

Lam, S.H. et al., 2004. Development and maturation of the immune system in zebrafish, Danio rerio: a gene expression profiling, in situ hybridization and immunological study. *Developmental and Comparative Immunology*, 28(1), pp.9–28.

Lavrik, I. et al., 2003. The active caspase-8 heterotetramer is formed at the CD95 DISC. *Cell Death and Differentiation*, 10(1), pp.144–145.

Lawrence, M.B. & Springer, T.A., 1991. Leukocytes roll on a selectin at physiologic flow rates: distinction from and prerequisite for adhesion through integrins. *Cell*, 65(5), pp.859–873.

Lawrence, M.B. & Springer, T.A., 1993. Neutrophils roll on E-selectin. *Journal of Immunology*, 151(11), pp.6338–6346.

Lazarus, G.S. et al., 1968. Human granulocyte collagenase. *Science*, 159(3822), pp.1483–1485.

Lee, A., Whyte, M.K. & Haslett, C., 1993. Inhibition of apoptosis and prolongation of neutrophil functional longevity by inflammatory mediators. *Journal of Leukocyte Biology*, 54(4), pp.283–288.

Lee, A.Y. et al., 2008. HS 1-associated protein X-1 is cleaved by caspase-3 during apoptosis. *Molecules & Cells*, 25(1), pp.86–90.

Lee, H.J., Kim, E. & Kim, J.S., 2010. Targeted chromosomal deletions in human cells using zinc finger nucleases. *Genome Research*, 20(1), pp.81–89.

Lees, D.M., Hart, I.R. & Marshall, J.F., 2008. Existence of multiple isoforms of HS1-associated protein X-1 in murine and human tissues. *Journal of Molecular Biology*, 379(4), pp.645–655.

Li, B. et al., 2012. Hax-1 is rapidly degraded by the proteasome dependent on its PEST sequence. *BioMed Central Cell Biology*, 13, p.20.

Li, T. et al., 2011. Modularly assembled designer TAL effector nucleases for targeted gene knockout and gene replacement in eukaryotes. *Nucleic Acids Research*, 39(14), pp.6315–6325.

Li, W.B. et al., 2009. Induction of apoptosis by Hax-1 siRNA in melanoma cells. *Cell Biology International*, 33(4), pp.548–554.
Lieschke, G.J. et al., 2001. Morphologic and functional characterization of granulocytes and macrophages in embryonic and adult zebrafish. *Blood*, 98(10), pp.3087–3096.
Lieschke, G.J., 2001. Zebrafish--an emerging genetic model for the study of cytokines and hematopoiesis in the era of functional genomics. *International Journal of Hematology*, 73(1), pp.23–31.
Lieschke, G.J. & Currie, P.D., 2007. Animal models of human disease: zebrafish swim into view. *Nature Reviews. Genetics*, 8(5), pp.353–367.
Liles, W.C. et al., 1996. Differential expression of Fas (CD95) and Fas ligand on normal human phagocytes: implications for the regulation of apoptosis in neutrophils. *The Journal of Experimental Medicine*, 184(2), pp.429–440.
Liu, X. et al., 1996. Induction of apoptotic program in cell-free extracts: requirement for dATP and cytochrome c. *Cell*, 86(1), pp.147–157.
Locksley, R.M., Killeen, N. & Lenardo, M.J., 2001. The TNF and TNF receptor superfamilies: integrating mammalian biology. *Cell*, 104(4), pp.487–501.
Lollike, K. et al., 1995. Lysozyme in human neutrophils and plasma. A parameter of myelopoietic activity. *Leukemia*, 9(1), pp.159–164.
Lomas, H. et al., 2008. Non-cytotoxic polymer vesicles for rapid and efficient intracellular delivery. *Faraday Discussions*, 139, pp.128–143,419–420.
Lotz, S. et al., 2004. Highly purified lipoteichoic acid activates neutrophil granulocytes and delays their spontaneous apoptosis via CD14 and TLR2. *Journal of Leukocyte Biology*, 75(3), pp.467–477.
Luo, H.R. & Loison, F., 2008. Constitutive neutrophil apoptosis: mechanisms and regulation. *American Journal of Hematology*, 83(4), pp.288–295.
Maeder, M.L. et al., 2008. Rapid “open-source” engineering of customized zinc-finger nucleases for highly efficient gene modification. *Molecular Cell*, 31(2), pp.294–301.
Maianski, N.A. et al., 2004. Functional characterization of mitochondria in neutrophils: a role restricted to apoptosis. *Cell Death and Differentiation*, 11(2), pp.143–153.
Maianski, N.A. et al., 2002. Granulocyte colony-stimulating factor inhibits the mitochondria-dependent activation of caspase-3 in neutrophils. *Blood*, 99(2), pp.672–679.
Martin, J.S. & Renshaw, S.A., 2009. Using in vivo zebrafish models to understand the biochemical basis of neutrophilic respiratory disease. *Biochemical Society Transactions*, 37, pp.830–837.
Martin, T.R. et al., 1985. The effects of chronic bronchitis and chronic air-flow obstruction on lung cell populations recovered by bronchoalveolar lavage. *The American Review of Respiratory Disease*, 132(2), pp.254–260.
Martinez, J. et al., 2002. Single-stranded antisense siRNAs guide target RNA cleavage in RNAi. *Cell*, 110, pp.563–574.
Mathias, J.R. et al., 2006. Resolution of inflammation by retrograde chemotaxis of neutrophils in transgenic zebrafish. *Journal of Leukocyte Biology*, 80(6), pp.1281–1288.
Matsubara, K. et al., 2007. Severe developmental delay and epilepsy in a Japanese patient with severe congenital neutropenia due to HAX1 deficiency. *Haematologica*, 92(12), pp.e123–5.

Matsumoto, T. et al., 1997. Pivotal role of interleukin-8 in the acute respiratory distress syndrome and cerebral reperfusion injury. *Journal of Leukocyte Biology*, 62(5), pp.581–587.
Matute-Bello, G. et al., 1997. Neutrophil apoptosis in the acute respiratory distress syndrome. *American Journal of Respiratory and Critical Care Medicine*, 156(6), pp.1969–1977.
McDonald, B. et al., 2010. Intravascular danger signals guide neutrophils to sites of sterile inflammation. *Science*, 330(6002), pp.362–366.
McEver, R.P. & Cummings, R.D., 1997. Perspectives series: cell adhesion in vascular biology. Role of PSGL-1 binding to selectins in leukocyte recruitment. *The Journal of Clinical Investigation*, 100(3), pp.485–491.
Medzhitov, R., 2010. Inflammation 2010: new adventures of an old flame. *Cell*, 140(6), pp.771–776.
Medzhitov, R., 2008. Origin and physiological roles of inflammation. *Nature*, 454(7203), pp.428–435.
Medzhitov, R., 2001. Toll-like receptors and innate immunity. *Nature Reviews. Immunology*, 1(2), pp.135–145.
Melley, D.D., Evans, T.W. & Quinlan, G.J., 2005. Redox regulation of neutrophil apoptosis and the systemic inflammatory response syndrome. *Clinical Science*, 108(5), pp.413–424.
Meng, X. et al., 2008. Targeted gene inactivation in zebrafish using engineered zinc-finger nucleases. *Nature Biotechnology*, 26(6), pp.695–701.
Miller, J.C. et al., 2011. A TALE nuclease architecture for efficient genome editing. *Nature Biotechnology*, 29(2), pp.143–148.
Miller, J.C. et al., 2007. An improved zinc-finger nuclease architecture for highly specific genome editing. *Nature Biotechnology*, 25(7), pp.778–785.
Mirmohammadsadegh, A. et al., 2003. HAX-1, identified by differential display reverse transcription polymerase chain reaction, is overexpressed in lesional psoriasis. *The Journal of Investigative Dermatology*, 120(6), pp.1045–1051.
Modem, S. & Reddy, T.R., 2008. An anti-apoptotic protein, Hax-1, inhibits the HIV-1 rev function by altering its sub-cellular localization. *Journal of Cellular Physiology*, 214(1), pp.14–19.
Mohr, W., Kohler, G. & Wessinghage, D., 1981. Polymorphonuclear granulocytes in rheumatic tissue destruction. II. Demonstration of PMNs in rheumatoid nodules by electron microscopy. *Rheumatology International*, 1(1), pp.21–28.
Moore, F.E. et al., 2012. Improved somatic mutagenesis in zebrafish using transcription activator-like effector nucleases (TALENs). *PloS One*, 7(5), p.e37877.
Moore, K.L. et al., 1995. P-selectin glycoprotein ligand-1 mediates rolling of human neutrophils on P-selectin. *Journal of Cell Biology*, 128(4), pp.661–671.
Moriceau, S., Lenoir, G. & Witko-Sarsat, V., 2010. In cystic fibrosis homozygotes and heterozygotes, neutrophil apoptosis is delayed and modulated by diamide or roscovitine: evidence for an innate neutrophil disturbance. *Journal of Innate Immunity*, 2(3), pp.260–266.
Morishima, T. et al., 2013. Genetic correction of HAX1 in induced pluripotent stem cells from a patient with severe congenital neutropenia improves defective granulopoiesis. *Haematologica*, 99(1), pp.19–27.

Motoyama, N. et al., 1995. Massive cell death of immature hematopoietic cells and neurons in Bcl-x-deficient mice. *Science*, 267(5203), pp.1506–1510.
Moulding, D.A. et al., 2001. BCL-2 family expression in human neutrophils during delayed and accelerated apoptosis. *Journal of Leukocyte Biology*, 70(5), pp.783–792.
Moulding, D.A. et al., 1998. Mcl-1 expression in human neutrophils: regulation by cytokines and correlation with cell survival. *Blood*, 92(7), pp.2495–2502.
Muhlrad, D. & Parker, R., 1994. Premature translational termination triggers mRNA decapping. *Nature*, 370(6490), pp.578–581.
Muller, W.A. et al., 1993. PECAM-1 is required for transendothelial migration of leukocytes. *The Journal of Experimental Medicine*, 178(2), pp.449–460.
Mussolino, C. et al., 2011. A novel TALE nuclease scaffold enables high genome editing activity in combination with low toxicity. *Nucleic Acids Research*, 39(21), pp.9283–9293.
Nasevicius, A. & Ekker, S.C., 2000. Effective targeted gene “knockdown” in zebrafish. *Nature Genetics*, 26(2), pp.216–220.
Nathan, C., 2006. Neutrophils and immunity: challenges and opportunities. *Nature reviews. Immunology*, 6(3), pp.173–182.
Nathan, C.F., 1987. Neutrophil activation on biological surfaces. Massive secretion of hydrogen peroxide in response to products of macrophages and lymphocytes. *The Journal of Clinical Investigation*, 80(6), pp.1550–1560.
Nobes, C.D. & Hall, A., 1999. Rho GTPases control polarity, protrusion, and adhesion during cell movement. *Journal of Cell Biology*, 144(6), pp.1235–1244.
Oltvai, Z.N., Milliman, C.L. & Korsmeyer, S.J., 1993. Bcl-2 heterodimerizes in vivo with a conserved homolog, Bax, that accelerates programmed cell death. *Cell*, 74(4), pp.609–619.
Oudijk, E.J. et al., 2006. Expression of priming-associated cellular markers on neutrophils during an exacerbation of COPD. *Respiratory Medicine*, 100(10), pp.1791–1799.
Owen, C.A. & Campbell, E.J., 1999. The cell biology of leukocyte-mediated proteolysis. *Journal of Leukocyte Biology*, 65(2), pp.137–150.
Pesci, A. et al., 1998. Neutrophils infiltrating bronchial epithelium in chronic obstructive pulmonary disease. *Respiratory Medicine*, 92(6), pp.863–870.
Pham, C.T., 2006. Neutrophil serine proteases: specific regulators of inflammation. *Nature Reviews. Immunology*, 6(7), pp.541–550.
Phillips, M.L. et al., 1995. Neutrophil adhesion in leukocyte adhesion deficiency syndrome type 2. *The Journal of Clinical Investigation*, 96(6), pp.2898–2906.
Pletz, M.W. et al., 2004. Reduced spontaneous apoptosis in peripheral blood neutrophils during exacerbation of COPD. *European Respiratory Journal*, 23(4), pp.532–537.
Premack, B.A. & Schall, T.J., 1996. Chemokine receptors: gateways to inflammation and infection. *Nature Medicine*, 2(11), pp.1174–1178.
Provost, E., Rhee, J. & Leach, S.D., 2007. Viral 2A peptides allow expression of multiple proteins from a single ORF in transgenic zebrafish embryos. *Genesis*, 45(10), pp.625–629.

Quinn, M.T. & Gauss, K.A., 2004. Structure and regulation of the neutrophil respiratory burst oxidase: comparison with nonphagocyte oxidases. *Journal of Leukocyte Biology*, 76(4), pp.760–781.

Van Raam, B.J., Verhoeven, A.J. & Kuijpers, T.W., 2006. Mitochondria in neutrophil apoptosis. *International Journal of Hematology*, 84(3), pp.199–204.

Radhika, V. et al., 2004. Galpha13 stimulates cell migration through cortactin-interacting protein Hax-1. *The Journal of Biological Chemistry*, 279(47), pp.49406–49413.

Ramsay, A.G. et al., 2007. HS1-associated protein X-1 regulates carcinoma cell migration and invasion via clathrin-mediated endocytosis of integrin alphavbeta6. *Cancer Research*, 67(11), pp.5275–5284.

Rather, L.J., 1971. Disturbance of function (functio laesa): the legendary fifth cardinal sign of inflammation, added by Galen to the four cardinal signs of Celsus. *Bulletin of the New York Academy of Medicine*, 47(3), pp.303–322.

Renshaw, S.A. et al., 2006. A transgenic zebrafish model of neutrophilic inflammation. *Blood*, 108(13), pp.3976–3978.

Renshaw, S.A. et al., 2000. Inflammatory neutrophils retain susceptibility to apoptosis mediated via the Fas death receptor. *Journal of Leukocyte Biology*, 67(5), pp.662–668.

Rinkenberger, J.L. et al., 2000. Mcl-1 deficiency results in peri-implantation embryonic lethality. *Genes & Development*, 14(1), pp.23–27.

Robu, M.E. et al., 2007. p53 activation by knockdown technologies. *PLoS Genetics*, 3(5), p.e78.

Sabroe, I. et al., 2002. Toll-like receptor (TLR)2 and TLR4 in human peripheral blood granulocytes: a critical role for monocytes in leukocyte lipopolysaccharide responses. *Journal of Immunology*, 168(9), pp.4701–4710.

Sander, J.D. et al., 2011. Selection-free zinc-finger-nuclease engineering by context-dependent assembly (CoDA). *Nature Methods*, 8(1), pp.67–69.

Van Der Sar, A.M. et al., 2006. MyD88 innate immune function in a zebrafish embryo infection model. *Infection and Immunity*, 74, pp.2436–2441.

Sarnowska, E. et al., 2007. Hairpin structure within the 3'UTR of DNA polymerase beta mRNA acts as a post-transcriptional regulatory element and interacts with Hax-1. *Nucleic Acids Research*, 35(16), pp.5499–5510.

Savill, J. et al., 2002. A blast from the past: clearance of apoptotic cells regulates immune responses. *Nature Reviews. Immunology*, 2(12), pp.965–975.

Savill, J., 1997. Apoptosis in resolution of inflammation. *Journal of Leukocyte Biology*, 61(4), pp.375–380.

Savill, J. et al., 1993. Phagocyte recognition of cells undergoing apoptosis. *Immunology Today*, 14(3), pp.131–136.

Savill, J. et al., 1990. Vitronectin receptor-mediated phagocytosis of cells undergoing apoptosis. *Nature*, 343(6254), pp.170–173.

Savill, J. & Haslett, C., 1995. Granulocyte clearance by apoptosis in the resolution of inflammation. *Seminars in Cell Biology*, 6(6), pp.385–393.

Savill, J.S., Wyllie, A.H., et al., 1989. Macrophage phagocytosis of aging neutrophils in inflammation. Programmed cell death in the neutrophil leads to its recognition by macrophages. *The Journal of Clinical Investigation*, 83(3), pp.865–875.

Savill, J.S., Henson, P.M. & Haslett, C., 1989. Phagocytosis of aged human neutrophils by macrophages is mediated by a novel “charge-sensitive” recognition mechanism. *The Journal of Clinical Investigation*, 84(5), pp.1518–1527.

Scaffidi, C. et al., 1998. Two CD95 (APO-1/Fas) signaling pathways. *The European Molecular Biology Organization Journal*, 17(6), pp.1675–1687.

Semerad, C.L. et al., 2002. G-CSF is an essential regulator of neutrophil trafficking from the bone marrow to the blood. *Immunity*, 17(4), pp.413–423.

Sharp, T. V et al., 2002. K15 protein of Kaposi’s sarcoma-associated herpesvirus is latently expressed and binds to HAX-1, a protein with antiapoptotic function. *Journal of Virology*, 76(2), pp.802–816.

Shendure, J. & Ji, H., 2008. Next-generation DNA sequencing. *Nature Biotechnology*, 26(10), pp.1135–1145.

Shi, J. et al., 2001. Role of the liver in regulating numbers of circulating neutrophils. *Blood*, 98(4), pp.1226–1230.

Shimizu, S., Narita, M. & Tsujimoto, Y., 1999. Bcl-2 family proteins regulate the release of apoptogenic cytochrome c by the mitochondrial channel VDAC. *Nature*, 399(6735), pp.483–487.

Shimizu, Y., Bhakta, M.S. & Segal, D.J., 2009. Restricted spacer tolerance of a zinc finger nuclease with a six amino acid linker. *Bioorganic & Medicinal Chemistry Letters*, 19(14), pp.3970–3972.

Siamakpour-Reihani, S. et al., 2010. Grb7 binds to Hax-1 and undergoes an intramolecular domain association that offers a model for Grb7 regulation. *Journal of Molecular Recognition*.

Silva, M.T., 2010. When two is better than one: macrophages and neutrophils work in concert in innate immunity as complementary and cooperative partners of a myeloid phagocyte system. *Journal of Leukocyte Biology* , 87 (1), pp.93–106.

Slayton, W.B. et al., 1998. The first-appearance of neutrophils in the human fetal bone marrow cavity. *Early Human Development*, 53(2), pp.129–144.

Sligh Jr., J.E. et al., 1993. Inflammatory and immune responses are impaired in mice deficient in intercellular adhesion molecule 1. *Proceedings of the National Academy of Sciences of the United States of America*, 90(18), pp.8529–8533.

Smith, J.A., 1994. Neutrophils, host defense, and inflammation: a double-edged sword. *Journal of Leukocyte Biology*, 56(6), pp.672–686.

Southgate, E.L. et al., 2008. Identification of formyl peptides from Listeria monocytogenes and Staphylococcus aureus as potent chemoattractants for mouse neutrophils. *Journal of Immunology*, 181(2), pp.1429–1437.

Spitznagel, J.K., 1990. Antibiotic proteins of human neutrophils. *The Journal of Clinical Investigation*, 86(5), pp.1381–1386.

Springer, T.A., 1994. Traffic signals for lymphocyte recirculation and leukocyte emigration: the multistep paradigm. *Cell*, 76(2), pp.301–314.

Srinivasula, S.M. & Ashwell, J.D., 2008. IAPs: what’s in a name? *Molecular Cell*, 30(2), pp.123–135.

Stainier, D.Y., Lee, R.K. & Fishman, M.C., 1993. Cardiovascular development in the zebrafish. I. Myocardial fate map and heart tube formation. *Development*, 119(1), pp.31–40.

Stein, C. et al., 2007. Conservation and divergence of gene families encoding components of innate immune response systems in zebrafish. *Genome Biology*, 8(11), p.R251.

Stewart, M. & Hogg, N., 1996. Regulation of leukocyte integrin function: affinity vs. avidity. *Journal of Cellular Biochemistry*, 61(4), pp.554–561.

Sumagin, R. & Sarelius, I.H., 2010. Intercellular adhesion molecule-1 enrichment near tricellular endothelial junctions is preferentially associated with leukocyte transmigration and signals for reorganization of these junctions to accommodate leukocyte passage. *Journal of Immunology*, 184(9), pp.5242–5252.

Summers, C. et al., 2010. Neutrophil kinetics in health and disease. *Trends in Immunology*, 31(8), pp.318–324.

Sun, S.J. et al., 2012. HAX-1 promotes the chemoresistance, invasion, and tumorigenicity of esophageal squamous carcinoma cells. *Digestive Diseases and Sciences*, 57(7), pp.1838–1846.

Susin, S.A. et al., 1996. Bcl-2 inhibits the mitochondrial release of an apoptogenic protease. *The Journal of Experimental Medicine*, 184(4), pp.1331–1341.

Suzuki, Y. et al., 1997. HAX-1, a novel intracellular protein, localized on mitochondria, directly associates with HS1, a substrate of Src family tyrosine kinases. *Journal of Immunology*, 158(6), pp.2736–2744.

Swain, S.D., Rohn, T.T. & Quinn, M.T., 2002. Neutrophil priming in host defense: role of oxidants as priming agents. *Antioxidants & Redox Signaling*, 4(1), pp.69–83.

Szczepek, M. et al., 2007. Structure-based redesign of the dimerization interface reduces the toxicity of zinc-finger nucleases. *Nature Biotechnology*, 25(7), pp.786–793.

Takeda, K., Kaisho, T. & Akira, S., 2003. Toll-like receptors. *Annual Review of Immunology*, 21, pp.335–376.

Takeuchi, O. & Akira, S., 2010. Pattern Recognition Receptors and Inflammation. *Cell*, 140, pp.805–820.

Tanaka, S. et al., 1998. A novel variant of human Grb7 is associated with invasive esophageal carcinoma. *The Journal of Clinical Investigation*, 102(4), pp.821–827.

Taneja, R. et al., 2004. Delayed neutrophil apoptosis in sepsis is associated with maintenance of mitochondrial transmembrane potential and reduced caspase-9 activity. *Critical Care Medicine*, 32(7), pp.1460–1469.

Theilgaard-Mönch, K. et al., 2005. The transcriptional program of terminal granulocytic differentiation. *Blood*, 105, pp.1785–1796.

Thelen, M. & Didichenko, S.A., 1997. G-protein coupled receptor-mediated activation of PI 3-kinase in neutrophils. *Annals of the New York Academy of Sciences*, 832, pp.368–382.

Trebinska, A. et al., 2014. Exploring the anti-apoptotic role of HAX-1 versus BCL-X in cytokine-dependent bone marrow-derived cells from mice. *Federation of European Biochemical Societies Letters*.

Trebinska, A. et al., 2010. HAX-1 overexpression, splicing and cellular localization in tumors. *BioMed Central Cancer*, 10, p.76.

Trede, N.S. et al., 2004. The use of zebrafish to understand immunity. *Immunity*, 20(4), pp.367–379.

Tsujimoto, Y. & Croce, C.M., 1986. Analysis of the structure, transcripts, and protein products of bcl-2, the gene involved in human follicular lymphoma.

Proceedings of the National Academy of Sciences of the United States of America, 83(14), pp.5214–5218.
Tucker, K.A. et al., 1987. Characterization of a new human diploid myeloid leukemia cell line (PLB-985) with granulocytic and monocytic differentiating capacity. *Blood*, 70, pp.372–378.
Turner, D.L. & Weintraub, H., 1994. Expression of achaete-scute homolog 3 in Xenopus embryos converts ectodermal cells to a neural fate. *Genes & Development*, 8(12), pp.1434–1447.
Usher, L.R. et al., 2002. Induction of neutrophil apoptosis by the Pseudomonas aeruginosa exotoxin pyocyanin: a potential mechanism of persistent infection. *Journal of Immunology*, 168(4), pp.1861–1868.
Vafiadaki *, E. et al., 2009. The anti-apoptotic protein HAX-1 interacts with SERCA2 and regulates its protein levels to promote cell survival. *Molecular Biology of the Cell*, 20(1), pp.306–318.
Vafiadaki, E. et al., 2007. Phospholamban interacts with HAX-1, a mitochondrial protein with anti-apoptotic function. *Journal of Molecular Biology*, 367(1), pp.65–79.
Vafiadaki, E. et al., 2009. The role of SERCA2a/PLN complex, Ca(2+) homeostasis, and anti-apoptotic proteins in determining cell fate. *Pflugers Archiv European Journal of Physiology*, 457(3), pp.687–700.
Veis, D.J. et al., 1993. Expression of the Bcl-2 protein in murine and human thymocytes and in peripheral T lymphocytes. *Journal of Immunology*, 151(5), pp.2546–2554.
Verhagen, A.M. et al., 2002. HtrA2 promotes cell death through its serine protease activity and its ability to antagonize inhibitor of apoptosis proteins. *Journal of Biological Chemistry*, 277, pp.445–454.
Walters, K.B. et al., 2010. Live imaging of neutrophil motility in a zebrafish model of WHIM syndrome. *Blood*, 116(15), pp.2803–2811.
Walz, A. et al., 1987. Purification and amino acid sequencing of NAF, a novel neutrophil-activating factor produced by monocytes. *Biochemical and Biophysical Research Communications*, 149(2), pp.755–761.
Ward, P.A. & Lentsch, A.B., 1999. The acute inflammatory response and its regulation. *Archives of Surgery*, 134(6), pp.666–669.
Wei, M.C. et al., 2001. Proapoptotic BAX and BAK: a requisite gateway to mitochondrial dysfunction and death. *Science*, 292(5517), pp.727–730.
Wei, M.C. et al., 2000. tBID, a membrane-targeted death ligand, oligomerizes BAK to release cytochrome c. *Genes & Development*, 14(16), pp.2060–2071.
Weiss, S.J., 1989. Tissue destruction by neutrophils. *The New England Journal of Medicine*, 320(6), pp.365–376.
Whyte, M.K., Meagher, L.C., et al., 1993. Impairment of function in aging neutrophils is associated with apoptosis. *Journal of Immunology*, 150(11), pp.5124–5134.
Whyte, M.K., Hardwick, S.J., et al., 1993. Transient elevations of cytosolic free calcium retard subsequent apoptosis in neutrophils in vitro. *The Journal of Clinical Investigation*, 92(1), pp.446–455.
Wong, S.H. et al., 2009. Lactoferrin is a survival factor for neutrophils in rheumatoid synovial fluid. *Rheumatology*, 48(1), pp.39–44.

Woodfin, A. et al., 2011. The junctional adhesion molecule JAM-C regulates polarized transendothelial migration of neutrophils in vivo. *Nature Immunology*, 12(8), pp.761–769.

Yamaguchi, H., Bhalla, K. & Wang, H.G., 2003. Bax plays a pivotal role in thapsigargin-induced apoptosis of human colon cancer HCT116 cells by controlling Smac/Diablo and Omi/HtrA2 release from mitochondria. *Cancer Research*, 63(7), pp.1483–1489.

Yang, J. et al., 1997. Prevention of apoptosis by Bcl-2: release of cytochrome c from mitochondria blocked. *Science*, 275(5303), pp.1129–1132.

Yap, S. V et al., 2010. HAX-1: a multifaceted antiapoptotic protein localizing in the mitochondria and the sarcoplasmic reticulum of striated muscle cells. *Journal of Molecular and Cellular Cardiology*, 48(6), pp.1266–1279.

Yap, S. V., Koontz, J.M. & Kontrogianni-Konstantopoulos, A., 2011. HAX-1: A family of apoptotic regulators in health and disease. *Journal of Cellular Physiology*, 226, pp.2752–2761.

Yedavalli, V.S. et al., 2005. Human immunodeficiency virus type 1 Vpr interacts with antiapoptotic mitochondrial protein HAX-1. *Journal of Virology*, 79(21), pp.13735–13746.

Yin, X.M., Oltvai, Z.N. & Korsmeyer, S.J., 1994. BH1 and BH2 domains of Bcl-2 are required for inhibition of apoptosis and heterodimerization with Bax. *Nature*, 369(6478), pp.321–323.

Yokomizo, T. et al., 1997. A G-protein-coupled receptor for leukotriene B4 that mediates chemotaxis. *Nature*, 387(6633), pp.620–624.

Yuan, J. et al., 1993. The C. elegans cell death gene ced-3 encodes a protein similar to mammalian interleukin-1 beta-converting enzyme. *Cell*, 75(4), pp.641–652.

Zeytun, A. et al., 2010. Induction of cytokines and chemokines by Toll-like receptor signaling: strategies for control of inflammation. *Critical Reviews in Immunology*, 30(1), pp.53–67.

Zha, H. et al., 1996. Proapoptotic protein Bax heterodimerizes with Bcl-2 and homodimerizes with Bax via a novel domain (BH3) distinct from BH1 and BH2. *The Journal of Biological Chemistry*, 271(13), pp.7440–7444.

Zhao, W. et al., 2009. The anti-apoptotic protein HAX-1 is a regulator of cardiac function. *Proceedings of the National Academy of Sciences of the United States of America*, 106(49), pp.20776–20781.

Zimmerman, G.A., Prescott, S.M. & McIntyre, T.M., 1992. Endothelial cell interactions with granulocytes: tethering and signaling molecules. *Immunology Today*, 13(3), pp.93–100.

Zinkernagel, R.M. et al., 1996. On immunological memory. *Annual Review of Immunology*, 14, pp.333–367.

Zou, H. et al., 1997. Apaf-1, a human protein homologous to C. elegans CED-4, participates in cytochrome c-dependent activation of caspase-3. *Cell*, 90(3), pp.405–413.